ADVANCES IN

QUANTUM CHEMISTRY

EDITED BY

PER-OLOV LÖWDIN

DEPARTMENT OF QUANTUM CHEMISTRY
UPPSALA UNIVERSITY
UPPSALA, SWEDEN
AND
QUANTUM THEORY PROJECT
UNIVERSITY OF FLORIDA
GAINESVILLE, FLORIDA

VOLUME 9—1975

LIST OF CONTRIBUTORS

Numbers in parentheses indicate the pages on which the authors' contributions begin.

ROBERT J. BUENKER,* Lehrstuhl für Theoretische Chemie, Universität Bonn, Bonn, West Germany (69)

J. ČIŽEK,† Quantum Theory Group, Department of Applied Mathematics, Faculty of Mathematics and Department of Chemistry, Faculty of Science, University of Waterloo, Waterloo, Ontario, Canada (105)

BRIAN J. DUKE, Department of Chemistry, University of Lancaster, Lancaster, England (1)

JAMES E. EILERS, Department of Chemistry, State University of New York College at Brockport, Brockport, New York (1)

WILLIAM A. LESTER, JR., IBM Research Laboratory, San Jose, California (199)

R. K. NESBET, IBM Research Laboratory, San Jose, California (215)

BRIAN O'LEARY, Department of Chemistry, University of Alabama at Birmingham, Birmingham, Alabama (1)

J. PALDUS, Quantum Theory Group, Department of Applied Mathematics, and Department of Chemistry, Faculty of Science, University of Waterloo, Waterloo, Ontario, Canada (105)

SIGRID D. PEYERIMHOFF, Lehrstuhl für Theoretische Chemie, Universität Bonn, Bonn, West Germany (69)

* Permanent address: Department of Chemistry, University of Nebraska, Lincoln, Nebraska.

† Present address: Centre de Mécanique Ondulatoire Appliquée, Centre National de la Recherche Scientifique, Paris, France.

PREFACE

In investigating the highly different phenomena in nature, scientists have always tried to find some fundamental principles that can explain the variety from a basic unity. Today they have not only shown that all the various kinds of matter are built up from a rather limited number of atoms, but also that these atoms are constituted of a few basic elements of building blocks. It seems possible to understand the innermost structure of matter and its behavior in terms of a few elementary particles: electrons, protons, neutrons, photons, etc., and their interactions. Since these particles obey not the laws of classical physics but the rules of modern quantum theory of wave mechanics established in 1925, there has developed a new field of "quantum science" which deals with the explanation of nature on this ground.

Quantum chemistry deals particularly with the electronic structure of atoms, molecules, and crystalline matter and describes it in terms of electronic wave patterns. It uses physical and chemical insight, sophisticated mathematics, and high-speed computers to solve the wave equations and achieve its results. Its goals are great, but perhaps the new field can better boast of its conceptual framework than of its numerical accomplishments. It provides a unification of the natural sciences that was previously inconceivable, and the modern development of cellular biology shows that the life sciences are now, in turn, using the same basis. "Quantum biology" is a new field which describes the life processes and the functioning of the cell on a molecular and submolecular level.

Quantum chemistry is hence a rapidly developing field which falls between the historically established areas of mathematics, physics, chemistry, and biology. As a result there is a wide diversity of backgrounds among those interested in quantum chemistry. Since the results of the research are reported in periodicals of many different types, it has become increasingly difficult for both the expert and the nonexpert to follow the rapid development in this new borderline area.

The purpose of this serial publication is to try to present a survey of the current development of quantum chemistry as it is seen by a number of the leading research workers in various countries. The authors have

been invited to give their personal points of view of the subject freely and without severe space limitations. No attempts have been made to avoid overlap—on the contrary, it has seemed desirable to have certain important research areas reviewed from different points of view. The response from the authors has been so encouraging that a tenth volume is now being prepared.

The editor would like to thank the authors for their contributions which give an interesting picture of the current status of selected parts of quantum chemistry. The topics covered in the volume range from the treatment of large-scale calculations of electronic spectra, diagrammatic studies of time-independent perturbation theory, over collision phenomena and low energy electron scattering to the question of the transferability of the molecular orbital theory. Some of the papers emphasize studies in fundamental quantum theory, and others applications to comparatively complicated systems.

It is our hope that the collection of surveys of various parts of quantum chemistry and its advances presented here will prove to be valuable and stimulating, not only to the active research workers but also to the scientists in neighboring fields of physics, chemistry, and biology, who are turning to the elementary particles and their behavior to explain the details and innermost structure of their experimental phenomena.

PER-OLOV LÖWDIN

Utilization of Transferability in Molecular Orbital Theory

BRIAN O'LEARY

Department of Chemistry
University of Alabama
at Birmingham
Birmingham, Alabama

BRIAN J. DUKE

Department of Chemistry
University of Lancaster
Lancaster, England

and

JAMES E. EILERS

Department of Chemistry
State University of New York College
at Brockport
Brockport, New York

I. General Introduction

The purpose of this review is to consider ways in which transferability can be utilized in the construction of wavefunctions for large systems. Although our particular concern will be with those methods that use such

transferability to mimic *ab initio* calculations on large molecules, we shall also look at the role played by transference in improving the numerical convergence of SCF cycling procedures.

The concept of transferability permeates the whole of chemistry. We constantly experience the phenomenon of transferability, but usually call it "chemical sense." Thus we expect a given bond to be essentially the same, no matter where it is located. We speak of whole ranges of different molecules as containing the same functional group and identify this group by its characteristic chemical reactivity, infrared spectrum, and so on. Notions such as the additivity of bond energy, bond dipole, and covalent bond radii all reinforce this feeling of transferability in nature. For the quantum chemist even the use of s and p functions arises from the experience that the solutions of the Schrödinger equation for the one-electron atom prove valuable when used (transferred) to provide a first approximation to the wavefunction for the n-electron atom. This concept of transference is further extended when these same atomic functions are used (transferred) to provide a set of "building blocks" for approximating molecular wavefunctions.

Clearly, a concept that can be interpreted so widely forces us to limit our considerations to certain specific notions of transference. The notion with which we shall be concerned is that of the use of transferability as an economic tool for obtaining wavefunctions for molecules of chemical interest. Such transferability is masked by the use of wavefunctions Ψ described as

$$\Psi = A(\phi_1\alpha(1)\phi_1\beta(2)\phi_2\alpha(3) \cdots \phi_n\beta(2n)) \tag{1}$$

where the ϕ_m are a set of mutually orthogonal molecular orbitals and A is the usual antisymmetrizer. If we chose the orbitals ϕ_m to be the usual delocalized canonical orbitals, we disguise just those transferability features of a molecule that our "chemical sense" tells us to expect. However, the process of expanding these molecular orbitals in terms of atomic centered basis functions χ_i

$$\phi_m = \sum_i C_{mi}\chi_i \tag{2}$$

and optimizing Ψ through the iterative solution of the Roothaan–Hartree–Fock equation

$$\mathbf{FC} = \mathbf{SC}\lambda \tag{3}$$

may reveal transferable features. In Eq. (3) S is the matrix of the overlap integrals, λ is the diagonal matrix of the eigenvalues or orbital energies, C is the matrix whose columns are the eigenvectors, and F is the matrix of elements over the Hartree–Fock operator. Thus several workers have considered the question of whether the individual matrix elements of F are transferable and hence provide a means of simulating the Fock matrix of a large system from that of a smaller system. An alternative approach is provided by recognizing that our choice of functions ϕ_m in Eq. (1) is not unique; the wavefunction may readily be subjected to a unitary transformation that localizes its constituent molecular orbitals in bonding regions. The question of the transference of these so called "localized orbitals" has been considered by a number of workers.

Although in the sections that follow we shall be considering both of the above approaches in detail, we shall not consider questions related to the transference of basis sets, even though this leads us to exclude the interesting work of Christoffersen. Christoffersen's use of a basis set of floating spherical Gaussian orbitals, optimized on small fragment molecules, to calculate the wavefunctions of large systems has recently been reviewed (Christoffersen, 1972).

Attempts to mimic *ab initio* molecular orbital wavefunctions through transference will be in direct competition with those semiempirical or approximate methods such as CNDO, NDDO, etc., which also aim to mimic *ab initio* results. Any competition is only in terms of economy and accuracy since transference methods are in many respects similar to semiempirical methods. One interpretation of transference methods is to consider them as simply using a specialized method for obtaining approximate parameters. We shall therefore exclude consideration of semiempirical methods unless: (a) parameters are obtained directly from *ab initio* results, or (b) the method aims to reproduce *ab initio* results. This excludes MINDO which aims to obtain superior results of "chemical accuracy."

Concerning the latter case Freed (1974) has raised the interesting question of whether, with such a scheme, parameters can be transferred from calculations on small molecules that go beyond the Hartree–Fock limit.

The sections that follow begin by considering the major area in which transference methods have been developed, namely, methods involving the transfer of matrix elements. We next deal with transference methods involving the use of localized orbitals, and finally we consider the use of both transferred matrix elements and transferred localized orbitals in improving the efficiency of SCF cycling procedures.

II. Transferability of Fock Matrix Elements

A. Introduction

Within the molecular orbital theory the transference of matrix elements from one molecule to another and their possible use in the construction of wavefunctions for large systems forms a natural alternative to the transferability of parts of a wavefunction such as localized orbitals.

Like most quantum chemical concepts the idea of transferring matrix elements over some effective Hamiltonian has its roots in π electron theory. Indeed, the very simplest Hückel theory employs just such transference. Thus, the Hückel parameters α and β representing the matrix elements over a one-electron Hamiltonian, since they are solely dependent on the presence of a given orbital in a molecule, are, for a series of molecules containing that orbital, transferable from one molecule to another; this transferability of Hückel parameters is independent of any difference in size between the molecules. Within this π-theory framework, Orloff and Fitts (1963) showed that, for heteroatomic systems, more accurate Hückel parameters could be obtained by transferring both diagonal and off-diagonal matrix elements from SCF Pariser–Parr–Pope calculations. Leroy and Jaspers (1967) employed a similar technique for alternant hydrocarbons and found, using the atom and bond classification notation devised by Hartmann (1947), transferable elements for atoms and bonds in similar environments. This approach has been extended to d-orbitals by Nanda and Narasimham (1972).

The Orloff–Fitts "π-electron only" approach has served as a starting point for extensions to all electron calculations. These extensions have concentrated on the direct application of the idea of transference to the solution of the Roothaan eigenvalue problem [Eq. (3)]. In the first of these approaches, the NonEmpirical Molecular Orbital (NEMO) scheme introduced by Newton et al. (1966; see also Boer et al., 1966), while the diagonal elements of F are obtained by transferring them from ab initio calculations on smaller model compounds, the off-diagonal elements of F are estimated in a semiempirical fashion. Recently, however, the idea of transference has been extended to all the elements of F by (1) Eilers and Whitman (1973) who, in their Simulated Ab initio Molecular Orbital (SAMO) scheme obtain the diagonal and off-diagonal elements of F by transferring them from ab initio calculations on smaller molecules and (2) by the work of Degand et al. (1973) who combine the notion of the transference of Fock matrix elements with that of the transference of localized orbitals.

B. The Nonempirical Molecular Orbital (NEMO) Technique

Although in the mid 1960's the chemist, when faced with the problem of performing a calculation on a molecule of "chemical interest," had a number of different techniques from which to choose, these techniques were all semiempirical (Pople and Beveridge, 1970; Klopman and O'Leary, 1970; Murrell and Harget, 1972). The first scheme not to use experimental parameters, the NEMO method (Newton *et al.*, 1966; see also Boer *et al.*, 1966), subsequently labeled by its authors NEMO I, was introduced as a nonempirical alternative to the then popular extended Hückel method (Hoffman, 1963; Hoffmann and Lipscomb, 1962).

1. Basis of the NEMO Method

Within the NEMO scheme the orbital energies and molecular orbitals are obtained by a single (noniterative) solution of the eigenvalue problem

$$\mathbf{FC} = \mathbf{SC\lambda} \tag{4}$$

where:

(a) The elements of $\mathbf{S}$, the overlap matrix, are evaluated exactly.

(b) The diagonal elements $(F_{ii} = \alpha_i)$ of $\mathbf{F}$, the Fock matrix, are transferred directly from *ab initio* calculations on small model compounds. In the hope that these α's will include most of the effects of the bonding environment, the model compounds are chosen such that their atoms have similar local environments to the atoms found in the larger molecules of interest.

(c) The off-diagonal elements F_{ij} of $\mathbf{F}$ over nonorthogonal orbitals are estimated, using parameters obtained from these same model calculations, via the two equations

$$F_{ij} = T_{ij} + U_{ij}, \tag{5}$$

$$U_{ij} = K_{ij}S_{ij}(U_{ii} + U_{jj})/2. \tag{6}$$

Here:

(i) T_{ij}, the kinetic energy component, is evaluated exactly.

(ii) U_{ij}, the potential energy component, is obtained by use of Eq. (6)—a modified Mulliken (1949) or Wolfsberg and Helmholtz (1952) equation.

The diagonal elements U_{ii} and U_{jj} of the potential energy matrix are obtained from Eq. (5) using the transferred F_{ii} values and the calculated T_{ii} values.

Since the Mulliken-type approximations are known to fail for kinetic

energy (Mulliken, 1949; Newton *et al.*, 1966; see also Boer *et al.*, 1966) it is to be expected that applying Eq. (6) only to the potential energy portion will result in better values for the F_{ij} elements.

(iii) K_{ij} is an adjustable parameter in the sense that its values are chosen so as to best reproduce the Fock elements arising in the *ab initio* calculations on the model compounds. Although, as shown in Table I, it is necessary to have different K_{ij}'s for different types of orbital interaction, there is, nevertheless, a remarkable similarity of K values for different atoms. Within classes average values for K_{ij} are obtained through

$$K_{ab} = \left(\sum_{ij} K_{ij} \, |\, U_{ij}\,| \right) \bigg/ \sum_{ij} |\, U_{ij}\,|. \tag{7}$$

The subscripts a, b on K refer to those given in the first column of Table I.

TABLE I

NEMO METHOD—COEFFICIENTS FOR UMATRIX ELEMENTS[a,b]

	CH$_4$	C$_2$H$_2$	C$_2$H$_4$	C$_2$H$_6$	HCN	H$_2$CO	NH$_3$	BH$_3$[e]	B$_2$H$_6$[f]
K_{1s2s} (one-center)	0.66	0.66	0.66	0.66	0.66	0.66	0.66	0.66	0.66
K_{1s2s}	—	0.82	0.81	0.80	0.81	0.81	—	—	0.81
K_{1s2p}	—	0.82	0.82	0.81	0.82	0.82	—	—	0.82
K_{2s2s}	—	1.08	1.02	0.94	1.07	1.00	—	—	1.05
K_{2s2p}	—	1.09	1.06	1.00	1.11	1.05	—	—	1.11
K_{2p2p}	—	1.12	1.05	0.99	1.17	1.07	—	—	1.13
K_{2p2p}[c]	—	1.07	1.10	—	1.05	1.05	—	—	—
K_{2p2p}[d]	—	—	0.73	0.69	—	0.74	—	—	1.14
K_{1sH}	0.83	0.83	0.83	0.83	0.83	0.83	0.84	0.81	0.81
K_{2sH}	1.05	1.07	1.05	1.04	1.07	1.04	1.06	1.05	1.04
K_{2pH}	1.00	0.95	0.98	0.99	0.92	0.94	1.02	1.02	1.05
K_{HH}	1.19	1.48	1.18	1.15	—	1.20	1.19	1.16	1.13

[a] Reprinted with permission from *J. Amer. Chem. Soc.*, **88**, 2353 (1966). Copyright by American Chemical Society.

[b] The K's listed were obtained from Eq. (6) and averaged over certain similar interactions via Eq. (7). H denotes the hydrogen 1s orbital. Except for the first entry, all K's refer to two-center interactions.

[c] This row represents π–π interactions in the π MO's of C$_2$H$_2$, C$_2$H$_4$, HCN, and H$_2$CO.

[d] This row contains K's for the in-plane π–π interactions in C$_2$H$_4$ and H$_2$CO and the C$_2$H$_6$ π–π interaction, and an average of the two K's for the B$_2$H$_6$ π–π interactions (see footnote f).

[e] For BH$_3$, $\alpha 2_p$ was taken as the α of one of the in-plane 2$_p$ orbitals, since the third 2$_p$ orbital is unoccupied.

[f] Since the value of $K_{\pi-\pi}$ for B$_2$H$_6$ is an average value, it differs appreciably from other values in the same row.

Use of this formula ensures that the K's for large potential terms are the most heavily weighted.

The average K values so obtained are shown to fairly adequately reproduce the model compound SCF values on which they are based (Newton *et al.*, 1966).

(d) The off-diagonal elements F_{ij} of **F** over orthogonal orbitals would, were the Wolfsberg–Helmholtz technique to be used, all be set equal to zero. This is incorrect, for many of these elements have a nonzero value. In view of this difficulty, Newton *et al.* (1966; see also Boer *et al.*, 1966) introduce the following second-order formulas to estimate what they consider to be the most significant of these nonzero elements, namely, those over 2s and 2p orbitals located on the same atomic center.

$$F_{2s, 2p} = K_{2s, 2p} \sum S_{2s, r} S_{2p, r} \alpha_r \qquad (8)$$

Here, the sum extends over all orbitals. As shown in Table II, when using this formula it is necessary to distinguish the atom involved and the type of bonding situation present. The inclusion of these off-diagonal Fock elements over orthogonal orbitals has a marked effect on the resulting charge distribution (Newton *et al.*, 1966; see also Boer *et al.*, 1966). The desired rotational invariance of the NEMO wavefunctions is attained by using α's and K_{ij}'s that are averaged over the $2p_x$, $2p_y$, and $2p_z$ orbitals. However, for planar systems this requirement can be relaxed and the needed anisotropy retained by treating σ and π basis functions differently.

TABLE II

NEMO METHOD—ONE-CENTER 2s–2p F MATRIX
ELEMENTS

Molecule	Atom	F_{2s2p} (a.u.)	$K_{2, 2p}$
B_2H_6	B	0.104	0.33
C_2H_2	C	0.185	0.48
C_2H_4	C	0.106	0.40
C_2H_6	C	0.029	0.22
H_2CO	C	0.170	0.45
	O	0.190	0.64
NH_3	N	0.119	0.86
N_2O	N (terminal)	0.325	0.50
	N (internal)	0.078	0.69
	O	0.213	0.49
HCN	C	0.232	0.51
	N	0.279	0.58

Molecular binding energy (A) and the total energy (E_{tot}) cannot be precisely evaluated within the NEMO scheme. These quantities are, however, approximated by means of the formulas (Boer et al., 1964)

$$A = (\sum \varepsilon_i^m - \sum \varepsilon_i^a)/2 \qquad (9)$$

$$E_{tot} = (\sum \varepsilon_i^m + \sum E_i^a)/2 \qquad (10)$$

where ε_i and E_i are molecular (m) or atomic (a) orbital eigenvalues and core energies.

Let us now consider the errors introduced by the four approximations used within the NEMO scheme.

(a) Transference of α's from smaller model compounds. Errors may arise here because:

(i) In order to ensure the rotational invariance of the NEMO wavefunctions, the α's for the $2p_x$, $2p_y$, and $2p_z$ orbitals are averaged even when they are substantially different. This procedure proves much more detrimental for boron hydrides than for hydrocarbons (Newton et al., 1966; see also Boer et al., 1966).

(ii) The α values are not adjusted to take account of environmental differences between the model compound and the molecule of interest; the NEMO wavefunctions are not self-consistent in the usual sense. This may lead to exaggerated charge transfer.

(iii) The environment of the orbital in the model compound and the larger molecule may not be sufficiently similar. However, to the extent that the environments are similar (thus justifying transfer), the α values and the resulting wavefunctions are thought to mimic the true SCF values more closely than other semiempirical methods and in particular those that do not explicitly include electron repulsions. A further point in this improved performance over other semiempirical techniques is that, in agreement with exact SCF closed shell calculations for neutral ground state molecules, Newton et al. (1966; see also Boer et al., 1966) find that unoccupied orbitals have positive eigenvalues. In contrast to this, most semiempirical methods tend to yield one or more negative eigenvalues for unfilled shells. Nevertheless, the ionization potentials predicted by NEMO are often too low and the error increases with molecular complexity.

(b) The use of a Wolfsberg–Helmholtz technique to obtain the potential energy components of the off-diagonal Fock matrix elements over pairs of nonorthogonal orbitals. Errors may arise here because: (i) of the use of the Wolfsberg–Helmholtz approach itself; the shortcomings of this

have been reviewed at great length by Nicholson (1970), and (ii) this approximation involves transferring diagonal potential energy components from model compounds and again no adjustment is made for environmental differences.

(c) The neglect of off-diagonal Fock matrix elements over pairs of orthogonal orbitals, a second-order formula being used to estimate only those elements involving orthogonal 2s and 2p orbitals located on the same atomic center.

(d) The approximation of total energy and bond energy. This approach may result in errors in the overall method which are not entirely due to transference. Coupled with the lack of true self-consistency, this approximation renders the application of NEMO to geometrical or conformational questions somewhat dubious (Newton *et al.*, 1966; see also Boer *et al.*, 1966; Ehrenson, 1968a).

Workers have commented on both the fundamental logic and the predictive powers of the NEMO theory. Thus, applying the NEMO technique to an addition complex of triethylamine and trimethyl-6-boron has caused Ehrenson (1968a) to become sceptical about the ability of the available parameters to fit such an environment. Consequently, Ehrenson (1968b) modifies the basic method to allow charge redistribution to alter the α's. In a later work Ehrenson (1969a) analyzes the reasons for NEMO being at least qualitatively correct about bond angles but incapable of useful predictions about bond lengths. The explicit inclusion of kinetic energy causes NEMO to predict bond lengths that are too short whereas extended Hückel predicts molecules to be far too large. In an accompanying paper (Ehrenson, 1969b) he discusses why charge redistribution procedures of the Hückel type are inherently inferior to SCF procedures that explicitly include electron repulsion. This view is not shared by Halgren and Lipscomb (1973).

The extent to which the NEMO method can be applied depends on the number of available *ab initio* calculations on small molecules in which the atoms "see" environments as similar as possible to those found in the large molecule of interest. Since the early work was parameterized from CH_4, C_2H_2, C_2H_6, HCN, H_2CO, NH_3, N_2O, BH_3, and B_2H_6, only a limited number of environmental distinctions could be made. Nevertheless, acceptable results were obtained for the orbital energies, binding energies, ionization energies, and charge distributions of an impressive number of hydrocarbons (Newton *et al.*, 1966; see also Boer *et al.*, 1966). Latterly, the increase in the number of exact calculations on small molecules has resulted in a greater degree of discrimination in the choice

of environmentally sensitive parameters, and consequently a significant improvement in the method.

Boer and Turley (1967) report a calculation on 2-nitrosoethane using the original parametrization (Newton *et al.*, 1966; see also Boer *et al.*, 1966). Newton and Lipscomb (1967) compare exact SCF and NEMO results for methylacetylene. Although, as expected, the α's transfer acceptably, the off-diagonal elements can be in error by as much as 2 eV, and the charge distributions show appreciable differences. Potenza and Poindexter (1968) have applied NEMO to both fluorocarbons and radicals. The validity of NEMO for either of these systems can be questioned. Lippert *et al.* (1969) have performed NEMO calculations on benzene, *p*-xylene, and tetracyanoethylene, but are dissatisfied with their results. Boer *et al.* (1968) have studied the rearrangement of 2-pentanone with NEMO calculations on neutral molecules, radicals, and ions. Although they recognize the inherent dangers of discussing the energetics of radicals and ions from NEMO theory they feel that they obtained useful information about changes in orbital features accompanying rearrangement. Smith and Shannon (1969) discuss the decomposition of metastable ions in a similar fashion. Work on carbon-13 chemical shifts for five-membered nitrogen heterocycles suggested to Pugmire and Grant (1968) that NEMO wavefunctions are superior to both extended Hückel and CNDO wavefunctions. Bushweller *et al.* (1970) report calculations of the rotational barriers for formamide, thioformamide, selenoformamide, urea, and carbonic acid. The sequence of calculated barriers is found to roughly parallel the experimentally observed trend. Comparison of NEMO and SCF wavefunctions for benzene (Stevens *et al.*, 1971) are not encouraging. Offenhartz (1970) notes that the NEMO scheme cannot adequately deal with off-diagonal matrix elements in charged species such as NiF_6^{4-}. Birnstock (1973) proves that shielding constants calculated with NEMO wavefunctions are able to reflect multiple bond effects. NEMO parameters for Ga, Ge, As, Se (Stevenson and Lipscomb, 1970); Si, S (Boer and Lipscomb, 1969); Sc, Ti (Stevenson and Lipscomb, 1969); Cl (Boyd, 1971) and P (Boyd and Lipscomb, 1967) have also been compiled.

Many NEMO calculations have been made for boranes and carboranes. Stevenson (1973) has looked at a number of geometries of $B_3H_8^-$ using parameters from B_2H_6 (Boer *et al.*, 1966). Molecular orbital studies of $B_7C_2H_{13}$ have been made using parameters from B_2H_6 (Voet and Lipscomb, 1967). It is found that the main effect of including simply the one-center zero overlap matrix elements is to transfer electron density

from B and C atoms to the terminal hydrogens. Beal and Lipscomb (1967) report results for m-$B_{10}H_{10}C_2H_2$ using parameters from SCF calculations on B_4H_4 (Palke and Lipscomb, 1966) and including, for the first time, two-center zero overlap matrix elements. Other calculations on $B_6H_6C_2(CH_3)_2$ (Hart and Lipscomb, 1968) and $B_7H_7C_2(CH_3)_2$ (Koetzle et al., 1968) use parameters from B_4H_4 and ethane. Later calculations on 1,6-$B_8C_2H_{10}$ use parameters from B_5H_9 as well (Koetzle and Lipscomb, 1970a). A subsequent series of calculations on carboranes uses parameters obtained from $B_4C_2H_6$ (Koetzle and Lipscomb, 1970b). Their attempts to regenerate the SCF wavefunction for $B_4C_2H_6$ from the NEMO parameters met with limited success.

2. Modified NEMO Schemes

In addition to the shortcomings of the Mulliken approximation (Nicholson, 1970), the basic NEMO scheme has two fundamental deficiencies:

(a) In three-dimensional molecules the α's for $2p_x$, $2p_y$, and $2p_z$ orbitals are, even when they are substantially different, averaged in order to guarantee rotational invariance of the wavefunctions. Clearly, the method would be improved if, at the same time as maintaining rotational invariance, these α's were allowed to develop anisotropies appropriate to the molecular symmetry.

(b) All α's may be expected to have slightly different values in the molecule being studied as compared with the reference molecules, even though the α's transfer well between similar molecules, they cannot be optimal values for the new system. In view of this it would be desirable if these transferred α values were allowed to adjust to values which reflect the related, but somewhat different, environment found in the new molecule. The need for this adjustment was painfully obvious in applications that showed large charge distortions, and in applications to radicals and ions.

The first reported modification to NEMO is that of Ehrenson (1968b) who accounts for charge redistributions by a self-consistent, linear dependence of α upon orbital charge adjustment method. The application of this scheme to a trimethylamine–trimethylboron reaction system found that the charge deficiency for boron readjusted to 1/3 to 1/5 of the zero-order results. The adjustment in $(CH_3)_3B$ was significantly greater than for $(CH_3)_3N$. While in this reaction system the charge redistribution appears empirically satisfactory with respect to the charges themselves, the modification does not uniformly improve the correspondence be-

tween the theoretically and experimentally determined observables for the system. Since part of the difficulty is probably due to a lack of proper parameters for the tetrahedral boron environment, judgement on the general efficiency of the charge redistribution method has been reserved (Ehrenson, 1968b).

By introducing their NEMO II scheme Boyd and Lipscomb (1968) took steps to alleviate the aforementioned difficulties and to unify the approach for evaluating all Fock matrix elements. Both diagonal and off-diagonal potential energy matrix elements between orbitals with both zero and nonzero overlap are computed using the formula

$$U_{pq} = C_{pq} \sum_r S_{pr}(\alpha_r^{Av.} - T_{rr})S_{rp} \tag{11}$$

where the sum is over the basis set and the C_{pq}'s are characteristic of the type of orbital interaction. Although Eq. (11) is related to Eq. (6), it is seen to be far more general. All elements of the Fock matrix are obtained as the sum of the U's and exactly calculated kinetic energy integrals. Thus, even though isotropic or averaged α values are used, the diagonal elements of the Fock matrix are free to develop anisotropies appropriate to their environment in the large molecule. To gain rotational invariance, the values for the α's and C_{pq}'s are averaged over all orbitals in the same atomic subshells (i.e. p's and d's).

Extensive comparisons with SCF calculations and the NEMO I method have been made (Boyd and Lipscomb, 1968). The anisotropies introduced to the F-matrix by the new method are shown to be in the proper direction, albeit sometimes exaggerated. Generally, an acceptable agreement with SCF calculations is found, although charge separation is even more exaggerated than with NEMO I. Comparisons with SCF results for GaH_3 show both NEMO I and II to be inadequate (Tossel and Lipscomb, 1972).

Subsequent nonempirical molecular orbital schemes have become far more ambitious in scope. Thus, a version called NEMO III formulated by Tossell and Lipscomb (1972) is every bit as complex as Pople's INDO theory (Pople *et al.*, 1967). The intent is to simulate *ab initio* calculations on transition metal compounds and complex ions. This requires a system to handle highly charged atoms, charged molecules, and the energetics of open shells. This is accomplished by the melding of INDO and traditional NEMO ideas into an iterative scheme.

The diagonal elements of the Fock matrix are quite accurately evaluated from the integrals of Hartree–Fock theory (all of which are computed exactly except for three-center repulsion integrals which are

approximated by the Ruedenberg expression, Ruedenberg, 1951). All ani-
sotropies are retained for all integrals. The NEMO I approach is used for
off-diagonal elements with finite overlap. The zero overlap elements are
calculated by yet another complex formula. The α's for core orbitals are
transferred from model compounds and then adjusted using Manne's
formula (Manne, 1967) for the new charge distribution at each step of the
iteration. All necessary parameters are obtained from exact SCF calcula-
tions on model compounds. Nesbet and Watson's (1960) symmetry and
equivalence restrictions are used for open shells.

The parametrizations and the method are shown to reproduce SCF
results on small molecules far more effectively than either the NEMO I or
NEMO II schemes. A calculation on CuF_4^{2-} indicates that the method is
capable of reproducing semiquantitatively the relative energies of differ-
ent ligand and metal orbitals and of giving correct metal orbital anisotro-
pies. Within the limitations imposed by their minimal basis set, they
expect qualitatively correct results for charge distributions and energy
trends in transition metal compounds.

Tossell and Lipscomb (1972) report that Switkes (1970) has developed
a self-consistent field extension to the NEMO method and that it is more
accurate than CNDO/2, INDO, or NDDO. Tossell (1973) has recently
combined elements of both the CNDO/2 and NEMO methods in an
application to $SiO4^{4-}$.

Halgren and Lipscomb (1973) have developed a very sophisticated
self-consistent field approach that deserves a brief mention here. The
method is a little outside our present emphasis in that no matrix elements
are transferred. However, in that it does appear to be one of the best
semiempirical schemes yet devised, that using the same basis set as an *ab
initio* calculation aims at mimicking the SCF wavefunction, it must on
economic grounds represent the closest competitor to methods that in-
volve transference. The method, which is based on the Partial Retention
of Diatomic Differential Overlap (PRDDO) over an orthogonal basis,
aims at approximating LCAO SCF molecular orbital wavefunctions at
the minimum basis set level for closed shell molecules.

The SCF equations are solved explicitly, retaining all one-electron
integrals and approximating two-electron Coulomb integrals, hybrid
integrals, and exchange integrals of the forms $(i_A j_A \mid i_A j_A)$ and $(i_A j_A \mid i_A j_B)$
for centers A and B. Single-center averaging processes otherwise required
for rotational invariance are avoided by the use of local atomic-centered
axes which are unique in anisotropic environments. It is interesting to
note that comparison of parametrized results with *ab initio* SCF results

for many molecules indicates that, by this PRDDO scheme, Fock matrix elements are mimicked to standard deviations of 0.007, density matrix elements to 0.007 electrons, orbital populations and atomic charges to 0.01 or 0.02 electrons, orbital energies to 0.01 a.u., and total energies to 0.03 a.u.

C. The Simulated *Ab Initio* Molecular Orbital (SAMO) Technique

1. *Basis of the Method (Closed Shells)*

   a. Introduction. The simulated *ab initio* molecular orbital (SAMO) technique aims at constructing wavefunctions of near *ab initio* accuracy for large molecules. It arises from the Eilers–Whitman observation (Eilers and Whitman, 1973) that matrix elements over the Hartree–Fock operator in an LCAO–SCF–MO treatment have closely similar numerical values for similar pairs of basis functions in similar molecules. Thus, for example, the Fock matrix elements for similar interactions in propane and butane are, since they are almost identical, found to be interchangeable. This transference is, however, generally useful only when a set of hybridized atomic orbitals is employed. The explanation for this is that hybrids are determined by the internal reference framework of the molecule, whereas unhybridized s and p functions are defined by reference to an often arbitrary external coordinate system.
   Like NEMO, the SAMO method for closed-shell molecules generates the molecular orbitals and orbital energies for large molecules by a single solution of the Roothaan eigenvalue problem [Eq. (3)]. Both diagonal and off-diagonal elements of F are transferred, truncated to four decimal figures, from *ab initio* calculations on similar small molecules known as "pattern molecules." In those cases where interactions between distant orbitals are unavailable from the pattern molecules, the Fock matrix elements are usually small and consequently can be set to zero when constructing the Fock matrix for the large molecule. The total energy is given by

$$E_T = \sum_{occ} (\varepsilon_i^{(0)} + \lambda_i) + V_{NN} \tag{12}$$

where the $\varepsilon_i^{(0)}$ are the expectation values of the one-electron operator, the λ_i are the eigenvalues of the Hartree–Fock operator, V_{NN} is the nuclear repulsion energy, and the summation is over occupied orbitals. From this it can be seen that using SAMO one can evaluate both the molecular

orbitals and the total energy without recourse to the time consuming evaluation of two-electron repulsion integrals.

A program, SAMOM (O'Leary *et al.*, 1974a) designed to implement this method is available from the Quantum Chemistry Program Exchange.

b. Choice of Pattern Molecules. As an example, to clarify the problems arising in selecting suitable pattern molecules to be used in the simulation of a target molecule, we shall consider the target molecule to be a linear molecule R—X where R is a hydrocarbon chain and X is a terminal group, e.g. $-CH_3$, $-OH$, $-NH_2$, etc. The SAMO method is designed to produce wavefunctions of near *ab initio* accuracy for molecules where the group R is very large and consequently an *ab initio* calculation on R—X would be prohibitively expensive. In SAMO calculations:

1. We use pattern molecules of the form R'—X' where although R' is small it is nevertheless large enough to include all relevant Fock matrix elements involving orbitals on or close to the group X.

2. We obtain other Fock matrix elements involving orbitals located on the hydrocarbon chain from a pattern hydrocarbon molecule R". Again, although R" is much smaller than R it is chosen to be of sufficient size to include all relevant Fock matrix elements involving orbitals on that part of the hydrocarbon chain.

3. We neglect Fock matrix elements that involve one orbital from the terminal group X and another orbital from further out along the chain (i.e. not included in R'—X').

Figure 1 serves to illustrate the simulation of the target molecule R—X from the pattern molecules R'—X and R". It illustrates the designation of the set of all orbitals (including hydrogen) associated with each group (e.g. $-CH_3$, $-CH_2$, $-NH_2$, etc.) present in the molecule. Thus, for example,

$$\{A\} \equiv \{1s(C), 4(sp^3(C)), 2(1s(H))\}.$$

That is, the set $\{A\}$ consists of the 1s and four sp^3 hybrid orbitals centered on carbon together with the 1s orbitals centered on each of the two hydrogens.

In what follows the set of Fock matrix elements $\langle \chi_i | F | \chi_j \rangle$, where χ_i and χ_j both belong to the same set of basis functions (e.g. $\chi_i \in \{A\}$ and $\chi_j \in \{A\}$), will be designated by $\{A, A\}$. Where χ_i and χ_j belong to different sets (e.g. $\chi_i \in \{A\}$ and $\chi_j \in \{B\}$) the set of associated Fock matrix elements will be designated $\{A, B\}$.
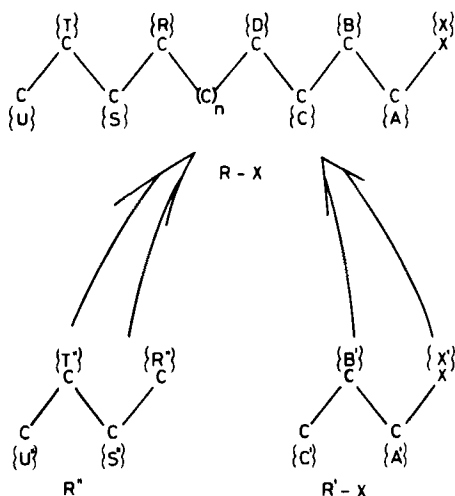
Fig. 1. Schematic representation of the simulation of the wavefunction for the target molecule R—X from the pattern molecules R'—X and R".

To obtain good results, we must select the pattern molecules in such a way as to balance the dual requirements of (i) obtaining all required Fock matrix elements, and (ii) performing economical *ab initio* calculations. Thus, referring to the hypothetical molecule shown in Fig. 1, the question boils down to finding the most economic way of obtaining the interactions

$$\{X, X\}, \{X, A\} \cdots \{X, U\},$$

$$\{A, A\}, \{A, B\} \cdots \{A, U\},$$

$$\{B, B\}, \{B, C\} \cdots \{B, U\},$$

$$\{U, U\}.$$

Were we to choose methane, the smallest conceivable pattern molecule, for the simulation of the Fock matrix elements of the set $\{A\}$ we would run into difficulties on two counts. First, we would be unable to obtain off-diagonal Fock matrix elements such as those in sets $\{A, B\}$, $\{A, X\}$, $\{C, B\}$, etc. Second, the elements of $\{A, A\}$ might not be transferable from such a small pattern molecule. Although to a first approximation it would seem that one could regard all C—H bonds in a given molecule as being equivalent, to obtain accurate results this environment must be taken into account. This is done by recognizing the difference between, say, the

C—H bonds in the methylene and methyl groups. Fock matrix elements involving the former must be taken from pattern molecules containing a suitable methylene group while pattern molecules for the latter must contain the appropriate methyl group.

Were one to go to the other extreme and select a very large pattern molecule, for example one containing all the sets from $\{X\}$ through $\{R\}$, the very purpose of SAMO would be defeated. Not only would such an *ab initio* calculation be uneconomic, but it would supply no Fock matrix elements of significant value ($> \sim 10^{-3}$ a.u.) that could not be obtained from a much smaller pattern molecule.

Considerations similar to the above clearly suggest an optimum size of pattern molecule. Our investigations have shown that pattern molecules consisting of four or at most five heavy centers (C, N, O, etc.) are usually of sufficient size to simulate the wavefunction of the largest molecules. In Table III we present a selection of target molecules together with their appropriate pattern molecules.

In the case of the hypothetical target molecule shown in Fig. 1, all

TABLE III

SAMO Method—Examples of Pattern Molecules

Target molecule	Associated pattern molecule(s)
R (saturated chain hydrocarbons)	R' (saturated chain hydrocarbons)
R (saturated rings)	R' (saturated chain hydrocarbons)
A (aromatic rings)	R' (unsaturated hydrocarbons)
R—X	$R'' + CH_3-CH_2-CH_2-X$
X = polar groups, radical group, or ionic group	X = polar group, radical group, or ionic group
$\begin{array}{c} O \\ \parallel \\ R'-C-R'' \end{array}$	$\begin{array}{c} O \\ \parallel \\ CH_2-CH_2-C-CH_3 + R''' \end{array}$
$\begin{array}{c} X \\ \mid \\ R'-CH-R'' \end{array}$	$\begin{array}{c} X \\ \mid \\ CH_3-CH_2-CH-CH_3 + R''' \end{array}$
$R'-O-R''$	$CH_3-CH_2-O-CH_3 + R'''$
$\begin{array}{c} X \\ \mid \\ R'-C-R'' \\ \mid \\ R'' \end{array}$	$\begin{array}{c} X \\ \mid \\ CH_3-CH_2-C-CH_3 + R''' \\ \mid \\ H \end{array}$

Fock elements arising in the sets $\{X, X\}$, $\{X, A\}$, $\{X, B\}$, $\{X, C\}$, $\{A, B\}$, $\{A, C\}$, and $\{B, C\}$ would be obtained from their counterpart in R'—X (e.g. $\{X, X\}$ from $\{X', X'\}$, $\{X, B\}$ from $\{X', B'\}$) while the remainder, Fock elements arising in such sets as $\{U, T\}$, $\{U, R\}$, and $\{T, S\}$, would be chosen from their counterpart in R''. Fock elements separated by distances greater than the size of the appropriate pattern molecule, e.g. $\{X, U\}$, $\{B, T\}$, $\{C, R\}$, etc., are set to zero.

The Fock matrix elements occurring in a given target molecule can be divided into two classes: the "in-range" elements, i.e. elements that are in the range of and hence can be obtained from the associated pattern molecules, and the "out-of-range" elements, i.e. elements that are outside the range of and hence cannot be obtained from the associated pattern molecule. The SAMO method rests on two approximations: transferring "in-range" Fock matrix elements, and neglecting "out-of-range" Fock matrix elements. What is the effect of these approximations on the accuracy of the calculations? To answer this question both *ab initio* and SAMO calculations were performed on a variety of molecules. In Table IV we present the overall root mean square (rms) deviation between Fock

TABLE IV

SAMO METHOD—ACCURACY OF FOCK MATRIX ELEMENTS

Molecule	Root mean square deviation between *ab initio* and SAMO Fock matrix elements
$CH_3-CH_2-CH_2-CH_2-OH$	0.0011
$CH_3-CH_2-CH_2-CH_2-NH_2$	0.0010
$CH_3-CH_2-CH_2-CH_2-CHO$	0.0010
$CH_3-CH_2-CH_2-COOH$	0.0021
Butane from propane	0.0011

matrix elements obtained from an *ab initio* calculation on a given molecule and the corresponding elements for the same molecule obtained by simulation as described above. Our investigation has shown that the errors incurred by transferring "in-range" Fock matrix elements and neglecting "out-of-range" Fock matrix elements are comparable. A statistical analysis of these errors (Eilers and Whitman, 1973) is in accordance with these results.

The actual act of transference involves the handling of a very large number of Fock matrix elements each having a different value. Since such

transference, when performed by hand, is an extremely slow and error prone process, it is desirable to adopt some kind of automatic retrieval system. Of the numerous different approaches used by us, the most generally successful involves (1) the storage of "libraries" of Fock matrix elements obtained from *ab initio* calculations on pattern molecules, and (2) routines for searching these libraries in order that the requirements of a given target molecule may be satisfied. A program, SAMOL (O'Leary *et al.*, 1974b), which, in addition to implementing both the above schemes, is also designed to allow the user to specify ranges of indices of Fock matrix elements, these indices coming from appropriate ranges in pattern molecules, is available from the Quantum Chemistry Program Exchange. We would introduce a word of caution here. None of the schemes implemented by the SAMOL program is foolproof. We have simply produced a system which allows the user to transfer the vast majority of Fock matrix elements in a form in which they can be readily checked and small modifications inserted. We are currently working on the development of a completely automatic system.

   c. Geometry and Basis Sets. In the SAMO method the geometry of those pattern molecules associated with a given target molecule is chosen to be the same as the geometry of that area of the target molecule they are required to mirror. This mirroring of geometry is of fundamental importance since accurate results cannot be expected to be obtained from pattern molecules whose geometry bears little or no relation to the geometry of the target molecule. In many of our applications of the SAMO method we have chosen idealized geometries for both the target and pattern molecules, e.g. all saturated C—C bond distances are set to 1.54 Å, all C—H bond distances to 1.10 Å, and all bond angles to 109° 28' or 120°. This idealization carries with it the advantage of economy—the same pattern molecule often mirrors a variety of positions within the target molecule. Thus, using a regular hexagonal geometry for our calculations of benzenoic hydrocarbons has enabled us to use butadiene as our pattern molecule, with all C—C bond lengths set to 1.40 Å and its bond angles set to 120°.

   The same basis set must be used for the *ab initio* calculations on all necessary pattern molecules and the evaluation of the overlap matrix and one-electron matrix of the target molecule. Having decided upon a given basis set one is committed to remain with that basis throughout the ensuing calculations, for Fock matrix elements obtained from calculations using different basis sets are not transferable. This fact is borne out
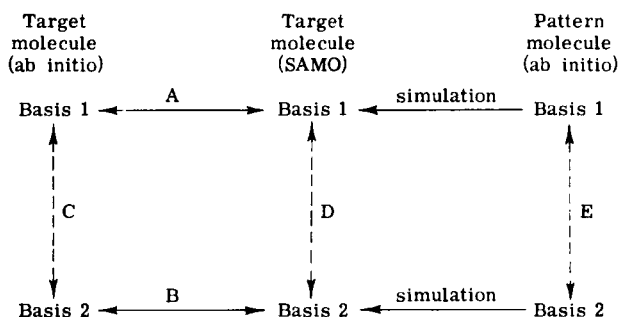
Fig. 2. Schematic representation of calculations in which simulation is carried out with the same basis set and in which the basis set is altered.

by a study (Duke and O'Leary, 1974) of the same molecule using two different basis sets. The general idea behind this investigation is represented in Fig. 2. In our particular study the target and pattern molecules were *n*-butane and propane, respectively, and the basis sets were:

Basis 1   Whitman–Hornback basis of contracted Gaussian orbitals (Whitman and Hornback, 1969)
Basis 2   Schmidt orthogonalized Slater type orbitals (STO's)

Paths A and B in Fig. 2 compare the *ab initio* and simulated Fock matrix obtained within the same basis set. Our study shows these to be both extremely good and of roughly similar accuracy. Paths C, D, and E compare *ab initio* and simulated Fock matrices obtained from different basis sets. Our study shows these to be very poor; the Fock matrix in basis 2 is very different from that obtained in basis 1. Unless otherwise stated, basis 1 has been used for all SAMO calculations.

Fock matrix elements over nonorthogonal hybrid orbitals are still of significant value even when the hybrids are located on atoms that are as far apart as three or four heavy centers. This leads us naturally to ask if there is a basis set that makes these long range terms smaller, but still allows transference of short range terms. Such a basis might be expected to be provided by the Löwdin symmetric orthogonalized orbitals (Löwdin, 1950). One might suppose terms involving Fock matrix elements over distant hybrid orbitals to be small when these hybrids have been symmetrically orthogonalized. This has been studied with disappointing results.

The Löwdin orthogonalized orbitals χ' (OAO basis) are formed from

the nonorthogonalized orbitals χ (AO basis) by means of the transformation

$$\chi' = \chi T \tag{13}$$

where

$$T = S^{-1/2} \tag{14}$$

and S is the overlap matrix with elements

$$S_{ij} = \langle \chi_i \mid \chi_j \rangle. \tag{15}$$

The Fock matrix F' in the new basis is related to the Fock matrix F in the old basis by the transformation

$$F' = TFT. \tag{16}$$

Transferability of the elements of F' has been studied (Duke and O'Leary, 1974) for the molecules butanol, butyl amine, pentanal, and butanoic acid. The results of this work are shown in Table V. This table serves to show that transferability does take place when an OAO basis is used. However, the errors in this transference are slightly worse than those obtained for the AO basis.

TABLE V

SAMO METHOD—ROOT MEAN SQUARE DEVIA-
TION OF FOCK MATRIX ELEMENTS

Molecule	AO basis	OAO basis
Butanol	0.0011	0.0014
Butyl amine	0.0010	0.0013
Pentanal	0.0010	0.0013
Butanoic acid	0.0024	0.0025

Our investigation has shown that the Fock matrix elements in the OAO basis transfer with much the same error as that found in the AO basis. The slightly poorer transferability lies in the sharp contrast between the values obtained for the "in-range" and "out-of-range" Fock matrix elements. Thus, although many of the "in-range" elements are of smaller value than the corresponding elements found with the AO basis, the

" out-of-range " elements are, surprisingly enough, larger than their counterpart in the AO basis. A possible explanation for this result is obtained by considering the expansion of the OAO's in the terms of χ, their component AO's. Terms in the expansion of F'_{ij} arising from the negative contribution to the OAO's (the so-called " tail ") must incorporate F_{pq} terms where χ_p and χ_q are AO's lying between χ_i and χ_j. Clearly, these terms must be more important in any such expansion of F_{ij} than the more long range terms F_{ij} in F'_{ij}; in spite of the fact that χ_i and χ_j are, by definition, the dominant terms in the expansion of χ'_i and χ'_j, respectively. The upshot of this is that the terms we neglect are larger in the OAO basis than in the AO basis.

A SAMO technique in the OAO basis can be developed as follows:

1. Transfer elements of $\mathbf{F}'$ for the target molecule from elements of $\mathbf{F}'$ for the pattern molecule in an exactly analogous manner to that used for the SAMO technique in the AO basis.
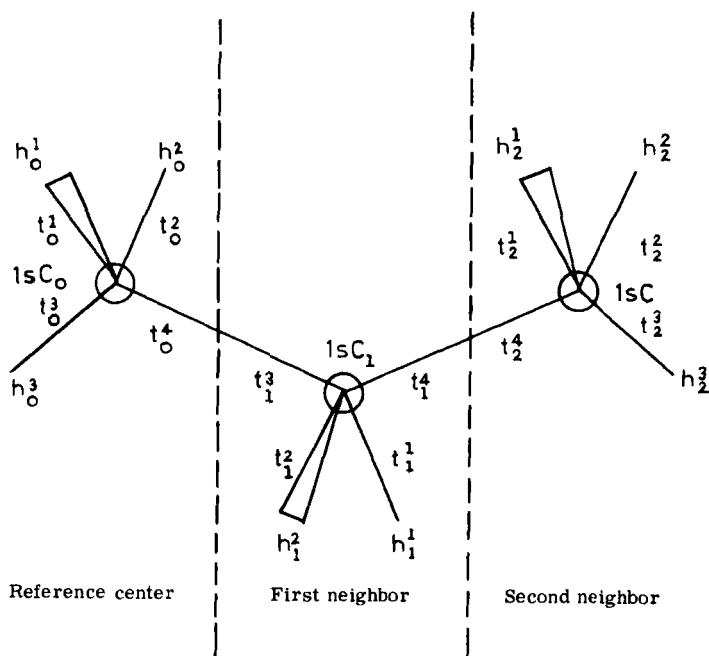

Fig. 3. Key to code used in Table VI—hybrid orbitals for propane. From Deplus *et al.*, (1974). Reprinted with permission from *Theor. Chim. Acta*, **36**, 109 (1974). Copyright by Springer-Verlag, Heidelberg.

TABLE VI

Fock Matrix Element Parameters by the Method of Deplus *et al.* (1974)

(a) Diagonal elements		(b) Elements within a center	
$h_0^1 h_0^1$	-0.0390	$1sC_0 h_0^i \ (i = 1, 2, 3)$	$+0.0314$
1sC1sC(CH$_4$)	-11.3737	$1sC_0 t_0^4$	$+0.1092$
1sC1sC (primary)	-11.3544	$h_0^1 h_0^i \ (i = 2, 3)$	-0.0698
1sC1sC (secondary)	-11.3457	$h_0^i t_0^i \ (i = 1, 2, 3)$	-0.5822
1sC1sC (tertiary)	-11.3407	$h_0^1 t_0^i \ (i = 2, 3, 4)$	-0.0587
$t_0^4 t_0^4$	-0.1441	$t_0^1 t_0^i \ (i = 2, 3, 4)$	-0.0204
$t_0^i t_0^i \ (i = 1, 2, 3)$	-0.1665		

(c) Elements between a center and its first neighbors		(d) Elements between a center and its second neighbors	
$1sC_0 h_1^i \ (i = 1, 2, 3)$	-0.0486	$1sC_0 t_2^4$	-0.0311
$1sC_0 t_1^3$	-0.4769	$t_0^4 t_2^4$	-0.0885
$1sC_0 t_1^i \ (i = 1, 2, 4)$	$+0.0371$	$t_0^4 t_2^i \ (i = 1, 2)$	$+0.0093$
$h_0^i h_1^i \ (i = 1, 2)$	-0.0230	$t_0^4 h_2^3$	-0.0229
$h_0^1 h_1^2$	-0.0153	$t_0^4 h_2^i \ (i = 1, 2)$	-0.0118
$h_0^i t_1^3 \ (i = 1, 2, 3)$	-0.0693	$t_0^3 t_2^3$	-0.0368
$t_0^4 t_1^3$	-0.6305	$t_0^3 h_2^i \ (i = 1, 2)$	$+0.0114$
$t_0^4 t_1^i \ (i = 1, 2, 4)$	-0.0463	$h_0^3 h_2^3$	-0.0075
$t_0^i t_1^i \ (i = 1, 2)$	$+0.0891$	$h_0^i h_2^i \ (i = 1, 2)$	-0.0256
$t_0^1 t_1^2$	-0.0353		

2. Solve

$$\mathbf{F'C'} = \mathbf{C'}\lambda \tag{17}$$

to give orbital energies and eigenvectors in the OAO basis.

3. For convenience transform the eigenvectors to the AO basis

$$\mathbf{C} = \mathbf{TC'}. \tag{18}$$

4. Use **C** to give population density terms, dipole moments, etc., as in the SAMO technique in the AO basis.

In Section II,C,(2) results using the technique outlined above will be compared with results using the AO basis.

The transferability of Fock matrix elements over an orthogonal basis has also been independently noted by Deplus *et al.* (1974). Their approach, although very similar to the SAMO approach outlined above, differs from it in one important respect. To obtain a simple parameter for a given Fock matrix element in a particular environment they take the average of a series of values of that element in a range of small molecules.

In obtaining these parameters they ignore interactions between a given center and its third neighbor or beyond, and set to zero all values lower than 7×10^{-3} a.u. The use of this averaging process results in a method which is somewhat simpler to apply than the SAMO approach in that fewer distinct parameters need to be transferred. This increased simplicity is, however, bought at a price, for it appears that the results are less accurate. In the only work so far reported, calculations are carried out on hydrocarbons. The parameters used by Deplus *et al.* are shown in Table VI (the key to the code used in Table VI is given in Fig. 3). Deplus *et al.* appear to be the first to notice the existence of a simple relationship between nondiagonal matrix elements and geometry. The element $t_0^i t_1^j$ can, for example, be obtained from the relationship

$$t_0^i t_1^j = 0.0011 + 0.0846 \cos \theta, \qquad i = 1, 2 \text{ or } 3, j = 1, 2 \text{ or } 4 \quad (19)$$

where θ is the dihedral angle defined by the sequence of atoms HCCH (see Fig. 3).

In Section II,C,(2) the results of the work of Deplus *et al.* will be compared with the results obtained using the SAMO method.

2. *Results and Modifications to the Basic SAMO Technique*

a. Introduction. The method outlined in the previous section has been successfully applied to chain hydrocarbons (Eilers and Whitman, 1973), aromatic rings (Eilers *et al.*, 1975b; Duke *et al.*, 1975c), simple polymers (Duke and O'Leary, 1973; Duke *et al.*, 1975b), certain organic radicals using a spin unrestricted open shell formalism (Duke *et al.*, 1974), cyclohexanes (Eilers *et al.*, 1975a), one large system of biological interest (O'Leary *et al.*, 1973), and molecules containing a polar functional group (Duke *et al.*, 1975a). A complete list of these calculations, target molecule, associated pattern molecule(s), properties calculated, etc., is given in Table VII.

TABLE VII

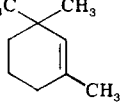LIST OF SAMO CALCULATIONS

Target molecule	Pattern molecule(s)	Ref.	Properties[i]	Comment
Ethane	Propane	[a]	A,B,C	1
Ethane	Av. hydrocarbon parameters	[b]	A,B	
Propane	Ethane	[a]	A,B,C	2

TABLE VII (*cont.*)

Target molecule	Pattern molecule(s)	Ref.	Properties[i]	Comment
n-Butane	Propane	*a*	A,B,C	2
Propane	Av. hydrocarbon parameters	*b*	A,B	
n-Butane	Av. hydrocarbon parameters	*b*	A,B	
i-Butane	Av. hydrocarbon parameters	*b*	A,B	
Neopentane	Av. hydrocarbon parameters	*b*	A	
Chair and boat cyclohexane	(i) Propanes			
	(ii) Propanes and methanes			
	(iii) Butanes	*c*	A,B	
Cyclohexane	Av. hydrocarbon parameters	*b*	A	
Polyethylene	*n*-Butane	*d*	E	
Benzene	*s-cis*-butadiene	*e*	A,B,C	
Naphthalene	*s-cis* butadiene			
	s-trans butadiene	*e*	A,B,C	
Anthracene	*s-trans* butadiene	*e*	A,B,C	
Phenanthrene	*s-trans* butadiene	*e*	A,B,C	
1,2 Benzanthracene	*s-trans* butadiene	*f*	A,F,G	
Pyrene	*s-trans* butadiene	*f*	A,F,G	
Dimethyldibenzopyrene	*s-trans* butadiene, pentene	*f*	A,F,G	
Dimethylanthanthrene	*s-trans* butadiene, pentene	*f*	A,F,G	
Benzonaphthacene	*s-trans* butadiene	*f*	A,F,G	
1,2; 5,6 Dibenzanthracene	*s-trans* butadiene	*f*	A,F,G	
3,4 Benzopyrene	*s-cis* butadiene			
	s-trans butadiene	*f*	A,F,G	
3,4; 9,10 Dibenzopyrene	*s-trans* butadiene	*f*	A,F,G	
Anthanthrene	*s-trans* butadiene	*f*	A,F,G	
Polyene	*s-trans* butadiene	*d*	E	
Toluene Me rotomers	(i) *s-cis* butadiene propene			
	(ii) *s-cis* butadiene pentene	*g*	A,B	3
Diphenyl— various conformers	Butadienes in various geometries	*g*	A,B	4
Butyl radical	Propyl radical			
	Propane	*h*	A,B,C	
Pentyl radical	(i) Butyl radical, Butane			
	(ii) Propyl radical, propane	*h*	A,B,C	

TABLE VII (cont.)

Target molecule	Pattern molecule(s)	Ref.	Properties[1]	Comment
Butyl cation and anion	Propyl cation and anion			
	Butane	i	A,B,C	
Acetic Acid	Formic Acid			
	Acetaldehyde	a	A,B	5
Butanoic Acid	CH_3-CH_2COOH			
	Butane	i	A,B,C	
Butanol	$CH_3CH_2CH_2OH$			
	Butane	i	A,B,C	
Butyl Amine	$CH_3CH_2CH_2NH_2$			
	Butane	i	A,B,C	
Pentanal	$CH_3-CH_2-CH_2-CHO$	i	A,B,C	
All-trans retinal		j	A,C	
	crotonaldehyde, various Me-butadienes, propylbutadiene			
Polyglycine	$CH_3-CO-NH-CH_3$ $NH_2-CH_2-CO-NH_2$ $CHO-NH-CH_2-CHO$	k	C,E	

[a] Eilers and Whitman (1973). [e] Eilers et al. (1975b). [i] Duke et al. (1975a).
[b] Deplus et al. (1974). [f] Duke et al. (1975c). [j] O'Leary et al. (1973).
[c] Eilers et al. (1975a). [g] Eilers et al. (1974). [k] Duke et al. (1975b).
[d] Duke and O'Leary (1973). [h] Duke et al. (1974).

[1] A—orbital energies, B—total energies, C—Mulliken populations, D—dipole moment, E—band structure, F—ionization potentials, G—carcinogenic activity.

Comments

1. This calculation is working in the "wrong" direction. However, it was an important test of the transferability and truncations utilized in the basic SAMO method.

2. This pair of calculations represent the first test of the SAMO method. Results show ethane to be too small a pattern molecule. Improved results are obtained using propane.

3. Using set (i) pattern molecules, rotomer with C—H perpendicular to ring was predicted to be the more stable by 2.5 kcal/mole. Using set (ii) pattern molecules the other rotomer was predicted to be the more stable by 6.3 kcal/mole. Experimentally the result is much lower (14 cal/mole, Rudolph et al., 1967).

4. Experimentally the most stable form is $42 \pm 2°$. The planar form of biphenyl is predicted, by SAMO, to be the most stable by 190 kcal/mole, and the 45° form to be marginally (3.75 kcal/mole) more stable than the 90° form. Repeating the calculation by increasing the central bond length in the planar pattern molecule (f) to 1.50 Å only increased the stability of the planar form of biphenyl.

5. This calculation represents a test of partial transferability. Not all Fock matrix elements are transferred, some being taken from acetic acid itself.

TABLE VIII

SAMO Method—Summary of Deviations from *Ab Initio* Results

Target[a] molecule	Reference	Total energy $\|\Delta E/\varepsilon\| \times 10^4$	Occupied orbital energy, rms $\times 10^3$
Butane	[b]	0.80	3.1
Benzene	[c]	8.20	16.8
Cyclohexane chair method III (PA)	[d]	0.91	3.4
boat method III (PA)	[d]	1.29	3.7
Butyl radical method (ii)	[e]	0.45	$2.7(\lambda^\alpha)\ 2.8(\lambda^\beta)$
Pentyl radical method a(ii)	[e]	0.67	$5.4(\lambda^\alpha)\ 5.7(\lambda^\beta)$
Butanol method (β)	[f]	0.26	1.6
Butyl amine method (β)	[f]	0.55	1.6
Pentanal method (β)	[f]	0.03	1.8
Butanoic acid method (β)	[f]	1.78	4.5
Butyl cation method (β)	[f]	2.64	5.8
Butyl anion method (β)	[f]	4.45	12.8

[a] Labels for method taken from original reference.
[b] Eilers and Whitman (1973).
[c] Eilers *et al.* (1975b).
[d] Eilers *et al.* (1975a).
[e] Duke *et al.* (1974).
[f] Duke *et al.* (1975a).

In Table VIII we present a summary of deviations from *ab initio* values for the total energy and occupied orbital energies. These values are calculated as the difference between the best SAMO result for a given molecule and the result obtained for an *ab initio* calculation on that molecule, using the same basis set and geometry. This table serves to clearly demonstrate the soundness of the SAMO method for it shows that

TABLE IX

SIMPLIFIED OAO SCHEME (DEPLUS *et al.*, 1974)—SUMMARY
OF DEVIATIONS FROM *Ab Initio* RESULTS

	RMS deviation in $\lambda_i \times 10^3$	$|\Delta E/E| \times 10^4$
Methane	9.2	21.8
Ethane	11.9	7.2
Propane	10.1	11.4
Butane	11.1	17.0
Iso-butane	8.8	32.2
Neopentane	12.5	—
Cyclohexane	10.9	—

total energies and orbital energies are in excellent agreement with the *ab initio* result.

The results shown in Table VIII, taken in conjunction with Table IX, allow us to compare the performance of the standard SAMO approach (Fock matrix elements transferred from smaller pattern molecules to larger target molecules) with that of the simplified scheme over orthogonalized orbitals developed by Deplus *et al.* (1974) (simulated parameter obtained by averaging Fock matrix elements for a range of small hydrocarbons). Whereas with the SAMO method one deliberately simulates only molecules larger than the pattern molecules, in the method of Deplus *et al.* it is possible, for example, to simulate methane by using parameters obtained from the range of hydrocarbons, methane through butane. It would be instructive to compare the results of Deplus *et al.* (1974) which use orthogonalized AO's with those obtained using nonorthogonalized AO's. Unfortunately Deplus *et al.* use a different basis set to that used in the SAMO calculations and, since their results are concerned exclusively with the OAO's, no exact direct comparison is possible. The change in basis set, however, is not going to be the most crucial point. Thus a comparison between Tables VIII and IX shows that their simplified scheme using averaged parameters leads to errors in the total energy and orbital energies which are significantly larger than those obtained from the SAMO method. The results, however, are still quite good and it is a matter of taste whether one is prepared to accept a somewhat larger error as the price of a simplified scheme.

For butyl alcohol, butylamine, pentanal, and butanoic acid, however, we do have a direct comparison within the SAMO technique between the

TABLE X

COMPARISON OF OAO AND AO SAMO CALCULATIONS

	Ab initio	SAMO AO	SAMO OAO
Butanol			
E	−231.107	−231.117	−231.113
μ	1.726	1.773	1.798
RMS deviation—occupied orbital energies	—	0.0016	0.0021
RMS deviation—orbital populations	—	0.0032	0.0025
Butyl amine			
E	−211.336	−211.351	−211.348
μ	1.555	1.599	1.515
RMS deviation—occupied orbital energies	—	0.0017	0.0022
RMS deviation—orbital populations	—	0.0026	0.0021
Pentanal			
E	−268.799	−268.805	−268.800
μ	2.225	2.287	2.293
RMS deviation—occupied orbital energies	—	0.0018	0.0024
RMS deviation—orbital populations	—	0.0035	0.0025
Butanoic acid			
E	−304.5444	−304.4971	−304.608
μ	0.986	1.012	1.051
RMS deviation—occupied orbital energies	—	0.0041	0.0048
RMS deviation—orbital populations	—	0.0086	0.0072

use of orthogonalized and nonorthogonalized atomic orbitals. This comparison is shown in Table X. As noted in Section II,C,1,c the Fock matrix elements over the OAO's transfer in a slightly poorer fashion than those over AO's. This leads to slightly larger errors in the orbital energies using the OAO basis. However, the errors in the density matrix are more evenly spread throughout the molecule. This results in an improved Mulliken population matrix and, in many cases, an improved total energy. Although the total errors in the density matrix using the AO basis are small they are formed from rather larger errors at some points and from negligible ones elsewhere. This is related to a certain ambiguity in choosing Fock matrix elements; a point discussed in the next section.

Our work with the SAMO technique has led us to an awareness of certain weaknesses within the basic method. Thus, for example, it is dependent on both the size of the pattern molecule and the degree of symmetry within the pattern molecule. In transference, ambiguity can arise over the question of from which part of a pattern molecule Fock elements should be chosen. The method as it stands fails to fully account for steric factors. These aspects of our work are dealt with in the following sections.

b. The Junction Effect between Pattern Molecules and Its Influence upon the Size of Pattern Molecules. The question of the optimum size of a pattern molecule(s) goes hand in hand with the problem of the junction effect. This problem is best considered in the light of our findings for molecules containing a polar functional group. Consider Fig. 1 showing the schematic representation of the simulation of the wavefunction for the target molecule $R—X$ from the pattern molecules $R'—X$ and R''. By the junction effect we mean the problem of deciding from where in the pattern molecule(s) we choose the elements of set $\{C, C\}$. Clearly, there are two possible choices:

1. Choose the elements of $\{C, C\}$ from $\{C', C'\}$ in the pattern molecule $R'—X$. The effects of this choice are: (i) Elements selected for $\{C, C\}$ are in the environment of the X group. This "environment effect" may well be an important factor to consider. (ii) Elements for $\{C, C\}$ are being selected from a set localized on a terminal group in $R'—X$. This introduces a "terminal error" as the elements of $\{C', C'\}$ must be expected to be different from the elements $\{C, C\}$, a set localized on an internal group.

2. Choose the elements of $\{C, C\}$ from $\{T'', T''\}$ in the pattern molecule R''. The effect of this choice is to (i) remove the terminal error and (ii) introduce an environment error, for the effect of the group X can no longer be taken into account.

It is the balancing of the errors arising in each of the above choices that decides the optimum size of pattern molecules. Thus, the larger $R'—X$ the more the environment error decreases; however, the terminal error remains constant. Hence the best results are obtained by choosing $R'—X$ to be of sufficient size to minimize the environment error as the terminal error may readily be eliminated through choice 2.

The original investigation (Eilers and Whitman, 1973) was confined to the simple hydrocarbons and showed that, while a pattern molecule containing two carbon centers was inadequate, one containing three carbon centers was of sufficient size for the simulation of the wavefunction of

butane. Subsequent investigation (Duke *et al.*, 1975a) has shown that for straight chain molecules containing a terminal polar group it is necessary to choose pattern molecules with at least four heavy centers (C, O, N, etc.) in a chain, counting the polar group as a single center even if it is —CHO or —COOH.

This rule of four carries over to ring systems. The investigation of aromatic ring systems (Eilers *et al.*, 1975b) has shown that satisfactory results can be obtained using pattern molecules containing four carbon centers. The study of cyclohexane (Eilers *et al.*, 1975a) was in part geared to an investigation of the effect of variations in the size of pattern molecules. Again it was found that, although propanes represent the smallest feasible pattern molecules for the simulation of boat and chair cyclohexane, results of acceptable accuracy were only obtained using butanes.

c. Steric Effects. A weakness of the basic SAMO method is its inability to account naturally for any steric effects that may be present in a given target molecule. Such steric effects may be regarded as a special case of the environment effect discussed in the previous section. In our investigation (Eilers *et al.*, 1974b, 1975b) we have met these effects through the interactions of the hydrogen atoms in the "bay" region in phenanthrene and through the interaction of the 1 and 4 groups in boat cyclohexane. In both these cases we have been able to correct for such effects by introducing a simple steric adjustment to the values of the appropriate Fock matrix elements obtained from the pattern molecule. In practice, by considering the values of the Fock elements associated with all relevant groups in the pattern molecule we are able to obtain a steric split, i.e. a measure of the value of the steric effect on the Fock matrix elements. The steric effect in the target molecule is then accounted for by using this steric split to modify the appropriate elements.

The effect of this steric adjustment has been to give more accurate values to individual Fock matrix elements and to improve energy calculations.

d. Second Bonding Pathway Effects in Cyclic Systems. The heavy centers in straight chain pattern molecules associated with cyclic target molecules can "interact" through only one bonding pathway. In the cyclic target molecule, however, the same centers can, by the very nature of the ring structure, "interact" through two bonding pathways; a pathway corresponding to that present in the pattern molecule and a second

bonding pathway having no equivalent in the pattern molecule. It would not be surprising, in view of the behavior of, for example, NMR coupling constants, if this altered the value of the Fock matrix elements.

The study of the cyclohexanes (Eilers *et al.*, 1975a) deals with the effect of this second bonding pathway on the simulation of wavefunctions for cyclic target molecules from noncyclic pattern molecules. Fock matrix data was obtained from three sources: (1) properly positioned pairs of methane molecules—no bonding pathway, (2) butanes—a single bonding pathway, and (3) the complete *ab initio* SCF calculation on the cyclohexanes—two bonding pathways. While the sign and size of the Fock elements for such long-range interactions are primarily determined by the type and spatial positioning of the interacting orbitals, the presence of the second bonding pathway in the target molecule has a small but noticeable effect on the magnitude of these Fock elements. Essentially, the effect of the bonding pathways is additive. Thus, the change between the methane approach and the butane approach gives a measure of the correction to be added to account for the effect of the second bonding pathway in the ring. Although correcting for the second bonding pathway improves the Fock matrix elements for long-range interactions in the cyclohexanes, it has a mixed effect on the overall calculation—improved eigenvalues and orbital populations but a marginally poorer energy.

A comparison of *ab initio* results with those obtained from the SAMO study of benzene (Eilers *et al.*, 1975b) suggests the presence of a second bonding pathway effect in this molecule. Although we are not able to correct for the effect here in quite the same way as we did in cyclohexane, possible methods of correction are currently under investigation. Multiple bonding pathway effects are expected to be important in all ring systems.

e. Conformational Studies. The determination of small energy differences between conformers or barriers to rotation is perhaps the application for which the SAMO technique is least suited. In *ab initio* studies it is at least known that the total energy calculated for a given molecule is higher than the "true value." Since the variation theorem does not apply to the SAMO method, the energies calculated for different conformations of a target molecule lie in a narrow region about the *ab initio* result. This randomness can, in extreme cases, lead to energy differences that are incorrect in both sign and size. The problem here is that since the requisite pattern molecules have differing degrees of symmetry, the errors in

each, arising from junction effects, steric effects, and, for cyclic systems, secondary bonding pathways, occur to different and indeterminable extents. Cyclohexane is a good example of this. The chair form has higher symmetry and requires fewer pattern molecules (in each case different butane conformations) than the boat form. As a result a more accurate SAMO result is obtained for the chair form. Unfortunately the errors for the two conformers are of opposite sign, giving an even poorer estimate of the energy difference. Even the best estimate of the energy difference is too large— ∼ 40 kcal/mole compared with *ab initio* results of 9.4 kcal/mole (Eilers *et al.*, 1975a) and 7.2 kcal/mole (Hoyland, 1969a) and an experimental estimate of 6.6 kcal/mole (Allinger *et al.*, 1968). Disappointing results have also been obtained for toluene and biphenyl (see Table VII) but further work is required to fully elucidate the problems in these molecules.

Although it may well be that we have chosen for study a number of particularly unfavorable situations—cyclohexane has a far greater degree of symmetry in its chair than in its boat form, toluene has an extremely small energy barrier to rotation, biphenyl has a steric effect which for SAMO is especially difficult to take into account, and the amount of conjugation and hence the central bond length differ in the rotomers— nevertheless, they are systems of real chemical interest. The toluene case is especially unfortunate, we would have expected to have predicted a much smaller barrier here. In the light of this experience the SAMO technique appears to be of little use in studying rotational barrier problems. Moreover, it would seem unwise to use the SAMO technique for problems involving energy differences between conformers when one conformer has a much greater degree of symmetry than the other(s) and hence can be expected to be more amenable to a SAMO treatment, and when, the energy difference(s) under consideration is extremely small.

f. The Ionic Effect. The work reported so far in this section has been confined to the consideration of neutral target molecules. The successful results obtained when the group X (Fig. 1) is a $-CH_3$, $-OH$, $-NH_2$, $-CHO$ or $-COOH$ group does not allow us to predict similar successes when the group X bears a full positive or negative charge. In the case of a neutral target molecule $R-X$, the fact that Fock matrix elements associated with orbitals belonging to the terminal set $\{U\}$ can be obtained from the hydrocarbon pattern molecule R'' means that those terms involving nuclear attraction and electron repulsion with the nuclei and electrons located on group X are canceling each other out. Where the

group X bears a positive or negative charge, such a cancellation cannot occur. In this case we would expect, and indeed find, that the values of F_{ij}^+, the matrix elements associated with orbitals belonging to set $\{U, U\}$ when X bears a positive charge, are very different to F_{ij}^-, those associated with $\{U, U\}$ when X bears a negative charge; the values of the corresponding elements F_{ij}^P taken from the hydrocarbon pattern molecule R" are roughly the mean of F_{ij}^+ and F_{ij}^-.
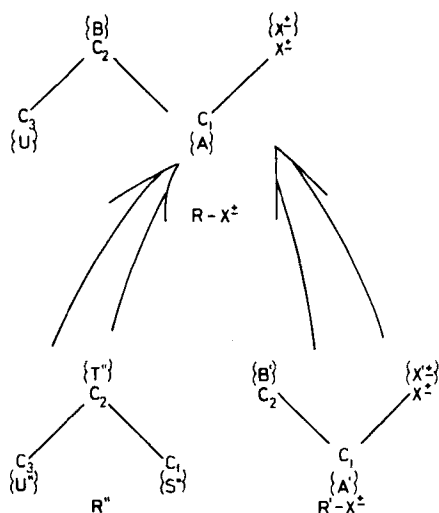
Fig. 4. Schematic representation of the simulation of the wavefunction for $R-X^\pm$, the target ions butyl cation and butyl anion ($X^\pm = CH_2^+$ and CH_2^-, respectively), from $R'-X^\pm$, the pattern ions propyl cation and anion, respectively, and R", the pattern molecule propane.

In a study (Duke *et al.*, 1975a), shown schematically in Fig. 4, of the simulation of the butyl cation and anion using propyl cation and anion as pattern ions and propane as pattern molecule we found that choosing $F_{ij}^\pm$, the matrix elements belonging to $\{U, U\}$ from the corresponding elements of $\{U'', U''\}$, with a correction from a single nuclear attraction integral, does not allow the direct simulation of the requisite target ion matrix elements. The problem here is that such a scheme can only work where the positive and negative charges are similarly distributed within their respective ions. Our investigation shows that as a consequence of their not being similarly distributed an ionic effect occurs.

We correct for this ionic effect by introducing a perturbation to the

term F_{ij}^{P}. The resulting formula (a formula now specifically designed to take into account the different distribution of positive and negative charges) is

$$F_{ij}^{\pm} \approx F_{ij}^{P} + \sum q_t^{\pm} \langle \chi_i \mid 1/r_t \mid \chi_j \rangle. \qquad (20)$$

Here $\langle \chi_i \mid 1/r_t \mid \chi_j \rangle$ is the nuclear attraction integral involving nucleus t bearing unit charge, and $q_t^{\pm}$ is the partial charge on atom t. The parameter $q_t^{\pm}$ approximates the spread of the total positive or negative charge in the target cation or target anion. This is obtained from the Mulliken orbital population charges in the pattern ion $R'-X^{+}$ or $R'-X^{-}$, corrected by subtracting movement of charge in $C_1 - C_2$ already taken into account in the matrix elements from R'', propane. The sum over t in Eq. (20) is taken over all nuclei where a nonzero q_t is available (i.e. all nuclei present in $R'-X^{\pm}$, the pattern ion). Equation (20) is used to obtain all those Fock elements that arise in the target ion and cannot be obtained by transference from the pattern ions. In the case of butyl ions we thus transferred all matrix elements from the propyl ions or from propane using Eq. (20).

The fact that the largest values of q_t arising in the cation are on the hydrogen atoms of the CH_2^{+} group, while the largest terms in the anion are to be found on the carbon atom of the CH_2^{-} group makes Eq. (20) a more satisfactory approximation for the cation than for the anion. In spite of this, the errors in our simulation of the wavefunction for the butyl cation and anion were still satisfactory, although somewhat larger than those for neutral molecules. This slight decline in accuracy, then, is due to the small size of pattern molecule and ion used and to the fact that in the cation the larger q_t charges are more remote from the terminal $\{U\}$ group than is the case for the anion.

3. Open Shell SAMO

a. The Problem of Open Shells. Within the framework of the molecular orbital theory, *ab initio* calculations on the ground states of open-shell systems have been performed in more than one way. Thus we have the single determinant, different orbitals for different spin approaches (the so-called spin unrestricted Hartree–Fock UHF open-shell approach) (Pople and Nesbet, 1954) and the pairing up of all but the odd-electron approach (the so-called restricted Hartree–Fock RHF open-shell approach) (Roothaan, 1960).

Since the SAMO method rests on the ability to choose suitable pattern molecules, it is not to be expected that the technique can be applied to the problem of simulating the wavefunction of those open-shell target radicals in which the odd electron is highly delocalized—in such cases it is not possible to choose pattern radicals that mimic the delocalization. Pattern radicals can, however, be chosen to mimic the spin density distribution when the odd electron is well localized. In such situations it is to be expected that the SAMO technique will have an application. A SAMO study of such target radicals, using both the UHF and RHF approach, has shown that transferability exists within each formalism. The RHF approach (Duke *et al.*, 1975d) was completed after the submission of this review, so only the UHF approach will be discussed (Duke *et al.*, 1974).

b. Different Orbitals with Different Spin SAMO (DODS/SAMO). Within the different orbitals with different spin or UHF approach the molecular orbital eigenvalues and eigenfunctions are obtained by solving the pair of matrix equations:

$$\mathbf{F}^\alpha \mathbf{C}^\alpha = \mathbf{S}\mathbf{C}^\alpha \lambda^\alpha, \tag{21}$$

$$\mathbf{F}^\beta \mathbf{C}^\beta = \mathbf{S}\mathbf{C}^\beta \lambda^\beta. \tag{22}$$

In the full *ab initio* method, the method used for pattern radicals, these equations are coupled, i.e. both $\mathbf{F}^\alpha$ and $\mathbf{F}^\beta$ depend on $\mathbf{C}^\alpha$ and $\mathbf{C}^\beta$. In the DODS/SAMO method $\mathbf{F}^\alpha$ and $\mathbf{F}^\beta$ are obtained for the target radical by transferring their values from calculations on pattern radicals and molecules. The overlap matrix $\mathbf{S}$ is evaluated exactly and equations are separately solved to give the eigenvalues and eigenfunctions for orbitals with α spin and β spin, respectively. As shown in Eq. (23), the total energy E_T can be obtained from a knowledge of the orbital energies λ_i^α and λ_i^β and the matrix over the one-electron part of the Hamiltonian.

$$E_\mathrm{T} = V_{\mathrm{NN}} + \tfrac{1}{2}(\textstyle\sum \lambda_i^\alpha + \sum \lambda_i^\beta) + \tfrac{1}{2}\mathrm{Tr}(\mathbf{RH}) \tag{23}$$

Here V_{NN} is the nuclear repulsion energy, and the summation over λ_i^α and λ_i^β is over the respective occupied orbitals. The total density matrix R is formed from the sum of $\mathbf{R}^\alpha$ and $\mathbf{R}^\beta$, where $\mathbf{R}^\alpha$ and $\mathbf{R}^\beta$ are themselves formed from $\mathbf{C}^\alpha$ and $\mathbf{C}^\beta$, respectively, and H is the matrix over the one-electron Hamiltonian.

Figure 5 is a schematic representation of the DODS/SAMO technique for the simulation of the wavefunction of R—X′, a target radical, from R′—X′, a pattern radical, and R″, a pattern molecule. The
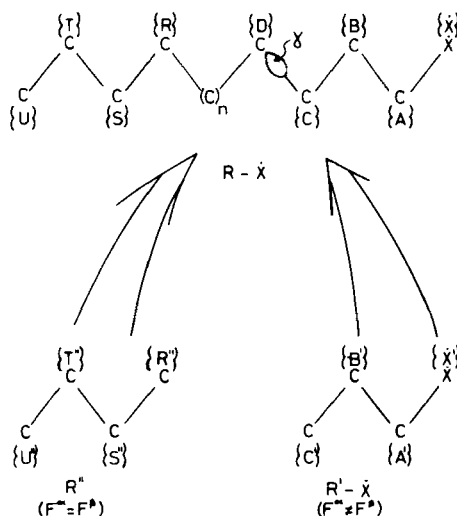
Fig. 5. Schematic representation of the simulation of the wavefunction for $R-X$, a target radical, from $R'-$, a pattern radical, and R'', a pattern molecule. In our study (Duke *et al.*, 1974): (i) $X = -CH_2$, $R = -CH_2-CH_2-CH_3$, $R' = -CH_2-CH_3$, and $R'' = CH_3-CH_2-CH_3$, and (ii) $X = -CH_2$, $R = -CH_2-CH_2-CH_2-CH_3$, $R' = -CH_2-CH_2-CH_3$, and $R'' = CH_3-CH_2-CH_2-CH_3$.

method by which the required values of F_{ij}^{α} and F_{ij}^{β} are obtained from the associated patterns depends upon whether or not the elements are subject to a junction effect.

Elements not subject to a junction effect. For these elements a procedure closely similar to that developed for closed shell systems is used.

(i) Within the area of localization of the odd electron both F_{ij}^{α} and F_{ij}^{β} are transferred from $R'-X$.

(ii) Outside the area of localization, i.e. for Fock elements involving orbitals that are fairly distant from the, essentially localized, odd electron the following approximation is made:

$$F_{ij}^{\alpha} = F_{ij}^{\beta} = F_{ij}.$$

Here, F_{ij} represents the value of the corresponding Fock element occurring in R''.

(iii) Elements out of range of both $R'-X$ and R'' are set to zero. The one exception to this occurs for those members of $\{X', D\}$ which involve the orbital labeled γ in Fig. 5, i.e. the orbital belonging to $\{D\}$ that points

back along the chain. Neglect of these elements gives rise to a principle
source of error. Surprisingly enough these can be approximated by those
interactions in $R'-X'$ involving $\{X'\}$ and the hydrogen in orbitals belong-
ing to the terminal $-CH_3$ group.

This approach has met with considerable success in application to the
simulation of the wavefunction for the butyl and propyl radicals, respec-
tively (Duke *et al.*, 1974); the DODS/SAMO work being compared with
results obtained from *ab initio* UHF calculations using identical basis sets
and geometries. This study has also served to illustrate the increased
importance of the junction effect in such calculations.

Elements subject to a junction effect. In closed shell work it is generally
sufficient to use a "one-to-one mapping," i.e. all the required matrix
elements arising in the target molecule can be obtained from one pattern
molecule. In open shell systems such an approach proves inadequate and
is replaced by a "two-to-one mapping." In other words, since $\{C\}$ is an
internal group in the target radical (see Fig. 5) and $\{C'\}$ a terminal $-CH_3$
group in $R'-X$, the absolute values of the elements of $\{C, C\}$ are best
transferred from $\{T'', T''\}$ (or equivalently $\{S'', S''\}$) in R''. However, the
splitting or difference between F_{ij}^{α} and F_{ij}^{β} occuring within the target
molecule, since it seems to be purely a function of distance, is best trans-
ferred from the target radical $R'-X'$. The "two-to-one mapping" for
correcting for junction effects arising in open-shell systems may be sum-
marized as follows:

(i) Determine the value of Δ_{ij}, the splitting occuring in the pattern
radical between F_{ij}^{α} and F_{ij}^{β}.

(ii) Obtain F_{ij}^{ρ}, the value of that element in the pattern molecule
corresponding to the element required for the target radical which, owing
to the junction effect, cannot be taken from the pattern radical.

(iii) Equate F_{ij} to the value of F_{ij}^{ρ} corrected by $\Delta_{ij}/2$, the value of the
average splitting. That is,

$$F_{ij} = F_{ij}^{\rho} \pm \tfrac{1}{2}\Delta_{ij}.$$

Table XI compares the results obtained from our DODS/SAMO work on
the butyl and pentyl radicals with those we obtained using the *ab initio*
UHF approach (Duke *et al.*, 1974). The DODS/SAMO technique seems
to provide a promising method for calculating wavefunctions for large
radicals in the spin unrestricted formalism. Since it appears to be partic-
ularly accurate for spin orbital populations it would seem to be a poten-
tially very useful technique for interpreting ESR experiments. No attempt
has been made in our work to compare the DODS/SAMO method with

TABLE XI

COMPARISON OF RESULTS OF CALCULATIONS ON THE BUTYL AND PENTYL RADICALS USING
THE DODS/SAMO AND *Ab Initio* UHF METHODS

Property	Butyl radical		Pentyl radical	
	Ab initio UHF	DODS/SAMO	*Ab initio* UHF	DODS/SAMO
Total energy E	−155.921	−155.913	−194.794	−194.807
$\langle S^2 \rangle$	0.7626	0.7626	0.7627	0.7626
RMS deviations				
Orbital energies for				
occupied orbitals λ_i^α	—	0.0027	—	0.0054
λ_i^β	—	0.0028	—	0.0057
Spin orbital populations	—	0.0004	—	0.0003
Total orbital populations	—	0.0021	—	0.0033

such experimental results. Rather, we have simply shown that if *ab initio* results are of value for large systems then they may be simulated with reasonable accuracy and at less expense.

A program, SAMOU, to implement the DODS/SAMO method has been developed (O'Leary *et al.*, 1974c) and is available from the Quantum Chemistry Program Exchange.

4. Polymers

Owing to the very considerable cost of full *ab initio* polymer calculations, in recent years there has been a growing interest in the development of some cheaper method of comparable accuracy. Unfortunately, such methods, based as they have been on semiempirical techniques, have usually produced the cheapness but not the accuracy. Since by definition polymers are made up of repeating units of identically arranged atoms (the so-called unit cell), the problem of evaluating molecular orbitals for such infinite polymer systems from smaller pattern units would seem to provide the SAMO technique with a natural area of application and the polymer chemist with a cheap and accurate method of calculation.

The method (Duke and O'Leary, 1973) applies the SAMO technique to lattices periodic in one dimension. The standard approach of incorporating translational symmetry by forming Bloch orbitals is used. This leads to the complex Hermitian eigenvalue problem

$$\mathbf{F}(k)\mathbf{C}(k) = \mathbf{S}(k)\mathbf{C}(k)\lambda(k) \qquad (24)$$

where

$$F_{pq}(k) = \sum_{s=-m}^{+m} e^{iks} F_{pq}^s; \qquad S_{pq}(k) = \sum_{s=-m}^{+m} e^{iks} S_{pq}^s. \qquad (25)$$

Hence, F_{pq}^s and S_{pq}^s are Fock and overlap matrix elements, respectively, between basis function χ_p in a typical cell, labeled zero, and basis function χ_q in cell s. The index s runs from $-m$ to m, where interactions of the zero cell with m cells are included. By following the usual practice of truncating the series given in Eq. (25) we achieve a "nearest" or "single cell" approximation in which the summation is taken from $m = -1$ to $m = 1$ and a "second nearest" or "two-cell" approximation where we sum from $m = -2$ to $m = 2$. The matrix elements F_{pq}^s are taken from *ab initio* calculations on pattern molecules or set to zero. Matrix elements S_{pq}^s are evaluated exactly. Equation (24) is solved by standard methods for a range of points $k(-\pi < k \leq \pi)$ in the reciprocal lattice space. The derivatives with respect to k, $d\lambda/dk$, of the orbital energies are also evaluated

TABLE XII

COMPARISON OF BAND STRUCTURES OF POLYETHYLENE AND POLYENE OBTAINED FROM *Ab Initio*, SAMO, CNDO, AND EXTENDED HÜCKEL METHODS

Properties	*Ab initio*	SAMO one-cell	SAMO two-cell	CNDO	Extended Hückel
			Polyethylene		
Ionization potential	0.489	0.439	0.469	0.430	0.443
Electron affinity	0.210	0.258	0.398	0.261	0.011
Energy gap	0.699	0.697	0.867	0.691	0.454
1s Bandwidth	0.001	0.0001	0.0001	—	—
σ Valency bandwidth	0.741	0.782	0.754	1.359	0.618
σ^* Conduction bandwidth	0.554	0.651	0.464	0.175	1.828
			Polyene		
Ionization potential	0.308	0.271		0.275	0.405
Electron affinity	−0.083	−0.024		−0.021	−0.385
Energy gap	0.225	0.247		0.253	0.019
1s Bandwidth	0.002	0.001		—	—
σ Valency bandwidth	0.639	0.707		1.268	0.636
π Valency bandwidth	0.247	0.275		0.570	0.119
π^* Conduction bandwidth	0.348	0.304		0.352	0.199
σ^* Conduction bandwidth	0.614	0.788		0.268	2.061

(André *et al.*, 1972). This is of considerable help in determining band crossing points.

In a study of polyethylene and polyene (Duke and O'Leary, 1973) results obtained from the SAMO approach were compared with those obtained by André *et al.* (1971) using *ab initio*, CNDO, and extended Hückel methods. Although the results are not directly comparable with the *ab initio* results they do display, as shown in Table XII, a much broader agreement with the *ab initio* values than do the results of semiempirical methods. Further, the SAMO approach is many times faster and consequently very much cheaper than the *ab initio* method. It may also be faster than iterative semiempirical methods.

The role played by polymers in systems of biochemical interest is well known. We are currently engaged in a study of polyglycine (Duke *et al.*, 1975b) and related polymers of biochemical interest.

A program, SAMOP, to implement the SAMO method, as applied to polymers, has been developed (O'Leary *et al.*, 1974d) and is available from the Quantum Chemistry Program Exchange.

III. Localized Orbitals

A. Introduction

A second major area of transference exploitation is the localized orbital approach. The essential idea, first used by Coulson (1937) and now well known, is to replace the fully delocalized canonical molecular orbitals ϕ by a set of orbitals θ localized in core, lone pair, and bond regions. Since the two sets θ and ϕ are related by a unitary transformation A,

$$\theta = \phi A, \tag{26}$$

a single determinant wavefunction built from the set θ is identical to that built from set ϕ. Further, while the set θ satisfy the Hartree–Fock equations

$$\hat{F}\phi_i = \lambda_i \phi_i \tag{27}$$

where the Lagrange multiples λ_i are in diagonal form, the set θ satisfy the equations

$$\hat{F}\theta_i = \sum_j \lambda_{ij} \theta_j \tag{28}$$

with the Lagrange multiples in nondiagonal form. If the canonical orbitals are known, the transformation matrix A can be chosen in a variety of

ways. Alternatively, several authors have suggested methods for obtaining the localized orbitals θ directly. For further details of these matters the reviews of Weinstein *et al.* (1971) and England *et al.* (1971) should be consulted.

Almost every worker using localized orbitals lists their possible transferability as one of the objectives of his study. In practice, however, there is surprisingly little direct and useful evidence for such transferability, and few useful methods have developed using localized orbitals to cheaply build up the wavefunction for a large molecule. This is partly due to the fact that until recently most localized orbitals have been obtained for diatomic molecules where transferability can be seen only in a qualitative fashion. Both experience with transferring matrix elements and direct evidence indicates that useful transferability will occur if and only if "similar" environments are carefully defined. Only two important methods have been developed which utilize transferability of localized orbitals to construct wavefunctions for larger molecules in an economic fashion. The most recent of these moves toward the matrix element approach is that both localized orbitals and Fock matrix elements over localized orbitals are transferred. This is the method of Leroy and co-workers. The other method, von Niessen's "molecules in molecules" approach, uses a wavefunction built from transferred localized orbitals and new molecular orbitals which are to be optimized. In addition to these "constructing wavefunctions by transferring localized orbitals" techniques there are several methods which construct localized orbitals directly in an economic fashion. In a few cases some transferability is used. Although beyond the scope of this review, it is worth noting that localized orbitals have important uses in providing a convenient basis for introducing correlation effects and thus going beyond the Hartree–Fock limit. Levy *et al.* (1970), for example, show that strongly orthogonal geminals localized in core, lone pair, or bond regions are transferable between H_2O and transplanar H_2O_2.

B. Evidence for Transferability of Localized Orbitals

Although localized orbitals are strongly localized, they still contain small contributions from basis functions not centered in a region of maximum density, i.e. core, lone pair, or bond region. Localized orbitals thus have delocalized "tails." Transferability between molecules cannot thus be exact unless the tails are absent. At best we can hope they will be negligible. We are not restricted to having localized orbitals which are mutually orthogonal. Indeed there is some evidence that nonorthogonal

orbitals are more strongly localized and that such nonorthogonal orbitals result from a neglecting of the delocalized tails.

In a classic paper of nearly ten years ago, Adams (1965) set forward a number of suggested criteria for transferability. He was concerned with what he calls molecular invariant orbitals for various subgroups of molecules. There has been surprisingly little exact work to confirm these suggestions. His three main criteria are particularly important:

(a) The subgroup orbitals in general should not be orthogonal to the orbitals of any other subgroup in a molecule.

(b) The subgroup orbitals should be well localized in the sense that they are small in the neighborhood of the nuclei of the other subsystems.

(c) The nuclear separation in the molecule from which the localized orbitals are taken and the nuclear separation in the molecule to which the orbitals are transferred should be identical.

Criteria (a) and (b) are related. If localized orbitals are orthogonalized, this introduces components from basis functions centered on distant nuclei. The choice of nonorthogonal orbitals is however surprising since their use is closely related to additive bond properties and particularly to those depending on a one-electron operator $\hat{\Omega}$. If

$$\Psi = A\{\theta_1 \alpha \theta_1 \beta \theta_2 \alpha \cdots \theta_n \alpha \theta_n \beta\} \tag{29}$$

and

$$\langle \theta_i \mid \theta_j \rangle = \delta_{ij} \tag{30}$$

then

$$\Omega = 2 \sum_{i=1}^{n} \langle \theta_i \mid \hat{\Omega} \mid \theta_i \rangle. \tag{31}$$

The use of orthogonal localized orbitals thus justifies the use of, for example, additive bond moments where the bond moment μ_i for a bond described by a localized orbital θ_i is given by

$$\mu_i = \langle \theta_i \mid \mathbf{r} \mid \theta_i \rangle. \tag{32}$$

It is this property that has encouraged research on the relationship between localized molecular orbitals and the chemical ideas of additive bond properties. However, orthogonal localized orbitals are not as well localized in the sense of Adams' criterion (b) as nonorthogonal ones. The avoidance of artificial orthogonalization of bond orbitals is stressed by Magnasco and Musso (1971a,b).

Several criteria for transferability can be used. The most direct is that used by Rothenburg (1969, 1971) for C—H bonds. The localized orbitals are superimposed with the C atoms and C—H bond axis coincident. The overlap between the localized orbitals for different C—H bonds is then evaluated. The overlap for C—H bonds in methane, ethane, and methanol is always greater than 0.996 (Rothenburg, 1969). In a later paper, Rothenburg (1971) extends his results to include ethylene and acetylene and reaches the conclusion that C—H bonds in these systems are still surprisingly similar to C—H bonds in saturated systems. Semi-empirical molecular orbital methods have been used by many authors to study transferability of localized orbitals. Trindle and Sinanõglu (1968) show transferability of C—C and C—H bonds in hydrocarbons, but not in CH_3F and CF_3H. They conclude that "it seems clear that successful transfer of bond moments and thus bond orbitals will occur only if the transfer is between similar environments." The $—CHF_2$ environment is clearly different from the $—CH_3$ environment. Caution must be used if transfer is between widely different environments. The question of transferability of semiempirical localized orbitals is also discussed by Gordon and England (1972). Their concern is again with C—H bonds, their bond moments, bond energies, and certain components of the localized charge distribution energies.

For useful transferability, localized orbitals have to be truncated by removal of the small components from the "delocalization tails." It is customary to remove all basis functions not centered on the two atoms of the bond. Several authors have studied the effect of this removal. Newton et al. (1970) propose a quantitative measure of the extent to which localized orbitals θ_i deviate from pure one-center or n-center orbitals θ_i^T, obtained by truncation and renormalization

$$d_i = \left(\int (\theta_i - \theta_i^T)^2 \, dr/2 \right)^{1/2} \times 100\%. \tag{33}$$

Inner shell orbitals deviate by less than 5% while valence orbitals can deviate by as much as 15%. The truncated orbitals, however, can give a total energy which is only slightly above the SCF energy. A few of the results quoted by Newton et al. are shown in Table XIII.

This criterion is also used by Leroy and Peeters (1974a). As shown in Tables XIV and XV, they find transferability of localized orbitals for a wide range of hydrocarbons. The mean square deviation of the *strictly* localized orbitals from the localized orbitals shows that the localized orbitals are very much better localized than those discussed by Newton et

TABLE XIII

MOLECULAR ENERGIES USING TRUNCATED LMO's[a]

	SCF MO	Truncated LMO's
CH_4	−40.1281	−40.0976
C_2H_6 st	−79.0999	−79.0292
C_2H_6 ec	−79.0946	−79.0258
C_2H_4	−77.8558	−77.8097
C_2H_2	−76.6416	−76.6167
H_2CO	−113.5228	−113.4296
HCN	−92.6095	−92.5684
$CH_3-C≡CH$	−115.6235	−115.5528

[a] From Newton *et al.* (1970).

al. The transferability of these orbitals can also be seen by inspection of the coefficients in the atomic orbitals; they are very similar. Leroy and Peeters (1974b) find similar results for unsaturated hydrocarbons.

Recently Fink (1973) has suggested a projection technique giving a new localized orbital restricted to a particular subset of the original basis set, which is superior to direct truncation followed by orthonormalization. The new orbital has a greater overlap with the original orbital.

The evidence is thus fairly strong that localized orbitals for C—C and

TABLE XIV

CHARACTERISTICS OF C—H LOCALIZED ORBITALS[a]

Orbital[b]	System	d_i	% s	LCAO-LO coefficients
CH(4)	CH_4	1.2	28.6	−0.0651(1s) + 0.3413(2s) + 0.5388(p) + 0.4809(H) −0.0656(H)(3x)
CH(3)	C_2H_6	1.5	28.0	−0.0647(1s) + 0.3388(2s) + 0.5439(p) + 0.4870(H) −0.0677(H)(2x) + 0.0616(H)
CH(3)	C_3H_8	1.5	27.3	−0.0641(1s) + 0.3358(2s) + 0.5479(p) + 0.4857(H) −0.0690(H)(2x) + 0.0607(H)
CH(2)	C_3H_8	1.8	26.2	−0.0635(1s) + 0.3316(2s) + 0.5567(p) + 0.4888(H) −0.0741(H) + 0.0636(H)(2x)
CH(1)	C_4H_{10}	2.0	26.3	−0.0640(1s) + 0.3337(2s) + 0.5582(p) + 0.4908(H) +0.0608(H)(3x)

[a] From Degand *et al.* (1973). Reprinted with permission from *Theor. Chim. Acta*, **30**, 243 (1973). Copyright by Springer-Verlag, Heidelberg.

[b] The number between brackets gives the number of hydrogen atoms bound to the carbon.

TABLE XV

CHARACTERISTICS OF C—C LOCALIZED ORBITALS[a]

Orbital[b]	System	d_i	% s	LCAO-LO coefficients
C(3)—C′(3)	C_2H_6	2.0	27.8	$-0.0651(1s) + 0.3081(2s) - 0.4967(2p) - 0.0651(1s')$ $+0.3081(2s') + 0.4967(2p') - 0.0575(H)(6x)$
C(3)—C′(2)	C_3H_8	2.3	28.1	$-0.0676(1s) + 0.3147(2s) - 0.4941(2p) - 0.0653(1s')$ $+0.3077(2s') + 0.5010(2p') - 0.0558(H)(3x)$ $-0.0591(H)(2x) + 0.0544(H)(1x)$
C(2)—C′(2)	C_4H_{10} n	2.5	28.2	$-0.0667(1s) + 0.3135(2s) - 0.5006(2p) - 0.0667(1s')$ $+0.3135(2s') + 0.5006(2p') - 0.0585(H)(4x)$ $+0.0529(H)(2x)$
C(3)—C′(1)	C_4H_{10} i	2.6	27.4	$-0.0643(1s) + 0.3046(2s) - 0.5110(2p) - 0.0679(1s')$ $+0.3150(2s') + 0.4981(2p') - 0.0578(H)(3x)$ $-0.0633(H)(1x) + 0.0539(H)(2x)$

[a] From Degand et al. (1973). Reprinted with permission from Theor. Chim. Acta, 30, 243 (1973). Copyright by Springer-Verlag, Heidelberg.

[b] The number between brackets gives the number of hydrogen atoms bound to the carbon.

C—H bonds are transferable but only suggestive that transferability is a useful concept elsewhere.

C. Approximate Localized Orbitals

To evaluate approximate localized orbitals economically a method must be found which does not use the total electronic energy, and hence all the electron repulsion integrals. Once one undertakes the evaluation and use of such integrals it is as economic to carry out an exact SCF-MO calculation and, if necessary, transform this wavefunction to localized orbitals. Nevertheless, some insight into localized orbitals has been obtained by methods which do use the total energy. Hoyland (1968, 1969b) has evaluated a number of bond orbital wavefunctions for small hydrocarbons; a bond orbital being a localized orbital consisting of basis functions centered only on two atoms. They are not mutually orthogonal. The bond orbital wavefunction for large molecules can be formed by transferring bond orbitals from small molecules. The energy calculation serves only to test the validity of such a wavefunction. Related calculations have been carried out by Petke and Whitten (1969) and Sovers et al. (1968). They are reviewed by Whitten (1973). Sovers et al. introduces a new feature by an optimization of the wavefunction using Hellmann–Feynman forces for ethane and its barrier to rotation. Fink (1974) has used his projection technique to construct ethane from methane in a most successful manner.

The use of maximum overlap concepts and related ideas to prescribe optimum hybrids provides another path to approximate localized orbitals (McWeeny and Del Re, 1968; Randić and Măksic, 1972). An ingenious method by Weinstein and Pauncz (1968) uses ideas closely related to the method of Magnasco and Perico (1967) for forming localized orbitals from canonical orbitals, to form approximate localized orbitals directly. This method has recently been reviewed by its originators (Weinstein *et al.*, 1971).

If localized orbitals θ_i could be obtained for a large molecule by transference from small molecules, an approximate wavefunction Ψ is available at once as in Eq. (29). The energy could not be evaluated unless all the electron repulsion integrals are known. This is precisely the problem that is tackled in a systematic way by von Niessen in the "molecules in molecules" method. He asks the question—"Can some orbitals θ_k be formed directly in an optimum way from a basis set for a dimer molecule AB where they cannot be obtained from separate calculations on A or B?" The optimization of these orbitals θ_k is in the fixed field of other orbitals which can be obtained by transference. The whole exercise is only worthwhile if this process can be carried out without the use of all the electron repulsion integrals and hence more economically than a full SCF calculation using the same basis set; this approach is considered in more detail in the next section. Trindle and Sinanŏglu (1970) have used transferred localized orbitals entirely in a semiempirical framework. Their results give more evidence for transferability of localized orbitals.

However, if the energy is not required the wavefunction Ψ, where all θ's are obtained by transference, can still be useful. Expectation values of a one-electron operator, such as the dipole moment, can be evaluated relatively easily. This procedure has been used in an inverse way by forming the θ_i directly in such a way that Ψ fits the experimental values of one-electron properties. Electronegativity considerations are also used to fix the localized orbitals (Letcher and Dunning, 1968; Winter *et al.*, 1968; Letcher *et al.*, 1969; Letcher and van der Wazer, 1966, 1967; Unland and Letcher, 1968; Unland, 1968; Unland *et al.*, 1969; Letcher, 1971). The direct use of transference to give one-electron properties for large molecules appears to still await a thorough test.

The problems of evaluating the total energy from localized orbitals has lead Leroy *et al.* to develop canonical orbitals as a linear combination of localized orbitals transferred from smaller molecules and investigate whether the Fock matrix elements in such a basis are transferable. We review this approach in detail in a later section.

D. The Method of "Molecules in Molecules"

Several techniques in π-electron theory aim at constructing a wavefunction for a large molecule by utilizing wavefunctions from small molecules. These have been used in particular to discuss excited states of composite molecules in relation to excited states of separate fragments (Longuet-Higgins and Murrell, 1955). The work of Dewar (1949, 1950, 1952), Dewar and Longuet-Higgins (1952), and Simpson (1962) is relevant and there have been several applications (see, e.g., Heilbronner *et al.*, 1966; Mori, 1961; Favini *et al.*, 1969; Favini and Gamba, 1968; Germer and Becker, 1972).

Extensions to *ab initio* all electron wavefunctions, made by von Niessen (1971, 1973a,c, 1974a), are concerned only with the ground state of closed shell molecules. This "molecules in molecules" (MIM) method appears to be particularly useful for loosely bound dimers A—B such as F—H $\cdots$ H—F (von Niessen, 1971), F—H $\cdots$ F—H (von Niessen, 1973b), NH_3H_2O (von Niessen, 1973c), and NeH_2O (von Niessen, 1974b), although there have been a few other applications by the same author (von Niessen, 1973a, 1974a).

The wavefunction employed is an antisymmetrized product of doubly occupied localized orbitals, the majority of which are transferred directly from wavefunctions for the components A and B,

$$\Psi = A\{\theta_1^A \cdots \theta_i^A \cdots \theta_{NA}^A \theta_1^B \cdots \theta_j^B \cdots \theta_{NB}^B \phi_1 \cdots \phi_K \cdots \phi_{NK}\}. \quad (34)$$

θ_i^A and θ_j^B are localized orbitals transferred without change from wavefunctions of A and B. ϕ_K are new molecular orbitals partially formed from orbitals on A or B, and describe the new bonds and modified old bonds in the dimer A—B. For example, NH_4Cl would be split such that A and B are the two closed-shell molecules NH_3 and HCl. The orbitals ϕ_K would describe the N lone pair and the H—Cl bond, since these parts of A and B would be most affected by dimer formation.

A division of A—B into ionic components is not the most appropriate choice, except for molecules with ionic bonds, because of the long-range character of the Coulomb interaction. A division into radical components A and B is also inappropriate due to the difficulties of open shell calculations.

The localized orbitals are not all mutually orthogonal, but the separate sets θ_i^A, θ_j^B, and ϕ_K are

$$\langle \theta_i^A | \theta_{i'}^A \rangle = \delta_{ii'} \qquad \langle \theta_j^B | \theta_{j'}^B \rangle = \delta_{jj'} \qquad \langle \phi_K | \phi_{K'} \rangle = \delta_{KK'} \quad (35)$$

$$\langle \theta_i^A | \theta_j^B \rangle \neq 0 \qquad \langle \theta_i^A | \phi_K \rangle \neq 0 \qquad \langle \theta_j^B | \phi_K \rangle \neq 0. \quad (36)$$

This nonorthogonality problem is one of the major problems in using the "molecules in molecules" method.

The wavefunction Ψ gives an energy E which, if properly evaluated, lies above the SCF energy (E_{SCF}) for A—B. If E is close to E_{SCF} the transferability of localized orbitals θ_i^A and θ_j^B from A and B is a good approximation. E can be improved by optimizing the orbitals ϕ_K in the fixed field of the orbitals θ_i^A and θ_j^B. ϕ_K need not be localized although their main components will arise from what von Niessen calls the interaction region—the region most modified by dimer formation. Because of the nonorthogonality relations [Eq. (36)], the evaluation of the total energy involves the use of all the electron repulsion integrals for A—B. This is unfortunate since the objective of any such approach is to evaluate the wavefunctions for A—B economically by utilizing information from A and B separately. Several approximations are therefore introduced:

(i) The first nonorthogonality relation [Eq. (36)] can be neglected since the orbitals θ_i^A and θ_j^B are spatially separate and hence have a small overlap.

(ii) The orbitals ϕ_K can be made orthogonal to the localized orbitals θ_i^A and θ_j^B by the use of a projection operator. Denoting a general member of the combined set $\{\theta_i^A, \theta_j^B\}$ by $|k\rangle$ or $|l\rangle$ and a member of the set ϕ_K by $|m\rangle$, we use the projection P given by

$$P = 1 - \sum_{k,l} |k\rangle S_{kl}^{-1}\langle l|. \tag{37}$$

S_{kl}^{-1} is the k, l element of $\mathbf{S}^{-1}$ where $\mathbf{S} = \langle k|l\rangle$. Variation of $|m\rangle$ in the restricted subspace created by P gives:

$$PFP|m\rangle = \varepsilon_m |m\rangle, \tag{38}$$

$$F = F_{core} + \sum_m (2J_m - K_m), \tag{39}$$

$$F_{core} = h + \sum_k (2J_k - K_k). \tag{40}$$

Equation (45) holds only if the orbitals $|k\rangle$ and $|l\rangle$ are orthogonal, as assumed in (i) above. In this case Eq. (37) gives

$$P = 1 - \sum_k |k\rangle\langle l|. \tag{41}$$

J_i and K_i are Coulomb and exchange operators

$$J_i = \langle i|r_{12}^{-1}|i\rangle j K_i = \langle i|r_{12}^{-1}|\rangle|i\rangle. \tag{42}$$

h is the one-electron part of the Hamiltonian operator. The Lagrangian matrix in Eq. (38) is diagonal because the MO's $|m\rangle$ are not required to be localized. This approach is computationally convenient, but does not solve the problem of handling all the electron repulsion integrals. Further restrictions must be imposed. The orbitals $|m\rangle$ are expanded in a LCAO form which is restricted to a subset Γ of the orbitals $|p\rangle$, including only those orbitals close to the interaction region. This gives

$$|m\rangle = \sum_{p \in \Gamma} |p\rangle C_{pm}. \tag{43}$$

Equation (43) decreases the size of matrix eigenvalue problems arising in (38) but the use of P retains all the electron repulsion integrals.

(iii) Basis functions distant from the interaction region will play a small part in P. The localized MO's $|k\rangle$ in P can be restricted to a subset Δ of all $|k\rangle$ and certain basis functions do not therefore appear in the expansions due to P. It is clear that Γ must be a subset of Δ. This approximation reduces the number of integrals arising in (38) but complete orthogonality between $|m\rangle$ and $|k\rangle$ is lost.

(iv) Denoting the set of basis functions used in $|m\rangle$ as Δ [(iii) above] and the sets arising in θ_i^A and θ_j^B as A and B, leaves Coulomb and exchange integrals

$$\langle \Delta | A \rangle \qquad \langle \Delta | B \rangle$$

where this nomenclature implies, in the Coulomb case, integrals of form

$$\langle pq | rs \rangle, \qquad p, q \in \Delta, \qquad r, s \in A \text{ or } B$$

and similarly for the exchange case. Integrals of form $\langle A | B \rangle$ do not arise in Eq. (38) but do arise in the evaluation of the total energy, which, neglecting nonorthogonality terms, is

$$E = 2 \sum_n \langle n | h | n \rangle + \sum_{n_1, n_2} \{2K_{n_1 n_2} - K_{n_1 n_2}\} \tag{44}$$

where $J_{n_1 n_2}$ and $K_{n_1 n_2}$ are Coulomb and exchange integrals between any orbitals $|n_1\rangle$ and $|n_2\rangle$. Use of these equations implies a neglect of nonorthogonality between the MO's, otherwise all integrals reenter the problem.

For these integrals of form $\langle A | B \rangle$, n_1 and n_2 are spatially separate and might be approximated by the point charge approximation

$$K_{ij} = 0, \qquad J_{ij} = |r_i - r_j|^{-1}, \qquad r_i = \langle i | R | i \rangle \tag{45}$$

where r_i is the charge centroid of $|i\rangle$.

To summarize, von Niessen introduces four major approximations:

1. A restricted expansion of the MO's in the interaction region to a subset Γ.

2. A restriction of the projection operator used to ensure orthogonality of these MO's to the localized "core" orbitals to the subset Δ.

3. Neglect of nonorthogonality between the MO's in evaluating the total energy.

4. Use of the point charge approximation in evaluating the total energy. The justification for each of these approximations has been examined.

In paper II (von Niessen, 1973a) a full examination of these approximations for the repulsive curve of Be_2 is reported. Inner shell LMO's are transferred and outer shell orbitals recalculated. A basis set of 9 s-type Gaussian functions is used in each atom. The subsets Γ and Δ are progressively reduced from 18 down to 12. The energy has been evaluated both with nonorthogonality of the MO's retained (case b) and by removing nonorthogonality using the Löwdin orthogonalization method (case a). The curves a and b for the energy difference between the "molecules in molecules" energy and the Be atom SCF energy do not meet in general for $R \to \infty$ and do not approach the limiting value of zero. They do, however, run parallel to the abscissa for large distances. If the set Γ is less than the full set of 18 functions the limiting value zero cannot be reached.

The major conclusion is that it is advisable to keep the sets Γ and Δ identical, since the difference between curves a and b, which determines the reliability of the calculations where nonorthogonality is neglected, is then minimal. There is, in fact, little computational advantage in allowing Γ and Δ to differ. The point charge approximation is only valid for distances greater than 6 a.u.

$Li_2 - Li_2$ in a linear form has been studied and gives an energy minimum (0.54 kcal/mole binding energy) at a distance of 7.5 a.u. Transferring all LMO's from Li_2 and thus calculating no interaction orbitals gives no binding. It is concluded that modification of the Li_2 bonding orbitals leads to the binding energy of two Li_2 molecules. The sets Γ and Δ are kept identical. Neglect of nonorthogonality and the use of the point charge approximation results in no serious error.

Paper II (von Niessen, 1973a) gives a large number of detailed figures and tables for the energies of both Be_2 and $Li_2 - Li_2$ at various levels of approximation. The first application to a system which is not a loosely bonded dimer is to C_2H_6. Here localized orbitals for the C core and the six C—H bonds are transferred from calculations on CH_4. A total of 34

basis functions is used and the subset Γ is varied from the full set of 34 down to 20. Several different schemes for producing localized orbitals are used and the results shown to not differ significantly. The main point of interest is the evaluation of the rotational barrier. This turns out to be almost independent of the size of the subset Γ but does depend on the use of the point charge approximation and on whether nonorthogonality is properly taken into account. These results for $\Gamma = 34$ basis functions are given in Table XVI. Neglect of nonorthogonality gives results which are seriously in error, but the point charge approximation is surprisingly good considering the closeness of the two CH_3 groups.

TABLE XVI

Rotational Barrier for Ethane by the "Molecules in Molecules" Method

	Rotational barrier (kcal/mole)
Exact energy— nonorthogonality taken into account	2.38
Exact energy— neglect of nonorthogonality	−2.06
Point charge approximation— nonorthogonality taken into account	3.34
Point charge approximation— neglect of nonorthogonality	1.52
Exact SCF—same basis set	3.01

In paper I, von Niessen (1971) develops this approach and in particular shows the necessity to force near orthogonality of the interaction region MO's to the fixed "core" LMO's. The numerical justification is shown by a calculation on $F-H \cdots H-F$.

In paper III (von Niessen, 1973b) the hydrogen bonded dimer $F-H \cdots F-H$ in a linear form is studied. For the proton donor molecule $-F_1-H_1$, all LMO's are transferred except the $F-H$ bond orbital. For the proton accepter molecule $-F_2-H_2$, the three lone pair orbitals are recalculated and the others transferred. The subset Γ is varied from the full basis of 34 orbitals down to a basis set of 24. The energy E does not approach the value $-E_{SCF}$ for $R \to \infty$ if nonorthogonality is neglected in evaluating the energy, but the energy curves are parallel for large R. Use of the point charge approximation reproduces the SCF value

for the bond length, but the binding energy is too large by a factor of 3. Decreasing the size of the subset Γ to 28 by removing the π-type basis functions on F_1 leads to little change in the results, but a further decrease to 26 by removing the s-type basis functions on F_1 and H_2 shows a wider deviation particularly at large R. The binding energy and bond lengths are still given remarkably well. A calculation with all LMO's transferred using the exact energy expression gives very good results, indicating that in this case, unlike $Li_2 - Li_2$, most of the bonding is due to the unperturbed fragments and not due to readjustment of the F—H orbitals.

Although when judged from an economic standpoint the method of "molecules in molecules" is rather poor, von Niessen has taken one important step. As shown in Table XVII he has attempted to answer the question "which LMO's contribute most to the energy?"

The energy with no LMO's adjusted is already giving 77% of the SCF binding energy (4.6 kcal/mole as compared with 6.4 kcal/mole). The terms arising from independently modifying the LMO's are essentially additive. Modification of the F—H bond orbital in the proton acceptor

TABLE XVII

CONTRIBUTIONS TO THE TOTAL HYDROGEN BONDING ENERGY OF TWO FH MOLECULES (AT THE DISTANCE $R_{FF} = 5.25$ a.u.) OBTAINED BY MODIFYING THE LMO's IN THE PROTON DONOR MOLECULE F_1H_1 AND IN THE PROTON ACCEPTOR MOLECULE F_2H_2[a,b]

Modified LMO	ΔE
None	4.6
Lone pair LMO's in F_1H_1	0.24
Bond LMO in F_1H_1	0.19
Lone pair LMO's in F_2H_2	0.5
Bond LMO in F_2H_2	0.78
Inner shell LMO in F_1H_1	0.014
Inner shell LMO in F_2H_2	0.056
	6.38

[a] All values in kcal/mole.
[b] Reprinted with permission from *Theor. Chim. Acta*, **31**, 297 (1973). Copyright by Springer-Verlag, Heidelberg.

molecule is surprisingly more important than modification of the donor
F—H bond, leading to an energy lowering of 0.78 kcal/mole. The lone
pair orbitals of the donor molecules on modification lead to an energy
lowering of 0.24 kcal/mole.

In paper IV (von Niessen, 1973c) the H_3N—HOH dimer is con-
sidered. For NH_3 all LMO's are transferred except for the lone pair. For
H_2O only the inner shell LMO and the OH bond orbital not involved in
the hydrogen bond are transferred. At a lower level of approximation
only the OH bond is reevaluated. The important feature of these calcula-
tions is that, unlike F_2H_2, the point charge approximation is totally
invalid leading to a repulsive energy curve. The other approximations
hold up very well, even when only the lone pair and the OH bond is
reevaluated.

Again, as shown in Table XVIII, von Niessen considers the question
"which LMO's contribute most to the energy?." With no orbitals
modified 52% of the binding energy (4.13 kcal/mole compared with
7.97 kcal/mole for the SCF energy) is obtained if the energy is evaluated
exactly. The energy analysis gives different conclusions from the F_2H_2
system. Modification of the lone pair and the OH bond yields
2.51 kcal/mole lowering of the binding energy. Modification of the N lone
pair is the most important factor.

TABLE XVIII

CONTRIBUTIONS TO THE TOTAL HYDROGEN BONDING ENERGY OF
$H_3N\cdot HOH$ (AT THE DISTANCE R_{NO} = 5.5 a.u. OBTAINED BY
MODIFYING THE LMO's IN THE PROTON ACCEPTOR MOLECULE
NH_3 AND IN THE PROTON DONOR MOLECULE $H_2O^{a,b}$

Modified LMO	ΔE
None	4.13
OH bond orbital involved in hydrogen bond	0.87
O lone pair LMO's	0.62
OH bond orbital not involved in hydrogen bond	0.25
N lone pair LMO	1.64
NH bond orbitals	0.40
O inner shell LMO	0.048
N inner shell LMO	0.016
	7.97

[a] All values in kcal/mole.
[b] Reprinted with permission from *Theor. Chim. Acta*, **32**, 13
(1973). Copyright by Springer-Verlag, Heidelberg.

Paper V (von Niessen, 1974a), the last paper in the present series, represents von Niessen's only attempt, so far, to apply his method to large molecules. The method is applied to covalent compounds following the same scheme as for ethane. The molecules considered are the disubstituted benzenes C_6H_4XY where X, Y = CH, OH, or F. Transfer of localized orbitals from C_6H_5X and HY is found to be good, but the "molecule in method" works well for the energy difference between ortho-, meta-, and para- compounds only if this energy difference is large. Von Niessen concludes that the treatment of nonorthogonality may need some improvement and the point charge approximation gives rise to the largest uncertainty in the results.

In conclusion, the "molecules in molecules" method is important in that it provides a further demonstration of the transferability of localized orbitals. It is difficult, however, to produce any great saving in computer time as it remains necessary to still evaluate a large number of molecular integrals. The use of approximate methods to decrease the number of electron repulsion integrals is not, in general, useful, but can be valuable in specific cases.

E. Fock Matrix Elements over Localized Orbitals

The transferability of localized orbitals discussed in Section III,B and the ideas of transferring Fock matrix elements have been combined in an interesting study by Degand *et al.* (1973). Using the localization method of Magnasco and Perico (1967) they form localized orbitals for the hydrocarbons methane, ethane, propane, *n*-butane, and iso-butane and show that these localized orbitals are transferable. The importance of this study, however, lies in the fact that a simple method is developed which utilizes this transferability to construct wavefunctions for larger molecules. The method has been extended to unsaturated hydrocarbons by Leroy and Peeters (1974, 1975) and to aliphatic compounds containing oxygen and fluorine by Clarisse (1974).

The approach used by all these authors relies on transferability of the elements, over localized orbitals, of the Fock matrix F^L defined by

$$F^L = T^T \lambda T \tag{46}$$

where T is the transformation matrix from molecular orbitals to localized orbitals and λ is the diagonal matrix of orbital energies. In Table XIX, taken from Leroy and Peeters (1975), the transferability of matrix elements is illustrated by giving their maximum, minimum, and mean values. The authors report localized orbitals obtained by the method of

TABLE XIX

FOCK MATRIX ELEMENTS OVER LOCALIZED ORBITALS[a]

Element	Maximal value	System	Minimal value	System	Mean value
h_{CH}	−0.7415	$i\,C_4H_{10}$	−0.7331	$n\,C_4H_{10}$	−0.735
h_{CC}	−0.8527	C_3H_8	−0.8361	C_2H_6	−0.840
$(h_{CH-CH})_0$	−0.1430	C_4H_{10}	−0.1360	C_2H_6	−0.136
$(h_{CH-CC})_0$	−0.1355	$i\,C_4H_{10}$	−0.1305	$n\,C_4H_{10}$	−0.134
$(h_{CH-1sC})_0$	−0.6447	CH_4	−0.6305	C_3H_8	−0.640
$(h_{CC-1sC})_0$	−0.6237	C_3H_8	−0.6071	$i\,C_4H_{10}$	−0.615
$(h_{CC-CC})_0$	−0.1285	$i\,C_4H_{10}$	−0.1266	$n\,C_4H_{10}$	−0.128
$(h_{CH-CH})_1$	−0.0145	$n\,C_4H_{10}$	−0.0137	$n\,C_4H_{10}$	−0.014
h_{CC_π}	−1.0386	C_2H_4	−1.0286	$i\,C_4H_8$	−1.035
h_{CC_π}	−0.4654	C_3H_6	−0.4629	$1-C_4H_8$	−0.464
$(h_{C_\pi C-CC_\pi})_0$	−0.1516	C_3H_6	−0.1431	$1-C_4H_8$	−0.145
$(h_{CC_\pi-CH})_1$	±0.0406	$1-C_4H_8$	±0.0382	$i\,C_4H_8$	±0.040

[a] From Leroy and Peeters (1975). Reprinted with permission from "Localization and Delocalization in Quantum Chemistry" (R. Daudel, ed.), Vol. 1, in press. Copyright D. Reidel Publ. Co., Dordrecht, The Netherlands.

Boys (1960) to be slightly less transferable than those obtained by the Magnasco and Perico (1967) method.

The transferability of matrix elements allows a simulation of the Fock matrix for a large molecule. The molecular orbitals ϕ_j are defined as a linear combination of localized orbitals θ_p

$$\phi_j = \sum_p A_{pj}\theta_p \qquad (47)$$

giving Roothaan equations in the form

$$F^L A = A\lambda \qquad (48)$$

where $F^L_{pq} = \langle \theta_p \,|\, \hat{F} \,|\, \theta_q \rangle$ and $\langle \theta_p \,|\, \theta_q \rangle = \delta_{pq}$.

The use of a linear combination of localized or equivalent orbitals has frequently been employed in semiempirical theories. These are reviewed in detail by Herndon (1972). Since the localized orbitals θ are defined in terms of atomic orbitals χ

$$\theta = \chi C \qquad (49)$$

the molecular orbitals ϕ can also be defined in terms of atomic orbitals

$$\phi = \theta A = \chi C A, \qquad (50)$$

thus allowing the usual evaluation of population density terms, etc. This of course, introduces a slight ambiguity for, since the localized orbitals are not exactly transferable, it may not be clear which particular localized orbital to choose.

The use of mean values of matrix elements for similar environments leads to the construction of a set of parameters for this simulated method. Tables of such parameters are found in the work of both Degand *et al.* (1973) and Leroy and Peeters (1974, 1975). These parameters can be used in the construction, at various levels of approximation, of the matrix F^L. Thus, to a first level of approximation, only one-center terms are included. To give more accurate results first neighboring terms are included and, finally, a third level of approximation is obtained by the inclusion of second neighbor terms. Degand *et al.* (1973) designate these three levels as stages I, II, and III, respectively, and report results for each of them. Leroy and Peeters (1974, 1975), on the other hand, appear to automatically include terms up to the second neighbor level (stage III).

This "Fock matrix-localized orbital" approach has been restricted to the evaluation of orbital energies. In Table XX, we report the root mean

TABLE XX

RMS DEVIATIONS FOR ORBITAL ENERGIES FOR "FOCK
MATRIX—LOCALIZED ORBITAL" METHOD

Stage Molecule	RMS × 10^3			
	I	II	III	SAMO
CH_4	3.8	—	—	—
C_2H_6	39.8	2.8	—	—
C_3H_6	44.9	8.1	5.6	23.5
n-C_4H_{10}	45.3	7.3	5.2	3.1
n-C_5H_{12}	—	—	5.5	—
Iso-C_5H_{12}	—	—	8.3	—
Neo-C_5H_{12}	—	—	10.7	—
n-C_6H_{14}	—	—	6.2	—
cyclohexane	—	—	9.0	3.4
1-C_5H_{10}	—	—	13.5	—
2-$trans$-C_5H_{10}	—	—	7.5	—
2-cis-C_5H_{10}	—	—	9.4	—
Me-2-butene-1	—	—	9.7	—
Me-2-butene-2	—	—	9.5	—
Cyclohexene	—	—	9.5	—

square deviations evaluated by us between the simulated and *ab initio* orbital energies reported in tabular form by Degand *et al.* (1973) and Leroy and Peeters (1974, 1975). The importance of including at least nearest neighbor matrix elements (stage II) is clear from these results. Where available, we have reported in Table XX analogous root mean square errors arising from the SAMO method. The SAMO propane results use matrix elements obtained from ethane while the butane results use matrix elements obtained from propane. It should be noted that the SAMO method always uses a pattern molecule smaller than the molecule to be studied while the "Fock matrix-localized orbital" approach used matrix elements obtained by averaging over a series of molecules. The SAMO results appear to be more accurate than the "Fock matrix-localized orbital" approach but this latter method is simpler.

In one sense the "Fock matrix-localized orbital" method has brought the localized orbital approach full circle. The method is essentially identical to the SAMO approach and particularly to the SAMO method over an orthogonal basis set, the difference being that now localized orbitals replace the orthogonal hybrids of the SAMO basis set.

IV. Improved SCF Cycling

Thus far we have been concerned with methods which utilize transferability to obtain approximate LCAO-MO wavefunctions for large molecules. Most of these methods, however, have the additional ability of producing wavefunctions which give very good initial estimates of the wavefunction in the SCF cycling procedure. This has two consequences. First, it can ensure convergence in cases where divergence can readily occur. Second, by decreasing the number of cycles required for convergence, the SCF stage of an *ab initio* calculation can be made more economic.

Orloff and Fitts (1963) show that their method of estimating the Fock matrix in π-electron theory leads to final convergence in a few cycles. In *ab initio* work similar ideas have been presented (Petke and Whitten, 1969). Letcher (1971) uses a set of initial eigenvectors obtained from localized orbitals and obtains good convergence. In a later communication Letcher *et al.* (1972) argue strongly for such a procedure in avoiding divergence difficulties. The SAMO method has similar uses (Eilers, 1971; Duke, 1974). In Table XXI the convergence of the total energy for a minimum basis set calculation on butylamine is shown. It can be seen that even one cycle and thus one pass through the integral list gives a good energy and one significantly better than the energy given by the SAMO method itself. The energy is given to four decimal place accuracy

TABLE XXI

CONVERGENCE OF SCF FROM SAMO INITIAL
EIGENVECTORS—BUTYL AMINE [a]

	Energy
SAMO wavefunction	−211.3475
Cycle 1	−211.3353503
2	−211.3358913
3	−211.3359110
4	−211.3359121
5	−211.3359122
Final SCF	−211.3359122

[a] Reprinted with permission from *Chem. Phys. Lett.* **28**, 437 (1974). Copyright by North-Holland Pub. Co., Amsterdam.

after two cycles. Letcher (1971) gives various examples for H_2O using localized orbitals as a starting point; four decimal place accuracy is obtained after three or four cycles. Clementi *et al.* (1973) suggest the use of atomic densities as a good starting point. Convergence by this method for ethane appears to be comparable or slightly better than Letcher's result for H_2O. Degand *et al.* (1973) suggest that their method might have similar uses, but no results are presented. Shipman and Christoffersen (1972) transfer elements of the density matrix from fragment molecules in order to give a reasonable initial estimate. This method appears to be of particular value for their method using floating spherical Gaussian orbitals obtained from fragment calculations.

Recently one of us (Duke, 1974) has suggested that, if good initial eigenvectors can be obtained and thus SCF convergence obtained in a few iterations, it might be more economic to avoid storing the large number of electron repulsion integrals and to reevaluate them at every cycle. This could be reasonable since such a program would require small amounts of core storage and backing store and could run as a background job, time sharing with data processing jobs requiring large amounts of backing store. For very large molecules the amount of backing store required by conventional programs may be the largest bottleneck.

The use of simulated wavefunctions to avoid divergence problems in SCF cycling is not straightforward. In some cases divergence occurs if a poor starting point is used (e.g. setting the initial density matrix to the null matrix or the unit matrix), but convergence is rapid if the starting density matrix is close to the final density matrix. Other cases, however,

are intrinsically divergent and simulated wavefunctions would be of no value in themselves. Such a case is discussed by Saunders and Hillier (1973) and their method of damping and level shifting is a sound theoretical method for ensuring convergence in all cases. Such an approach could be combined with the use of simulated wavefunctions as starting points. In some circumstances, extrapolation techniques as discussed for example by Winter and Dunning (1971) are valuable.

V. General Conclusions

The steady increase in the efficiency of both numerical techniques and computer hardware has resulted in a progressive decrease in the cost of full *ab initio* calculations. To compete with this trend, any method which aims to successfully mimic *ab initio* molecular orbital calculations must satisfy the following three criteria: (1) it must be considerably more economic than the full *ab initio* SCF calculation, (2) it must give accurate results, and (3) it must have wide, if not general applicability.

Criterion 1: Economy. With the exception of "molecules in molecules," the main methods discussed in this review are very fast and use few computer resources. The SAMO method is, however, slightly less economic than the Fock matrix over the localized orbital method or the related method developed by Leroy and co-workers using OAO's. The "molecules in molecules" method comes up against the fundamental problem of *ab initio* work, namely, the evaluation and use of a large number of integrals. As yet it has not been able to overcome this problem.

Criterion 2: Accuracy. When considering the question of accuracy, transference methods must be viewed in the context of other approximate methods. Thus, for example, when the NEMO (transference) method is compared with semiempirical (nontransference) methods such as PRDDO, a method which represents the best semiempirical (nontransference) scheme yet devised to mimic *ab initio* SCF wavefunctions with the same basis set, the NEMO method is seen to be the less accurate. As well as being more accurate than the Fock matrix over the localized orbitals method or the related method developed by Leroy and co-workers using OAO's, the SAMO method appears to be more accurate than the PRDDO method. Thus the PRDDO method mimics the Fock matrix elements to a standard deviation of 0.007 a.u., an error that is approximately five times greater than that obtained using the SAMO technique. A similar situation arises in the PRDDO method in the mimicking of overlap populations and atomic charges; here the error is approximately six times

greater than that obtained using the SAMO technique. Although in terms of accuracy the method of " molecules in molecules " does extremely well (by making it progressively more elaborate the method can gradually approach the true *ab initio* result) its ability to satisfy criterion 2 is somewhat reduced by its lack of economy. When the methods review here are compared with the approximate *ab initio* method of Christoffersen it is seen that while Christoffersen's approach is superior in its ability to calculate energy differences and perform geometry searches, the methods reviewed here do give better results in terms of total energies and Mulliken populations and are, on the whole, cheaper. This serves to illustrate the general principle that methods that are not truly variational cannot be expected to correctly predict energy differences between conformers or molecular geometries.

Criterion 3: General Applicability. All the methods reviewed here have some weaknesses in this area. Indeed, their lack of general applicability is immediately seen by the fact that few calculations on transition metal complexes have been discussed. The prospect for successful transference in this field seems rather poor. A main limitation to general applicability of the methods is the expense of repeating the calculations at a range of different geometries. Thus, for example, SAMO requires *ab initio* calculations on " patterns " at a range of geometries, mimicking the required geometry of the target molecule. Only NEMO can carry out geometry searches cheaply, but, unfortunately, it cannot do so very accurately. The simplified methods of Leroy and co-workers do introduce some dependence of parameters on geometry, but the use of these for geometry searches has not been carried out. However, transference methods, since they are not variational, are unable to correctly predict the difference in total energies at different geometries. Further, since these energies can be of opposite sign, the error encountered in calculating small energy differences between conformers can be substantial. This was found to be the case in the SAMO calculations on chair and boat cyclohexane. The method of " molecules in molecules " does seem particularly suitable for calculations on dimers where one is especially interested in the small charges occuring among the molecules on dimer formation. It may well be that the method will have its greatest application in the dimer field and hence it may be well worth trying to improve its computational features to this end.

Having discussed the criteria of economy, accuracy, and applicability we must now consider the criteria for whether or not one would expect transferability. In this connection we are led to the following two criteria:

Criterion 1: Geometry. Our experience supports Adams' (1965) suggestion that for either Fock matrix elements or localized orbitals to be transferable the geometry of the pattern molecule must be the same as that of the target molecule.

Criterion 2: Environment. (a) Fock matrix elements F_{ij} over the same or neighboring centers i and j are transferable if the environment up to and including one nearest neighbor center on either side of i and j are similar, i.e. for i and j neighboring centers:

$$k \qquad\qquad i \qquad\qquad\qquad j \qquad\qquad\qquad l$$
$$\text{C}————————\text{C}————————\text{C}————————\text{C}$$

k, first nearest neighbor center to i	i, j neighboring centers	l first nearest neighbor center to j
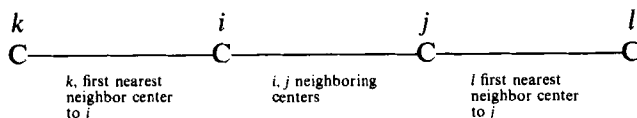
(b) Fock matrix elements F_{kl} where k and l are further apart than first nearest neighbors are transferable if the environment between k and l is similar. It follows from this that it is of no great importance if k and l are terminal centers.

(c) Localized orbitals are transferable if the environment up to and including first nearest neighbors is similar.

In this review we have restricted ourselves to considering transferability within *ab initio* methods up to the limit of Hartree–Fock theory. Clearly, however, some of the ideas we have discussed are capable of being employed beyond the Hartree–Fock level; consequently, there is a need for such extensions. The ideas are, in themselves, not new; a number of the key concepts go back quite a long way to the work of Moffitt (1951, 1953), Moffitt and Scanlan (1953) and Hurley (1955, 1956) (atoms in molecules); that of Arai (1957) and Arai and Sakamoto (1958) (deformed atoms in molecules); that of Ellison (1963) and Ellison *et al.* (1963) (diatomics in molecules); and that of Klessinger and McWeeny (1965), Klessinger (1965, 1967, 1968, 1969, 1970a,b), Franchini and Vergani (1969), Franchini *et al.* (1970), and Franchini and Zandomeneghi (1971) on group functions.

An interesting recent approach is the PCILO method which uses localized bonding and antibonding orbitals as a basis for a perturbative expansion equivalent to a configuration interaction treatment. There are a few *ab initio* applications of this method (Masson *et al.*, 1970; Daudey and Diner, 1972), but the main development has been within the semiempirical framework (Diner *et al.*, 1970). The PCILO method (Diner *et al.*, 1969a,b,c; Jordan *et al.*, 1969; Langlet and Malrieu, 1972; Langlet *et al.*, 1970, 1971; Maigret *et al.*, 1970; Langlet, 1972) has had many applica-

tions, particularly to conformers of biologically interesting compounds. There may be scope for the use of transference within this approach, or other approaches which aim to go beyond the Hartree–Fock limit. The recent work of Daudey and co-workers (Daudey *et al.*, 1974a,b; Daudey, 1974) is of particular interest in this respect.

REFERENCES

Adams, W. H. (1965). *J. Chem. Phys.* **42**, 4030.
Allinger, N. L., Hirsch, J. A., Miller, M. A., Tyminsky, I. J., and Van Catledge, F. A. (1968). *J. Amer. Chem. Soc.* **90**, 1199.
André, J. M., Kapsomenos, G. S., and Leroy, G. (1971). *Chem. Phys. Lett.* **8**, 195.
André, J. M., Delhalle, J., Kapsomenos, G. S., and Leroy, G. (1972). *Chem. Phys. Lett.* **14**, 485.
Arai, T. (1957). *J. Chem. Phys.* **26**, 435, 451.
Arai, T., and Sakamoto, M. (1958). *J. Chem. Phys.* **28**, 32.
Beal, H., and Lipscomb, W. N. (1967). *Inorg. Chem.* **6**, 874.
Birnstock, F. (1973). *Mol. Phys.* **26**, 343.
Boer, F. P., and Lipscomb, W. N. (1969). *J. Chem. Phys.* **50**, 989.
Boer, F. P., and Turley, J. W. (1967). *J. Amer. Chem. Soc.* **89**, 1034.
Boer, F. P., Newton, M. D., and Lipscomb, W. N. (1964). *Proc. Nat. Acad. Sci. U.S.* **52**, 890.
Boer, F. P., Newton, M. D., and Lipscomb, W. N. (1966). *J. Amer. Chem. Soc.* **88**, 2361.
Boer, F. P., Shannon, T. W., and McLafferty, F. W. (1968). *J. Amer. Chem. Soc.* **90**, 7239.
Boyd, D. B. (1971). *Theor. Chim. Acta* **20**, 273.
Boyd, D. B., and Lipscomb, W. N. (1967). *J. Chem. Phys.* **46**, 910.
Boyd, D. B., and Lipscomb, W. N. (1968). *J. Chem. Phys.* **48**, 4955.
Boys, S. F. (1960). *Rev. Mod. Phys.* **32**, 296.
Bushweller, C. H., Stevenson, P. E., Golini, J., and O'Neil, J. W. (1970). *J. Phys. Chem.* **74**, 1155.
Christoffersen, R. E. (1972). *Advan. Quant. Chem.* **6**, 333.
Clarisse, Fr. (1974). Memoire de licence, Univ. Catholique de Louvain, Louvain.
Clementi, E., Kistenmacher, H., and Popkie, H. (1973). *J. Chem. Phys.* **58**, 4699.
Coulson, C. A. (1937). *Trans. Faraday Soc.* **33**, 388.

Daudey, J. P. (1974). *Int. J. Quantum Chem.* **8**, 29.

Daudey, J. P., and Diner, S. (1972). *Int. J. Quantum Chem.* **6**, 575.

Daudey, J. P., Claverie, P., and Malrieu, J. P. (1974a). *Int. J. Quantum Chem.* **8**, 1.

Daudey, J. P., Malrieu, J. P., and Rojas, O. (1974b). *Int. J. Quantum Chem.* **8**, 17.

Degand, P., Leroy, G., and Peeters, D. (1973). *Theor. Chim. Acta* **30**, 243.

Deplus, A., Leroy, G., and Peeters, D. (1974). *Theor. Chim. Acta* **36**, 109.

Dewar, M. J. S. (1949). *Proc. Cambridge Phil. Soc.* **45**, 638.

Dewar, M. J. S. (1950). *J. Chem. Soc., London* p. 329.

Dewar, M. J. S. (1952). *J. Chem. Soc., London* pp. 3532, 3534.

Dewar, M. J. S., and Lonquet-Higgins, H. C. (1952). *Proc. Roy. Soc., Ser. A* **214**, 482.

Diner, S., Malrieu, J. P., and Claverie, P. (1969a). *Theor. Chim. Acta* **13**, 1, 18.

Diner, S., Jordan, F., and Gilbert, M. (1969b). *Theor. Chim. Acta* **15**, 100.

Diner, S., Malrieu, J. P., Claverie, P., and Jordan, F. (1969c). *Chem. Phys. Lett.* **2**, 319.

Diner, S., Malrieu, J. P., Jordan, F., and Claverie, P. (1970). *Theor. Chim. Acta* **15**, 86.

Duke, B. J. (1974). *Chem. Phys. Lett.* **28**, 437.

Duke, B. J., and O'Leary, B. (1973). *Chem. Phys. Lett.* **20**, 459.

Duke, B. J., and O'Leary, B. (1974). *In* "Quantum Chemistry—The State of the Art,"
    Proceedings of the Atlas Computer Conference (V. R. Saunders and J. Brown, eds.),
    No. 4, *Sci. Res. Counc.*, London. (Preliminary publication; final publication to appear
    in 1975).

Duke, B. J., Eilers, J. E., and O'Leary, B. (1974). *J. Chem. Soc. (Faraday II)* **70**, 386.

Duke, B. J., Pickering, M., O'Leary, B., and Eilers, J. E. (1975a). *J. Chem. Soc. (Faraday II)*
    (in press).

Duke, B. J., Eilers, J. E., and O'Leary, B. (1975b). *Chem. Phys. Lett.* **32**, 602.

Duke, B. J., Eilers, J. E., Kang, S., Liberles, A., and O'Leary, B. (1975c). *Int. J.
    Quantum Chem. Symp.* (in press).

Duke, B. J., Collins, M. P., Eilers, J. E., and O'Leary, B. (1975d). To be published.

Ehrenson, S. (1968a). *Theor. Chim. Acta* **10**, 193.

Ehrenson, S. (1968b). *Theor. Chim. Acta* **10**, 209.

Ehrenson, S. (1969a). *J. Amer. Chem. Soc.* **91**, 3693.

Ehrenson, S. (1969b). *J. Amer. Chem. Soc.* **91**, 3702.

Eilers, J. E. (1971). Ph.D. Thesis, Case Western Reserve Univ., Cleveland, Ohio.

Eilers, J. E., and Whitman, D. R. (1973). *J. Amer. Chem. Soc.* **95**, 2067.

Eilers, J. E., O'Leary, B., and Duke, B. J. (1974). Unpublished work.

Eilers, J. E., O'Leary, B., Duke, B. J., Liberles, A., and Whitman, D. R. (1975a). *J. Amer.
    Chem. Soc.* **97**, 131.

Eilers, J. E., O'Leary, B., Liberles, A., and Whitman, D. R. (1975b). *J. Amer. Chem. Soc.*
    (in press).

Ellison, F. O. (1963). *J. Amer. Chem. Soc.* **85**, 3540.

Ellison, F. O., Huff, N. T., and Patel, J. C. (1963). *J. Amer. Chem. Soc.* **85**, 3544.

England, W., Salmon, L. S., and Ruedenburg, K. (1971). *Fortschr. Chem. Forsch.* **23**, 31.

Favini, G., and Gamba, A. (1968). *Gazz. Chim. Ital.* **98**, 627.

Favini, G., Gamba, A., and Simonetta, M. (1969). *Theor. Chim. Acta* **13**, 175.

Fink, W. H. (1973). *Int. J. Quantum Chem.* **7**, 1045.

Fink, W. H. (1974). *J. Chem. Phys.* **60**, 402.

Franchini, P. F., and Vergani, C. (1969). *Theor. Chim. Acta* **13**, 46.

Franchini, P. F., and Zandomeneghi, M. (1971). *Theor. Chim. Acta* **21**, 90.

Franchini, P. F., Moccia, R., and Zandomeneghi, M. (1970). *Int. J. Quantum Chem.* **4**, 487.

Freed, K. F. (1974). *J. Chem. Phys.* **60**, 1765.

Germer, H. A., and Becker, R. S. (1972). *Theor. Chim. Acta* **28**, 1.

Gordon, M. S., and England, W. (1972). *J. Amer. Chem. Soc.* **94**, 5168.

Halgren, T. A., and Lipscomb, W. N. (1973). *J. Chem. Phys.* **58**, 1569.

Hart, H., and Lipscomb, W. N. (1968). *Inorg. Chem.* **7**, 1070.

Hartmann, B. (1947). *Z. Naturforsch. A* **2**, 259.

Heilbronner, E., Weber, J., Michl, J., and Zahradnik, R. (1966). *Theor. Chim. Acta* **6**, 141.

Herndon, W. C. (1972). *Progr. Phys. Org. Chem.* **9**, 99.

Hoffmann, R. (1963). *J. Chem. Phys.* **39**, 1397.

Hoffmann, R., and Lipscomb, W. N. (1962). *J. Chem. Phys.* **36**, 2179, 3489.

Hoyland, J. R. (1968). *J. Amer. Chem. Soc.* **90**, 2227.

Hoyland, J. R. (1969a). *J. Chem. Phys.* **50**, 2775.

Hoyland, J. R. (1969b). *J. Chem. Phys.* **50**, 473.

Hurley, A. C. (1955). *Proc. Phys. Soc., London, Sect. A* **68**, 149; **69**, 49.

Hurley, A. C. (1956). *Proc. Phys. Soc., London, Sect. A* **69**, 301.

Jordan, F., Gilbert, M., Malrieu, J. P., and Pincelli, U. (1969). *Theor. Chim. Acta* **15**, 211.

Klessinger, M. (1965). *J. Chem. Phys.* **43**, S117.

Klessinger, M. (1967). *J. Chem. Phys.* **46**, 3261.

Klessinger, M. (1968). *Chem. Phys. Lett.* **2**, 562.

Klessinger, M. (1969). *Chem. Phys. Lett.* **4**, 144.

Klessinger, M. (1970a). *J. Chem. Phys.* **53**, 225.

Klessinger, M. (1970b). *Int. J. Quantum Chem.* **4**, 191.

Klessinger, M., and McWeeny, R. (1965). *J. Chem. Phys.* **42**, 3343.

Klopman, G., and O'Leary, B. (1970). *Fortschr. Chem. Forsch.* **15**, 445.

Koetzle, T. F., and Lipscomb, W. N. (1970a). *Inorg. Chem.* **9**, 2279.

Koetzle, T. F., and Lipscomb, W. N. (1970b). *Inorg. Chem.* **9**, 2743.

Koetzle, T. F., Scarbrough, F. E., and Lipscomb, W. N. (1968). *Inorg. Chem.* **7**, 1076.

Langlet, J. (1972). *Theor. Chim. Acta* **27**, 223.

Langlet, J., and Malrieu, J. P. (1972). *J. Amer. Chem. Soc.* **94**, 7254.

Langlet, J., Pullman, B., and Berthod, H. (1970). *J. Chim. Phys.* **67**, 480.

Langlet, J., Gilbert, M., and Malrieu, J. P. (1971). *Theor. Chim. Acta* **22**, 80.

Leroy, G., and Jaspers, S. (1967). *J. Chim. Phys.* **64**, 479.

Leroy, G., and Peeters, D. (1974). *Theor. Chim. Acta* **36**, 11.

Leroy, G., and Peeters, D. (1975). *In* "Localisation et Delocalisation en Chimie Quantique" (R. Daudel, ed.), Vol. 1. Reidel Publ., Dordrecht, Netherlands. In press.

Letcher, J. H. (1971). *J. Chem. Phys.* **54**, 3215.

Letcher, J. H., and Dunning, T. H. (1968). *J. Chem. Phys.* **48**, 4538.

Letcher, J. H., and van der Wazer, J. R. (1966). *J. Chem. Phys.* **44**, 815; **45**, 2916, 2926.

Letcher, J. H., and van der Wazer, J. R. (1967). *In* "Topics in Phosphorus Chemistry" (M. Grayson and E. J. Griffith, eds.), Vol. 5, Ch. 2. Wiley, New York.

Letcher, J. H., Unland, M. L., and van der Wazer, J. R. (1969). *J. Chem. Phys.* **50**, 2185.

Letcher, J. H., Absar, I., and van der Wazer, J. R. (1972). *Int. J. Quantum Chem., Symp.* **6**, 451.

Levy, M., Stevens, W. J., Shull, H., and Hagstrom, S. (1970). *J. Chem. Phys.* **52**, 5483.

Lippert, J. L., Hanna, M. W., and Trotter, P. J. (1969). *J. Amer. Chem. Soc.* **91**, 4035.

Löwdin, P.-O. (1950). *J. Chem. Phys.* **18**, 365.

Longuet-Higgins, H. C., and Murrell, J. N. (1955). *Proc. Phys. Soc., London, Sect. A* **68**, 601.

McWeeny, R., and Del Re, G. (1968). *Theor. Chim. Acta* **10**, 13.

Magnasco, V., and Musso, G. F. (1971a). *J. Chem. Phys.* **54**, 2925.

Magnasco, V., and Musso, G. F. (1971b). *Chem. Phys. Lett.* **9**, 433.

Magnasco, V., and Perico, A. (1967). *J. Chem. Phys.* **47**, 971.

Maigret, B., Pullman, B., and Caillet, J. (1970). *Biochem. Biophys. Res. Commun.* **40**, 808.

Manne, R. (1967). *J. Chem. Phys.* **46**, 4695.

Masson, A., Levy, B., and Malrieu, J. P. (1970). *Theor. Chim. Acta* **18**, 193.

Moffitt, W. (1951). *Proc. Roy. Soc., Ser. A* **210**, 224, 245.

Moffitt, W. (1953). *Proc. Roy. Soc., Ser. A* **218**, 486.

Moffitt, W., and Scanlan, J. (1953). *Proc. Roy. Soc., Ser. A* **218**, 464; **220**, 530.

Mori, Y. (1961). *Bull. Chem. Soc.* **34**, 1031, 1036.

Mulliken, R. S. (1949). *J. Chim. Phys.* **46**, 497, 675.

Murrell, J. N., and Harget, A. J. (1972). "Semi-empirical Self-consistent-field Molecular Orbital Theory of Molecules." Wiley (Interscience), New York.

Nanda, D. M., and Narasimham, P. T. (1972). *Mol. Phys.* **24**, 1341.

Nesbet, R. K., and Watson, R. E. (1960). *Ann. Phys. (New York)* **9**, 260.

Newton, M. D., and Lipscomb, W. N. (1967). *J. Amer. Chem. Soc.* **89**, 4261.

Newton, M. D., Boer, F. P., and Lipscomb, W. N. (1966). *J. Amer. Chem. Soc.* **88**, 2353, 2367.

Newton, M. D., Switkes, E., and Lipscomb, W. N. (1970). *J. Chem. Phys.* **53**, 2645.

Nicholson, B. J. (1970). *Advan. Chem. Phys.* **18**, 249.

Offenhartz, P. O'D. (1970). *J. Amer. Chem. Soc.* **92**, 2599.

O'Leary, B., Duke, B. J., Eilers, J. E., and Abrahamson, E. W. (1973). *Nature (London)* **246**, 166.

O'Leary, B., Duke, B. J., and Eilers, J. E. (1974a). Program SAMOM. Q.C.P.E., Chem. Dep., Univ. of Indiana, Bloomington. Part of program 263 (SAMOS).

O'Leary, B., Duke, B. J., and Eilers, J. E. (1974b). Program SAMOL. Q.C.P.E., Chem. Dep., Univ. of Indiana, Bloomington. Part of program 263 (SAMOS).

O'Leary, B., Duke, B. J., and Eilers, J. E. (1974c). Program SAMOU. Q.C.P.E., Chem. Dep., Univ. of Indiana, Bloomington. Part of program 263 (SAMOS).

O'Leary, B., Duke, B. J., and Eilers, J. E. (1974d). Program SAMOP. Q.C.P.E., Chem. Dep., Univ. of Indiana, Bloomington. Part of program 263 (SAMOS).

Orloff, M. K., and Fitts, D. R. (1963). *J. Amer. Chem. Soc.* **85**, 3721.

Palke, W. E., and Lipscomb, W. N. (1966). *J. Chem. Phys.* **45**, 3945.

Petke, J. D., and Whitten, J. L. (1969). *J. Chem. Phys.* **51**, 3166.

Pople, J. A., and Beveridge, D. L. (1970). "Approximate Molecular Orbital Theory." McGraw-Hill, New York.

Pople, J. A., and Nesbet, R. K. (1954). *J. Chem. Phys.* **22**, 571.

Pople, J. A., Beveridge, D. L., and Dobosh, P. A. (1967). *J. Chem. Phys.* **47**, 2026.

Potenza, J. A., and Poindexter, E. H. (1968). *J. Amer. Chem. Soc.* **90**, 6309.

Pugmire, R. J., and Grant, D. M. (1968). *J. Amer. Chem. Soc.* **90**, 4232.

Randić, M., and Mãksic, Z. B. (1972). *Chem. Rev.* **72**, 43.

Roothaan, C. C. J. (1960). *Rev. Mod. Phys.* **32**, 179.

Rothenburg, S. (1969). *J. Chem. Phys.* **51**, 3389.

Rothenburg, S. (1971). *J. Amer. Chem. Soc.* **93**, 68.

Rudolph, H. D., Dreizler, H., Jaeschke, A., and Winding, P. (1967). *Z. Naturforsch. A* **22**, 940.

Ruedenberg, K. (1951). *J. Chem. Phys.* **19**, 1433.

Saunders, V. R., and Hillier, I. H. (1973). *Int. J. Quantum Chem.* **7**, 699.

Shipman, L. L., and Christoffersen, R. E. (1972). *Chem. Phys. Lett.* **15**, 469.

Simpson, W. T. (1962). "Theories of Electrons in Molecules." Prentice-Hall, Englewood Cliffs, New Jersey.

Smith, K. C., and Shannon, T. W. (1969). *J. Chem. Phys.* **51**, 4633.

Sovers, O. J., Kern, C. W., Pitzer, R. M., and Karplus, M. (1968). *J. Chem. Phys.* **49**, 2592.

Stevens, R. M., Switkes, E., Laws, E. A., and Lipscomb, W. N. (1971). *J. Amer. Chem. Soc.* **93**, 2603.

Stevenson, P. E. (1973). *J. Amer. Chem. Soc.* **95**, 54.

Stevenson, P. E., and Lipscomb, W. N. (1969). *J. Chem. Phys.* **50**, 3306.

Stevenson, P. E., and Lipscomb, W. N. (1970). *J. Chem. Phys.* **52**, 5343.

Switkes, E. (1970). Ph.D. Thesis, Harvard Univ., Cambridge, Massachusetts.

Tossell, J. A. (1973). *J. Phys. Chem. Solids* **34**, 307.

Tossell, J. A., and Lipscomb, W. N. (1972). *J. Amer. Chem. Soc.* **94**, 1505.

Trindle, C., and Sinanòglu, O. (1968). *J. Chem. Phys.* **49**, 65.

Trindle, C., and Sinanòglu, O. (1970). *In* "Sigma Molecular Orbital Theory," (O. Sinanòglu and K. Wiberg, eds.) p. 209. Yale Univ. Press, New Haven, Connecticut.

Unland, M. L. (1968). *J. Chem. Phys.* **49**, 4514.

Unland, M. L., and Letcher, J. H. (1968). *J. Chem. Phys.* **49**, 2706.

Unland, M. L., van der Wazer, J. R., and Letcher, J. H. (1969). *J. Amer. Chem. Soc.* **91**, 1045.

Voet, D., and Lipscomb, W. N. (1967). *Inorg. Chem.* **6**, 113.

von Niessen, W. (1971). *J. Chem. Phys.* **55**, 1948.

von Niessen, W. (1973a). *Theor. Chim. Acta* **31**, 111.

von Niessen, W. (1973b). *Theor. Chim. Acta* **31**, 297.

von Niessen, W. (1973c). *Theor. Chim. Acta* **32**, 13.

von Niessen, W. (1974a). *Theor. Chim. Acta* **33**, 7.

von Niessen, W. (1974b). Personal communication.

Weinstein, H., and Pauncz, R. (1968). *Symp. Faraday Soc.* **2**, 23.

Weinstein, H., and Pauncz, R. (1968). *In* "Molecular Wave Functions," *Symp. Faraday Soc.* **2**, 23.

Weinstein, H., Pauncz, R., and Cohen, M. (1971). *Advan. At. Mol. Phys.* **7**, 97.

Whitman, D. R., and Hornback, C. J. (1969). *J. Chem. Phys.* **51**, 398.

Whitten, J. L. (1973). *Accounts Chem. Res.* **6**, 238.

Winter, N. W., and Dunning, T. H. (1971). *Chem. Phys. Lett.* **8**, 169.

Winter, N. W., Dunning, T. H., and Letcher, J. H. (1968). *J. Chem. Phys.* **49**, 1871.

Wolfsberg, M., and Helmholtz, L. (1952). *J. Chem. Phys.* **20**, 837.

A Series of Electronic Spectral Calculations Using Nonempirical CI Techniques*

SIGRID D. PEYERIMHOFF and
ROBERT J. BUENKER†

Lehrstuhl für Theoretische Chemie
Universität Bonn
Bonn, West Germany

I. Introduction

While *ab initio* calculations for molecular systems have been practical for over a decade now, very little emphasis in such work has been placed on the description of molecular excited states. In the past few years, however, there has been significant progress in altering this basic stance. Efforts in this direction are met with inherently greater difficulties than in more conventional studies involving only ground states for the obvious reason that it becomes necessary in such expanded treatments to deal with a *variety* of electronic states on a more or less common footing, including species which run the gamut from typical valence-shell states, with relatively compact charge distributions, to those of pure Rydberg

character, which are much more diffuse in appearance. In addition, states
of differing multiplicity must be handled with nearly equivalent accuracy
to achieve the theoretical goals sought by means of such calculations.

In general the required degree of balance in the treatment of a whole
series of electronic states cannot be satisfactorily achieved in *ab initio*
calculations unless one goes beyond the SCF or Hartree–Fock method
and introduces a certain amount of correlation into the wavefunctions of
the various species of interest. For the most part this objective has been
pursued by means of the introduction of at least a moderate amount of
configuration interaction (CI) into the overall theoretical treatment. It is
the purpose of the present article to examine the degree to which such *ab
initio* CI methods are capable of effecting a satisfactory representation of
both ground and excited states of various polyatomic molecules, as
measured in large part by the success of such treatments in describing
basic features of the electronic spectra of the systems considered, includ-
ing the energy locations of observed transitions and the values of the
corresponding oscillator strengths. A discussion of the error limits in-
volved in the quantitative aspects of this work is also given, along with a
somewhat more qualitative interpretation of the calculated results as they
pertain to the general description of the electronic spectra of molecular
systems.

II. Importance of the AO Basis in Excited State Calculations

The influence of the AO basis set on molecular properties such as
energy values (e.g. with reference to the Hartree–Fock limit), potential
surfaces (through binding energies and equilibrium internuclear separa-
tions), dipole moments, and related quantities has been thoroughly tested
for a number of molecular systems, particularly in their respective ground
states. It is well established, for example, that molecular dissociation is
very poorly described by means of minimal-basis set calculations
(Schaefer and Harris, 1968) because the functions employed therein are
invariably optimized for the individual (separated) *atoms* and con-
sequently are much less suitable for the corresponding combined
molecule, with its more complex nonspherical charge distribution. The
flexibility introduced by using double-zeta sets (typically obtained by
decomposing larger contracted groups when Gaussian-type functions are
employed) is known to improve this situation markedly, at least in the
sense that it generally leads to fairly accurate determinations of geometri-

cal parameters. Nevertheless additional functions are invariably required for the description of polarization effects before reliable estimates of *binding energies* can be obtained in *ab initio* calculations (regardless of how extensive a CI treatment might be employed in their absence); these species can be either higher order spherical harmonics centered at the nuclei or various types of bond functions strategically located between constituent atoms.

There is very little reason to expect that AO basis set composition is less critical for the calculation of excited state potential surfaces, although there is the distinct possibility that the influence of at least some types of functions could be essentially the same for all states *at a given geometry,* thereby not significantly affecting the calculation of *vertical energy differences* (and thus transition energies) between such potential curves. On the other hand, it is obvious that addition of long-range united-atom type functions not generally present in basis sets employed for ground state calculations is essential in order to allow for a valid description of typical excited Rydberg (diffuse) species. Furthermore the experience of early excited state calculations for the H_2 molecule (Phillipson and Mulliken, 1958) and also the beryllium atom (Roothaan and Bagus, 1963) has shown that relatively long-range functions are also required for an adequate description of certain valence-like species such as the $^1(\sigma_g, \sigma_u)$ state in H_2 and the $^1(2s, 2p)$ state in Be. Such *semidiffuse* states actually appear to bridge the gap between pure valence species and those of conventional Rydberg (hydrogenic) type, and as a result their existence would seem to further complicate the problem of designing AO basis sets of universal validity for the entire spectrum of electronic states characterizing a given system.

It seems clear from existing calculations that single-zeta AO basis sets can only be effective in obtaining a *rough idea* of the relative spacing of electronic energy levels in a given system, and then only among its valence-shell states (Bender and Davidson, 1967; Schaefer and Harris, 1968; Kouba and Öhrn, 1970a,b; Thulstrup and Öhrn, 1972; Tseng and Grein, 1974). Species of at least double-zeta quality appear to be required for a generally reliable treatment of excited states and even more flexibility is probably necessary before truly quantitative predictions of transition energies and associated oscillator strengths can be expected. Addition of various types of polarization functions has generally not led to any *pronounced* change in the calculated transition energies between electronic states but nevertheless their influence is certainly of quantitative significance in most cases, as can be judged from results obtained for

ethylene, thioformaldehyde, and O_2 at both the SCF and CI level of treatment (Table I). Generally speaking such changes in the relative locations of two states are likely to be least significant for species of quite similar character, such as among the various Rydberg states of ethylene or the valence π_g^2 multiplets in O_2, but beyond this no simple pattern in the transition energy results obtained with and without polarization functions is really discernible.

TABLE I

Comparison of Calculated Transition Energies (eV) in Several Systems Obtained by Employing a Double-Zeta Type AO Basis with (Basis II) and without (Basis I) Polarization Functions

Molecule	Excitation	Basis I		Basis II	
		SCF	CI	SCF	CI
H_2CS^a	$^3(n, \pi^*)$	1.00		1.18	
(SCF)	$^1(n, \pi^*)$	1.25		1.44	
	$^3(\pi, \pi^*)$	2.13		2.20	
	$^3(\sigma, \pi^*)$	5.30		5.60	
	$^1(\sigma, \pi^*)$	6.31		6.67	
$C_2H_4^b$	$^3(\pi, \pi^*)$, T	3.29	4.34	3.35	4.32
(SCF)	$^1(\pi, 3s)$, R	6.06	7.13	5.99	7.01
	$^1(\pi, 3py)$, V_g	6.64	7.75	6.57	7.63
	$^1(\pi, \pi^*)$, V_u	7.41	8.31	7.32	8.08
	$^1(\pi, 3d\sigma)$	8.69	9.86	8.57	9.71
	$^1(\pi, \infty)$, I^+	8.96	10.12	8.89	10.01
O_2^c	$(\pi_g)^2$, $^1\Delta_g$	1.29	0.96	1.28	1.01
	$(\pi_g)^2$, $^1\Sigma_g^+$	2.57	1.64	2.55	1.75

^{a} Bruna et al. (1974).
^{b} Polarization species represented by bond functions with optimized exponents $\alpha(s) = 1.4$, $\alpha(p) = 0.5$, $\alpha(d) = 1.02$.
^{c} Peyerimhoff and Buenker (1972b).

As far as the upper orbitals in pure Rydberg states are concerned experience indicates that a satisfactory description can be obtained through the use of single primitive Gaussians centered at either the midpoint of the molecule (the center of the united atom) or at one or more of its constituent (nonhydrogenic) nuclei (Fischbach, 1973; Fischbach et al., 1974; Peyerimhoff and Buenker, 1974). The value of the orbital exponent in such functions is usually a rather critical factor, however, as can be
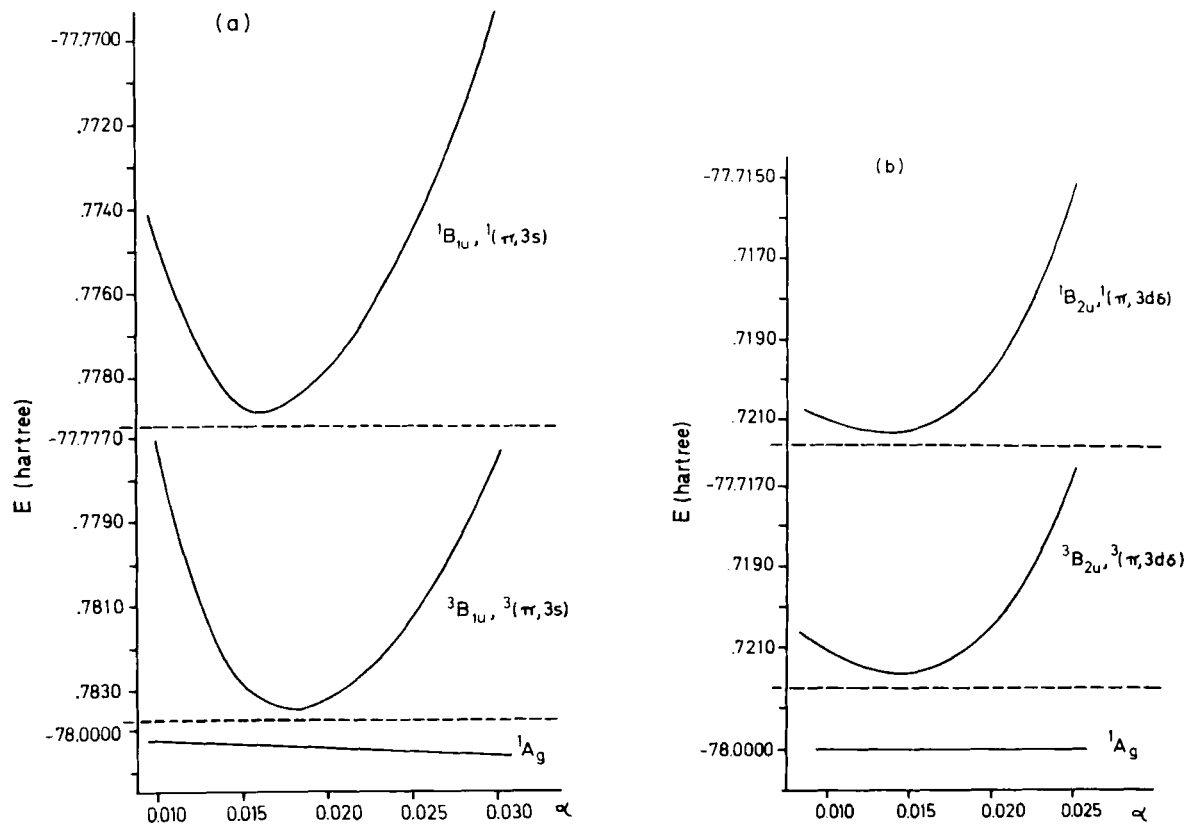
Fig. 1. Total SCF energy of the $(\pi, 3s)$ (a) and $(\pi, 3d\delta)$ (b) Rydberg states of ethylene as a function of the corresponding orbital exponent α. From Fischbach *et al.* (1974), with permission.

judged by the results obtained from SCF calculations for the $(\pi, 3s)$ and $(\pi, 3d)$ states of ethylene given in Figs. 1a and 1b, respectively; failure to optimize these exponents can lead to considerable underestimations of the stability of associated Rydberg states. Yet the exact location of such diffuse functions does not appear to be of much consequence, as for example can be seen from the fact that comparable results for the Rydberg states of H_2CO are obtained regardless of whether the long-range upper orbitals used are located at the carbon or the oxygen nucleus (Peyerimhoff *et al.*, 1971; Whitten and Hackmeyer, 1969).

For the states which can be described as semidiffuse in character similar long-range functions are of importance, as has been pointed out in the early work of Huzinaga (1962). Such states generally arise from in-plane excitations ($\pi \rightarrow \pi^*$ or $\sigma \rightarrow \sigma^*$), most often with singlet spin couplings, as for example in the cases of the various $^1(\pi, \pi^*)$ states of ethylene, butadiene, and benzene, as well as related species for various diatomics such as $^3\Sigma_u^-$ and $^3\Pi_u$ states of O_2 at relatively short distances. The indication thereby is that such states are quite likely to occur whenever Rydberg and valence species of the same symmetry are found in very nearly the same energetic region. Often geometry changes are quite important in determining the exact degree of mixing between such states. There is also still some uncertainty about what role correlation effects play in the description of these semidiffuse states (Mulliken, 1974), but there seems little doubt at this point that such species remain even in very large CI calculations.

In conclusion then it is clear that much more care must be exercised in choosing AO basis sets for treatments of excited states than is necessary for conventional ground state calculations. Nevertheless there is a good deal of evidence that double-zeta basis sets, when augmented with appropriate diffuse functions, are sufficiently flexible in nature to accomplish at least the most pressing objectives in such excited state studies.

III. Use of the SCF Method for the Description of Excited States

Although it is clear that SCF calculations by themselves are generally not capable of giving reliable predictions for transition energies between ground and excited states (especially between closed- and open-shell species, respectively) because of the different amounts of correlation energy inherent in the various electronic states, it is nevertheless true that

such treatments can play a useful role in spectral studies by affording at least a good qualitative picture of the energy relationships among the great majority of the most interesting states of a given system. The main advantage of the SCF method in this connection is that it generally entails very little additional computational effort beyond what is needed to obtain a given ground state solution. At the same time the resulting excited state wavefunctions are generally much preferable to the corresponding single configuration functions constructed solely from the appropriate occupied and virtual MO's of the ground state calculation, since in most cases electron reorganization from one state to another is quite substantial. The latter fact is obviously quite important if satisfactory properties are to be obtained from the excited state wavefunctions, including reliable geometrical characteristics of the excited molecule.[1]

The success of the SCF method in giving relatively accurate determinations of the stability orderings of various excited states can be judged from a number of examples given in Fig. 2 for formaldehyde, thioformaldehyde, ethylene, and water, respectively. Although the SCF transition energies are all invariably too low, and not always by the same amount compared to experiment (or corresponding CI result), it is still safe to say that the relative ordering of the states at the SCF level is essentially correct in these examples. That is to argue that the correlation energy errors in the various states, while by no means exactly equal (especially when comparing valence-shell states with those of pure Rydberg character), are nonetheless close enough to one another in many instances to enable SCF treatments to yield *fairly reliable estimates* of the energy *differences* between large numbers of excited states; this observation is particularly true for states of quite similar character, such as for all Rydberg states of the same principal quantum number[2], a point which serves as the quantitative basis for a number of investigations of species of this

---

[1] One major drawback of the SCF method is the fact that not all excited states are accessible in such treatments, particularly those higher-lying species which cannot be distinguished on the basis of orbital symmetry characteristics from each of the lower energy states; the difficulty in this case centers largely around the necessity of maintaining orthogonality with these other states. If electron reorganization between states of equivalent orbital symmetry is small, however, it is possible to use virtual SCF orbital energies to obtain a good estimate of the higher energy state's position in the spectrum in a manner akin to Koopman's theorem, but of course it is not always possible to predetermine the extent to which such an approximate method is valid in a given case.

[2] But only when they have the same initiating orbital, a point which comes out quite clearly in calculations for ethane (Buenker and Peyerimhoff, 1975c).

Fig. 2. Comparison of energy levels in H_2CO, H_2CS, C_2H_4, and H_2O obtained by SCF calculations with the corresponding CI values.

type (Peyerimhoff *et al.*, 1971; Whitten and Hackmeyer, 1969; Buenker *et al.*, 1971a; Fischer-Hjalmars and Kowalewski, 1972, 1973). In all the examples of Fig. 2 the correlation energy error is greatest for the respective (closed-shell) ground states, thereby leading to the situation in which all excitation energies are underestimated, but cases can also be found for which this simple result does not obtain [the ethane ground state appears to possess a relatively small amount of correlation energy compared to many of its excited states (Buenker and Peyerimhoff, 1975a), for instance]. Thus it still should be stressed that one cannot rely too heavily on the results of the SCF method alone for the purpose of assigning electronic transitions without giving some thought to the importance of correlation effects in a given case.

It has also been found in many applications that the SCF method can be quite effective in deducing geometrical characteristics of individual excited states. The SCF results for various excited state inversion barriers in formaldehyde given in Table II, for example, are clearly more reliable than data derived from small CI calculations for the corresponding states which are based solely on the SCF MO's of the ground state (GSMO's). Calculated SCF potential curves for CO stretch and CH_2 flapping in H_2CO, respectively (Buenker and Peyerimhoff, 1970), have also been found to agree with pertinent experimental findings, and similar success has been noted with regard to SCF treatments of the excited state poten-

TABLE II

Equilibrium Angles ϑ_0 and Inversion Energies ΔE for the $^{3,\,1}A_2(n, \pi*)$
States in Formaldehyde Obtained from Several Treatments (Angles
in Degrees, Energies in eV)

Treatment	$\vartheta_0(^1A_2)$	$\Delta E(^1A_2)$	$\vartheta_0(^3A_2)$	$\Delta E(^3A_2)$
Single configuration (GSMO's)	0	0.0	25	—
CI(GSMO)[a]	0	0.0	0	0.0
CI(PCMO)[a]	31.9	0.073	32.7	0.090
SCF	31.1	0.054	32.0	0.060
Exptl.[a]	20.5–31	0.044	35–36	0.096

[a] For details see Buenker and Peyerimhoff (1970).

tial curves of ethylene (Buenker *et al.*, 1971b), particularly those of the various Rydberg species in this system. In addition a number of calculations for diatomic molecules have indicated that SCF oscillator strengths can be expected to have at least an order-of-magnitude accuracy (Huo, 1968; Henneker and Popkie, 1971; Popkie and Henneker, 1971; Popkie, 1971).

IV. Use of CI Methods in Electronic Spectral Calculations

In order to get a balanced treatment of all states of interest in a given system it is clearly necessary to go beyond the single-configuration approach, usually by means of configuration interaction, in an attempt to account simultaneously for both electron reorganization and electron correlation effects. In applying such CI techniques[3] one is faced with the usual problem of keeping the amount of computational work to within practical limits. For all but the simplest systems a full CI for a sufficiently flexible AO basis is out of the question and thus it becomes necessary to restrict the scope of such calculations without greatly jeopardizing the reliability of the resulting theoretical treatment. Such restrictions can generally be put into two different classes, namely, limitations to the number of MO's allowed variable occupation in the calculations or

[3] In this endeavor our main interest is in the study of general polyatomic systems. Nevertheless the early work on diatomic molecules, particularly that in which better than minimal basis sets have been employed (e.g., Fougere and Nesbet, 1966; Chan and Davidson, 1968, 1970), is clearly relevant in this connection.

systematic elimination of the most weakly interacting configurations from the final CI problem to be explicitly solved. Each of these possibilities is considered below.

A. Full CI for Restricted MO Basis

One way to hold down the number of MO's allowed variable occupation in a given treatment is of course to employ a quite restrictive AO basis set in the first place, for example, one of single-zeta quality. At the outset it is clear from the general discussion in Section II that such calculations are completely ineffective in describing Rydberg states and also certain semidiffuse species. In addition one must expect potential curves for dissociative processes calculated in this manner to be strongly biased toward the separated atoms because of the manner in which minimal basis sets are generally obtained, i.e. via atomic SCF calculations. Nevertheless such restrictive treatments should still be expected to yield a good qualitative picture of the *ordering* of the important *pure valence shell* states of a system, as has in fact been the experience of various authors (Schaefer and Harris, 1968; Tseng and Grein, 1974; Schaefer, 1972) in applying full minimal-basis CI calculations to a series of diatomics (Table III). If one is aware of these limitations, it is certainly possible that such calculations can be of value in arriving at a rough assignment of the measured lines in a given electronic spectrum. At the very least one is guaranteed in these treatments that dissociative processes are described in a formally satisfactory manner (since the Wigner–Witmer rules must be satisfied in even the minimal-basis full CI), although one must keep in mind that the state correlation so indicated may be misleading, again as a consequence of the quite restrictive nature of such AO basis sets.

For larger systems or for more flexible AO basis sets the framework of a full CI can still be maintained by arbitrarily limiting the set of MO's (in the general sense, including NO's) which are allowed variable occupation in the construction of configurations. A core of doubly occupied MO's, derived from some appropriate SCF solution, is usually assumed in such calculations, while some species of the corresponding virtual set are simply never occupied at all. Examples of this type of approach include full π CI treatments for systems such as butadiene and benzene, with a well-defined σ nuclear framework. If a minimal basis set is used the same limitations discussed previously for smaller systems are again present, but use of more flexible basis sets augmented with appropriate diffuse functions can often improve the situation substantially. In butadiene (Buenker and Whitten, 1968; Shih *et al.*, 1972; Dunning *et al.*, 1973), for

TABLE III

Transition Energies (eV) to Several States of O_2 and PO
Obtained from a Full Valence-Shell CI Using a Minimal AO
Basis, and Corresponding Experimental Values

O_2			PO		
State	Calc.[a]	Exptl.	State	Calc.[b]	Exptl.[b]
a $^1\Delta_g$	1.00	0.98	B' $^2\Pi$	2.64	(4.10)
b $^1\Sigma_g^+$	1.36	1.63	$^4\Sigma^-$	3.53	4.61*
c $^1\Sigma_u^-$	2.87	4.49	D' $^2\Pi$	4.26	4.75
C $^3\Delta_u$	3.11	4.26	C' $^2\Delta$	4.65	5.42
A $^3\Sigma_u^+$	3.16	4.34	F $^2\Sigma^+$	4.83	(6.20)
B $^3\Sigma_u^-$	6.01	6.12	C' $^2\Sigma^-$	5.08	5.42
$^1\Delta_u$	8.64		C $^2\Sigma^-$	5.95	5.66
$^1\Sigma_u^+$	10.28				

[a] Schaefer and Harris (1968); data given are T_0 values.
[b] Tseng and Grein (1974); values in parentheses are uncertain.
Data are T_e values with the exception of the one marked with an
asterisk, which corresponds to T_0.

example, it is found that many of the $^1(\pi, \pi^*)$ states prefer a significant
admixture of diffuse $p\pi$ character (Table IVa), while virtually all the
excited states benefit in comparison to the ground state from introduction
of a double-zeta basis. This work has led to a reassignment (Shih *et al.*,
1972) of the important N–V$_1$ and N–V$_2$ transitions for this system in
terms of *dipole-allowed* excitations to *semidiffuse* (π, π^*) species rather
than as allowed and forbidden transitions, respectively, involving purely
valence upper states (Mulliken, 1942; Pariser and Parr, 1953;
Dumbacher, 1972). Similarly large improvements in the descriptions of
the excited states of benzene have been obtained as a result of analogous
basis set extensions (Buenker *et al.*, 1968; Peyerimhoff and Buenker,
1970; Hay and Shavitt, 1973, 1974) (see Table IVb).

One consequence of assuming a large fixed core in the CI calculations
is that such a procedure makes the choice of the molecular orbital basis
actually employed a critical factor. First of all, it requires that the charge
reorganization of the core which invariably occurs upon excitation must
be accounted for *outside* the normal CI procedure. In an attempt to gauge
the importance of such effects comparative CI treatments for the excited

TABLE IV

COMPARISON OF CALCULATED VERTICAL (π, π^*) TRANSITION ENERGIES (eV) OBTAINED FROM CI(GSMO) AND CI(PCMO) CALCULATIONS BY EMPLOYING PURE VALENCE-SHELL AO BASIS SETS AND THOSE AUGMENTED WITH DIFFUSE FUNCTIONS, FOR BUTADIENE (a) AND BENZENE (b)

	State[b]	Minimal basis[a] π CI(GSMO)	Double-zeta plus diffuse π[a] CI(GSMO)	CI(PCMO)	Exptl.[a]
	$2\ ^1A_g$ v	7.69	6.67	6.67	(6.26–6.63)
	$3\ ^1A_g$ s-d		7.79	7.79	
	^3A_g v	5.52	4.96	4.95	4.93
	$1\ ^1B_u$ s-d		6.90	6.60	{(5.71–6.29) / 5.92, 6.2
(a)	$2\ ^1B_u$ s-d		8.15	7.98	7.2?, 7.25
	$3\ ^1B_u$ v	10.19	8.88	9.16	
	$1\ ^3B_u$ v	3.81	3.28	3.24	3.22
	$2\ ^3B_u$ s-d		7.04	7.55	
	$3\ ^3B_u$ v	9.04	8.08	7.92	

		Minimal basis[c] π CI(GSMO)	Somewhat extended $p\pi$'s CI(GSMO)[d]	Diffuse π's CI(GSMO)[e]	Exptl.
	$^1B_{2u}$ v	5.26	5.20	5.0	4.9, 5.0
	$^1B_{1u}$ v (s-d)	9.48	8.08	7.63	6.2, 6.3
	$1\ ^1E_{1u}$ d			7.26	7.41
	$2\ ^1E_{1u}$ s-d	10.61	9.41	8.34	7.0
(b)	$3\ ^1E_{1u}$ d			8.74	
	$1\ ^1E_{2g}$ d			7.90	7.98
	$2\ ^1E_{2g}$ v (s-d)	8.62	8.56	8.33	7.3
	$^3B_{1u}$ v	3.98	4.12	3.83	3.9
	$^3E_{1u}$ v	5.39	5.20	4.98	4.7
	$^3B_{2u}$ v (s-d)	8.61	7.35	7.0	5.6
	$^3E_{2g}$ v	7.48	7.59	7.28	6.55

[a] Shih et al. (1972).

[b] The abbreviations v, s-d, and d on the right indicate whether the state in question is best characterized as valence, semidiffuse, or diffuse, respectively.

[c] Buenker et al. (1968).

[d] Peyerimhoff and Buenker (1970).

[e] Hay and Shavitt (1973, 1974).

states of butadiene have been carried out using each state's own characteristic SCF MO's in the CI, as well as those of the ground state. The results in Table IVa show energy lowerings of as much as 0.3 eV to result from employing the excited state's SCF MO's in each case instead of the ground state set, an obvious reflection of the beneficial effects of allowing for charge reorganization of the core in such restrictive CI procedures. But even the use of characteristic SCF MO's for each state is undoubtedly not enough in itself to completely compensate for the restriction of a large core, although it provides a useful means of going beyond the clearly unbalanced situation which results from exclusive use of the ground state SCF MO's for ground and excited states alike.

One even more obvious problem with full π CI treatments in general is their exclusion of a large number of potentially important states in which σ-type molecular orbitals are formally involved in the excitation process. In butadiene, for example, it has been found that Rydberg (π, 3s) states fall at roughly the same energy as the $^1(\pi, \pi^*)$ species which have generally dominated consideration (compare Tables IVa and V).

TABLE V

VERTICAL EXCITATION ENERGIES (eV) TO (π, 3s) RYDBERG STATES OF BUTADIENE OBTAINED FROM A CI(PCMO) TREATMENT[a]

State	ΔE_e
$1\ ^1A_u$	6.50
$2\ ^1A_u$	6.76
$1\ ^3A_u$	6.48
$2\ ^3A_u$	6.67
$1\ ^1B_g$	6.24
$2\ ^1B_g$	7.31
$1\ ^3B_g$	6.17
$2\ ^3B_g$	7.29

[a] Shih et al. (1972).

Especially in view of the fact that the $^1(\pi, \pi^*)$ species are themselves relatively diffuse in character, there is good reason to believe that the practice of designing theoretical treatments of electronic spectra which completely ignore such pure Rydberg states can be hazardous. There are at least six band systems which have thus far been identified in the far UV

spectrum of butadiene (Herzberg, 1966, p. 656; Price and Walsh, 1940), for example, and it seems highly unlikely that *all* of these species can realistically be assigned as (π, π^*) transitions; nor should one expect the situation to become any less complicated as the size of the π system is increased. In summary there is a distinct likelihood in such restrictive CI treatments of completely missing key transitions simply because not all low-lying states in a given system can be represented even approximately at this level, and this fact should certainly not be ignored in attempting to use such calculations to make spectral assignments.

B. Limited CI with Minimal Core

In view of the pitfalls associated with restricting the set of orbitals involved in the excitation process, there is a strong incentive for investigating alternative CI procedures which do not rely on the assumption of a large doubly occupied core. For large basis sets such a practice effectively rules out a full CI treatment (at least in an explicit sense) and thus it becomes necessary to seek other means of limiting the amount of computations to a practical size. One of the most promising methods of achieving the latter objective involves the use of a systematic selection procedure to eliminate large numbers of the most weakly interacting configurations from the final CI secular equations actually to be solved in the treatment. This whole question of configuration selection has been discussed in detail elsewhere (Gershgorn and Shavitt, 1968; Buenker and Peyerimhoff, 1974a) and only a brief summary of the basic features of this technique will be included in the present work.

To begin with a series of dominant (main) configurations for a given state is chosen as the nucleus of its respective CI treatment. All singly and doubly excited configurations with respect to *each* of these dominant species are then tested individually for their capacity to lower the energy of the state in question relative to its value obtained in a zero-order secular equation involving only the main configurations themselves. Configurations whose energy lowerings do not exceed a predefined threshold value T are thereupon eliminated from the final CI secular equation in each case; in addition an extrapolation procedure can then be used to estimate the potential contribution of the neglected species. In essence what is obtained in this method is equivalent to a CI for all single and double excitations with respect to a *series* of the most important configurations in a given state. One of the most significant advantages of such a treatment is that core reorganization is directly accounted for to a large extent, especially as the size of the main configuration set is ex-

panded. The use of special MO (NO) basis sets is also helpful for convergence properties in this connection but this feature will not be discussed further at this point.

In practice a small core of MO's is often still maintained in such calculations, generally consisting entirely of species of inner-shell type. Extremely short-range complements of the latter MO's may also be excluded from the excitation process without adversely affecting the calculated findings; results of calculations of this type will be discussed in the next section. As with the more restrictive treatments discussed in Section IV,A, the goal in these calculations is to obtain a realistic description of the electronic spectra of the systems of interest, i.e. a proper balance in the correlation energy errors of all the various states, rather than to account for the total correlation energy in any given case. The success with which this relatively limited objective is accomplished in such nonempirical studies can then be determined to a large extent via direct comparison with experimental findings.

V. Electronic Spectra of Systems with Twelve Valence Electrons

The family of molecules with twelve valence electrons, including such species as molecular oxygen, ethylene, and formaldehyde, has probably received more attention in the area of spectra calculations than any other group of isovalent systems. The low-lying excited states in these molecules run the full gamut from typical valence species on the one hand to those of pure Rydberg character on the other, and include a number of examples of the semidiffuse variety discussed earlier. Consequently it seems appropriate to use this family of molecules to illustrate the effectiveness of the various CI methods outlined in the previous section in predicting details of the electronic spectra of such systems.

A. Quantitative Results

1. Formaldehyde

Calculated vertical transition energies to the low-lying states of H_2CO are collected in Table VI from a variety of CI treatments. A relatively consistent series of theoretical estimates for the excitation energies is obtained in these investigations, and practically all the results are found to be in good agreement with the respective experimental data. Probably the simplest of these treatments is that referred to as the CI(PCMO)

method (Peyerimhoff *et al.*, 1971), in which a fairly small valence set of MO's has been employed in constructing the various configurations. The AO basis in this case is of double-zeta quality augmented with s and p diffuse functions at each nonhydrogenic center (see Section II). Reorganization of the core electrons in the various states is accounted for in large part through the use of each state's own set of SCF MO's (MO's of the *parent* configuration) in the individual cases; analogous calculations employing only ground state MO's for all states lead to overestimations of the corresponding transition energies of from 1.0 to 2.0 eV. Whitten and Hackmeyer (1969) and more recently Davidson (1974) and co-workers have employed larger CI expansions with smaller core sizes (using SCF ground state MO's) and their results do not differ greatly from those obtained in the less extensive CI(PCMO) calculations (Table VI).

The most important features of the formaldehyde spectrum are as follows. The lowest-lying pair of excited states is the pure valence-shell $^{3,1}(n, \pi^*)$ species in the neighborhood of 3.5 eV. The first *fully allowed* transition in this spectrum occurs at much shorter wavelength and is of Rydberg (n, 3s) type. The next absorption system (at 8.0 eV) was once believed (Pople and Sidman, 1957) to result from an intravalence transition, with a $^1(\pi, \pi^*)$ upper state, but it is now established that it corresponds instead to an $(n, 3pa_1)$ Rydberg excitation. The location of the actual (π, π^*) singlet is still a matter of controversy, with estimates ranging from 9.9 to 11.4 eV; by contrast the corresponding triplet state is widely agreed to lie in the neighborhood of 5.6 eV. The simple CI(PCMO) calculations [and more recently a treatment employing the equations-of-motion method (Yeager and McKoy, 1974)] have also predicted an allowed transition of (σ, π^*) type in the neighborhood of 9.0 eV, and recent experimental investigations (Mentall *et al.*, 1971) have tended to substantiate this assignment, including the finding that the state in question should possess a repulsive CO stretch potential curve (Buenker and Peyerimhoff, 1970). Geometrical characteristics for the other H_2CO states are also included in Table VI and are likewise found to be in generally good agreement with experimental findings.

The calculated triplet–singlet energy splittings for H_2CO are seen to fall into three distinct categories according to the character of the initial and final MO's involved in the formal excitation process. The smallest of these quantities invariably occur for Rydberg-type transitions, thereby clearly reflecting the *diffuse nature of the upper orbital* in these cases (which in turn leads to a quite small exchange integral between this species and the MO from which excitation is initiated). On the other hand

TABLE VI

VERTICAL TRANSITION ENERGIES (eV) OF H_2CO OBTAINED FROM DIFFERENT TREATMENTS

State		Approximate[a] geometry	CI(PCMO)[b]	A[c]	B[d]	CI[e]	Exptl.[b]
$^1A_1$		Planar	0.0	0.0	0.0	0.0	$\tilde{X}$ 0.0
$^3A_2$	(n, π^*)	Bent ($\approx 30°$)	3.41	3.38	3.77		$\tilde{a}$ 3.12–3.44
$^1A_2$		R_{CO} increased (≈ 0.1 Å)	3.81	3.80			$\tilde{A}$ 3.50–5.39
$^3A_1$	(π, π^*)	Bent ($\approx 25°$) R_{CO} increased (≈ 0.2 Å)	5.56	5.66	5.97		
$^3B_2$	$(n, 3s)$	Approximately	7.32				First Rydberg
$^1B_2$		same geometry as ion	7.38	7.48			$\tilde{B}$ 7.08–7.51
2 $^3A_1$	$(n, 3pb_2)$	Approximately	8.09	8.10			Second Rydberg
2 $^1A_1$		same geometry as ion	8.11	8.30		8.05	$\tilde{C}$ 7.97
$^3B_1$	(σ, π^*)	Bent ($\approx 25°$)	8.14				
$^1B_1$		R_{CO} increased (0.2–0.3 Å)	9.03	9.35			
2 $^3A_2$	$(n, 3pb_1)$	Approximately	9.06				
2 $^1A_2$		same geometry as ion	9.07				
2 $^3B_2$	$(n, 3pa_1)$	Approximately	8.29				Third Rydberg
2 $^1B_2$		same geometry as ion	8.39				$\tilde{D}$ 8.14
3 $^1A_1$	(π, π^*)	CO repulsive	11.41 (9.9)	11.31	11.3	10.96	

[a] Buenker and Peyerimhoff (1970).
[b] Peyerimhoff et al. (1971).
[c] Whitten and Hackmeyer (1969) and Whitten (1972).
[d] Langhoff et al. (1974) and Davidson (1974).
[e] Results of a CI calculation (with selection) with four core orbitals and a valence set of 19. Zero of energy is -113.9487 hartree.

the largest splittings observed occur for in-plane excitations between MO's which are both of valence type, such as for the (π, π^*) transitions; generally speaking the exchange integrals between initial and final MO's are quite large in this case. Finally one finds splittings of intermediate magnitude (approximately 0.5–1.0 eV) for intravalence excitations of the out-of-plane variety, such as for the (n, π^*) and (σ, π^*) species, respectively. In the great majority of cases these energy splittings can be predicted with reasonable accuracy purely on the basis of SCF results (Section III) without the use of any CI whatsoever, particularly

when the splittings are relatively small, i.e. when the character of corresponding singlet and triplet states is not greatly different.

The only real uncertainty concerning the H_2CO spectrum seems to be the location of the $^1(\pi, \pi^*)$ species. Since this state possesses the same symmetry as the ground state [as well as the $^1(n, 3pa_1)$ species], the simple CI(PCMO) treatment cannot be applied in the usual way but rather the same set of MO's must be employed as in the ground state case in order to ensure mutual orthogonality in each instance. Hence it could be argued that a more extended CI treatment is necessary to give a reliable value for the $^1(\pi, \pi^*)$ excitation energy. Davidson (1974) and co-workers do obtain a somewhat lower value for this quantity in a larger CI but it is still above the minimum I.P. of 10.9 eV and well above the 9.9 eV result obtained by Whitten (1972) using less straightforward methods. A fairly extended CI treatment with a core of 4 MO's and a valence set of 19 orbitals employing the same AO basis as in the aforementioned CI(PCMO) calculations has been carried out by the authors to investigate this point further; a total of five main configurations was thereby used as $\{\psi_0\}$ (see Buenker and Peyerimhoff, 1974b, for details) and optimal configurations were selected for all three of the lowest-lying $^1A_1$ states. As shown in Table VI the calculated $^1(\pi, \pi^*)$ transition energy resulting from this treatment is 10.96 eV after extrapolation to zero threshold (Buenker and Peyerimhoff, 1974a) (it is 11.07 eV at $T = 20$ μhartree); the corresponding value for the $^1(n, 3pa_1)$ species is also somewhat lower than in the earlier CI(PCMO) calculation, but in general the discrepancies are not substantial. It is also worth noting that the $^1(\pi, \pi^*)$ state, though basically a valence species, is nevertheless found to possess a significant amount of diffuse character, in definite contrast to the case for the corresponding triplet; as pointed out in Section II this distinction is quite common for states of different multiplicity resulting from the same *in-plane* excitation.

2. Thioformaldehyde

A CI treatment employing a double-zeta basis including diffuse functions has also recently been reported (Bruna *et al.*, 1974) for the ground and excited states of the thiocarbonyl analog of formaldehyde, H_2CS. In this case a core of eight electron pairs has been assumed (six of which correspond to inner shells) and configuration selection has been used to keep the sizes of the final secular equations to within practical limits. A summary of the results of these calculations is given in Table VII; agreement between calculated and experimental results (wherever comparison is possible) again appears to be quite good.

TABLE VII

VERTICAL TRANSITION ENERGIES ΔE_c FOR H_2CS OBTAINED FROM A CI(PCMO)
CALCULATION AND COMPARISON WITH EXPERIMENTAL DATA[a]

State		Calculated geometrical characteristics	ΔE_c (eV)	Exptl.
$^1A_1$		Planar		
$^3A_2$	(n, π^*)	R_{CS} increased (≈ 0.1 Å)	1.84	
$^1A_2$		planar or weakly bent ($\approx 15°$)	2.17	$\tilde{A}$ 2.33–2.50
$^3A_1$	(π, π^*)	R_{CS} increased (≈ 0.2 Å) planar or weakly bent ($\approx 13°$)	3.28	
$^3B_2$	$(n, 3s)$	Approximately	5.72	
$^1B_2$		same geometry as ion	5.83	$\tilde{B}$ 5.85–5.95
$2\,^3A_1$	$(n, 3pb_2)$	Approximately	6.58	
$2\,^1A_1$		same geometry as ion	6.62	$\tilde{C}$ 6.0–5.6[b]
$^3B_1$	(σ, π^*)	R_{SC} increased (≈ 0.25 Å)	6.38	
$^1B_1$		probably weakly bent	7.51	
$3\,^1A_1$	(π, π^*)		7.92	
$2\,^3A_2$	$(n, 3pb_1)$	Approximately	7.79[c]	
$2\,^1A_2$		same geometry as ion	7.88[c]	

[a] Bruna *et al.* (1974); ground state energy is -436.5317 hartree.

[b] Experimental range is based on extrapolations of analogous results for higher thiones.

[c] Values too high by approximately 0.5–1.0 eV; see original reference.

The replacement of oxygen by sulfur has a quite predictable effect (see also Section V,B) on the stability of the various valence-shell MO's and this influence is easily recognizable in a comparison of the spectral data for H_2CO and H_2CS. The transitions originating from the n MO, which is less stable in the sulfur compound, are found to occur at significantly longer wavelengths in this system than in H_2CO; this is particularly true for excitations into the π^*MO, which becomes somewhat more stable upon substitution of sulfur. In addition the greater diffuseness of the second-row atom shows up clearly in the magnitudes of the various triplet–singlet splittings observed for these two systems. These quantities are slightly greater than in H_2CO for Rydberg states (since the upper orbitals in such species have a larger overlap with the more diffuse sulfur valence MO's than with their counterparts for the oxygen-containing system) but are decidedly smaller for valence-shell states (for the analogous reason). One of the important consequences of this behavior is the

occurrence of the $^1(\pi, \pi^*)$ transition *at a much lower energy* in H_2CS than in H_2CO, well below the minimum I.P. for the thiocarbonyl system. Geometrical characteristics for the H_2CS states are also included in Table VII and again a strong similarity to the corresponding H_2CO data is noted (Buenker and Peyerimhoff, 1974b).

3. *Ethylene*

Of all the 12-valence-electron polyatomic systems the one whose electronic spectrum has been studied most extensively is ethylene. Most of the attention in this case has centered around the characterization of the $^{3,1}(\pi, \pi^*)$ states but again, as in formaldehyde, it is well established that the majority of the low-lying excited species of this system are actually of the pure Rydberg type. A summary of calculated transition energies to the various C_2H_4 excited states is given in Table VIII for comparison with existing experimental data. For the most part only allowed Rydberg transitions are given explicit consideration in this table but information concerning the neighboring forbidden species is also available in the original references (Fischbach, 1973; Fischbach *et al.*, 1974; Buenker *et al.*, 1971a).

TABLE VIII

Vertical Transition Energies (eV) for Ethylene Obtained from Different Treatments and Comparison with Corresponding Experimental Data[a]

State		CI1	CI(32)	CI(38)	Exptl.
^1A_g	N	0.0	0.0	0.0	0.0
					4.4–4.7
$^3B_{1u}$	T (π, π^*)	4.17	4.34	4.32	or 4.22
$^3B_{3u}$	T_R $(\pi, 3s)$	6.80		6.86	
$^1B_{3u}$	R $(\pi, 35)$	6.94	7.13	7.01	7.11
$^3B_{1g}$	$(\pi, 3py)$	7.47			
$^1B_{1g}$	V_g $(\pi, 3py)$	7.52	7.75	7.63	7.45
$^1B_{2g}$	$(\pi, 3p\sigma)$	7.55	7.79		
$^1B_{1u}$	V_u (π, π^*)	8.25	8.31	8.09	7.66
2 $^1B_{3u}$	$(\pi, 3d\sigma)$	8.44	8.69	8.57	?8.26
3 $^1B_{3u}$	$(\pi, 3d\delta)$		8.75		8.62
4 $^1B_{3u}$	$(\pi, 4s)$		8.92		8.92

[a] Zero of energy for CI(38) is -78.2275 hartree. CI1 values are taken from Buenker *et al.* (1971a); the other data are taken from Buenker and Peyerimhoff (1975b).

Again the simplest of the CI treatments considered in Table VIII is of the CI(PCMO) type, employing a double-zeta AO basis (including diffuse functions), a core of 5 MO's, and valence sets with as few as 9 MO's (denoted CI1). The much more extended treatment [denoted CI(32)] uses the same AO basis but includes only the two inner-shell orbitals in the core and expands the corresponding valence set to comprise 26 MO's; selection and extrapolation methods (Buenker and Peyerimhoff, 1974a) as outlined in Section IV,B are also applied in this case. Finally in the calculation referred to as CI(38) a larger AO basis with additional bond-type polarization functions of s, $p\pi$, and $d\pi$ character is employed, and selection of configurations (arising from a core of two and a valence set of 31 MO's, respectively) is again implemented. Despite the fact that the absolute energies for a given state in the various treatments differ by as much as 0.20 hartree it is seen that their relative location with respect to one another is not greatly affected by such improvements in the calculations.

A detailed discussion of the various Rydberg members in ethylene is given elsewhere (Fischbach, 1973; Fischbach et al., 1974); the agreement between experimental and calculated transition energies in these cases is generally quite good. There is still some question about the correct assignment of the band systems at 8.26 and 8.62 eV, respectively, however, with both $(\pi, 3d\sigma)$ and $(\pi, 3d\delta)$ transitions calculated to lie in the 8.6 eV region of the spectrum. Fischer-Hjalmars and Kowalewski (1972, 1973) have suggested that the longer wavelength of these systems may correspond to a *dipole-forbidden* $(\pi, 3p\sigma)$ excitation but the afore-mentioned *ab initio* calculations find this species to lie at significantly lower energy (7.6–7.7 eV); in addition the intensity of the 8.26 eV system is not noticeably smaller than that of other dipole-allowed Rydberg species. An alternative assignment for this transition as an allowed $(\pi, 3d\sigma)$ species has been suggested on the basis of model potential calculations (Betts and McKoy, 1971).

The lowest pure valence-shell transition in ethylene is the $^3(\pi, \pi*)$ species found in the 4.2–4.4 eV region of the spectrum, and in this case the CI calculations at each of the levels discussed above are again in good agreement with the experimental findings. The results for the $^1(\pi, \pi*)$ excited states, on the other hand, have been a matter of considerable controversy (Basch and McKoy, 1970; Peyerimhoff et al., 1971; Bender et al., 1972), primarily because the vertical energy differences obtained by *ab initio* SCF and CI calculations consistently exceed the observed location of the Franck–Condon maximum of the corresponding V–N band system

by 0.4–0.6 eV, and also because the calculations attribute a significant amount of diffuse character to the upper orbital in this case [in distinct contrast to what is found for the corresponding $^3(\pi, \pi^*)$ species], although it is now established that CI leads to a rather noticeable reduction in the amount of this diffuseness. The value for $\langle \pi^* | x^2 | \pi^* \rangle$, for example, decreases from 32.4 a.u. for the upper orbital in the $^1(\pi, \pi^*)$ SCF state to 23.0 a.u. for the corresponding species after transformation to a natural orbital basis is carried out [CI(38) treatment], while that for $\langle \pi^* | 1/r | \pi^* \rangle$ increases accordingly from 0.154 to 0.231 a.u. for the same comparison. Ryan and Whitten (1972) have reported a vertical energy difference of only 8.05 eV obtained from a calculation without additional diffuse functions in the AO basis, but at the same time the transition energy to the $^3(\pi, \pi^*)$ state in this treatment is calculated to be unusually high (4.89 eV).

Another interesting aspect of these calculations is the fact that the $^1(\pi, \pi^*)$ state is calculated to undergo an avoided crossing with the $(\pi, 3py)$ Rydberg state (of lower vertical energy) as CH_2 twisting of the molecule occurs (Buenker et al., 1971b). The best calculations carried out to date still find the $(\pi, 3py)$ species at least 0.4 eV below the $^1(\pi, \pi^*)$ state at the ground state nuclear geometry of the molecule. This finding adds support to the idea that nonvertical transitions (Salem, 1966) are actually responsible for the absorption maximum in the V–N band system, with its unusually broad appearance (Wilkinson and Mulliken, 1955). In fact, explicit calculations of the vibrational excitation energies (Peyerimhoff and Buenker, 1972a) and associated oscillator strengths indicate that the *vertical electronic energy difference* in this instance is approximately 0.4 eV *above the location of the most probable vibrational transition*. If this result is correct the values calculated for the $^1(\pi, \pi^*)$ vertical energy are obviously much closer to the true situation than would otherwise be expected on the basis of the naive application of the Franck–Condon Principle.

In this context it should also be mentioned that the origin of the $^1(\pi, \pi^*)$ band is calculated to lie at 6.3 eV in the CI (32) treatment, in wide disagreement with the value of 4.9 eV assumed (Merer and Mulliken, 1969) on the basis of extrapolation of the twisting frequency of the upper state, but in rather good agreement with the 5.9–6.0 eV estimate given more recently for this quantity by McDiarmid (1971). Closely related calculations for the ground state rotational barrier height in ethylene compare quite favorably with the corresponding experimental quantity in this case (Buenker et al., 1971b). In summary the $^1(\pi, \pi^*)$ excited state in

ethylene appears to be marked with a number of exceptional qualities not found in any of the other ethylene states nor in any of the excited species in either of its isovalent counterparts previously discussed in this section.

4. The HNO Spectrum

The electronic spectrum of HNO has not been completely characterized experimentally because of the relatively short lifetime of this system in the gas phase. Nevertheless two relatively strong transitions have been tentatively assigned (Herzberg, 1966, p. 589; Callear and Wood, 1971). Wu *et al.* (1975) have recently carried out *ab initio* SCF and CI calculations for the ground and excited states of this system, using different characteristic sets of SCF MO's as the basis for the treatment of the various states; a double-zeta AO basis augmented with diffuse functions has again been employed in this work. In all cases a core of 4 MO's has been maintained along with a valence set of 17 orbitals; the ground state CI energy lowering relative to the SCF result is 0.10 hartree in this treatment. The resulting calculated transition energies at the ground state equilibrium geometry (∡ HNO = 108.5°) are given in Table IX for comparison with existing experimental data.

There have been some questions concerning the identity of the HNO ground state, a point which is underscored by the relatively small energy difference calculated by Wu for the two lowest energy species of this

TABLE IX

CALCULATED VERTICAL TRANSITION ENERGIES (eV) FOR HNO AND COMPARISON WITH CORRESPONDING EXPER-IMENTAL DATA[a]

State	Approximate ∡ HNO	ΔE_c	Exptl.[b]
$^1A'$	108.5	0.0	0.0
$^3A''$ $(7a', 2a'')$		0.71	
$^1A''$ $(7a', 2a'')$	115	1.60	1.63
$2\ ^1A'$ $(2a''^2)$	180	4.27	
$^3A'$ $(1a'', 2a'')$	110	5.30	
$2\ ^3A''$ $(6a', 2a'')$	Bent	6.07	
$3\ ^1A'$ $(7a', 8a')$	Weakly bent	6.17	
$2\ ^1A''$ $(6a', 2a'')$	Bent	6.28	5.98

[a] Calculated results of Wu *et al.* (1975) and Wu (1975).
[b] Herzberg (1966) and Callear and Wood (1971).

system. Nevertheless it seems safe to say that the HNO ground state is a singlet at the equilibrium geometry (⋆ HNO = 108.5°), although it is clear that the triplet species is the more stable in the *linear* nuclear arrangement. The first allowed transition is to the $1(7a', 2a'')$ state of the same configuration as the aforementioned triplet; the calculated excitation energy is seen to agree quite well with the corresponding experimental result. The next singlet state is found to be a double-excitation species, but in all likelihood has not yet been observed experimentally. The following two singlets are of Rydberg $(7a', 3s)$ and valence-shell $(6a', 2a'')$ type, respectively, and are calculated to lie within 0.11 eV of one another. Both values are in relatively good agreement with the second experimental band center studied by Callear and Wood (1971) at 5.98 eV, which these authors have in fact assigned as the valence-shell $(6a', 2a'')$ excitation.

5. *Molecular Oxygen*

The last 12-valence-electron system to be considered in the present work is molecular oxygen, for which of course accurate potential data (Krupenie, 1972) are available for a large number of electronic states. Several CI treatments for various states of O_2 exist in the literature (Schaefer and Harris, 1968; Schaefer, 1971; Schaefer and Miller, 1971; Morokuma and Konishi, 1971) and their results are compared in Table X with the known experimental data for energy differences relative to the O_2 ground state in its equilibrium geometry [as taken directly from the experimental potential curves (Krupenie, 1972)]. In addition data obtained from several other (preliminary) CI treatments carried out by the authors are given for comparison. In both cases a standard double-zeta AO basis augmented by diffuse functions is employed; in treatment A only valence-shell MO's are allowed variable occupation (eight of π and four of σ type) and a core of four σ MO's is maintained, while in treatment B five σ species are always kept doubly occupied and the full complement of 12 π MO's in the present basis comprises the valence set, thereby allowing Rydberg $(\pi_g, 2\pi_{uR})$ excited states to be represented in the second but not in the first of these treatments. The SCF MO's of the $^3\Sigma_g^-$ ground state are used exclusively in constructing the various configurations considered in this work.

As expected the minimal-basis-set full CI treatment is moderately successful in predicting the relative locations of the various valence-shell O_2 states. Treatment A is somewhat better for the $\pi_u^3 \pi_g^3$ valence-shell species, but the use of the ground state SCF MO's tends to favor the π_g^2

TABLE X

VERTICAL TRANSITION ENERGIES (eV) FOR O_2 OBTAINED FROM SEVERAL TREATMENTS[a]

State	Minimal basis, full CI[b]	M, K[c]	A	B	Exptl.
X $^3\Sigma_g^-$ $(\pi_g)^2$	0.0	0.0	0.0	0.0	0.0
a $^1\Delta_g$ $(\pi_g)^2$	1.03	1.16	1.04	0.97	0.98
b $^1\Sigma_g^+$ $(\pi_g)^2$	1.57	1.75	1.85	1.77	1.65
c $^1\Sigma_u^-$ $(\pi_u)^3$ $(\pi_g)^3$	5.75	6.18	6.07	5.57	(5.9–6.0)
C $^3\Delta_u$ $(\pi_u)^3$ $(\pi_g)^3$	5.97	6.41	6.24	5.73	(6.0–6.2)
A $^3\Sigma_u^+$ $(\pi_u)^3$ $(\pi_g)^3$	6.08	6.54	6.38	5.87	(6.3–6.5)
B $^3\Sigma_u^-$ $(\pi_u)^3$ $(\pi_g)^3$	10.25	9.51	9.74	9.85	(8.5–8.9)
$^1\Delta_u$ $(\pi_u)^3$ $(\pi_g)^3$	13.01	14.53	12.20	14.09	(11.6–12.0)
$^1\Sigma_u^+$ $(\pi_u)^3$ $(\pi_g)^3$	14.55		14.58	16.44	(13.0–13.5)
$^1\Sigma_u^-$ (π_g) $(p\pi_R)^d$				10.24 ⎫	
$^3\Delta_u$ (π_g) $(p\pi_R)$				10.30 ⎪	
$^1\Delta_u$ (π_g) $(p\pi_R)$				10.31 ⎬	
$^3\Sigma_u^+$ (π_g) $(p\pi_R)$				10.36 ⎪ (9.3–9.7)	
$^1\Sigma_u^+$ (π_g) $(p\pi_R)$		11.61		10.51 ⎪	
$^3\Sigma_u^-$ (π_g) $(p\pi_R)$				11.93 ⎭	

[a] See also Table I.

[b] The T_0 values for the minimal-basis-set full CI calculation are contained in Table III; the present values are from M, K.[c]

[c] Morokuma and Konishi (1971), values taken from their DZD CI calculation.

[d] Rydberg states.

configuration (see Section IV,B), and hence the transition energies to most of the six $\pi_u^3\pi_g^3$ species are overestimated; this is particularly true for the $^1\Delta_u$ and $^1\Sigma_u^+$ excited states, which are definitely semidiffuse in character and hence relatively poorly represented in such a valence-shell oriented treatment.

Replacing some of the σ valence MO's by diffuse π species (treatment B) allows for a reasonably good description of the $(\pi_g, 2\pi_{uR})$ Rydberg states of O_2, but at the same time this procedure leads to a relatively poorer representation of the various valence-shell states of lower energy, particularly those stemming from the π_g^2 configuration. As a result the transition energies to the three most stable $\pi_u^3\pi_g^3$ multiplets are also predicted to be somewhat smaller than their corresponding experimental values (by 0.3–0.5 eV). Nevertheless the opposite trend is noted for both the $^1\Delta_u$ and $^1\Sigma_u^+$ semidiffuse multiplets of the $\pi_u^3\pi_g^3$ configuration and also for the various $\pi_g p\pi_R$ Rydberg series, thereby indicating that larger

valence sets are needed before Rydberg and valence species of the same symmetry can be *simultaneously* represented in a satisfactory manner.

More extensive CI calculations using the selection techniques described in Section IV,B are clearly needed in order to bring the level of the theoretical treatment for O_2 more nearly in line with what has been employed for the other systems discussed earlier in this section.

NOTE ADDED IN PROOF

Since completion of this manuscript such calculations have been reported [Buenker and Peyerimhoff (1975a,b)] and quite good agreement with the experimental transition energies for this system has been obtained.

B. Interpretation of the Calculated Data

Regardless of how accurate spectral calculations become in the near future there will still be a need for a good qualitative model with which to organize and analyze the corresponding experimental results in a consistent and intuitively reasonable manner. The molecular orbital theory approaches this goal through an independent particle model in which differences in orbital energy levels are used to approximate transition energies between corresponding molecular states. To a good extent the broad outlines of this scheme can be realized in *ab initio* calculations through the use of a canonical orbital energy correlation diagram such as that shown in Fig. 3 (only results for MO's occupied in the ground state are included in each case). In particular it is instructive to examine the manner in which the relative location of corresponding orbital energy levels in such a diagram varies from one system to another.

The stability of the π-type MO, for example, is seen to decrease in a monotonic fashion from O_2 to C_2H_4 as the composition of this orbital changes from the p AO's of oxygen to those of carbon. Thus the energy difference between the n and π MO is significantly smaller in H_2CO than between the corresponding levels in HNO (the composition of the n orbital is quite similar in both cases). The presence of the hydrogen atom in (bent) HNO leads to a splitting of the formerly degenerate π (and also π^*) levels of O_2, with the in-plane component being selectively stabilized through mixing with the hydrogen 1s AO. Similarly the splitting between the corresponding levels in H_2CO and C_2H_4 becomes even larger, with
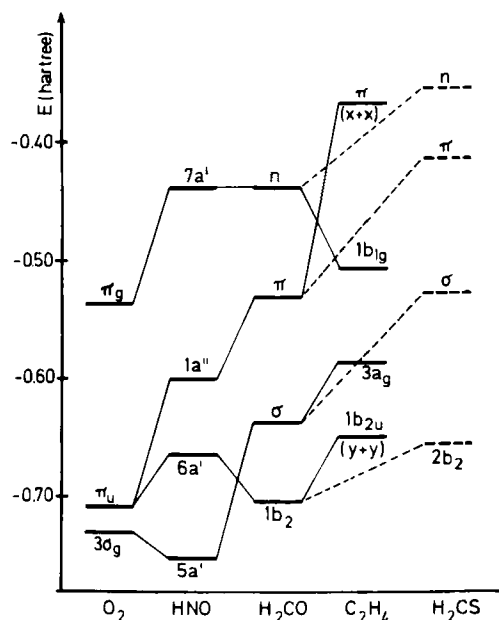
Fig. 3. Correlation of canonical orbital energies in several molecules containing 12 valence electrons.

more hydrogens involved in these systems. This fact leads to an inversion in the highest (originally) σ- and lowest (originally) π-type levels in H_2CO relative to HNO, with the effect that $\sigma \rightarrow \pi^*$ transitions occur at relatively low energy in the former system but not in the latter, for example. The effect of the constituent H atoms becomes even more critical for ethylene, in which *all* of the in-plane MO's gain considerable stability as a result of interaction with hydrogen AO's (at least for the planar molecule), and this in turn leads to the result that the π MO is the highest occupied species in this case, in distinct contrast to the other 12-valence-electron species discussed earlier. In comparing H_2CO and H_2CS the major effects quite naturally stem from the interchange of sulfur and oxygen; MO's which have a great deal of O character in formaldehyde, such as the n and π species, are considerably less stable in thioformaldehyde (because of the smaller electronegativity of sulfur), whereas those composed mainly of carbon AO's are much less affected.

The general orbital energy trends noted above are apparent in the corresponding transition energy data, at least as long as attention is

restricted to the lowest energy multiplets of each configuration. The intra-valence $\pi \rightarrow \pi^*$ transition energy, for example, increases from ethylene to O_2, while that for the $n \rightarrow \pi^*$ excitations shows the opposite behavior; as a result no transitions out of the $n(1b_{1g})$ MO of ethylene are expected below 9.0 eV. As remarked earlier differences in H_2CO and H_2CS results are also understandable on the basis of the corresponding orbital energy data. The same type of argumentation is valid for Rydberg excitations because of the role the ionization potential plays in determining the energy location of species of this type. The underlying principle in all of this discussion is essentially that of Koopmans' theorem, and as a result one can only expect to obtain satisfactory results with such a simple model as long as the constitution of the various MO's of interest does not vary greatly from one system to another (i.e. as long as the basic assumption of Koopmans' theorem remains valid).

No matter how well the simple orbital energy model can account for the stability of *electronic configurations* in a given system, such an approach can never be entirely adequate without considering the relative energetics of the individual multiplets contained within each such species. As shown in Section V,A the magnitudes of the triplet–singlet energy splittings vary widely between different electronic configurations, but these results can generally be understood for nondegenerate systems in terms of key exchange integrals connecting initial and final MO's in the transitions of interest.

Although the situation is somewhat more complicated for degenerate species, similar reasoning is quite often possible. In diatomic molecules, for example, Σ^+ states result when the open-shell component MO's lie in the *same* plane while in Σ^- species the analogous MO's must be found in mutually perpendicular planes; Δ states fall somewhere in between these two extremes. These considerations lead to the familiar energy ordering of π^2 multiplets, namely $^3\Sigma^- < ^1\Delta < ^1\Sigma^+$. They also provide at least a qualitative explanation for the observed triplet–singlet splittings for $\pi\pi$ (or $\pi_u^3\pi_g^3$) electronic configurations in such systems, with $^{3,\,1}\Sigma^-$ splittings being much smaller than those for Σ^+ states, and $^{3,\,1}\Delta$ energy differences again falling somewhere in between. In the case of the $\pi_g p\pi_R$ Rydberg states of O_2 the splittings are all much smaller than for multiplets of the same *valence-shell* configuration, again as expected, although the results of Table X do contain an apparent violation of the aforementioned rules, namely with respect to the large energy difference calculated for the $^{3,\,1}\Sigma_u^- \pi_g p\pi_R$ states. But this finding is closely connected with the fact

that the $^3\Sigma_u^-$ Rydberg species lies very close to the $\pi_u^3\pi_g^3$ valence-type multiplet of the same symmetry; hence it is impossible for the limited treatment employed in this work to obtain a proper representation for both of these O_2 states. Finally it should be mentioned that the same trends in valence-shell multiplet splittings are observed in the spectra of the 10-valence-electron species N_2 and acetylene C_2H_2, leading, for example, to an inversion in the order of the singlet states arising from the important $\pi_u^3\pi_g$ configuration relative to the order of the corresponding triplets (Buenker and Peyerimhoff, 1968; Kammer, 1970, 1974).

VI. Outlook for Future Calculations

In the calculations discussed in the preceding section attention has been centered primarily on predicting the location of the intensity maxima in electronic transitions. It is clear, however, that the ultimate goal in such work is to be able to predict details concerning the pattern of the intensity variation in an entire electronic band system, including the location and strength of individual vibrational and rotational lines (in addition to the total oscillator strength of the transition). Some progress in this direction has been made in the past few years but further work in these areas is definitely necessary if unambiguous assignments of electronic transitions on a purely theoretical basis are to become possible on a general scale. A number of points germane to this aspect of electronic spectral calculations will be taken up in the remaining section of this article, and in addition an attempt will be made to identify possible sources of error in the more conventional investigations on this general subject, namely in determinations of transition energies between ground and excited states of many-electron systems.

A. Calculation of Structural Characteristics of Electronic Transitions

The Franck–Condon method for calculating details of the electronic spectra of molecules is well-known, being derived in a straightforward manner from the Born–Oppenheimer approximation. In its simplest form all that is required is a knowledge of at least a portion of the potential energy surfaces of both ground and excited electronic states (from which vibrational wavefunctions are to be computed), in addition to the value of

the corresponding electronic transition moment calculated for the equilibrium nuclear conformation of the ground state. The intensities of individual vibrational transitions are simply assumed to be proportional to the squares of the overlaps of corresponding vibrational wavefunctions (Franck–Condon factors) in this procedure. For more detailed work it is necessary to compute the electronic transition moment as a function of nuclear geometry rather than at a single point, but for dipole-allowed transitions this additional effort generally does not lead to any significant change in the calculated results. More details concerning the computations involved in this theoretical method can be found in a recent treatment of the vibrational characteristics of various electronic transitions of ethylene (Peyerimhoff and Buenker, 1972a). The treatment of rotational transitions can be carried out in a completely analogous fashion.

A fairly typical example of this kind is the calculation of the vibrational structure of the N–R transition in C_2H_4. The potential curve for CH_2 twisting in the R $^1(\pi, 3s)$ state of ethylene is given in Fig. 4, complete with calculated vibrational energy levels; analogous results have been obtained for the electronic ground state N, and corresponding CC-stretch potential curves have also been calculated. When these data are used in the above-mentioned Franck–Condon formalism, the series of vibra-
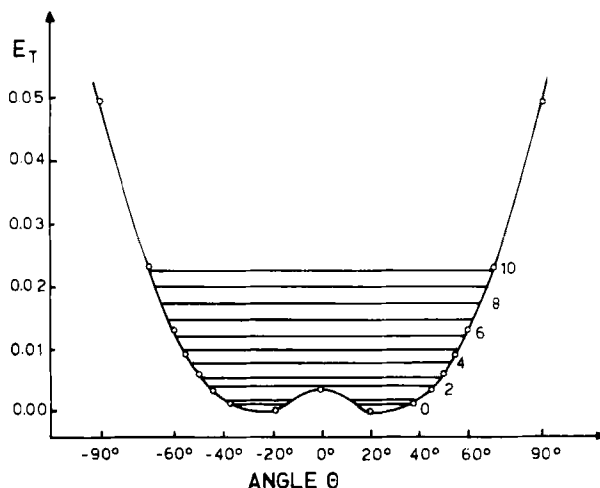
Fig. 4. Calculated CH_2 twisting potential curve and vibrational levels for the R state in ethylene. From Peyerimhoff and Buenker (1972), with permission.

tional oscillator strengths given in Table XI ensues. A progression of doublets in the upper state stretching frequency v'_2 is found, with maximum intensity almost equally divided in each case between the $v'_4 = 0$ and $v'_4 = 1$ twisting vibrational states of the R species. Quite similar behavior is in fact observed experimentally for the N–R band system, and indeed for all other Rydberg series of the C_2H_4 system.

TABLE XI

TABULATION OF THE CALCULATED OSCILLA-
TOR STRENGTHS FOR THE R–N TRANSITION OF
ETHYLENE[a]

v'_4	$v'_2 = 0$	$v'_2 = 1$	$v'_2 = 2$
0	0.0192	0.0138	0.0060
2	0.0196	0.0141	0.0062
4	0.0091	0.0065	0.0029
6	0.0026	0.0019	0.0008
8	0.0008	0.0005	0.0002
10	0.0002	0.0002	0.0001
12	0.0001	0.0001	0.0000
14	0.0000	0.0000	0.0000
16	0.0000	0.0000	0.0000
Σ	0.0516	0.0371	0.0162

[a] All results are obtained relative to the lowest vibrational level of the ^1A_g ground state $(v''_2 = 0, \ v''_4 = 0)$. Peyerimhoff and Buenker (1972a).

From a more general point of view an interesting aspect of this calculation is the finding that the location of the *most probable* transition (ΔE_{max}) is at least 0.2 eV below the value calculated for the so-called *vertical* energy difference ΔE_e between these electronic states. This result clearly emphasizes that a certain amount of caution must be exercised in equating calculated ΔE_e values with the location of the intensity maxima in the corresponding observed band system. Discrepancies between ΔE_e and ΔE_{max} values are expected to be especially large in situations for which the excited state potential surface possesses a *maximum* at the

nuclear arrangment which is optimal for the electronic ground state, as it does, for example, in the case of the $^1(\pi, \pi^*)$ transition discussed in Section V,A,3.

B. Possible Improvements in Transition Energy Calculations

In addition to seeking a realistic description of the intensity distribution in electronic band systems there is also a need to improve the accuracy with which calculations can predict the *relative stabilities* of different electronic states in a given system. The treatments of the various 12-valence-electron molecules discussed in Section V,A have shown that relatively simple CI calculations employing an adequate AO (and MO) basis can yield reasonably reliable estimates of vertical transition energies, oftentimes to within a few tenths of an electron volt of the corresponding experimental quantity. Nevertheless more extensive calculations are clearly required before further improvement in the agreement between theory and experiment can be expected. As efforts proceed in this direction a discussion of possible errors in the theoretical methods seems appropriate.

Calculations for accurate transition energy values require only that an *equalization* of the correlation energy errors inherent in the description of the various states be achieved and not necessarily that an accurate determination of the *total* correlation energy be carried through. In other words when considering the impact of a given technical development in such calculations the question is always whether it can be expected to have a *selective* influence on some electronic states relative to others. At the present time data from existing calculations allow some fairly general conclusions to be drawn concerning the effects of a number of commonly employed approximations in the context of such theoretical investigations.

The choice of orbital transformation employed in CI calculations is quite important, particularly for relatively limited CI treatments. For states of greatly different character use of the same set of MO's in such calculations can easily lead to errors in transition energies of more than 1.0 eV (see Section IV,A). For CI treatments employing configuration selection in which essentially all orbitals are allowed variable occupation much smaller discrepancies are expected, but results obtained for the same state with different sets of MO's can still vary by several tenths of an electron volt (Buenker and Peyerimhoff, 1974a). In addition for states which are represented by several dominant configurations approximate

natural orbitals often lead to improvements of 0.1–0.2 eV compared to the analogous results obtained from use of the corresponding SCF MO's.

The effect of employing a larger core in the CI treatment is more difficult to judge but indications are that proper allowance for electron reorganization through the use of different (optimized) sets of MO's greatly minimizes the influence of such restrictions on transition energy results. Similarly addition of polarization functions to the AO basis does not seem to have a profound effect on the relative location of the various states, at least as long as such species are optimized via SCF techniques, thereby emphasizing the description of only the set of occupied MO's of the leading configuration. In ethylene, for example, transition energies to all Rydberg states (Table VIII) are lowered by roughly the same amount (0.1 eV) upon inclusion of such functions. Especially since it appears that the *vertical* energy differences obtained for these species (compared to the ground state) are already underestimated [by 0.2 eV in the CI(32) calculation, for example], even without the use of such functions, other factors must also clearly be involved in producing the observed discrepancies between calculated and experimental transition energies in such systems.

This view is further supported by calculations for the $C_2H_4^+$ ion, which yield a minimum I.P. in the CI(32) treatment which is 0.4 eV above the corresponding experimental value. Furthermore, just as for the $^1(\pi, 3s)$ Rydberg state, addition of polarization functions is observed to worsen the agreement by an additional 0.1 eV. The fact that *SCF transition energies* to the C_2H_4 Rydberg states and positive ion underestimate the corresponding experimental quantities by *much greater margins* demonstrates that the CI treatments carried out to date only partially account for the actual differences in correlation energy between the ground and excited states of such molecules. Thus it seems reasonable to conclude that basis functions which improve the representation of important configurations other than the leading species, or in other words, functions which are optimized in the CI treatment itself in order to specifically account for electron correlation effects, are also necessary in general in order to afford more accurate determinations of transition energy values. Without such functions CI treatments can quite generally be expected to lead to transition energy *errors* which, *though significantly smaller*, continue to be *in the same direction* as in the corresponding SCF calculations. By the same token it seems quite likely that the aforementioned discrepancies will be smallest for states of essentially the same character, and from this point of view the generally good agreement found to exist for calculated and experimental energy differences between the ground

state and at least the most compact of the Rydberg species (which clearly possess far different characteristics than the corresponding ground state) must be counted as an encouraging development in this general study.

REFERENCES

Basch, H., and McKoy, V. (1970). *J. Chem. Phys.* **53**, 1628.
Bender, C. F., and Davidson, E. R. (1967). *J. Chem. Phys.* **46**, 3313.
Bender, C. F., Dunning, T. H., Jr., Schaefer, H. F., III, and Goddard, W. A. (1972). *Chem. Phys. Lett.* **15**, 171.
Betts, T., and McKov, V. (1971). *J. Chem. Phys.* **54**, 113.
Bruna, P., Peyerimhoff, S. D., Buenker, R. J., and Rosmus, P. (1974). *Chem. Phys.* **3**, 35.
Buenker, R. J., and Peyerimhoff, S. D. (1968). *J. Chem. Phys.* **48**, 354 (Appendix II).
Buenker, R. J., and Peyerimhoff, S. D. (1970). *J. Chem. Phys.* **53**, 1368.
Buenker, R. J., and Peyerimhoff, S. D. (1974a). *Theor. Chim. Acta* **35**, 33.
Buenker, R. J., and Peyerimhoff, S. D. (1974b). *Chem. Rev.* **74**, 127.
Buenker, R. J., and Peyerimhoff, S. D. (1975a). *Chem. Phys.* **8**, 324.
Buenker, R. J., and Peyerimhoff, S. D. (1975b). *Chem. Phys. Lett.*, in press.
Buenker, R. J., and Peyerimhoff, S. D. (1975c). *Chem. Phys.* **8**, 56.
Buenker, R. J., and Whitten, J. L. (1968). *J. Chem. Phys.* **49**, 5381.
Buenker, R. J., Whitten, J. L., and Petke, J. D. (1968). *J. Chem. Phys.* **49**, 2261.
Buenker, R. J., Peyerimhoff, S. D., and Kammer, W. E. (1971a). *J. Chem. Phys.* **55**, 814.
Buenker, R. J., Peyerimhoff, S. D., and Hsu, H. L. (1971b). *Chem. Phys. Lett.* **11**, 65.
Callear, A. B., and Wood, P. M. (1971). *Trans. Faraday Soc.* **67**, 3399.
Chan, A. C. H., and Davidson, E. R. (1968). *J. Chem. Phys.* **49**, 727.
Chan, A. C. H., and Davidson, E. R. (1970). *J. Chem. Phys.* **52**, 4108.
Davidson, E. (1974). *Proc. Int. Congr. Quantum Chem., 1st, Menton,* p. 17.
Dumbacher, B. (1972). *Theor. Chim. Acta* **23**, 346.
Dunning, T. H., Jr., Hosteny, R. P., and Shavitt, I. (1973). *J. Amer. Chem. Soc.* **95**, 5067.
Fischbach, U. (1973). Diplomarbeit Mainz.
Fischbach, U., Buenker, R. J., and Peyerimhoff, S. D. (1974). *Chem. Phys.* **5**, 265.

Fischer-Hjalmars, I., and Kowalewski, J. (1972). *Theor. Chim. Acta* **27**, 197.
Fischer-Hjalmars, I., and Kowalewski, J. (1973). *Theor. Chim. Acta* **29**, 345.
Fougere, P. F., and Nesbet, R. K. (1966). *J. Chem. Phys.* **44**, 285.
Gershgorn, Z., and Shavitt, I. (1968). *Int. J. Quantum Chem.* **2**, 751.
Hay, P. J., and Shavitt, I. (1973). *Chem. Phys. Lett.* **22**, 33.
Hay, P. J., and Shavitt, I. (1974). *J. Chem. Phys.* **60**, 2865.
Henneker, W. H., and Popkie, H. E. (1971). *J. Chem. Phys.* **54**, 1763.
Herzberg, G. (1966). "Molecular Spectra and Molecular Structure," Vol. 3. Van Nostrand-Reinhold, Princeton, New Jersey.
Huo, W. M. (1968). *J. Chem. Phys.* **49**, 1482.
Huzinaga, S. (1962). *J. Chem. Phys.* **36**, 453.
Kammer, W. E. (1970). *Chem. Phys. Lett.* **6**, 529.
Kammer, W. E. (1974). *Chem. Phys.* **5**, 408.
Kouba, J., and Öhrn, Y. (1970a). *J. Chem. Phys.* **52**, 5387.
Kouba, J., and Öhrn, Y. (1970b). *J. Chem. Phys.* **53**, 3923.
Krupenie, P. H. (1972). *J. Phys. Chem. Ref. Data* **1**, 423.
Langhoff, S. R., Elbert, S. T., Jackels, C. F., and Davidson, E. R. (1974). *Chem. Phys. Lett.* **29**, 247.
McDiarmid, R. (1971). *J. Chem. Phys.* **55**, 4669.
Mentall, J. E., Gentien, E. P., Krauss, M., and Neumann, D. (1971). *J. Chem. Phys.* **55**, 5471.
Merer, A. J., and Mulliken, R. S. (1969). *Chem. Rev.* **69**, 639.
Morokuma, K., and Konishi, H. (1971). *J. Chem. Phys.* **55**, 402.
Mulliken, R. S. (1942). *Rev. Mod. Phys.* **14**, 765.
Mulliken, R. S. (1974). *Chem. Phys. Lett.* **25**, 305.
Pariser, R., and Parr, R. (1953). *J. Chem. Phys.* **27**, 767.
Peyerimhoff, S. D., and Buenker, R. J. (1970). *Theor. Chim. Acta* **19**, 1.
Peyerimhoff, S. D., and Buenker, R. J. (1972a). *Theor. Chim. Acta* **27**, 243.
Peyerimhoff, S. D., and Buenker, R. J. (1972b). *Chem. Phys. Lett.* **16**, 235.
Peyerimhoff, S. D., and Buenker, R. J. (1974). *Proc. NATO Advan. Study Inst. Chem. Spectrosc. Photochem. Vac. Ultraviolet*, p. 257.
Peyerimhoff, S. D., Buenker, R. J., Kammer, W. E., and Hsu, H. L. (1971). *Chem. Phys. Lett.* **8**, 129.
Phillipson, P. E., and Mulliken, R. S. (1958). *J. Chem. Phys.* **28**, 1248.
Popkie, H. E. (1971). *J. Chem. Phys.* **54**, 4597.
Popkie, H. E., and Henneker, W. E. (1971). *J. Chem. Phys.* **55**, 617.
Pople, J. A., and Sidman, J. W. (1957). *J. Chem. Phys.* **27**, 1270.
Price, W. C., and Walsh, A. D. (1940). *Proc. Roy. Soc., Ser. A* **174**, 220.
Roothaan, C. C. J., and Bagus, P. S. (1963). *Methods Comput. Phys.* **2**, 48.
Ryan, J. A., and Whitten, J. L. (1972). *Chem. Phys. Lett.* **15**, 119.
Salem, L. (1966). "The Molecular Orbital Theory of Conjugated Systems," p. 364. Benjamin, New York.
Schaefer, H. F., III (1971). *J. Chem. Phys.* **54**, 2207.
Schaefer, H. F., III (1972). "The Electronic Structure of Atoms and Molecules: A Survey of Rigorous Quantum Mechanical Results." Addison-Wesley, Reading, Massachusetts.
Schaefer, H. F., III, and Harris, F. E. (1968). *J. Chem. Phys.* **48**, 4946.
Schaefer, H. F., III, and Miller, W. H. (1971). *J. Chem. Phys.* **55**, 4107.
Shih, S., Buenker, R. J., and Peyerimhoff, S. D. (1972). *Chem. Phys. Lett.* **16**, 244.
Thulstrup, E. W., and Öhrn, Y. (1972). *J. Chem. Phys.* **57**, 3716.

Tseng, T.-J., and Grein, F. (1974). "Low-lying Valence States of the PO Molecule According to Configuration Interaction Calculations," preprint communicated to the authors.

Whitten, J. L. (1972). *J. Chem. Phys.* **56**, 5458.

Whitten, J. L., and Hackmeyer, M. (1969). *J. Chem. Phys.* **51**, 5584.

Wilkinson, P. G., and Mulliken, R. S. (1955). *J. Chem. Phys.* **23**, 1895.

Wu, A. (1975). *Theor. Chim. Acta,* in press.

Wu, A., Peyerimhoff, S. D., and Buenker, R. J. (1975). *Chem. Phys. Lett.,* in press.

Yeager, D. L., and McKoy, V. (1974). *J. Chem. Phys.* **60**, 2714.

Time-Independent Diagrammatic Approach to Perturbation Theory of Fermion Systems

J. PALDUS and J. ČÍŽEK*

Quantum Theory Group
Departments of Applied Mathematics and Chemistry
University of Waterloo, Waterloo, Ontario, Canada

* *Present address:* Centre de Mécanique Ondulatoire Appliquée, Centre National de la Recherche Scientifique, Paris, France.

"... For some time I have been worrying about what new developments in
theoretical chemistry are likely to be most important in the next 10–15 years. One
has to hazard a guess. Twenty years ago we opted for group theory, and turned
out to be absolutely right.... Today something new must be encouraged. Rightly
or wrongly we have decided on diagram methods. ..."

C. A. COULSON (1910–1974)
(*Progress Report, Theoretical Chemistry Department
of Oxford University, 1972–1973*)

I. Introduction

Over the past decade we have been working on the development of a
time-independent form of the diagrammatic approach to the many-body
problem, which we have used in a variety of applications. This approach
is based on the second quantization formalism, the time-independent
form of Wick's theorem, and, finally, on Feynman-like diagrams. The
main characteristic of our approach, as opposed to those of Goldstone
(1957), Bloch (1958a,b), Hubbard (1957, 1958a,b), Tolmachev (1963a,b,
1969), Kelly (1964, 1968, 1969) and others (e.g., cf. Morrison, 1968; Fetter
and Walecka, 1971) is that while these latter derivations are invariably
based on the time-dependent theory of the S-matrix, our formalism is
strictly time-independent. In fact, the use of time-dependent theory seems
to be an unnecessary complication if one is only interested in stationary
problems. Our approach resembles most nearly that of Brandow (1967),
and to some extent, at least conceptually, that of Hugenholtz (1957), even
though we do not use the resolvent and convolution techniques, which
are basic characteristics of the latter approach.[1]

Indeed, a straightforward introduction of diagrams to the second
quantized form of the problem and a graphical interpretation of the
time-independent Wick theorem makes it possible to obtain rather easily
the answers to many complex problems. Using this technique, we were
able to derive the general equations determining the cluster expansion

[1] The formalism of Hugenholtz (1957) is in fact, roughly speaking, a Fourier transform
of Goldstone (1957) formalism.

components of the exact closed-shell wavefunction (Čížek, 1966, 1969), and obtain formulas, which are readily used in practice, including all linked doubly and the most important triply excited clusters (Paldus *et al.*, 1972a). Further, we were able to generalize the Thouless (1972) stability conditions to the simple open-shell case and define the so-called doublet instabilities (Paldus and Čížek, 1969, 1970) as well as to derive the stability conditions for the Brueckner (maximum overlap) wavefunctions (Paldus *et al.*, 1973). We also derived, using this technique, very compact expressions for the configuration interaction matrix elements between the spin symmetry adapted mono- and doubly-excited configurations for all pertinent spin multiplets. Finally, we were able to use this formalism to derive general expressions for the matrix elements of one-, and two-particle operators between arbitrary antisymmetrized products of geminals, that is either strongly or weakly orthogonal, nonorthogonal, or identical ones (Paldus, 1972; Paldus *et al.*, 1972b). In fact, the well-known Rumer diagrams of the valence bond theory may be shown to represent a special case of these general diagrams introduced for calculations with geminal-type wavefunctions. In all these cases the time-independent approach proved to be not only very simple and straightforward but also very effective.

In our recent paper (Paldus and Čížek, 1974; see also Čížek and Paldus, 1972) dealing with the direct calculation of excitation energies we have used a more conventional, and for the given problem certainly a very appropriate approach; that of the Green function formalism. Indeed, in this formalism the excitation energies appear very naturally as the poles of the Fourier transform of the double time particle–hole Green function.

The advantages of the direct calculation of excitation energies, compared with the approach in which the total energies of the pertinent electronic states are calculated separately for each state and then the excitation energies are obtained by subtracting the appropriate state energies, are quite obvious. The situation here is not unlike the direct calculation of correlation effects, dissociation energies, and many other important quantities, which are given as the energy difference of pertinent states. These differences are usually very small compared to the total energy of the states concerned.

Particularly in the case of the perturbation calculation of the excitation energies the direct approach will avoid the calculation of the most difficult terms, which enter the total energies of both pertinent states and exactly cancel each other when the difference is taken, as was first shown by Malrieu *et al.* (1967) and Malrieu (1967).

There is little doubt that the Green function formalism is the most natural one to use for this problem as we have already stated. Unfortunately, this formalism does not yet seem to be a standard item in the conventional quantum chemists "toolbox." More importantly, the use of this rather complex time-dependent formalism for the excitation energy calculations, which is basically a stationary problem, may be rather confusing at first sight. Indeed, this is very much the same argument which has been used with respect to the derivation of Goldstone's perturbation theory using the S-matrix formalism. The same S-matrix formalism is used in the perturbative approach to the Green functions. In fact, as Brandow (1967) showed, and as follows easily from the general coupled-pair many electron formalism (Čížek, 1966, 1969), the Goldstone perturbation theory may indeed be obtained in a much more straightforward manner, without using the time-dependent formalism.

We would like to show in this paper that even the Rayleigh–Schrödinger perturbation expressions for the direct calculation of the excitation energies may be obtained in a rather simple way without involvement of the Green function formalism. This is not intended to imply that the Green function formalism is an unnecessary complication to this problem, which should be used only for the study of more complex time-dependent phenomena. On the contrary, our simple approach using the ordinary perturbation theory for separate levels will show very clearly certain desirable features of the Green function formalism. For example, the so-called "double projection" scheme we have proposed (Paldus and Čížek, 1974; Čížek and Paldus, 1972), which enables one to obtain very compact perturbation expressions for the excitation energies, particularly for the higher orders, would be difficult to discover without using the Green function formalism. On the other hand, when we combine the classical perturbative approach with the time-independent diagrammatic technique mentioned at the outset, we will be able to show these formulas from a different point of view. Further, we will be able to demonstrate how effective these graphical methods may be and how clearly they indicate the above-mentioned cancellations.

The significance of such an approach is not only pedagogical. Indeed, very much the same *time-independent* techniques may be employed for a number of other very important problems, as indicated earlier. We feel very strongly that this technique, eventually coupled with the graph theoretical methods of spin algebras, is extremely powerful and useful.

We would also like to point out briefly that in a similar manner we can derive the Rayleigh–Schrödinger perturbation expansion for ioniza-

tion potentials and electron affinities, which in turn may be obtained directly as poles of the pertinent Fourier transformed one-particle Green functions (cf. Csanak *et al.*, 1971; Reinhardt and Doll, 1969; Reinhardt and Smith, 1973; Doll and Reinhardt, 1972). These quantities have been computed using the Green function technique (in the Brillouin-Wigner perturbative form) by the Münich group (Ecker and Hohlneicher, 1971; Cederbaum *et al.*, 1971, 1973; Albat, 1972) and in the Rayleigh–Schrödinger form by Hubač *et al.* (1973). In fact, the pertinent formulas may be obtained easily as a special case of the excitation energy expressions, using the class of so-called self-energy diagrams (Paldus and Čížek, 1974). We will show briefly how the same formulas may be obtained with the simple time-independent approach, just as in the excitation energy case.

Finally, we will present in this paper much more general formulas for the direct calculation of the excitation energies than those given earlier, which were limited to the use of a ground state Hartree–Fock molecular orbital basis. It is well-known that this is not the best basis to use if we want to get a rapidly converging perturbation expansion (Kelly, 1968, 1969). We will thus present the general formulas up to and including the third order of perturbation theory based on an arbitrary one-electron basis.

In the limited space available to us here we cannot give a detailed and complete account of the time-independent diagrammatic technique which we shall be using. We sincerely hope, however, that together with the numerous previous applications using this approach, the reader will not only get a better understanding of the Green function and ordinary perturbative approaches, but also of the general diagrammatic time-independent technique mentioned at the outset, which makes such a comparison possible. This is indeed the primary aim of this article.

II. Rayleigh–Schrödinger Perturbation Theory for a Nondegenerate Level

In order to familiarize readers with the time-independent graphical techniques used in this paper, we will first expose them to the well-known case of the perturbation theory for a nondegenerate level. The formulas derived will also serve as a starting point for the subsequent consideration of the excitation and ionization energies. Let us first recall the Rayleigh–Schrödinger (RS) perturbation theory (PT) for the case of a nondegenerate level of some Hamiltonian operator $\hat{K}$, which may be

written as a sum of the unperturbed operator $\hat{K}_0$ and of the perturbation $\hat{W}$,

$$\hat{K} = \hat{K}_0 + \hat{W}. \tag{1}$$

We assume the exact eigenvalues and corresponding eigenvectors of $\hat{K}_0$ to be known,

$$\hat{K}_0 |\Phi_i\rangle = \kappa_i |\Phi_i\rangle, \tag{2}$$

and we are interested in the perturbation theoretical expression for the eigenvalues of the operator $\hat{K}$,

$$\hat{K} |\Psi_i\rangle = k_i |\Psi_i\rangle, \tag{3}$$

assuming that the nondegenerate state $|\Phi_i\rangle$ goes over into the state $|\Psi_i\rangle$ as the perturbation $\hat{W}$ is switched on.

As is well-known (see, e.g., Roman, 1965; Raimes, 1972) the perturbation theoretical expansion for the eigenvalue k_i has the form

$$k_i = \kappa_i + \sum_{n=0}^{\infty} \langle \Phi_i | \hat{W}[\hat{P}_i(\hat{W} + \kappa_i - k_i)]^n | \Phi_i\rangle, \tag{4}$$

where

$$\hat{P}_i = \sum_{\substack{j \\ (j \neq i)}} \frac{|\Phi_j\rangle\langle\Phi_j|}{\kappa_i - \kappa_j} = \frac{1 - |\Phi_i\rangle\langle\Phi_i|}{\kappa_i - \hat{K}_0}. \tag{5}$$

Clearly, we have that

$$\hat{P}_i |\Phi_i\rangle = 0. \tag{6}$$

Approximating k_i on the right-hand side of (4) again by the expansion (4), we can group together the terms of the same order in the coupling constant (i.e. in the perturbation $\hat{W}$) and write

$$k_i = \sum_{j=0}^{\infty} k_i^{(j)}, \tag{7}$$

where $k_i^{(j)}$ designates the jth-order contribution. The $j = 0$ term represents the unperturbed mean value,

$$k_i^{(0)} = \langle \Phi_i | \hat{K}_0 | \Phi_i\rangle, \tag{8}$$

while the first three orders are given as follows [in view of (6)]

$$k_i^{(1)} = \langle \Phi_i \mid \hat{W} \mid \Phi_i \rangle, \tag{9a}$$

$$k_i^{(2)} = \langle \Phi_i \mid \hat{W} \hat{P}_i \hat{W} \mid \Phi_i \rangle, \tag{9b}$$

$$k_i^{(3)} = \langle \Phi_i \mid \hat{W} \hat{P}_i (\hat{W} - k_i^{(1)}) \hat{P}_i \hat{W} \mid \Phi_i \rangle. \tag{9c}$$

We observe that the so-called renormalization terms appear for the first time in the third order.

The higher order terms in the RS expansion (7) may be easily obtained, if desired, by using the so-called "bracketing technique,"[2] explained in Appendix A. We shall content ourselves in this paper with the third-order contributions, since higher order terms are rather laborious to calculate in most practical applications. However, the theory may be extended along the lines indicated to any desired order.

The general formulas given above, even though very compact, are not very useful for practical calculations. In the latter case, $\hat{K}_0$ will be separable and its eigenstates will be best characterized using the occupation number representation or configuration description. Thus, the most convenient form of the expressions (9) for actual calculations will be obtained by reducing them to the form containing only the one-particle eigenvalues associated with $\hat{K}_0$ as well as the one- and two-particle matrix elements of the perturbation $\hat{W}$ in the representation of the single particle states generated by $\hat{K}_0$. Let us now show how we can obtain this form of the theory using second quantization and the diagrammatic techniques.

A. Ground State Case

Let us consider the ground state of some Hamiltonian $\hat{H}$, containing at most two-particle interactions,

$$\hat{H} = \hat{Z} + \hat{V}, \tag{10}$$

where

$$\hat{Z} = \sum_i \hat{z}(i), \qquad \hat{V} = \sum_{i<j} \hat{v}(i,j). \tag{11}$$

Assume, further, that this Hamiltonian may be approximated by the

---

[2] In order to avoid any misunderstanding we would like to stress that the "bracketing technique" described in this article is not related in any way to the "bracketing function" technique developed by Löwdin (1966).

separable unperturbed Hamiltonian $\hat{H}_0$, which we can write in the form

$$\hat{H}_0 = \hat{Z} + \hat{U}, \qquad \hat{U} = \sum_i \hat{u}(i), \tag{12}$$

$\hat{U}$ representing some one-electron approximation to $\hat{V}$ as, for example, the Hartree–Fock potential. At this stage, however, we shall not place any restrictions on $\hat{U}$, except that it enables us to obtain $\hat{H}_0$ such that the corresponding single particle states $|A\rangle$ and corresponding energies ω_A, given by

$$(\hat{z} + \hat{u})|A\rangle = \omega_A |A\rangle, \tag{13}$$

are known. Ordering these one-particle states according to their increasing eigenenergies, we shall also assume that the unperturbed N-particle ground state wavefunction $|\Phi_0\rangle$, given as an antisymmetrized product of the first N eigenstates $|A\rangle$, is nondegenerate.

Thus, we wish to find the perturbation expansion for the ground state energy of $\hat{H}$, given by the Schrödinger equation

$$\hat{H}|\Psi_i\rangle = E_i |\Psi_i\rangle \tag{14}$$

for $i = 0$, knowing the solutions of the unperturbed problem

$$\hat{H}_0 |\Phi_i\rangle = \varepsilon_i |\Phi_i\rangle. \tag{15}$$

B. Unperturbed Problem

Since we intend to use the diagrammatic technique to simplify our derivations, we shall find it very convenient to consider only the operators in the normal product (N-product) form (cf. Appendices B, C, and D). Indeed, the generalized Wick theorem (cf. Appendix C) may then be used, considerably reducing the number of terms which must be considered.

Let us therefore define new operators $\hat{K}$ and $\hat{K}_0$ to be used for the perturbation expansion as follows:

$$\hat{K} = \hat{H} - \langle\Phi_0 | \hat{H} | \Phi_0\rangle \tag{16}$$

and

$$\hat{K}_0 = \hat{H}_0 - \langle\Phi_0 | \hat{H}_0 | \Phi_0\rangle. \tag{17}$$

The unperturbed ground state $|\Phi_0\rangle$ will be used as the Fermi vacuum in the hole–particle second quantization formalism. Thus the first N spin orbitals $|A\rangle$ occupied in $|\Phi_0\rangle$ will be referred to as hole states, and the unoccupied virtual spin orbitals as particle states.

The pertinent characteristic problems now take the form

$$\hat{K} \, | \, \Psi_i \rangle = k_i \, | \, \Psi_i \rangle \qquad (18)$$

and

$$\hat{K}_0 \, | \, \Phi_i \rangle = \kappa_i \, | \, \Phi_i \rangle, \qquad (19)$$

where

$$k_i = E_i - \langle \Phi_0 \, | \, \hat{H} \, | \, \Phi_0 \rangle \qquad (20)$$

and

$$\kappa_i = \varepsilon_i - \varepsilon_0; \quad \varepsilon_0 = \langle \Phi_0 \, | \, \hat{H}_0 \, | \, \Phi_0 \rangle. \qquad (21)$$

We thus calculate the energy with respect to the ground state unperturbed energy of the system $\langle \Phi_0 \, | \, \hat{H} \, | \, \Phi_0 \rangle$.

The unperturbed eigenstates $| \, \Phi_i \rangle$ may be conveniently classified by their reference to the ground state $| \, \Phi_0 \rangle$ as mono-, bi-, tri-, etc., excited configuration states. Using the second quantization representation (cf. Appendix B) on the basis of single particle states $| \, A \rangle$, we can write a general k-fold excited configuration K as

$$| \, \Phi_K^{(k)} \rangle \equiv \left| \begin{array}{ccc} A_1'' & \cdots & A_k'' \\ A_1' & \cdots & A_k' \end{array} \right\rangle = \prod_{j=1}^{k} (\hat{X}^\dagger_{A_{j''}} \hat{X}_{A_{j'}}) \, | \, \Phi_0 \rangle, \qquad (22)$$

where the hole and particle states are labeled by singly and doubly primed capitals, respectively. The subscript K is an abbreviation for the ordered set of spin orbital indices characterizing a given configuration,

$$K \equiv (A_1'' \, \cdots \, A_k''; \, A_1' \, \cdots \, A_k'). \qquad (23)$$

The order of the terms in the product is immaterial, since the operators appear in mutually commuting pairs (all spin orbital labels in K are distinct).

Using the creation and annihilation operators $\hat{Y}^\dagger_A$ and $\hat{Y}_A$, respectively, of the hole–particle formalism, defined with respect to the Fermi vacuum $| \, \Phi_0 \rangle$ [cf. Eqs. (B.33) of Appendix B], we can rewrite (22) as

$$| \, \Phi_K^{(k)} \rangle = \prod_{j=1}^{k} (\hat{Y}^\dagger_{A_{j''}} \hat{Y}^\dagger_{A_{j'}}) \, | \, \Phi_0 \rangle. \qquad (24)$$

This notation expresses a given excitation as the creation of particle–hole pairs. Thus, we write the unperturbed problem (19) as follows:

$$\hat{K}_0 \, | \, \Phi_K^{(k)} \rangle = \kappa_K^{(k)} \, | \, \Phi_K^{(k)} \rangle, \qquad (0 \leq k \leq N), \qquad (25)$$

where $|\Phi^{(0)}\rangle \equiv |\Phi_0\rangle$; $|\Phi_K^{(k)}\rangle$ ($k > 0$) is given by (22) or (24) with K defined by (23), and

$$\kappa_K^{(k)} = \varepsilon_K^{(k)} - \varepsilon_0 = \sum_{i=1}^{k} (\omega_{A_i''} - \omega_{A_i'}). \tag{26}$$

Using this notation, the operator $\hat{P}_0$, Eq. (5), has the form

$$\hat{P}_0 = \sum_{k=1}^{N} \hat{P}_0^{(k)}, \tag{27}$$

where

$$\hat{P}_0^{(k)} = \sum_{K} \frac{|\Phi_K^{(k)}\rangle\langle\Phi_K^{(k)}|}{\kappa_0 - \kappa_K^{(k)}}, \tag{28}$$

the sum extending over all distinct k-fold excited configurations K. Since $\kappa_0 = 0$, we can write (28) more explicitly using (22) or (24) as

$$P_0^{(k)} = \sum_{\substack{A_1' < \cdots < A_k' \\ A_1'' < \cdots < A_k''}} \frac{\left| \begin{matrix} A_1'' & \cdots & A_k'' \\ A_1' & \cdots & A_k' \end{matrix} \right\rangle \left\langle \begin{matrix} A_1'' & \cdots & A_k'' \\ A_1' & \cdots & A_k' \end{matrix} \right|}{-\kappa_K^{(k)}}$$

$$= \frac{1}{(k!)^2} \sum_{\substack{A_1', \ldots, A_k' \\ A_1'', \ldots, A_k''}} \left\{ \prod_{i=1}^{k} (\hat{Y}_{A_i''}^\dagger \hat{Y}_{A_i'}^\dagger) \right\} |\Phi_0\rangle\langle\Phi_0|$$

$$\times \left\{ \prod_{j=1}^{k} (\hat{Y}_{A_j'} \hat{Y}_{A_j''}) \right\} (-\kappa_K^{(k)})^{-1}. \tag{29}$$

C. Perturbation

Consider now the perturbation $\hat{W}$,

$$\hat{W} = \hat{K} - \hat{K}_0 = \hat{H} - \hat{H}_0 - \langle\Phi_0|\hat{H} - \hat{H}_0|\Phi_0\rangle$$

$$= \hat{V} - \hat{U} - \langle\Phi_0|\hat{V} - \hat{U}|\Phi_0\rangle, \tag{30}$$

which will also be cast in the N-product form. In second quantization we have (cf. Appendix B)[3]

$$\hat{Z} = \sum_{A, B} \langle A|\hat{z}|B\rangle \hat{X}_A^\dagger \hat{X}_B, \qquad \hat{U} = \sum_{A, B} \langle A|\hat{u}|B\rangle \hat{X}_A^\dagger \hat{X}_B,$$

---

[3] Note that the order of operators in (31) is different from the order of the indices in the matrix element.

and

$$\hat{V} = \frac{1}{2} \sum_{A, B, C, D} \langle AB | \hat{v} | CD \rangle \hat{X}_A^\dagger \hat{X}_B^\dagger \hat{X}_D \hat{X}_C .\qquad(31)$$

We shall designate the pertinent N-product form of these operators by the subscript N, for example

$$\hat{V}_N = \frac{1}{2} \sum_{A, B, C, D} \langle AB | \hat{v} | CD \rangle N[\hat{X}_A^\dagger \hat{X}_B^\dagger \hat{X}_D \hat{X}_C],\qquad(32)$$

with the N-product defined with respect to the Fermi vacuum $| \Phi_0 \rangle$ (cf. Appendices B and D), so that

$$\hat{V} - \langle \Phi_0 | \hat{V} | \Phi_0 \rangle = \hat{V}_N + \hat{G}_N ,\qquad(33)$$

where

$$\hat{G}_N = \sum_{A, B} \langle A | \hat{g} | B \rangle N[\hat{X}_A^\dagger \hat{X}_B],\qquad(34)$$

and

$$\langle A | \hat{g} | B \rangle = \sum_{C'} \langle AC' | \hat{v} | BC' \rangle_A ,\qquad(35)$$

where

$$\langle AB | \hat{v} | CD \rangle_A = \langle AB | \hat{v} | CD \rangle - \langle AB | \hat{v} | DC \rangle\qquad(36)$$

is the antisymmetrized matrix element of the two-particle potential $\hat{v}$. The operator $\hat{g}$ represents, in fact, the Hartree–Fock potential.

Similarly

$$\hat{U} - \langle \Phi_0 | \hat{U} | \Phi_0 \rangle = \hat{U}_N ,\qquad(37)$$

so that finally

$$\hat{W} = \hat{Q}_N + \hat{V}_N = \hat{W}^{(1)} + \hat{W}^{(2)},\qquad(38)$$

where

$$\hat{W}^{(1)} \equiv \hat{Q}_N = \hat{G}_N - \hat{U}_N, \qquad \hat{W}^{(2)} \equiv \hat{V}_N\qquad(39)$$

and

$$\langle A | \hat{q} | B \rangle = \langle A | \hat{g} | B \rangle - \langle A | \hat{u} | B \rangle.\qquad(40)$$

Thus, the perturbation $\hat{W}$ consists now of one- and two-particle parts $\hat{Q}_N$ and $\hat{V}_N$, respectively, both in the N-product form. We see immediately

that choosing our single particle potential $\hat{U}$ to be the Hartree–Fock potential, the perturbation $\hat{W}$ contains only the two-particle part. However, for the arbitrary one-particle potential $\hat{U}$, which we consider, both one- and two-particle parts of $\hat{W}$ must be taken into account, the one-particle part being given by the difference between the Hartree–Fock potential and the chosen potential $\hat{U}$.

III. Diagrammatic Method

We now have the creation and annihilation operators in both $\hat{W}$ and $\hat{P}$ in the normal product form, since $\hat{P}_0^{(k)}$ may also be written as

$$\hat{P}_0^{(k)} = \frac{1}{(k!)^2} \sum_{\substack{A_{1'} \cdots A_{k'} \\ A_{1''} \cdots A_{k''}}} \{ N[\hat{Y}^{\dagger}_{A_{1''}} \hat{Y}^{\dagger}_{A_{1'}} \cdots \hat{Y}^{\dagger}_{A_{k''}} \hat{Y}^{\dagger}_{A_{k'}}] \, |\Phi_0\rangle\langle\Phi_0|$$

$$\times N[\hat{Y}_{A_{k'}} \cdots \hat{Y}_{A_{1''}}]/(-\kappa_K^{(k)})\}. \quad (41)$$

The problem of calculating the expressions of the type (9) then reduces to the calculation of Fermi vacuum mean values of various N-products of the creation and annihilation operators. We can conveniently exploit the generalized Wick theorem as formulated in Appendix C so that only contractions between operators appearing in different N-products must be considered. Let us recall that these contractions (pairings) must also be defined with respect to the Fermi vacuum $|\Phi_0\rangle$.

We should thus first transform all the operators $\hat{X}^{\dagger}_A, \hat{X}_A$, defined with respect to the true vacuum $|0\rangle$, into the operators $\hat{Y}^{\dagger}_A, \hat{Y}_A$, defined with respect to the Fermi vacuum $|\Phi_0\rangle$, using Eqs. (B.33). However, in the operator $\hat{W}$ the summations extend over all the spin orbital indices. Thus, in order to make this transition, we would have to replace each sum by two separate summations over the particle and hole states, respectively. Consequently, $\hat{Q}_N$ and $\hat{V}_N$ would be given by 4 and 16 different terms, respectively, differing by the number of particle and hole summations and the number of creation and annihilation operators $\hat{Y}$. Indeed, in this case the expressions for the contractions of the two $\hat{Y}$ operators are very simple [cf. Eq. (B.38)], but we would have to consider 4 and 16 different terms separately. It is thus much more convenient to use the "mixed" notation, keeping the operators $\hat{W}$ defined through the true vacuum operators $\hat{X}^{\dagger}_A, \hat{X}_A$ and to derive the contractions between these mixed operators (that is, contractions defined with respect to the Fermi vacuum), as shown in Appendix B, Eqs. (B.39).

A. Basic Graphs

The use of Wick's theorem may now be greatly facilitated by introducing a convenient graphical representation of the operators and contractions between them. This representation will be particularly useful if there is a one-to-one correspondence between the graphs and the algebraic expressions, so that one can easily make the transition from one form to the other. Let us introduce such a representation.

In general, we shall associate with each creation or annihilation operator a full oriented line attached to an appropriate vertex, characterizing a given algebraic quantity containing this operator. Moreover, the creation operator $\hat{X}_A^{\dagger}$ will be represented by an oriented line leaving the vertex, and the annihilation operator $\hat{X}_A$ by a line entering some vertex.

We shall also distinguish diagrams (graphs in which full oriented lines are labeled with spin orbital indices) from skeletons (diagrams stripped of those spin orbital indices which represent summation variables).[4] The latter are essential for the topological considerations which enable us to determine the numerical coefficients in the corresponding algebraic expressions. This is possible by assigning to each skeleton S a weight factor w_S, given as the reciprocal value of the number of all automorphisms of S, including the identical one. An automorphism of S is defined in this case as a topological deformation transforming S into itself, while all supervertices and all labeled lines (fixed labels) are also transformed into themselves. A supervertex (multiple vertex) consists of a number of simple vertices (each simple vertex having one full line entering and one leaving) connected by nonoriented lines.

Thus, the allowed topological deformations can interchange equivalent oriented unlabeled lines among themselves but not the vertices (supervertices) and distinctly labeled lines. In order to distinguish different automorphisms as defined here it is best to number consecutively all unlabeled oriented lines and, separately (say with Roman numerals), the vertices (supervertices) and labeled lines. Then the distinct automorphisms will correspond to distinct permutations of the integers, which we associated with the unlabeled oriented lines, while the vertex and labeled line numerals must always yield the identity permutation.[5] An example of

---

[4] These will be referred to as free labels, while those which are not summed over and are given *a priori* will be called fixed labels.

[5] In fact, all automorphisms of a given graph form a group and the weight factor is the reciprocal order of the group of all automorphisms. Using this representation of the automorphisms by permutations and Cayley's theorem, we can see that we can systematically find this group of automorphisms by considering all permutations of the symmetric group $\mathscr{S}_n$ and retaining those which describe some automorphism, i.e. transform a skeleton into itself without permuting the supervertices and labeled lines.
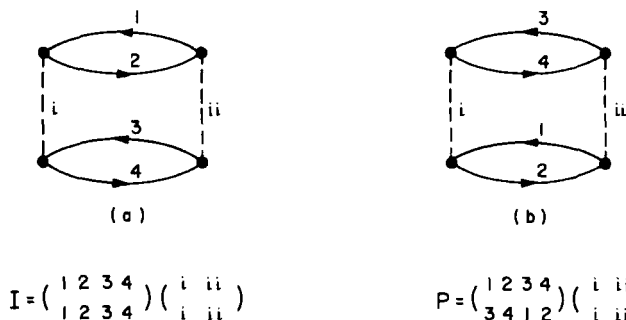
Fig. 1. An example of the identical (a) and a nontrivial (b) automorphism of the skeleton (a), used in the definition of the weight (topological) factor of the skeleton (diagram).

a graph in Fig. 1 shows that in addition to the identity permutation I, there is another permutation P, describing a nontrivial automorphism as defined above. The permutation P interchanges the simple vertices (belonging to the same supervertex) but transforms supervertices (i) and (ii) into themselves. Since, further, P is the only such nontrivial automorphism for this graph, the weight factor is $1/2$. It should also be emphasized that the numbers 1, 2, 3, and 4 are *not* labels but are simply used to distinguish the individual lines of a skeleton (see above).

We shall see later that for the perturbation theory diagrams the problem of weight factors is very simple indeed, since w can take on only two values, namely 1 and $\frac{1}{2}$.

Let us now briefly introduce the pertinent skeletons and diagrams, which we associate with the individual operators appearing in the matrix elements (9) (cf. Čížek, 1966, 1969; Paldus and Čížek, 1970; and others).[6]

With the one-particle operator $\hat{Q}_N$, Eq. (39) or (40),

$$\hat{Q}_N = \sum_{A, B} \langle A \,|\, \hat{q} \,|\, B \rangle N[\hat{X}^\dagger_A \hat{X}_B] \tag{42}$$

we shall associate the Q-skeleton, shown in Fig. 2a and the Q-diagram, shown in Fig. 2b, obtained from the Q-skeleton by labeling its oriented lines with spin orbital indices $\chi \equiv (A; B)$. The weight factor is clearly

$$w_Q = 1. \tag{43}$$

---

[6] Let us mention that originally we were using a more intuitive approach. It was the criticism of Prof. V. V. Tolmachev which motivated us to devise the formalism used here.
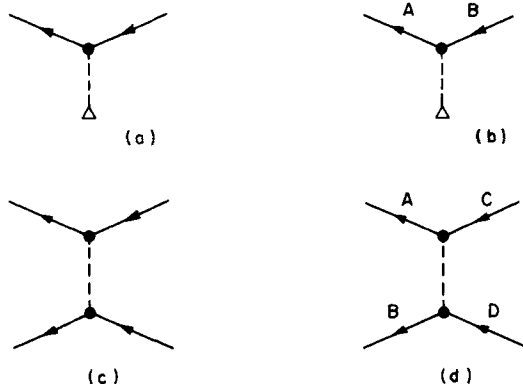
Fig. 2. Basic operator skeletons (vertices) and diagrams. (a) Q-skeleton (vertex), (b) Q-diagram, (c) V-skeleton (vertex), (d) V-diagram.

Further, with the Q-diagram (Fig. 2b) we associate the scalar quantity $d_Q(\chi)$,

$$d_Q(\chi) = \langle A \,|\, \hat{q} \,|\, B \rangle, \tag{44}$$

as well as the operator $\hat{D}_Q^N(\chi)$,

$$\hat{D}_Q^N(\chi) = d_Q(\chi) N[\hat{X}_A^\dagger \hat{X}_B]. \tag{45}$$

The pertinent vertex appearing in this skeleton (diagram) will be referred to as a Q-vertex. Notice that the outgoing and incoming lines of a Q-diagram (Fig. 2b) determine, respectively, the left- and right-hand side spin orbital in the matrix element (44) and the index of the creation and annihilation operator in (45), and are listed in the same order in the label set χ. Thus, we can write

$$\hat{Q}_N = w_Q \sum_{\chi} \hat{D}_Q^N(\chi), \tag{46}$$

the summation extending over all possible spin orbital sets χ.

Similarly, to the two-particle part $\hat{V}_N$ of $\hat{W}$, we shall assign a V-skeleton (Fig. 2c) and a corresponding V-diagram (Fig. 2d). The V-skeleton consists of a "two-particle" vertex, (called V-vertex or supervertex) indicated by two simple vertices joined by a dashed line, and of four external oriented lines. Clearly, the weight factor is

$$w_V = \tfrac{1}{2}, \tag{47}$$

the scalar quantity $d_V(\chi)$, $\chi = (A, B; C, D)$ is defined by the matrix element of the two-particle potential

$$d_V(\chi) = \langle AB | \hat{v} | CD \rangle \tag{48}$$

and the corresponding operator $\hat{D}_V^N(\chi)$ is

$$\hat{D}_V^N(\chi) = d_V(\chi) N[\hat{X}_A^\dagger \hat{X}_B^\dagger \hat{X}_D \hat{X}_C], \tag{49}$$

so that

$$\hat{V}_N = w_V \sum_\chi \hat{D}_V^N(\chi). \tag{50}$$

To represent the configurations (22) [or (24)] we define the so-called $T(k)$ (or, simply, T)-skeletons and diagrams[7] [and, for corresponding bra-states, $\bar{T}(k)$-skeletons and diagrams], shown in Fig. 3. The weight of a $T(k)$- [or $\bar{T}(k)$-] skeleton is

$$w_T(k) = (k!)^{-1}. \tag{51}$$

The definition of the pertinent scalar quantity $d_T(k, K)$ assigned to a T-diagram of Fig. 3b will depend on the state considered. Generally, for the state $|\Psi\rangle$, which may be expressed using (22) and (B.18) as

$$|\Psi\rangle = \sum_k \sum_K C_K^{(k)} |\Phi_K^{(k)}\rangle = \hat{C} |\Phi_0\rangle, \tag{52}$$

we define the scalar and operator quantities as follows:

$$d_T(k, K) = C_K^{(k)} \tag{53}$$

and

$$\hat{D}_T(k, K) = d_T(k, K) \prod_{j=1}^k (\hat{X}_{A_{j''}}^\dagger \hat{X}_{A_{j'}}). \tag{54}$$

We can thus write the operator $\hat{C}$ in (52) in the form

$$\hat{C} = \sum_k w_T(k) \sum_K \hat{D}_T(k, K). \tag{55}$$

Clearly, if we consider only a single k' excited configuration K' (22) by itself, then

$$d_T(k', K') = 1 \quad \text{and} \quad w_T(k') = 1, \tag{56}$$

since all labels are now fixed labels. Notice that in view of (24) the

---

[7] These skeletons will be needed only in the intermediate derivations and will not appear as parts of the final perturbation theory diagrams.
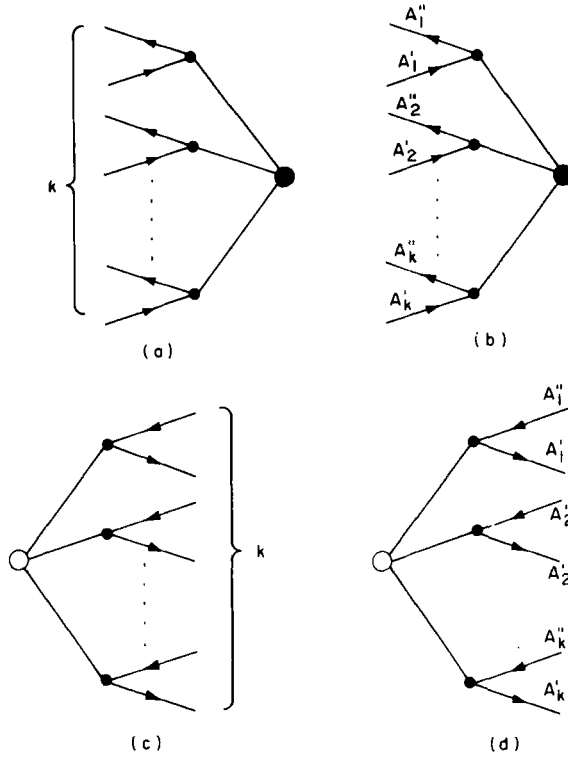
Fig. 3. An example of T- and $\bar{T}$-skeletons [(a) and (c)] and of corresponding T- and $\bar{T}$-diagrams [(b) and (d)], respectively.

operator $\hat{D}_T(k,\ K)$, Eq. (54), is automatically in the N-product form. The corresponding quantities associated with the $\bar{T}$-diagram are

$$d_{\bar{T}}(k,\ K) = \bar{d}_T(k,\ K)$$

and (57)

$$\hat{D}_{\bar{T}}(k,\ K) = \hat{D}_T^\dagger(k,\ K),$$

where $\bar{d}$ designates the complex conjugate of d.

B. Diagrammatic Representation of Wick's Theorem and Resulting Diagrams

Having introduced a diagrammatic representation of the basic quantities, we can now represent Wick's theorem graphically and apply it to the calculation of the matrix elements of the type (B.37). We shall simply

represent each contraction by joining together the appropriate oriented lines associated with the pertinent operators. Using the operators $\hat{X}^{\dagger}_{A}$ and $\hat{X}_{A}$, defined with respect to the true vacuum, we find easily, using relationships (B.39), that for the nonvanishing contractions defined with respect to the Fermi vacuum $|\Phi_0\rangle$ the orientation of full lines must be preserved in this operation. This is schematically illustrated in Fig. 4 for
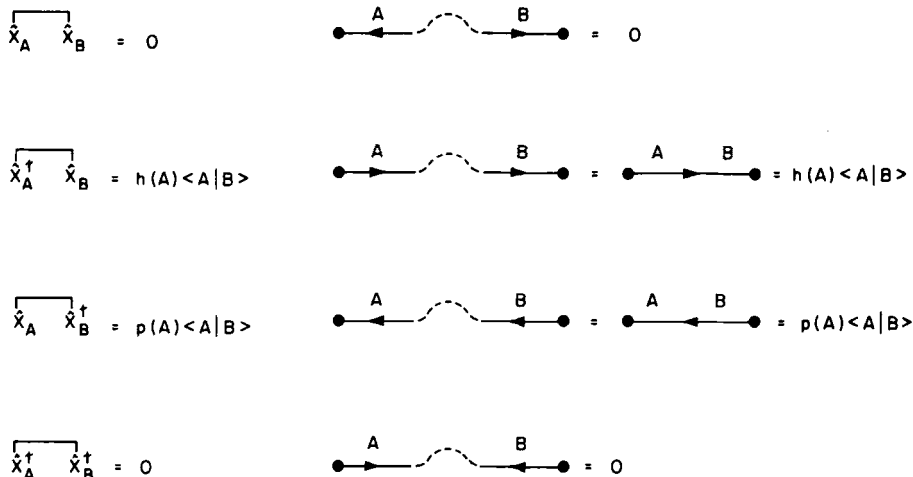
Fig. 4. A graphical representation of contractions (pairings) defined with respect to the Fermi vacuum for operators defined with respect to the true vacuum.

the four possible cases which can arise [cf. last column in (B.39)]. We shall also see shortly that this procedure automatically picks up the correct hole–particle component of the operators involved [cf. discussion following (41)].

Moreover, we see immediately two additional useful properties of this representation, namely:

(i) The contraction vanishes unless the labels on both "ends" are identical. Clearly, if both labels A and B represent summation indices over all spin orbital states, we can simply label the resulting internal line[8] with a single spin orbital summation index. This automatically takes care of the Kronecker symbol $\langle A \mid B \rangle$.

(ii) Moreover, we can also eliminate the functions $p(A)$ and $h(A)$ from the final expressions (again, as long as A is a summation index) by making the convention that the internal lines oriented from left to right are hole lines and, thus, are labeled by hole state indices and summed

over the hole states. Similarly, the internal lines oriented from right to left are particle lines and are summed over particle states only (assuming, of course, they are summation indices).

We can now see why we have to preserve the left–right ordering of individual vertices in our diagrams and, thus, why topological deformations permuting distinct vertices (supervertices) are not allowed in our considerations. Both properties (i) and (ii) are schematically represented in Fig. 5.
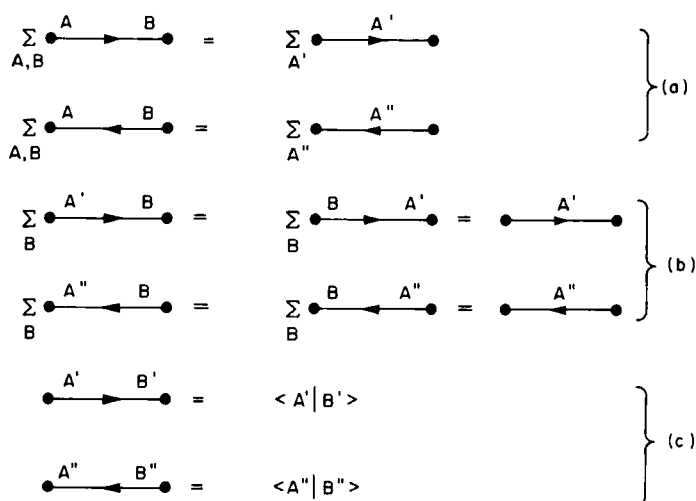
Fig. 5. A graphical illustration of the rules for labeling of oriented lines of resulting diagrams with fixed and summation (free) indices.

Thus, applying Wick's theorem to the calculation of a Fermi vacuum mean value of some product of creation and annihilation operators, using the property (B.37), we find that we can proceed as follows:

(i) We represent the creation and annihilation operators by oriented lines attached to appropriate vertices (supervertices) as described in Section III,A.

(ii) The left–right ordering of the supervertices must be the same as the ordering of the corresponding quantities, represented by these diagrams, in the calculated matrix element.

---

[8] An internal line is defined as an oriented line leaving some vertex and entering another vertex in contrast to an external line, which represents some creation or annihilation operator.

(iii) Joining all the oriented lines pairwise we next draw all possible *resulting diagrams* (Čížek, 1966, 1969; Paldus and Čížek, 1970; and others) (*R*-diagrams), each one representing a possible nonvanishing system of contractions on the right-hand side of (B.37). In doing so we must take care that the orientation of full lines is preserved and that *all* oriented lines are joined together pairwise. In other words, all oriented lines of the resulting diagram must be internal lines.

(iv) Each pair of spin orbital summation indices associated with a given internal line is replaced by a single particle or hole spin orbital summation label, depending on whether the line is a particle or hole line, respectively (cf. Fig. 5a). If only one spin orbital label is summed over while the other one is fixed, then we simply drop the summation label (cf. Fig. 5b). Finally, if both labels are fixed labels, we keep both and assign to this line in the final algebraic expression the appropriate Kronecker symbol (and p or h function, if applicable) (cf. Fig. 5c).

More generally, if we calculate the Fermi vacuum mean value of a product of N-products of creation and annihilation operators using the generalized Wick theorem (Appendix C), the above rules are simply modified in such a way that the systems of contractions containing pairings between the operators, which appear in the same N-product, are discarded. Since, normally, the oriented lines representing the creation and annihilation operators appearing in the same N-product are associated with the same supervertex (i.e. a single vertex or vertices joined by nonoriented lines, cf. Section III,A), the above rule simply means that we exclude the resulting diagrams in which the vertices of the same supervertex are joined by oriented lines.

Thus, forming all possible resulting diagrams, we obtain a graphical representation of the individual nonvanishing terms in the summation on the right-hand side of (B.37) (or of an analogous expression containing N-products on the left-hand side). Clearly, since there are no external lines present in the resulting diagrams, only a scalar quantity has to be associated with each resulting diagram. This must be done in such a way that this scalar quantity will give directly the desired algebraic expression for the calculated matrix element.

In calculating the general matrix elements, like (9) for example, the creation and annihilation operators, whose vacuum mean value(s) we calculate, originate in various operators like $\hat{Q}_N$, $\hat{V}_N$, etc., or come from the configurations (22) appearing in these expressions. Thus, in addition to the vacuum mean values of the operator products, like (B.37), our expression also contains various matrix elements (or scalar quantities). These are simply associated with each particular vertex or supervertex as

appropriate scalar quantities defined above. Thus, in order to obtain the final algebraic expression directly from the resulting diagrams, we simply assign the appropriate scalar quantity to each vertex (supervertex) of a resulting diagram, form their product, and carry out summation over the remaining summation indices.

In this way, we obtain the desired final expression, up to possibly a sign factor resulting from the "unscrambling" of the system of contractions into their simple product as defined in (B.25). Moreover, a number of different contraction schemes may yield the same resulting diagram. Thus, we must formulate the rules determining this number and yielding the correct numerical factor in the final result.

It is exactly these rules wherein the real power of the diagrammatic technique lies, since a conventional determination of these quantities usually requires very laborious and complex combinatorial considerations. We shall see that in the diagrammatic approach these intricate combinatorial considerations are replaced by very simple topological considerations, which only require a counting of hole lines and closed loops of oriented lines and a determination of weight factors.

A derivation of these rules for the general case is obviously rather difficult. However, the final rules are very simple indeed. Due to the limited scope of this article, we shall refrain from a consideration of the general case and will only formulate these rules later on for the specific case of the resulting perturbation theory diagrams needed here.

Let us now illustrate the above outlined ideas with a simple example. Calculate, for example, the following matrix element

$$Q_{01} = \langle \Phi_0 | \hat{Q}_N | {}^{A_1''}_{A_1'} \rangle, \tag{58}$$

where $\hat{Q}_N$ is given by (42) and the ket monoexcited configuration by (22) or (24), so that

$$Q_{01} = \sum_{A, B} \langle A | \hat{q} | B \rangle \langle \Phi_0 | N[\hat{X}^\dagger_A \hat{X}_B] N[\hat{X}^\dagger_{A_1''} \hat{X}_{A_1'}] | \Phi_0 \rangle. \tag{59}$$

Using directly the generalized Wick theorem (Appendix C), and the property (B.37) and (B.22), we get for the Fermi vacuum mean value in the above expression

$$\langle \Phi_0 | N[\hat{X}^\dagger_A \hat{X}_B] N[\hat{X}^\dagger_{A_1''} \hat{X}_{A_1'}] | \Phi_0 \rangle = \langle \Phi_0 | N[\hat{X}^\dagger_A \overrightarrow{\hat{X}_B \hat{X}^\dagger_{A_1''}} \hat{X}_{A_1'}] | \Phi_0 \rangle$$

$$= \overrightarrow{\hat{X}^\dagger_A \hat{X}_{A_1'}} \cdot \overrightarrow{\hat{X}_B \hat{X}^\dagger_{A_1''}} N[\varnothing] \langle \Phi_0 | \Phi_0 \rangle$$

$$= \langle A | A_1' \rangle \langle B | A_1'' \rangle, \tag{60}$$

since only one contraction scheme gives a nonvanishing result [cf. Eqs. (B.39)]. Thus, we get

$$Q_{01} = \langle A'_1 | \hat{q} | A''_1 \rangle, \tag{61}$$

one of the well-known Slater rules.

We can obtain the same result using the graphical method. The individual parts of this matrix element are represented by the diagrams shown in Fig. 6a. The scalar quantity assigned to the T-diagram representing the monoexcited state in (58) [diagram (2) in Fig. 6a] is in this case equal to unity. In greater detail we can represent the operator $\hat{Q}_N$ by the four diagrams shown in Fig. 6b, which indicate explicitly all four components one gets when considering explicitly the hole and particle states, which result when each spin orbital summation in (42) is expressed as a separate summation over the particle and hole states. [For the $\hat{V}_N$ operator we
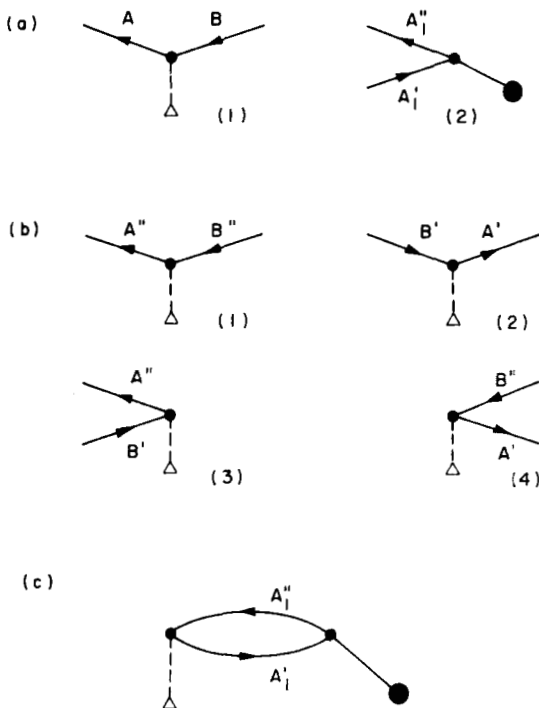
Fig. 6. An illustration of the diagrammatic evaluation of the matrix element (58). (a) Q- and T-vertices (diagrams) representing the component parts of (58). (b) Representation of a Q-vertex using the creation and annihilation operators defined with respect to the Fermi vacuum ($\hat{Y}$-type operators). (c) Resulting diagram for (58).

get similarly 16 terms (diagrams); cf. discussion following (41).] We can see that this is not in fact necessary since our procedure picks up automatically the pertinent component of the operator(s) when the oriented lines of the operator vertices are appropriately distorted in forming the resulting diagram.

Now, following the above rules, we can construct only one resulting diagram, as shown in Fig. 6c. Recalling that the spin orbital labels A_1', A_1'' are fixed (i.e. not summation indices), we immediately obtain the result (61), since this is the scalar quantity assigned to the Q-vertex in the resulting diagram, Fig. 6c, while to the T-vertex we assigned unity. We notice that in this case we have also obtained the correct sign, since the system of pairings in the second expression in (60) may be brought to a simple product of pairings without a sign change (even permutation of labels).

IV. Diagrams for Perturbation Theory

We now return to consider the matrix elements (9), giving various orders of perturbation theory, and will apply the above outlined rules to their evaluation.

We observe that in the operator $\hat{P}_0$ [Eqs. (27) and (28)] the ket and bra states in the "projector" numerator part correspond to the same configuration. Thus, in the diagrammatic representation all the oriented lines extending to the left-hand side of the T-diagram (representing the ket state) must be exactly the same as those on the right-hand side of the corresponding $\bar{T}$-diagram (representing the bra state), as shown in Fig. 7a. We can thus replace this pair of T- and $\bar{T}$-diagrams by the simple P-diagram shown in Fig. 7b, with which we can associate the pertinent denominator (26) as a scalar quantity assigned to this P-vertex

$$d_P(k, K) = (-\kappa_K^{(k)})^{-1} = \left[\sum_{i=1}^{k} (\omega_{A_{i'}} - \omega_{A_{i''}}) \right]^{-1}. \tag{62}$$

In fact, we can go even one step further in our simplification and make the following convention:

We shall omit the P-vertices (Fig. 7b) (which are always surrounded from each side by the interaction, i.e. either Q- or V- vertices) from our resulting diagrams and interconnect the identical oriented lines[9] as shown in Fig. 7c. Then, with each pair of neighboring interaction Q- or V-vertices (which were surrounding a given P-vertex) we associate a

---

[9] This will not only simplify our diagrams but it will also *automatically* ensure that we have the same ket and bra states in each term representing the operator $\hat{P}_0$.
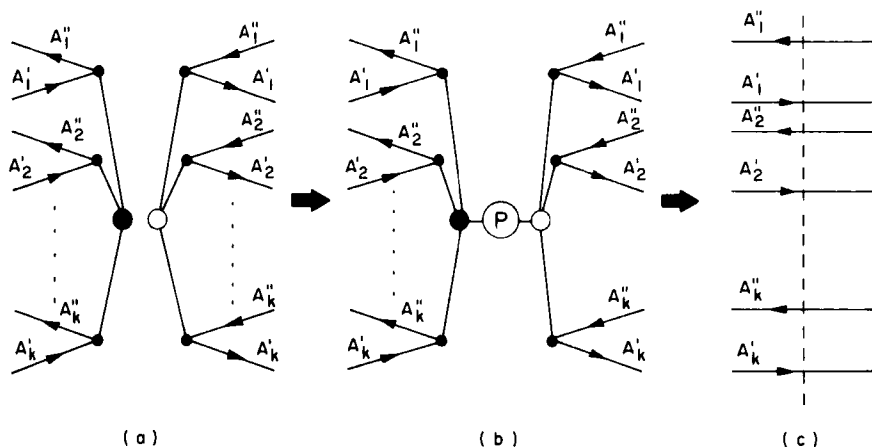
Fig. 7. Graphical representations of the operator $\hat{P}_i$ [Eq. (5)] of the perturbation theory. (a) Representation of the numerator part of $\hat{P}_i$ using T- and $\bar{T}$-diagrams. (b) Intermediate representation of the operator $\hat{P}_i$. (c) Final representation of $\hat{P}_i$ using the convention assigning the appropriate denominator (62) to each pair of neighboring interaction (i.e. Q or V) vertices. The dashed line represents here an imaginary line intersecting all oriented lines passing through the interval between the given pair of neighboring interaction vertices. This line is not shown explicitly in the resulting diagrams. The oriented lines of the resulting diagram intersecting this imaginary line determine the pertinent denominator (62) as explained in the text.

denominator (62), which we obtain by assigning the orbital energies ω_A to all oriented lines crossing an imaginary line separating these neighboring vertices (indicated by dashed line in Fig. 7c) and taking those corresponding to the hole lines with a positive sign and to the particle lines with a negative sign. It is easily seen that it is then irrelevant if the individual oriented lines are arbitrarily distorted and intersect the imaginary dividing line more than once. We also observe that the number of particle lines crossing a given imaginary line must be equal to the number of hole lines crossing it.

This representation has the additional advantage that we can now also easily eliminate the ground state projector $|\Phi_0\rangle\langle\Phi_0|$ from the sum [cf. the summation restriction in (5)] by considering only the so-called connected diagrams.[10]

[10] A connected diagram is a diagram in which any two vertices are connected by at least one path consisting of oriented and nonoriented lines. The path is then a sequence of internal lines. Notice, however, that disconnected diagrams may result even when the ground state projector is eliminated. This type of disconnected diagrams will be eliminated from our considerations later on (cf. Section IV,C and Appendix F).

A. Simple Examples

Let us illustrate these ideas on a simple second-order term involving only one-particle operators $\hat{Q}$, i.e. consider

$$k_0^{(2)'} = \langle \Phi_0 \mid \hat{W}^{(1)} \hat{P}_0 \hat{W}^{(1)} \mid \Phi_0 \rangle, \tag{63}$$

where $\hat{W}^{(1)} \equiv \hat{Q}_N$ is given by (39) and (42), and $\hat{P}_0$ by (27) and (28).

Clearly, we can simply consider the matrix element

$$k'' = \langle \Phi_0 \mid \hat{W}^{(1)} \hat{W}^{(1)} \mid \Phi_0 \rangle \tag{64}$$

avoiding the disconnected terms and associating the denominator with the pairs of neighboring vertices as outlined above.

Thus, we have

$$k'' = \sum_{A, B, C, D} \langle A \mid \hat{q} \mid B \rangle \langle C \mid \hat{q} \mid D \rangle \langle \Phi_0 \mid N[A^\dagger B] N[C^\dagger D] \mid \Phi_0 \rangle, \tag{65}$$

using the convention (D.8). From the generalized Wick theorem (Appendix C) and the property (B.37) we have, further,

$$\langle \Phi_0 \mid N[A^\dagger B] N[C^\dagger D] \mid \Phi_0 \rangle = \langle \Phi_0 \mid N[\overline{A^\dagger B C^\dagger D}] \mid \Phi_0 \rangle$$
$$= h(A) p(B) \langle A \mid D \rangle \langle B \mid C \rangle, \tag{66}$$

as in (60). Thus

$$k'' = \sum_{A', A''} \langle A' \mid \hat{q} \mid A'' \rangle \langle A'' \mid \hat{q} \mid A' \rangle \tag{67}$$

and, including the denominator part, we obtain the well-known formula

$$k_0^{(2)'} = \sum_{A', A''} \frac{\langle A' \mid \hat{q} \mid A'' \rangle \langle A'' \mid \hat{q} \mid A' \rangle}{\omega_{A'} - \omega_{A''}}. \tag{68}$$

Graphically, we represent each $\hat{W}^{(1)}$ by the diagram introduced in Section III,A, as shown in Fig. 8a, and form all possible connected resulting diagrams. Clearly, only one such diagram, shown in Fig. 8b, is
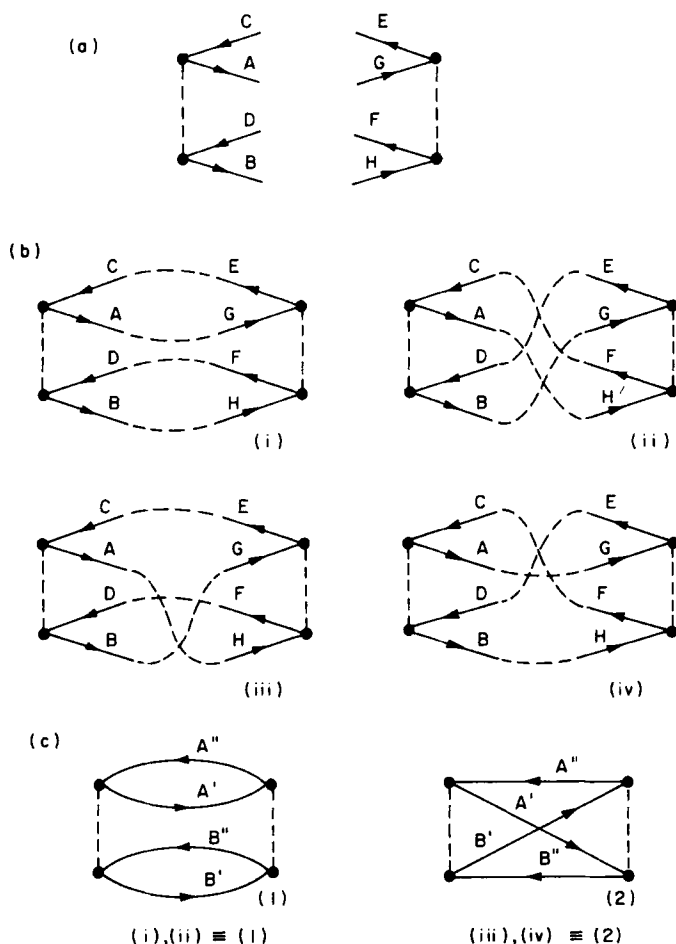

(a)   (b)
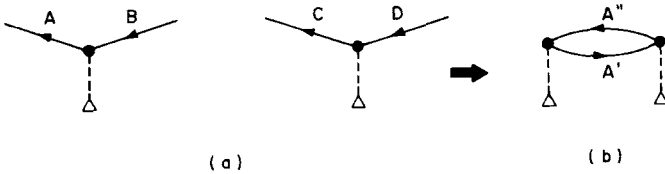
Fig. 8. Diagrammatic evaluation of the one-particle second-order contribution to the ground state energy. (a) Diagrammatic representation of the operators involved. (b) Resulting diagram.

possible, which again gives immediately the final expression (68) using the rules introduced earlier.

We can easily convince ourselves that considering the projector part $|\Phi_K^{(k)}\rangle\langle\Phi_K^{(k)}|$ of the operator $\hat{P}_0$ explicitly would not change the final result in any way. Indeed, we can always find an appropriate configuration among all possible ones which will do the job. In the example just given, these were the monoexcited configurations which played the role, as seen easily from the diagram in Fig. 8b, while all other configurations in $\hat{P}_0$ gave a vanishing result (yielding N-products with at least one uncontracted operator). Even the requirement that the number of particle lines equals the number of hole lines in any interval between two neighboring interaction vertices (supervertices) may be shown to be automatically satisfied for any resulting diagram, since every simple vertex has only one incoming and one outgoing oriented line. Thus, the procedure of drawing the resulting perturbation theory diagrams only on the basis of the interaction Q- and V-vertices is seen to select automatically the pertinent configurations from the projector part of the $\hat{P}_0$ operator, while the corresponding denominators, which remain in the final expressions, are given by the simple rule stated above.

Consider now another second-order term containing, however, the two-particle operators $\hat{W}^{(2)} \equiv \hat{V}_N$,

$$k_0^{(2)''} = \langle \Phi_0 \mid \hat{W}^{(2)} \hat{P}_0 \hat{W}^{(2)} \mid \Phi_0 \rangle, \tag{69}$$

or, the associated simpler expression

$$k'' = \langle \Phi_0 \mid \hat{W}^{(2)} \hat{W}^{(2)} \mid \Phi_0 \rangle$$

$$= \frac{1}{4} \sum_{A, B, C, D} \sum_{E, F, G, H} \langle AB \mid \hat{v} \mid CD \rangle \langle EF \mid \hat{v} \mid GH \rangle$$

$$\times \langle \Phi_0 \mid N[A^\dagger B^\dagger DC] N[E^\dagger F^\dagger HG] \mid \Phi_0 \rangle. \tag{70}$$

Again, using (B.36) and (C.1) we get

$$\langle \Phi_0 \mid N[A^\dagger B^\dagger DC] N[E^\dagger F^\dagger HG] \mid \Phi_0 \rangle$$

$$= \langle \Phi_0 \mid N[A^\dagger B^\dagger DC \; E^\dagger F^\dagger HG] \mid \Phi_0 \rangle \tag{i}$$

$$+ \langle \Phi_0 \mid N[A^\dagger B^\dagger DC \; E^\dagger F^\dagger HG] \mid \Phi_0 \rangle \tag{ii}$$

$$+ \langle \Phi_0 \mid N[A^\dagger B^\dagger DC \; E^\dagger F^\dagger HG] \mid \Phi_0 \rangle \tag{iii}$$

$$+ \langle \Phi_0 \mid N[\overline{A^\dagger \overline{B^\dagger \overline{DC} \; \overline{E^\dagger} F^\dagger H} G}] \mid \Phi_0 \rangle \qquad \text{(iv)}$$

$$= h(A)h(B)p(C)p(D)[\langle A \mid G \rangle \langle B \mid H \rangle \langle D \mid F \rangle \langle C \mid E \rangle \qquad \text{(i)}$$

$$+ \langle A \mid H \rangle \langle B \mid G \rangle \langle D \mid E \rangle \langle C \mid F \rangle \qquad \text{(ii)}$$

$$- \langle A \mid H \rangle \langle B \mid G \rangle \langle D \mid F \rangle \langle C \mid E \rangle \qquad \text{(iii)}$$

$$- \langle A \mid G \rangle \langle B \mid H \rangle \langle D \mid E \rangle \langle C \mid F \rangle], \qquad \text{(iv)} \quad (71)$$

which finally yields

$$k_0^{(2)''} = \frac{1}{2} \sum_{\substack{A', B' \\ A'', B''}} \frac{\langle A'B' \mid \hat{v} \mid A''B'' \rangle (\langle A''B'' \mid \hat{v} \mid A'B' \rangle - \langle A''B'' \mid \hat{v} \mid B'A' \rangle)}{\omega_{A'} + \omega_{B'} - \omega_{A''} - \omega_{B''}}.$$

$$(72)$$

We see that the terms (i) and (ii) [(iii) and (iv)] yield the same resulting expression.

In graphical language, we assign the V-vertices to the $\hat{W}^{(2)}$ operators, as shown in Fig. 9a (where the oriented lines are already distorted in such a way as to facilitate the diagrammatic representation of contractions). The individual contraction schemes (i)–(iv), Eq. (71), are represented graphically in Fig. 9b. Since all spin orbital labels are summation variables, we see easily that both schemes (i) and (ii) yield the same R-diagram (1) of Fig. 9c and the (iii) and (iv) schemes yield R-diagram (2) of the same figure. This is why we have the factor $1/2$ in the final expression (72). Also, unscrambling the individual contractions brings a negative sign to the term corresponding to the R-diagram (2) of Fig. 9c. Thus, we shall have to formulate the rules which will enable us to obtain the appropriate numerical factors directly from the R-diagrams. Indeed, except for these numerical factors the expression (72) can be written down immediately solely on the basis of R-diagrams of Fig. 9c using the rules formulated earlier.

We would like to stress another point concerning our "shortcut" calculation of this second-order term using expression (70) instead of (69). Should we have used directly the expression (69) and considered the operator $\hat{P}_0$ explicitly (using, for example, the vertices of Fig. 7b) we would have excluded from the doubly excited configurations, intervening here, those which violate the Pauli principle (and thus automatically vanish), i.e. the configurations having either two identical particle and/or two identical hole states. Clearly such states do not appear in $\hat{P}_0$ and automatically vanish. However, these states were not excluded in our

Fig. 9. Diagrammatic evaluation of the two-particle second-order contribution to the ground state energy. (a) Diagrammatic representation of the operators involved (with the oriented lines appropriately distorted to facilitate the construction of resulting diagrams). (b) Diagrammatic representation of the nonvanishing systems of pairings [cf. Eq. (71)]. (c) Resulting diagrams.

consideration based on the expression (70), where no restriction is made on the summations over the spin orbital states. In graphical language this means that we also consider diagrams (Fig. 9c), in which either both particle states and/or both hole states are identical. This is the simplest example of the so-called exclusion (Pauli) principle violating (EPV) diagrams.

We see immediately that in our example the contributions from the diagrams of this type will exactly cancel, since the direct term [Fig. 9c, (1)] always gives the same contribution, up to a sign, as the exchange term [Fig. 9c, (2)], which we also see immediately from the algebraic expression (72), since $\langle AA \,|\, \hat{v} \,|\, BC \rangle = \langle AA \,|\, \hat{v} \,|\, CB \rangle$ and $\langle AB \,|\, \hat{v} \,|\, CC \rangle = \langle BA \,|\, \hat{v} \,|\, CC \rangle$. Thus, we conclude that whether we consider or exclude these contributions is immaterial in this simple case.

We will see later on that another type of EPV diagrams appears in higher orders of PT, when one excludes the so-called unlinked terms. In this case, however, we will show (cf. Section IV,C and Appendix F) that, excluding the unlinked terms from our considerations, the EPV linked terms must be retained in order to obtain the correct result.

B. Rules for the Determination of Numerical Factors

Let us first consider how to determine the absolute value of the correct numerical factor by which we have to multiply the resulting algebraic expression, given as a product of scalar quantities associated with the vertices of the R-diagram and with pairs of neighboring (super) vertices (denominators). A clue to this problem is to determine in how many distinct ways we can form a given R-skeleton from the component Q- and V-skeletons. An answer to this problem gives the following general graph theoretical theorem, which we will accept without proof[11] (cf. Čížek, 1966, 1969):

THEOREM: *Let A, B, and C be skeletons, having weights w_A, w_B, and w_C, respectively, and let the connected skeleton C be obtained by joining pairwise a given number of oriented lines of skeletons A and B. Then the number N of distinct ways in which the skeleton C may be obtained from skeletons A and B is*

$$N = w_C/(w_A w_B). \tag{73}$$

Clearly, it is possible to generalize this theorem for an arbitrary finite number of component graphs. Let us first see how this theorem applies to the second example of the preceding section. Clearly, in this case $w_A = w_B = w_V = \frac{1}{2}$ [cf. Eq. (47)], as well as $w_C = \frac{1}{2}$, where C is the skeleton associated with either of the diagrams of Fig. 9c (cf. example in Section III,A, Fig. 1). Thus, we obtain $N = 2$ in agreement with the fact that each of the diagrams of Fig. 9c is obtained twice (i.e. as two different systems of pairings).

---

[11] Our resulting diagrams correspond to the so-called *star product* of the component graphs used in the graphical representation of generating functions (Stell, 1967). Realizing this fact the theorem given here becomes trivial.

It is now easy to realize that the desired numerical factor (absolute value) for each R-diagram is simply given by its weight factor. Indeed, consider a set of diagrams (skeletons) S_i with weights $w_S(i)$, from which we form some R-diagram (skeleton) with weight w_R. The desired numerical factor is given as a product of individual weight factors $w_S(i)$, appearing in the original algebraic expressions for these quantities (operators) [cf. Eqs. (46), (50), or (55)], times the multiplicity N, Eq. (73),

$$N = w_R \bigg/ \prod_i w_S(i), \tag{74}$$

which yields simply w_R.

For example, consider some connected nth-order resulting PT diagram R, containing only two-particle (i.e. V) vertices. The corresponding skeleton may be obtained from the n V-skeletons in $N = w_R/(\tfrac{1}{2})^n$ different ways. Since each $\hat{V}$ operator introduces a factor $\tfrac{1}{2}$ [cf. Eq. (31) or (32)] we see that the resulting factor is w_R.

Finally, let us mention that for the connected PT R-diagrams of an arbitrary order, the weight factor w_R is either 1 or $\tfrac{1}{2}$. Moreover, the latter case can only occur when no Q-vertices are present (i.e. all vertices must be V-vertices).

It remains now to find the correct sign of the numerical factor, whose absolute value is simply equal to the weight of the resulting diagram. This sign is clearly given by the parity of the permutation, which unscrambles the individual contractions into a simple product of pairings. In graphical language it may be shown, as indicated in Appendix E, that this sign factor is simply given by the following expression

$$(-1)^{l+h}, \tag{75}$$

where l is the number of closed paths of oriented lines (called loops or oriented loops)[12] and h is the number of hole lines in the given R-diagram.

For example, in the case of the diagrams of Fig. 9c we have in both cases $h = 2$, but $l = 2$ for (1) and $l = 1$ for (2), thus giving the correct signs in the final formula (72).

Thus, the overall numerical factor which we have to associate with each R-diagram is simply

$$w_R(-1)^{l+h}. \tag{76}$$

[12] This terminology deviates from conventional graph theoretical nomenclature, where the loop is an arc (line) originating and ending on the same node (vertex).

C. Renormalization Terms

As we have seen in Section II the so-called "unlinked" terms will appear in higher orders of PT. In our formulation, they appear for the first time in the third-order formula (9c), which we can rewrite as follows

$$k_i^{(3)} = \langle \Phi_i \mid \hat{W} \hat{P}_i \hat{W} \hat{P}_i \hat{W} \mid \Phi_i \rangle - \langle \Phi_i \mid \hat{W} \hat{P}_i^2 \hat{W} \mid \Phi_i \rangle k_i^{(1)}. \qquad (77)$$

For the ground state case ($i = 0$) we are now considering, and using the operators $\hat{K}$ and $\hat{K}_0$ defined by (16) and (17), respectively, the perturbation $\hat{W}$ is given by (30) or (38) and is in the N-product form. Due to this fact the first-order contribution $k_0^{(1)}$ vanishes, as we can see immediately from (30), so that for $i = 0$ we have instead of (9) the following simpler formulas:

$$k_0^{(0)} = 0,$$

$$k_0^{(1)} = 0,$$

$$k_0^{(2)} = \langle \Phi_0 \mid \hat{W} \hat{P}_0 \hat{W} \mid \Phi_0 \rangle,$$

$$k_0^{(3)} = \langle \Phi_0 \mid \hat{W} \hat{P}_0 \hat{W} \hat{P}_0 \hat{W} \mid \Phi_0 \rangle. \qquad (78)$$

Since $\hat{W}$ is in the N-product form, we can only get connected (linked)[13] diagrams for these first three orders, as we shall see explicitly in Section IV,G. This is due to the fact that redefining conveniently our Hamiltonian [cf. Eq. (16)] we avoided an explicit consideration of the so-called Hartree–Fock diagrams (cf. Section IV,H).

However, it is quite obvious that in the higher orders of PT the disconnected (unlinked)[13] diagrams will appear. For example, in the fourth-order term

$$k_0^{(4)'} = \langle \Phi_0 \mid \hat{W} \hat{P}_0 \hat{W} \hat{P}_0 \hat{W} \hat{P}_0 \hat{W} \mid \Phi_0 \rangle \qquad (79)$$

we shall have to consider, for example, the disconnected diagram shown in Fig. 10. Indeed, this diagram will result (among a number of other diagrams, of course) when one chooses biexcited configurations in the first and last operator $\hat{P}_0$ and a tetraexcited one in the second (central) operator $\hat{P}_0$ in (79). However, as is shown in Appendix F, all such diagrams will be cancelled by the contributions from other fourth-order terms, which we may obtain by using the bracketing technique of Appen-

---

[13] An unlinked diagram is generally defined as a diagram containing a disconnected vacuum part (i.e. a diagram having only internal oriented lines and, thus, no external lines). In the case of vacuum diagrams themselves, as is the case here, connected is synonymous with linked.
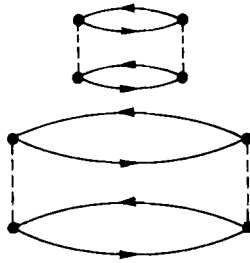
Fig. 10. An example of the fourth-order unlinked (disconnected) diagram.

dix A. Moreover, as shown in Appendix F, in order to make this cancella-
tion of unlinked terms complete, we have to consider all diagrams,
including the EPV ones. Thus, we find the result of the so-called *linked
cluster theorem*, namely that a PT contribution for a given order may be
obtained by considering all *linked* diagrams of the given order in which
the Pauli principle is ignored. The latter requirement is automatically
taken care of when the summations over the hole and particle states are
not restricted in any way.

D. Summary of Rules

Let us now summarize the rules obtained above, which enable one to
obtain explicit formulas for the kth order $(k \geq 2)$ of the ground state PT:

(i) Draw all possible connected (linked) vacuum skeletons having n_1
Q-vertices and n_2 V-vertices, $n_1, n_2 = 0, 1, \ldots, k$ and $n_1 + n_2 = k$, and
determine their weights w_R.

(ii) Label the particle and hole lines of these skeletons with particle
and hole spin orbital labels, respectively, thus forming all possible kth
order diagrams.

(iii) Write down the contributions from each diagram following these
rules:

(a) Assign matrix elements $\langle A | \hat{q} | C \rangle$ and $\langle AB | \hat{v} | CD \rangle$ to each Q-
and V-vertex, respectively, where A, B are labels of the outgoing lines and
C, D are labels of the incoming lines, A and C (B and D) being associated
with the same single vertex.

(b) With each pair of neighboring vertices associate a denominator
factor $[\sum_i (\omega_{A_{i'}} - \omega_{A_{i''}})]^{-1}$, taking the orbital energies ω_A associated with
the hole (particle) lines with positive (negative) sign.

(c) Determine the numerical factor given by $w_R(-1)^{l+h}$ [cf. Eq. (76)].

(d) Multiply together all the above factors and sum over all hole and
particle states labeling internal lines.

Thus, once we have all pertinent skeletons (diagrams), we can instantly write down the explicit algebraic expressions for any order of PT. Let us next examine how we can effectively obtain all pertinent skeletons.

E. Hugenholtz Diagrams

The graphs which we have been using so far are called Goldstone diagrams and represent a special case of the more general Feynman diagrams. These diagrams are very convenient since we can easily establish a one-to-one correspondence with the pertinent algebraic expressions. However, their number increases very rapidly with increasing order of PT.

We shall now introduce another type of diagram, called Hugenholtz (or degenerate, cf. Čížek, 1969) diagrams, which represent a homomorphic mapping of the Goldstone diagrams and are less numerous than the latter. Since a systematic transition from Hugenholtz diagrams to those of Goldstone is readily found, it is much better to initially generate all Hugenholtz diagrams and then to carry out the transition to the Goldstone diagrams.[14]

The Hugenholtz diagrams are obtained from the Goldstone ones by reducing the two-particle V-vertex to a single point (or degenerate) vertex as shown in Fig. 11a. These vertices should be associated with the antisymmetrized matrix elements (36), since both incoming (both outgoing) lines are now equivalent. Consequently, direct and exchange Goldstone diagrams are represented by the same Hugenholtz diagram. For example, both diagrams of Fig. 9c are mapped into the same Hugenholtz diagram shown in Fig. 12.

The reverse transition from Hugenholtz to Goldstone diagrams is simply achieved by replacing each Hugenholtz vertex by the direct and exchange Goldstone vertices as shown schematically in Fig. 11b. Thus, from a Hugenholtz diagram containing n_2 two-particle vertices we can obtain up to 2^{n_2} Goldstone diagrams. Clearly, a number of these 2^{n_2} diagrams may be topologically equivalent, as a reverse transition from the diagram of Fig. 12 to the diagrams of Fig. 9c clearly indicates.

We would like to mention here that we have formulated (Paldus and Wong, 1973) and programmed (Wong and Paldus, 1973) an algorithm for a systematic generation of Hugenholtz diagrams of different types,

[14] We would like to mention here that it is most convenient to use the mixed Hugenholtz–Goldstone formalism as introduced by Brandow (1967). However, since we are interested primarily in spin-independent Hamiltonians, it will be essential to use the Goldstone notation to carry out easily the summations over spin variables (cf. Section IV,F).

(a)

(b)
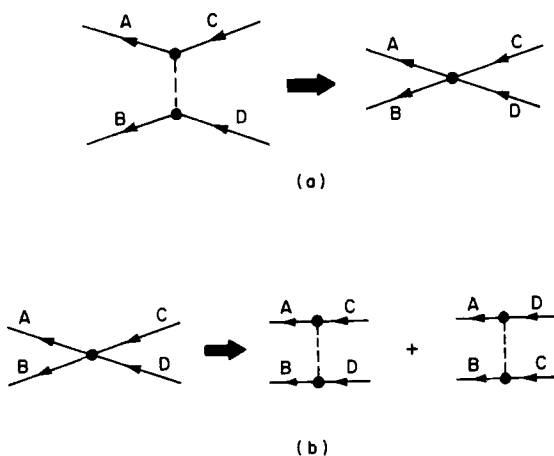
Fig. 11. Schematic representation of the transitions between Goldstone and Hugenholtz form of diagrams. (a) A transition from the Goldstone form to the Hugenholtz form achieved by the merger of simple vertices of the V-vertex. (b) A reverse transition achieved by the replacement of each Hugenholtz vertex by the direct and exchange Goldstone vertices.
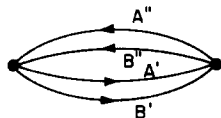
Fig. 12. Hugenholtz form of the resulting diagram for the two-particle second-order contribution.

namely vacuum PT diagrams and various one- and two-particle Green function diagrams (or, if you like, excitation energy and ionization potential PT diagrams). With the existing version any set of diagrams up to and including the fourth order may be generated. Generalization to higher orders is straightforward but hardly desirable at the present time.

F. Spin-Independent Formalism

For spin-independent Hamiltonians, we can easily carry out the summations over the spin variables in the PT formulas and thus eliminate the explicit spin dependence completely. Let us see how this transition from the spin orbital to the orbital formalism may be very simply achieved for the closed-shell case, using the diagrammatic representation.

Consider a closed-shell system for which $|\Phi_0\rangle$ consists of doubly

occupied orbitals $|a'\rangle$, and $|A'\rangle = |a'\rangle |\eta\rangle$, $\eta = \pm\frac{1}{2}$ [cf. Eqs. (B.14) and (B.15)]. Similarly the unoccupied orbitals are labeled with double primes. Clearly, every summation over the spin orbitals may now be written as a summation over the orbitals and a summation over the two spin states. For spin-independent interactions (potentials), the spin state must be preserved along each oriented path of our diagrams [cf. (B.15)]. Thus, for each closed loop of oriented lines there are two possibilities for spin states, each one yielding the same result in view of the spin independence of our potentials. Thus, going over to orbital summations, we simply have to add a factor of two for each closed loop of oriented lines.

This yields a very simple rule for the desired transition to the orbital formalism: (i) replace spin orbital indices with orbital ones, and (ii) multiply the contribution from the diagram by an additional factor 2^l. As an example, let us write down the second-order energy $k_0^{(2)''}$, Eq. (72), given by the diagrams of Fig. 9c, in the spin-independent form. Clearly the spin factor for the direct term is equal to 4 $(l = 2)$ and for the exchange term is equal to 2 $(l = 1)$, so that we get immediately

$$k_0^{(2)''} = \sum_{\substack{a', b' \\ a'', b''}} \langle a'b' | \hat{v} | a''b'' \rangle (2\langle a''b'' | \hat{v} | a'b' \rangle - \langle a''b'' | \hat{v} | b'a' \rangle)$$
$$\times [\omega_{a'} + \omega_{b'} - \omega_{a''} - \omega_{b''}]^{-1}. \tag{80}$$

G. Example: Third-Order Contribution

We shall first illustrate the above exposed theory on the derivation of the explicit spin-independent formulas for the third-order contribution $k_0^{(3)}$, Eq. (78), assuming that the Hartree–Fock solution is used as the unperturbed state, so that $\hat{Q}_N = 0$ and $\hat{W} = \hat{V}_N$.

We shall follow the rules of Section IV,D and first determine the pertinent Hugenholtz diagrams. To do so we must consider all possible ways of obtaining connected diagrams from three two-particle vertices, shown schematically in Fig. 13a. To simplify our problem we first consider a simpler case ignoring the orientation of lines. We also recall that we must not connect lines of the same vertex since we eliminated the HF diagrams. We can proceed in a systematic way considering that we connect vertices (I) and (II) of Fig. 13a with k lines, $k = 0, 1, 2, 3, 4$. We can immediately discard cases $k = 0$ and $k = 4$, since they would require that we join lines belonging to the same vertex. The same is also true for cases $k = 1$ and $k = 3$ [which are obtained from each other by a reflection
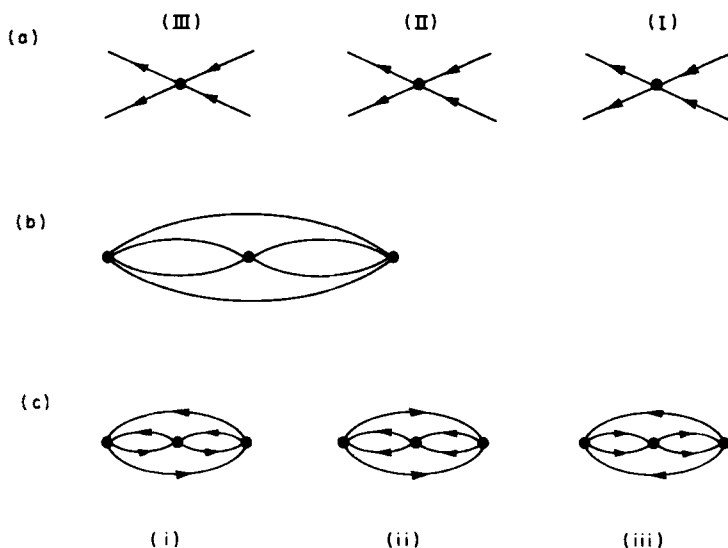
Fig. 13. Diagrammatic evaluation of the two-particle third-order contribution to the ground state energy. (a) Diagrammatic representation of the operators involved (in Hugenholtz form) and vertex numbering used. (b) Intermediate resulting diagram, in which the orientation of particle and hole lines is ignored. (c) Resulting Hugenholtz diagrams.

(I) ↔ (III)], so that only the case $k = 2$ yields a possible prototype of a third-order Hugenholtz diagram, shown in Fig. 13b. Considering now all possible orientations of lines, we find the three Hugenholtz diagrams (skeletons) shown in Fig. 13c. According to the type of interaction on the central vertex (II), we shall refer to them and to the corresponding terms as (i) particle–hole (p–h), (ii) particle–particle (p–p), and (iii) hole–hole (h–h) diagrams (terms).

We shall next find the corresponding Goldstone diagrams. A convenient way to effectuate this transition is (i) to first draw the Goldstone diagram having the maximum number of closed loops, (ii) to form exchange diagrams by "switching" two oriented lines at single V-vertices, pairs of V-vertices, etc., and (iii) to eliminate equivalent skeletons (diagrams). The resulting diagrams are shown in Fig. 14a. In the third column of Table I we have indicated at which vertices we carried out step (ii) above. We see that for the p–h diagram (i) of Fig. 13c all $2^3 = 8$ corresponding Goldstone diagrams are distinct, while only two are distinct in the p–p and h–h cases.

In order to write down the corresponding algebraic expressions, we first observe that we shall have certain matrix elements repeated a
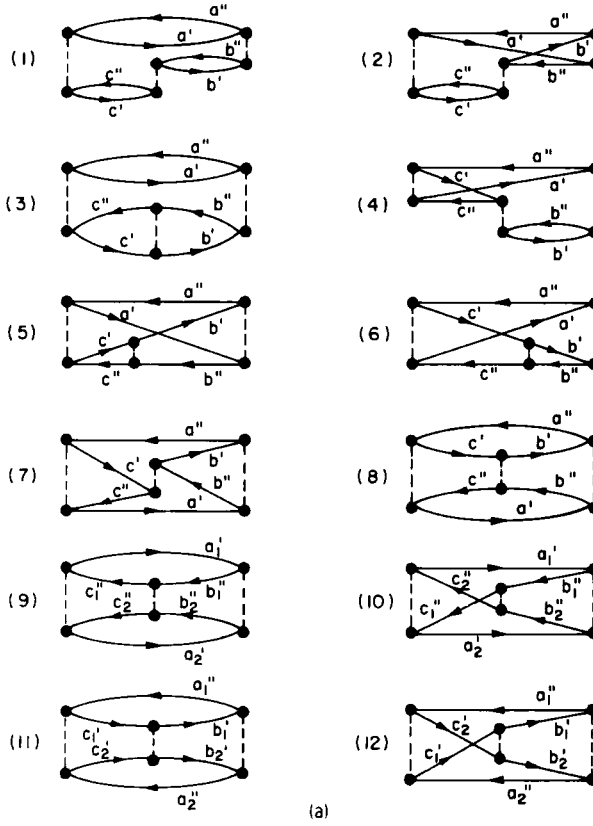
Fig. 14a. Goldstone form of the resulting diagrams for the two-particle (type A) third-order contribution to the ground state energy.

number of times in different diagrams. We therefore define

$$A_0 = \langle a''b'' \,|\, \hat{v} \,|\, a'b' \rangle \qquad A_1 = \langle a''b'' \,|\, \hat{b} \,|\, b'a' \rangle$$

$$B_0 = \langle b'c'' \,|\, \hat{v} \,|\, b''c' \rangle \qquad B_1 = \langle b'c'' \,|\, \hat{v} \,|\, c'b'' \rangle$$

$$C_0 = \langle a'c' \,|\, \hat{v} \,|\, a''c'' \rangle \qquad C_1 = \langle a'c' \,|\, \hat{v} \,|\, c''a'' \rangle \qquad (81)$$

for p–h terms and, similarly,

$$A_0' = \langle b_1'' b_2'' \,|\, \hat{v} \,|\, a_1' a_2' \rangle$$

$$B_0' = \langle c_1'' c_2'' \,|\, \hat{v} \,|\, b_1'' b_2'' \rangle$$

$$C_0' = \langle a_1' a_2' \,|\, \hat{v} \,|\, c_1'' c_2'' \rangle \qquad C_1' = \langle a_1' a_2' \,|\, \hat{v} \,|\, c_2'' c_1'' \rangle \qquad (82)$$

TABLE I

CONTRIBUTIONS FROM THE NON-HF THIRD-ORDER PT DIAGRAMS TO THE GROUND STATE ENERGY[a]

Hugenholtz diagram (Fig. 13c)	Goldstone diagram (Fig. 14a)	Exchange at vertices (cf. Figs. 13a,c)	w	l	h	Algebraic contribution of the diagram
(i)	1	NONE	1	3	3	$8R_{ph}A_0B_0C_0$
	2	I	1	2	3	$-4R_{ph}A_1B_0C_0$
	3	II	1	2	3	$-4R_{ph}A_0B_1C_0$
	4	III	1	2	3	$-4R_{ph}A_0B_0C_1$
	5	I, II	1	1	3	$2R_{ph}A_1B_1C_0$
	6	II, III	1	1	3	$2R_{ph}A_0B_1C_1$
	7	I, III	1	1	3	$2R_{ph}A_1B_0C_1$
	8	I, II, III	1	2	3	$-4R_{ph}A_1B_1C_1$
(ii)	9	NONE; I, II; I, III; II, III	$\frac{1}{2}$	2	2	$2R_{pp}A_0'B_0'C_0'$
	10	I; II; III; I, II, III	$\frac{1}{2}$	1	2	$-R_{pp}A_0'B_0'C_1'$
(iii)	11	NONE; I, II; I, III; II, III	$\frac{1}{2}$	2	4	$2R_{hh}A_0''B_0''C_0''$
	12	I; II; III; I, II, III	$\frac{1}{2}$	1	4	$-R_{hh}A_0''B_0''C_1''$

[a] The first and the second columns give the pertinent Hugenholtz and Goldstone diagrams, respectively; the third column lists the vertices at which the exchange has to be performed in the Goldstone diagram, containing maximum number of loops, in order to get a given diagram (cf. text for details); the next three columns list the weights (w), number of closed loops of oriented lines (l), and number of (internal) hole lines (h), and the last column gives the algebraic form of the given contribution [cf. Eqs. (81)–(84)].

and

$$A_0'' = \langle a_1'' a_2'' \,|\, \hat{v} \,|\, b_1' b_2' \rangle$$

$$B_0'' = \langle b_1' b_2' \,|\, \hat{v} \,|\, c_1' c_2' \rangle$$

$$C_0'' = \langle c_1' c_2' \,|\, \hat{v} \,|\, a_1'' a_2'' \rangle \qquad C_1'' = \langle c_1' c_2' \,|\, \hat{v} \,|\, a_2'' a_1'' \rangle \qquad (83)$$

for p–p and h–h terms, respectively.

Next we observe that the denominators of all Goldstone diagrams originating in the same Hugenholtz diagram are identical. Thus, the denominator factors will be

$$R_{ph} = [(\omega_{a'} + \omega_{c'} - \omega_{a''} - \omega_{c''})(\omega_{a'} + \omega_{b'} - \omega_{a''} - \omega_{b''})]^{-1}$$

$$R_{pp} = [(\omega_{a_1'} + \omega_{a_2'} - \omega_{c_1''} - \omega_{c_2''})(\omega_{a_1'} + \omega_{a_2'} - \omega_{b_1''} - \omega_{b_2''})]^{-1}$$

$$R_{hh} = [(\omega_{c_1'} + \omega_{c_2'} - \omega_{a_1''} - \omega_{a_2''})(\omega_{b_1'} + \omega_{b_2'} - \omega_{a_1''} - \omega_{a_2''})]^{-1}. \qquad (84)$$

Finally, the topological factor w, the number of closed loops l, and the number of hole lines h are easily determined for each Goldstone diagram of Fig. 14a and are given in Table I. The resulting algebraic expression is then given in the last column of Table I in terms of the quantities just defined. It should be noted how the product of matrix elements is related to the exchanges we have carried out in order to generate all Goldstone diagrams. It is not difficult to see that all these contributions may be conveniently expressed as follows

$$
\begin{aligned}
k_0^{(3)} = \sum_{\substack{a', b', c' \\ a'', b'', c''}} R_{ph}[(2A_0 - A_1)(2B_0 - B_1) \\
\times (2C_0 - C_1) - 3A_1 B_1 C_1] \\
+ \sum_{\substack{a_1', a_2' \\ b_1'', b_2'', c_1'', c_2''}} R_{pp} A_0' B_0'(2C_0' - C_1') \\
+ \sum_{\substack{b_1', b_2', c_1', c_2' \\ a_1'', a_2''}} R_{hh} A_0'' B_0''(2C_0'' - C_1'').
\end{aligned}
\tag{85}
$$

Defining the antisymmetrized orbital matrix elements as follows

$$
\langle ab \,|\, \hat{v} \,|\, cd \rangle_a = 2\langle ab \,|\, \hat{v} \,|\, cd \rangle - \langle ab \,|\, \hat{v} \,|\, dc \rangle
\tag{86}
$$

i.e.

$$
X_a = 2X_0 - X_1, \quad X = A, B, C, C', C'',
\tag{87}
$$

we get finally

$$
k_0^{(3)} = \sum R_{ph}(A_a B_a C_a - 3A_1 B_1 C_1) + \sum R_{pp} A_0' B_0' C_a' + \sum R_{hh} A_0'' B_0'' C_a'',
\tag{88}
$$

where the summations extend over the same hole and particles index sets as in (85).

In a completely analogous way we can find the explicit spin-independent expressions for the nonHartree–Fock basis. Clearly, in this case, the two-particle (type A) contribution is again given by (88) and we only have to find the additional mixed contributions involving both Q- and V-vertices as well as the pure one-particle contribution.

Proceeding along the same lines as in the case of the two-particle contribution, we first find all pertinent resulting Goldstone diagrams and then write down immediately the explicit algebraic expressions using the rules given in Sections IV,D and F. The latter step being straightforward we only present here the relevant diagrams. We observe that the mixed

(b)
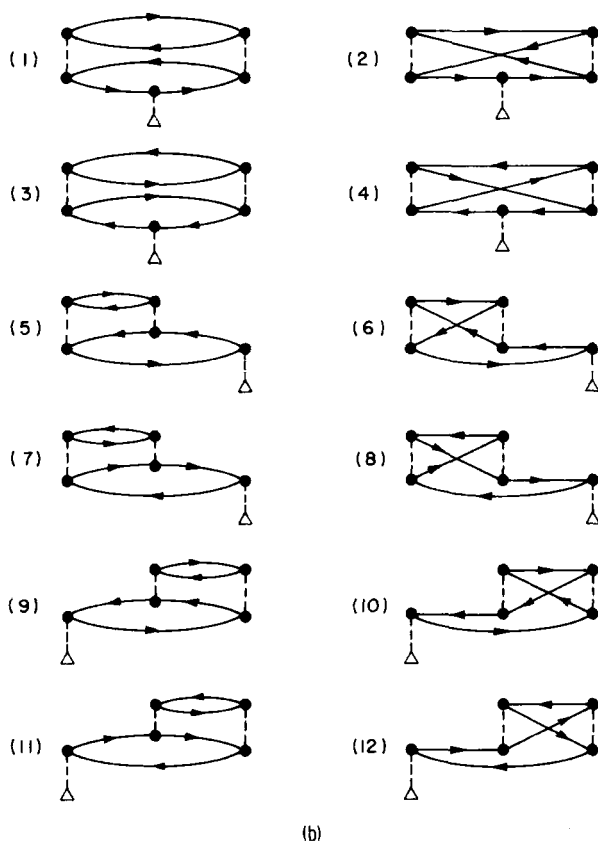
Fig. 14b. Resulting Goldstone diagrams for the mixed (type B, i.e. one Q- and two V-vertices) third-order contribution to the ground state energy.

terms can be of two basic types, depending on whether they contain one Q-vertex and two V-vertices (B type) or two Q- and one V-vertices (type C). The resulting Goldstone diagrams of both types are given in Figs. 14b and c, respectively. Finally, the one-particle contribution (type D, three Q-vertices) is given by the diagrams shown in Fig. 14d.

We would like to illustrate with this example one interesting feature of these resulting diagrams, which we shall conveniently exploit in the more complex excitation energy case treated in the next section. Consider, for example, a B-type mixed contribution given by the diagrams of Fig. 14b. We first observe that all the odd numbered diagrams are in fact the

(c)
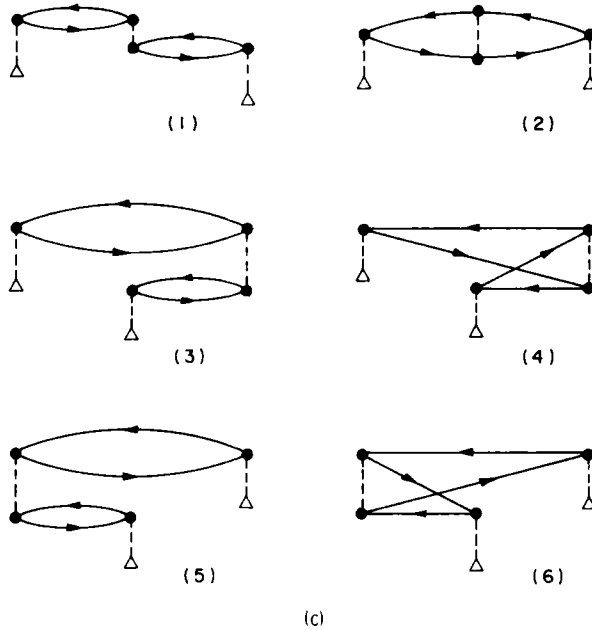
Fig. 14c. Resulting Goldstone diagrams for the mixed (type C, i.e. two Q- and one V-vertices) third-order contribution to the ground state energy.

exchange diagrams corresponding to the direct (even numbered) ones. Moreover, all these odd (even) numbered diagrams are easily obtained from the first (second) listed diagram by permuting the left–right ordering of vertices in all possible $3! = 6$ ways. Such grouping of diagrams, which differ only by a vertex permutation, follows naturally when using the time-dependent formalism of Goldstone (1957). The diagrams related in this way are referred to as different *time versions* of the same diagrams.

This grouping is particularly important in higher orders and in the excitation energy case, where we have to deal with large sets (several

(d)
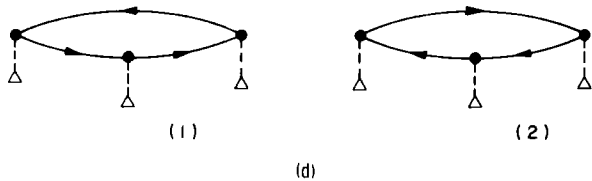
Fig. 14d. Resulting Goldstone diagrams for the one-particle (type D) third-order contribution to the ground state energy.

hundreds or even thousands) of Goldstone diagrams. Indeed, this is one of the homomorphic "projections" used in our "double projection scheme" (Paldus and Čížek, 1974; Čížek and Paldus, 1972), which enables one not only to write down the compact explicit expressions for higher orders of the PT, but also makes possible their efficient numerical evaluation. For example, in the considered case of B-type diagrams of Fig. 14b we see that all these diagrams are easily generated from a single Hugenholtz diagram, which will be referred to as the *essentially distinct diagram* (cf. Paldus and Wong, 1973; also Section V).

H. Hartree–Fock Diagrams

Using the operators in the N-product form [cf. Eqs. (16), (17), (30), (38) and Appendix D], we have achieved a considerable simplification of the PT formulas. Indeed, this fact enabled us to use the generalized Wick theorem (Appendix C) rather than the ordinary one and thus to eliminate the explicit consideration of a great number of diagrams, in which the oriented lines associated with the same Q- or V-vertex are joined together. This elimination is helpful in every order of the PT. In the first order we get a particularly simple result, namely that $k_0^{(1)} = 0$ [cf. Eq. (78)] regardless of whether we use the Hartree–Fock basis or some other independent particle model orbitals.

Should we apply the PT directly to the Hamiltonians $\hat{H}$ and $\hat{H}_0$ [Eqs. (10) and (12), respectively], we will not have the perturbation operator $\hat{W}$ in the N-product form and will have to associate the basic interaction vertices with the ordinary operator products (cf. Goldstone, 1957; Brandow, 1967; and others) rather than with the N-products. Consequently, we shall have to consider also contractions between the creation and annihilation operators of the same $\hat{V}$ or $\hat{U}$ operator when we apply Wick's theorem. Designating the one-particle vertex characterizing the
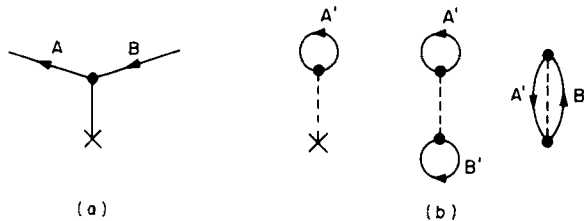
Fig. 15. (a) Diagrammatic representation of the one-particle potential $\hat{U}$ [cf. Eqs. (12), (31)] by U-diagram (skeleton, vertex). (b) First-order Hartree–Fock diagrams.

operator $\hat{U}$ as shown in Fig. 15a, and assigning to it the scalar quantity

$$d_U(\chi) = -\langle A \,|\, \hat{u} \,|\, B \rangle, \tag{89}$$

and using the same V-vertex as before for the two-particle part of the perturbation (which is not any more in the N-product form, however), we obtain easily in the first order of PT [cf. Eq. (9a)] the diagrams shown in Fig. 15b.

We find that the internal lines originating and ending on the same vertex or supervertex must always be hole lines. Otherwise the same rules as given in Sections IV,D and F will apply to their evaluation. Thus, we get immediately from the diagrams of Fig. 15b

$$\Delta E_0^{(1)} = -\sum_{A'} \langle A' \,|\, \hat{u} \,|\, A' \rangle$$

$$+ \frac{1}{2} \sum_{A', B'} (\langle A'B' \,|\, \hat{v} \,|\, A'B' \rangle - \langle A'B' \,|\, \hat{v} \,|\, B'A' \rangle)$$

$$= \sum_{A'} (\tfrac{1}{2}\langle A' \,|\, \hat{g} \,|\, A' \rangle - \langle A' \,|\, \hat{u} \,|\, A' \rangle), \tag{90}$$

yielding the first-order contribution in this formalism, which is generally different from zero. As may be seen from Eqs. (38)–(40), we get for the case of the Hartree–Fock potential

$$\Delta E_0^{(1)} = -\frac{1}{2} \sum_{A'} \langle A' \,|\, \hat{u} \,|\, A' \rangle, \tag{91}$$

since $\hat{U} = \hat{G}$. We find easily that the zero and the first orders, $E_0^{(0)}$ and $\Delta E_0^{(1)}$, respectively, give the well-known expression for the Hartree–Fock energy.

Similarly, in the second order, the additional diagrams which appear in this conventional approach (not using the N-product form of the operators) are shown in Fig. 16. However, the explicit consideration of these diagrams[15] is avoided in our approach based on the N-product form of the perturbation, even if we use an arbitrary one-particle potential in the unperturbed problem. Indeed, these diagrams are "hidden" in the one-particle potential (represented by Q-vertices) diagrams, since the definition of this potential, Eqs. (39) and (40), may be graphically represented as shown in Fig. 17. Thus, all the nine diagrams of Fig. 16 are represented in our formalism by the single diagram shown in Fig. 8b.

[15] Summing the contributions from the diagrams of this type to the infinite order of PT may be shown to be equivalent to the use of Hartree–Fock orbitals as a basis for the PT (Tolmachev, 1962). This is why the diagrams of this type are called Hartree–Fock diagrams.
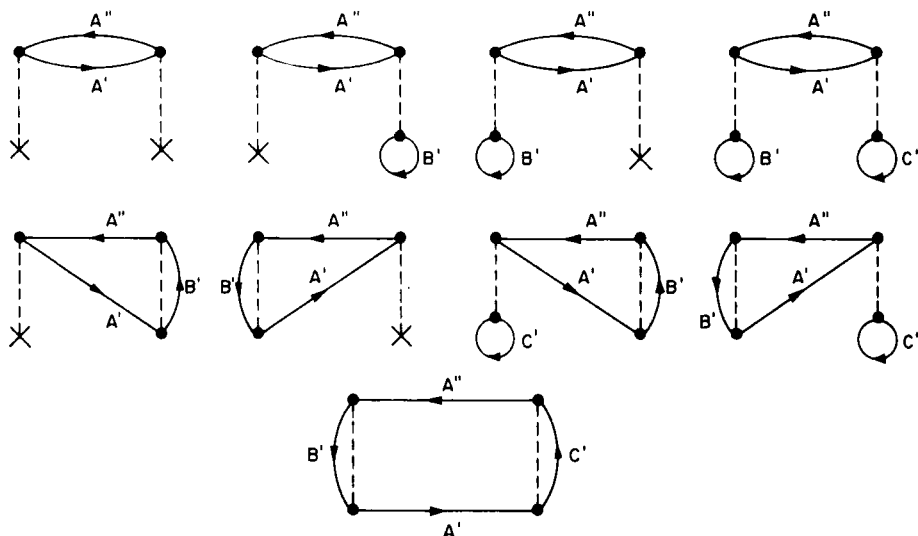
Fig. 16. Second-order Hartree–Fock diagrams.

In general, a graph containing k Q-vertices represents in fact 3^k diagrams. We hope that this example shows the advantages of introducing the potential $\hat{Q}$, Eqs. (39) and (40), into our theory very clearly indeed.
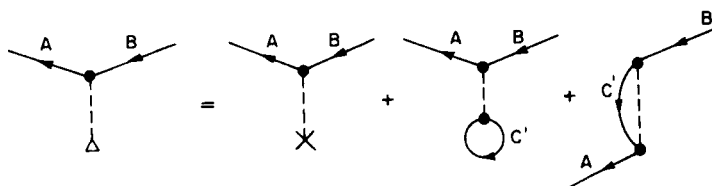
Fig. 17. Diagrammatic representation of the definition of the operator $\hat{Q}$ [Eq. (40)].

V. Perturbation Theory for Excitation Energies of Closed-Shell Systems

We shall now apply the diagrammatic technique of Sections III and IV to obtain the perturbation expansion for the direct calculation of excitation energies of closed-shell fermion systems. This approach will clearly show the compensation of terms appearing in the perturbation expansions for both levels and will yield the same expressions as those obtained in the Green function approach (Paldus and Čížek, 1974).

For the sake of clarity we shall restrict ourselves in this section to specific examples up to the second order of PT. In the next section we will present a generalization of our previous results (Paldus and Čížek, 1974), based on the Hartree–Fock approximation, for an arbitrary (i.e. nonHartree–Fock) unperturbed potential $\hat{U}$, giving explicit expressions up to and including the third order.

Having developed the ground state perturbation theory in the preceding section, we will mainly concentrate here on the perturbation expansion for low-lying excited states.

A. General Formulation

Consider again the Hamiltonian (10), (11) and the unperturbed Hamiltonian (12) in the normal product form defining operators $\hat{K}$ and $\hat{K}_0$, Eqs. (16) and (17), respectively. Thus, $\hat{W}$ is also in the N-product form (with respect to the unperturbed ground state $|\Phi_0\rangle$ chosen as a Fermi vacuum) and given by (38).

Consider next a nondegenerate low-lying excited state $|\Psi_1\rangle$, whose unperturbed counterpart[16] is described by the monoexcited configuration $|\Phi_1\rangle$,

$$|\Phi_1\rangle = \hat{X}^\dagger_{A''}\hat{X}_{A'}|\Phi_0\rangle = N[\hat{X}^\dagger_{A''}\hat{X}_{A'}]|\Phi_0\rangle. \tag{92}$$

We assume that the unperturbed levels $|\Phi_i\rangle$, $i = 0, 1$, become exact states $|\Psi_i\rangle$, $i = 0, 1$, as the perturbation is switched on. These states are eigenstates of $\hat{K}$ and $\hat{K}_0$, respectively [cf. Eqs. (2) and (3)], and the perturbation expansion of the eigenvalues for both $i = 0$ and $i = 1$ is given by (7). Similarly, the pertinent operators $\hat{P}_i$, $i = 0, 1$, are defined by (5). Thus, to the first three orders of the PT the ground state contributions are given by (78), while for the excited state $i = 1$ we have

$$k_1^{(0)} = \kappa_1 = \omega_{A''} - \omega_{A'},$$

$$k_1^{(1)} = \langle\Phi_1 \mid \hat{W} \mid \Phi_1\rangle,$$

$$k_1^{(2)} = \langle\Phi_1 \mid \hat{W}\hat{P}_1\hat{W} \mid \Phi_1\rangle,$$

$$k_1^{(3)} = \langle\Phi_1 \mid \hat{W}\hat{P}_1(W - k_1^{(1)})\hat{P}_1\hat{W} \mid \Phi_1\rangle. \tag{93}$$

---

[16] We assume for the moment that even $|\Phi_1\rangle$ is nondegenerate, and will discuss the degenerate case shortly.

The corresponding excitation energy is then

$$\Delta E_1 = E_1 - E_0 = k_1 - k_0 = \Delta k = \sum_{i=0}^{\infty} (k_1^{(i)} - k_0^{(i)})$$

$$= \sum_{i=0}^{\infty} \Delta k^{(i)}$$

$$= \sum_{i=1}^{\infty} \Delta E_1^{(i)}.$$

In the case where the unperturbed level is degenerate, we have to use the appropriate formalism for a degenerate level. Designate $|\Phi_{1i}\rangle$ $(i = 1, \ldots, s)$ the degenerate levels belonging to κ_1,

$$\hat{K}_0 |\Phi_{1i}\rangle = \kappa_1 |\Phi_{1i}\rangle, \qquad i = 1, \ldots, s. \tag{94}$$

Then instead of simple diagonal matrix elements (93) we have to calculate the whole matrix $k_1^{(n)}$ (i, j),

$$k_1^{(1)}(i, j) = \langle \Phi_{1i} | \hat{W} | \Phi_{1j}\rangle,$$

$$k_1^{(2)}(i, j) = \langle \Phi_{1i} | \hat{W} \hat{P}_1 \hat{W} | \Phi_{ij}\rangle,$$

$$k_1^{(3)}(i, j) = \langle \Phi_{1i} | \hat{W} \hat{P}_1 (\hat{W} - k_1^{(1)}) \hat{P}_1 \hat{W} | \Phi_{1j}\rangle,$$

$$\text{etc.,} \tag{95}$$

where $k_1^{(1)}$ in the third-order renormalization term is the first-order correction for the appropriate calculated energy level obtained from the first-order calculation. Thus, for each level we shall have to carry out a new diagonalization using the appropriate $k_1^{(1)}$ corrections.

In order for our expressions to apply to a general case, we shall evaluate a general matrix element of the type (95). Let us designate the appropriate independent particle model excitations as $A_2' \rightarrow A_1''$ and $A_4' \rightarrow A_3''$, i.e.

$$|\Phi_{1j}\rangle = N[\hat{X}_{A_1''}^{\dagger} \hat{X}_{A_2'}] |\Phi_0\rangle,$$

$$\langle \Phi_{1i} | = \langle \Phi_0 | N[\hat{X}_{A_4'}^{\dagger} \hat{X}_{A_3''}], \tag{96}$$

or simply $2 \rightarrow 1$ and $4 \rightarrow 3$, writing symbolically

$$|\Phi_{1j}\rangle = N[1^{\dagger}2] |\Phi_0\rangle,$$

$$\langle \Phi_{1i} | = \langle \Phi_0 | N[4^{\dagger}3], \tag{97}$$

and labeling the diagrams accordingly.

In fact, except for the accidental degeneracy case, we can always remove the degeneracy problem here by finding the appropriate symmetry (spin, space, alternancy, etc.) adapted independent particle states to which the nondegenerate form of the theory will apply. In any case, however, matrix elements of the type (95) (between single determinantal states) will be needed for evaluation of these matrix elements between the symmetry adapted states.

B. Diagrammatic Approach

Representing the bra and ket configurations $\langle \Phi_{1i} |$ and $| \Phi_{1j} \rangle$ by $\bar{T}(1)$ and $T(1)$ diagrams (skeletons), respectively, and the operator $\hat{W} = \hat{Q}_N + \hat{V}_N$ by the Q- and V-diagrams (skeletons), as defined in Section III,A, we can proceed in exactly the same way as in the ground state case. We must, however, change the rule for obtaining the denominators as well as to avoid all diagrams in which the intermediate state is one of the degenerate states $| \Phi_{1i} \rangle$ $(i = 1, \ldots s)$.[17] On the other hand, we now have to consider also the disconnected diagrams resulting from the use of the ground state projector $| \Phi_0 \rangle \langle \Phi_0 |$ in $\hat{P}_1$ [cf. Eq. (5), $i = 1$].

We find from Eqs. (5), (21), and (26) that the new denominator rule is simply obtained by adding to the denominator as obtained by rule (iii b) of Section IV,D the zero-order excitation energy, i.e. the new denominator factor is

$$\left[\omega_{A''} - \omega_{A'} + \sum_i (\omega_{A_{i'}} - \omega_{A_{i''}}) \right]^{-1}, \tag{98}$$

the summation extending again over all pairs of hole and particle lines passing through the interval between two given neighboring Q- or V-vertices. We see that for diagrams having as an intermediate state one of the degenerate states $| \Phi_{1i} \rangle$ $(i = 1, \ldots, s)$, which are called dangerous diagrams and which must be discarded, the denominator in (98), referred to appropriately as a dangerous denominator, vanishes.

In assigning the algebraic expressions to the resulting diagrams we also have to keep in mind that the monoexcitation labels A''_1, A'_2, A''_3, A'_4 or, simply, 1, 2, 3, 4, are fixed labels which are not summed over. We also notice that the weight of all resulting skeletons will be equal to unity.

Thus, in order to obtain the nth-order correction to the excited energy

---

[17] The nondegenerate case, when $s = 1$, represents a special case of this more general degenerate case.

level we have to construct all possible connected and disconnected result-
ing diagrams having one $\bar{T}(1)$-vertex on the left-hand side, one $T(1)$-
vertex on the right-hand side and n, Q- or V-vertices in between, and
assign to these diagrams the scalar quantities following the modified rules
just outlined.

Considering, for example, the first-order terms, we find immediately
that the only possible resulting Goldstone diagrams are those shown in
Fig. 18. This yields

$$k_1^{(1)}(i, j) = \langle A_3'' \,|\, \hat{q} \,|\, A_1'' \rangle \langle A_2' \,|\, A_4' \rangle - \langle A_2' \,|\, \hat{q} \,|\, A_4' \rangle \langle A_3'' \,|\, A_1'' \rangle$$
$$- \langle A_3'' A_2' \,|\, \hat{v} \,|\, A_1'' A_4' \rangle + \langle A_3'' A_2' \,|\, \hat{v} \,|\, A_4' A_1'' \rangle. \qquad (99)$$

C. Spin-Independent Formalism

The rules for obtaining the orbital form of the resulting expressions
must be modified since 1, 2, 3, and 4 represent fixed labels. Moreover, for
the spin-independent Hamiltonian, the resulting states must be eigen-
states of $\hat{S}_z$ and $\hat{S}^2$. In the unperturbed limit we thus have to use appro-
priate linear combinations of the degenerate spin orbital configurations,
which are proper eigenfunctions of $\hat{S}_z$ and $\hat{S}^2$. Considering monoexcita-
tion $a' \to a''$ we get the following singlet and triplet configurations corre-
sponding to $s_z = 0$ case

$$|\Phi_1^s\rangle = \left(\left| \begin{matrix} a''\alpha \\ a'\alpha \end{matrix} \right\rangle + \left| \begin{matrix} a''\beta \\ a'\beta \end{matrix} \right\rangle \right) / 2^{1/2},$$

$$|\Phi_1^t\rangle = \left(\left| \begin{matrix} a''\alpha \\ a'\alpha \end{matrix} \right\rangle - \left| \begin{matrix} a''\beta \\ a'\beta \end{matrix} \right\rangle \right) / 2^{1/2}, \qquad (100)$$

where α, β are one-particle spin up $(\eta = \frac{1}{2})$ and spin down $(\eta = -\frac{1}{2})$
eigenfunctions. The other two triplet components will have the same
energy as the $s_z = 0$ one and do not have to be considered explicitly.

Using the $s_z = 0$ components we find again that the spin state must be
preserved along each path of oriented lines, irrespective of the vertices
through which it passes.[18]

Forming the linear combinations (100) we realize that we have to
distinguish two types of diagrams, depending on whether a given spin
state propagates from a $T(1)$-vertex through the whole diagram to a
$\bar{T}(1)$-vertex or not. Clearly, only the terms where the spin state does not
propagate through the whole diagram will contribute to the cross terms

---

[18] This would not be true for the other two triplet components. Here the spin state
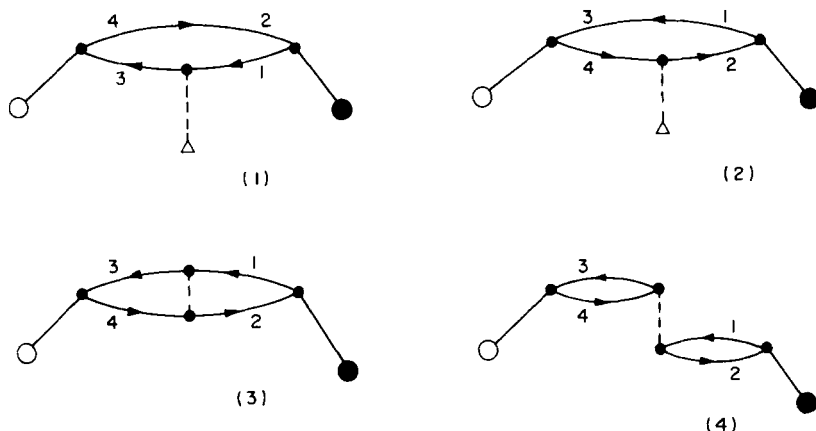would have to be reversed in going through the $T(1)$-vertex.

Fig. 18. First-order excitation energy Goldstone diagrams (or Green function particle-hole diagrams deleting $\bar{T}$- and T-vertices).

between the spin orbital configurations in (100). We shall refer to these two types of diagrams as forward and backward ones:

(i) A *forward* diagram results when there exists an oriented path connecting $\bar{T}$- and T-vertices, [cf., for example, diagrams (1)–(3) of Fig. 18].

(ii) In *backward* diagrams no such oriented path exists and the path leaving the T- (or $\bar{T}$-) vertex returns to the same vertex [for example, diagram (4) of Fig. 18].

Calculating the spin symmetry adapted matrix elements for various orders of perturbation theory we get in general four terms, as shown schematically in Fig. 19. Clearly, the first two terms on the right-hand

Fig. 19. A schematic representation of the derivation of rules for the forward and backward diagram contributions to the singlet and triplet excited state (or excitation) energies.

side will contribute irrespective of whether a given diagram is a forward or a backward one. However, the last two terms will give a nonvanishing result only for backward diagrams [cf. Eq. (B.15)].

We can thus formulate the following simple rules for the transition to the orbital formalism (compare with rules of Section IV,F):

(i) Replace spin orbital summation indices with the orbital ones.

(ii) Assign factors f and b to forward and backward diagrams, respectively.

(iii) Multiply the contribution of a diagram by an additional factor 2^{l-1}.

Then the singlet excitation energy will result for $f = b = 1$, triplet excitation energy for $f = 1$ and $b = 0$ (i.e. only forward diagrams contribute to the triplet energy), and the singlet–triplet separation for $f = 0$ and $b = 1$.

Note that in this case the additional numerical factor is 2^{l-1} since we get an additional factor of $\frac{1}{2}$ from the normalization factors in (100).

As an example, the first-order contribution (99) in the orbital form gives the well known result

$$k_1^{(1)}(i, j) = f[\langle a_3'' | \hat{q} | a_1'' \rangle \langle a_2' | a_4' \rangle - \langle a_2' | \hat{q} | a_4' \rangle \langle a_3'' | a_1'' \rangle$$
$$- \langle a_3'' a_2' | \hat{v} | a_1'' a_4' \rangle] + 2b \langle a_3'' a_2' | \hat{v} | a_4' a_1'' \rangle. \tag{101}$$

D. Example: Second-Order Contribution to the Excitation Energy

Let us see in detail how in the second-order case a cancellation of various terms occurs and how we can get the explicit expressions, which are the same as those obtained using the Green function approach. No such cancellation occurs in the first order, since owing to our choice of the operators $\hat{K}$ and $\hat{K}_0$ the first-order ground state contribution vanishes [cf. Eqs. (78)] so that the expression (101) represents directly the first-order excitation energy correction.

Consider first the single particle terms, i.e. the terms which result when we consider two Q-vertices. All possible resulting diagrams are easily found and are listed in Fig. 20. The first disconnected diagram (1) corresponds to a ground state projector part in $\hat{P}_1$, the diagrams (2)–(4) are obtained with monoexcited intermediate states, and the remaining ones with the biexcited intermediate states. Those diagrams of type (2)–(4), which yield dangerous denominators, must be discarded. In fact, it is easily seen that all diagrams of type (4) are dangerous diagrams and may be omitted.
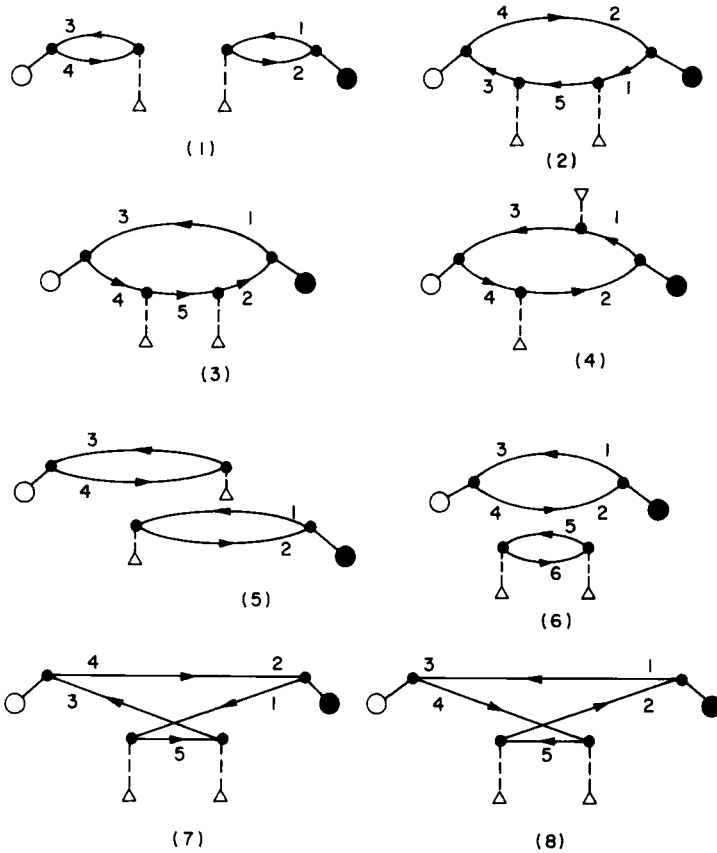
Fig. 20. Resulting diagrams for the one-particle second-order contribution to the excited state.

Further, we see immediately that the diagrams (1) and (5) of Fig. 20 cancel

$$k(1) = \langle 2 | \hat{q} | 1 \rangle \langle 3 | \hat{q} | 4 \rangle / (\omega_1 - \omega_2),$$

$$k(5) = \frac{\langle 2 | \hat{q} | 1 \rangle \langle 3 | \hat{q} | 4 \rangle}{(\omega_1 - \omega_2) + 2(\omega_2 - \omega_1)} = -k(1), \tag{102}$$

since $\omega_1 - \omega_2 = \omega_3 - \omega_4$ due to the assumption of degeneracy (in the nondegenerate case $1 = 3$, $2 = 4$). We are thus left with diagrams (2), (3), and (6)–(8). In order to get the excitation energy contribution from these one-particle terms, we must subtract the second-order one-particle ground state diagrams. Obviously, there is only one diagram of this type,

shown in Fig. 8b. Again we find that this diagram cancels exactly the contribution of the disconnected diagram (6).

Thus, only four diagrams [(2), (3), (7), and (8) of Fig. 20] contribute to the excitation energy. In fact all these diagrams are easily obtained from the diagram (2) by the following operations: (i) Particle–hole reversal, in which the direction of arrows on all oriented lines is reversed or, equivalently, the so called "time reversal" in which the diagram is reflected in the plane parallel to the vertex dashed lines.[19] (ii) "Time-version" formation, obtained by permuting the left–right ordering of Q- and V-vertices in all possible ways.

These "symmetry" operations on graphs follow naturally from the Green function approach and enable us to write very compact final expressions as we explained in detail earlier (Paldus and Čížek, 1974).

Diagrams which may not be obtained one from another by these two operations we call "essentially distinct diagrams" (Paldus and Wong, 1973, and Section IV,G). Thus, in this one-particle second-order case, we get only one essentially distinct diagram [say, diagram (2) of Fig. 20]. Its contribution to the excitation energy, in the orbital form, is given explicitly in the next section.

Let us also note here that this diagram [and, of course, the diagrams (3), (7), and (8) of Fig. 20, which we can generate from it] represents a so-called "self-energy" diagram. These diagrams are distinguished by the fact that they are always forward diagrams and all interactions involve only one oriented path connecting the $\bar{T}$- and T-vertices, while the other path propagates directly without any interactions. These diagrams are in fact the diagrams yielding the ionization potentials or electron affinities, as we shall see in Section VII.

Similarly we can consider the second-order contribution containing two V-vertices. In this case we obtain the Hugenholtz diagrams shown in Fig. 21. Again, diagram (1) results from using monoexcited states as the intermediate ones and the dangerous diagrams of this type must be excluded. The diagrams (2)–(7) then have biexcited intermediate states and (8)–(11) the triexcited ones. We see that the only disconnected diagram in this case is the last diagram, (11), which is again canceled by the corresponding ground state diagram of Fig. 12. The remaining ten diagrams are then easily obtained from the four essentially distinct diagrams, given in Fig. 13 of paper by Paldus and Čížek (1974), where the compact expression for their contribution may also be found.

---

[19] These two operations do not generally yield the same diagram but in totality all the diagrams so generated will be equivalent.
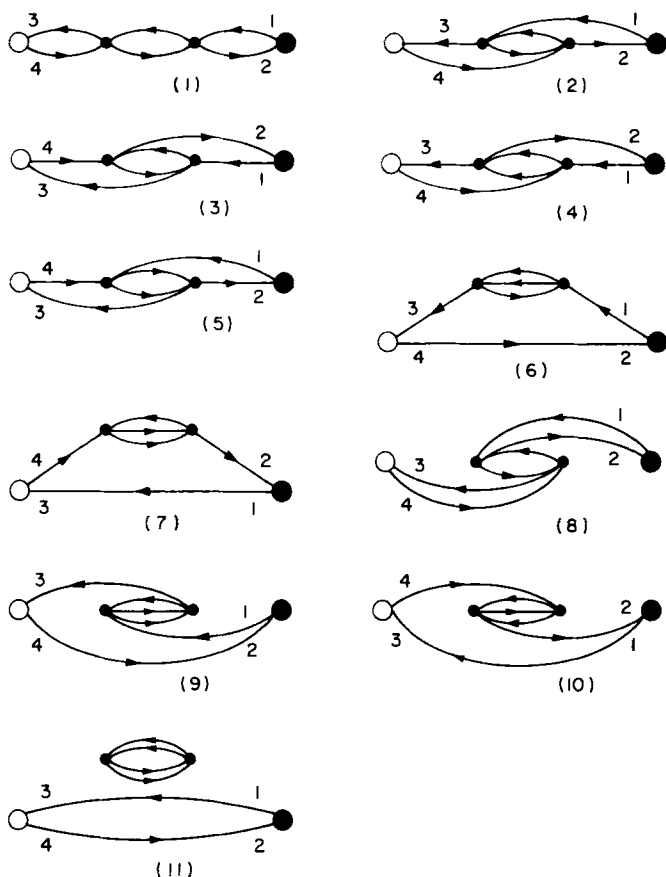
Fig. 21. Resulting diagrams for the two-particle second-order contribution to the excited state energy.

Considering, finally, the "mixed" contributions containing one Q- and one V-vertex, we find that only connected diagrams result (the essentially distinct Hugenholtz diagrams of this type in the Green function form are illustrated in Fig. 22). Since there is no ground state contribution of this type, these diagrams give directly the contribution to the excitation energy, the exact form of which is given in the next section.

We thus see that we indeed get the same resulting expressions by this direct approach as those obtained earlier from the Green function formalism. We have also seen very clearly the type of cancellation which occurs.
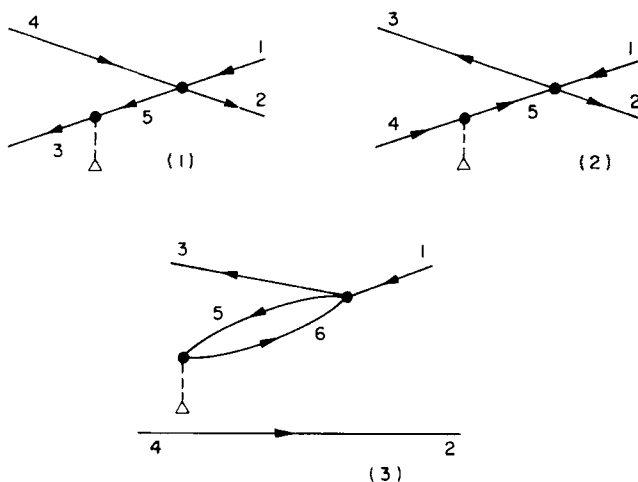
Fig. 22. Essentially distinct p–h diagrams for the mixed second-order contribution to the irreducible vertex part (or excitation energy resulting diagrams if the external lines are joined into the appropriate $\bar{T}$- and T-vertices).

In fact, we find that generally the diagrams most difficult to evaluate numerically (i.e. diagrams containing the largest number of summations) will cancel out in the direct approach. One can also better appreciate the reduction in the number of diagrams, which one has to consider explicitly, which follows naturally from the Green function formalism. On the other hand it is very instructive and gratifying to see that the same formulas may be obtained with a simple time-independent perturbation theory.

VI. General Explicit Formulas for the Second- and Third-Order Excitation Energy Contributions

We shall now extend the formulas using the Hartree–Fock basis given earlier [Paldus and Čížek (1974); hereafter referred to as PC(74)][20] to a general case enabling one to use an arbitrary unperturbed potential and corresponding orbitals. Clearly, the two-particle part of the perturbation $\hat{W}$ yields exactly the same expressions as those obtained for the Hartree–Fock basis. Thus, we need only consider the contributions involving the one-particle matrix elements $\langle a \,|\, \hat{q} \,|\, b \rangle$ which vanish identically when the Hartree–Fock potential is used for the unperturbed problem.

[20] For the details of notation used we refer the reader to this paper.

The essentially distinct diagrams of this type may be easily generated by the algorithm described earlier (Paldus and Wong, 1973; Wong and Paldus, 1973). The total number of essentially distinct diagrams of each vertex structure is shown in Table II. For a comparison, we also list these total numbers for the fourth-order diagrams. The explicit expressions for the contributions containing one-particle vertices, which were not given earlier [PC(74)], follow.

TABLE II

NUMBER OF ESSENTIALLY DISTINCT PARTICLE-HOLE HUGENHOLTZ DIAGRAMS IN
VARIOUS ORDERS OF PERTURBATION THEORY

PT order	Number of one-particle vertices	Number of two-particle vertices	Total number of essentially distinct Hugenholtz diagrams	Number of self-energy diagrams
1	1	0	1	1
	0	1	1	0
2	2	0	2	1
	1	1	3	1
	0	2	4	1
3	3	0	2	1
	2	1	10	3
	1	2	17	5
	0	3	14	3
4	4	0	3	1
	3	1	20	6
	2	2	70	17
	1	3	102	23
	0	4	76	14

A. Second Order

The second-order contribution $M^{(2)}$ to the compact vertex part M [cf. PC(74)] or to the excitation energy part of the matrix elements (95) (i.e. with the ground state component subtracted) is given as a sum of three components

$$M^{(2)} = M_A^{(2)} + M_B^{(2)} + M_C^{(2)}. \qquad (103)$$

The first component $M_A^{(2)}$, corresponding to the two-particle part of the perturbation, is given by Eq. (41) of PC(74) and will not be repeated here.

The second component $M_B^{(2)}$ corresponds to the "mixed" one-particle–two-particle contribution, while the last term $M_C^{(2)}$ gives a single particle contribution only.

For the "mixed" second term $M_B^{(2)}$ there are three essentially distinct diagrams (cf. Table II) shown in Fig. 22. We now draw these diagrams in the Green function form, which we simply obtain by "chopping off" the $\bar{T}$- and T-vertices on both ends. In this case the time-reversal symmetry parameter $g_i{}^{21}$ is always equal to unity and is not explicitly listed. We obtain

$$M_B^{(2)} = \sum_{i=1}^{3} (\theta_i^B + \bar{\theta}_i^B), \tag{104}$$

where

$$\theta_i^B(1, 2, 3, 4) = \sum_5 \Theta_i^B \kappa(\alpha_1^i, \alpha_2^i; 3), \qquad i = 1, 2,$$

$$\theta_3^B(1, 2, 3, 4) = \sum_{5, 6} \Theta_3^B \kappa(\alpha_1^3, \alpha_2^3; 4), \tag{105}$$

are the contributions from the set of Goldstone diagrams mapped into the ith essentially distinct Hugenholtz diagram of Fig. 22, the last term ($i = 3$) corresponding to the self-energy diagram (3) of Fig. 22. The numerators Θ_i^B have the form

$$\Theta_i^B = \langle b_1^i \,|\, \hat{q} \,|\, b_2^i \rangle \sum_{j=0}^{1} d_j^i A_j^i, \tag{106}$$

where A_j^i are the two-particle matrix elements [cf. Eq. (44) of PC(74)]

$$A_0^i = \langle a_1^i a_2^i \,|\, \hat{v} \,|\, a_3^i a_4^i \rangle,$$

$$A_1^i = \langle a_1^i a_2^i \,|\, \hat{v} \,|\, a_4^i a_3^i \rangle, \tag{107}$$

and the parameters d_j^i, a_j^i, and b_j^i are listed in Table III. The denominator parts, which differ from those defined by Eq. (45) in PC(74), have the following form

$$\kappa(\alpha_1^i, \alpha_2^i; 3) = \alpha_1^i - \alpha_2^i,$$

$$\kappa(\alpha_1^i, \alpha_2^i; 4) = (\alpha_1^i + \alpha_2^i)\delta_{2, 4}, \tag{108}$$

where the denominators α_i^i are given by Eq. (46) of PC(74), and the hole

---

[21] This parameter equals unity if the distinct diagram (skeleton) is obtained by the time-reversal (particle–hole reversal) operation (cf. Section V,D) and equals two if the skeleton is invariant to this operation.

and particle index sets ξ_l^i, η_l^i, appearing in the definition of α_l^i, are listed in Table III. The contributions $\tilde{\theta}_i^B$ from the time-reversed diagrams are obtained using the rules outlined in PC(74).

TABLE III

VALUES OF THE PARAMETERS b_j^i, a_j^i, d_j^i AND THE PARTICLE AND HOLE INDEX SETS ξ_j^i AND η_j^i, RESPECTIVELY, CHARACTERIZING THE SECOND-ORDER P–H DIAGRAMS OF TYPE B (FIG. 22) AND APPEARING IN THE EXPLICIT EXPRESSIONS (104)–(108)

i	Q_1^i		A_j^i				α_1^i		α_2^i		d_0^i	d_1^i
	b_1^i	b_2^i	a_1^i	a_2^i	a_3^i	a_4^i	ξ_1^i	η_1^i	ξ_2^i	η_2^i		
1	3	5	2	5	1	4	5	4	1, 3	2, 5	$2b$	$-f$
2	5	4	2	3	1	5	3	5	1, 5	2, 4	$-2b$	f
3	6	5	3	5	1	6	3, 5	2, 6	1, 6	2, 5	$2f$	$-f$

The single particle part $M_C^{(2)}$ is determined by the two essentially distinct diagrams shown in Fig. 23 [i.e. by diagrams (2) and (4) of Fig. 20]. As we already mentioned earlier, the contribution from the second diagram vanishes (always yielding a dangerous denominator).
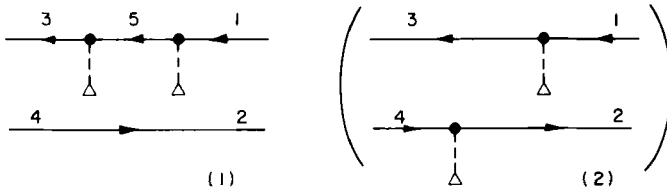
Fig. 23. Essentially distinct p–h diagrams for the one-particle second-order contribution to the excitation energy (cf. also caption to Fig. 22).

Thus, we obtain simply

$$M_C^{(2)} = \theta^C + \tilde{\theta}^C, \tag{109}$$

where

$$\theta^C(1, 2, 3, 4) = \sum_5 \Theta^C \delta_{2,4}(\alpha_1 - \alpha_2) \tag{110}$$

and

$$\Theta^C = f \langle 3 | \hat{q} | 5 \rangle \langle 5 | \hat{q} | 1 \rangle. \tag{111}$$

The particle and hole sets defining the denominators α_j $(j = 1, 2)$ are simply: $\xi_1 = \{5\}$, $\eta_1 = \{2\}$, $\xi_2 = \{1, 3\}$, and $\eta_2 = \{2, 5\}$, as may be seen instantly from diagrams (2) and (7) of Fig. 20.

B. Third Order

In the third order a considerable number of new diagrams appear when a nonHartree–Fock basis is used, as Table II indicates. However, these additional terms are much easier to evaluate than the corresponding two-particle terms of PC(74), since they always contain fewer summations.

We write

$$M^{(3)} = M_A^{(3)} + M_B^{(3)} + M_C^{(3)} + M_D^{(3)}, \tag{112}$$

where again the first term $M_A^{(3)}$ gives the two-particle contribution [Eqs. (49)–(53) of PC(74)] corresponding to 14 essentially distinct two-particle diagrams [Fig. 14 of PC(74)]. The last term $M_D^{(3)}$ gives the one-particle contribution, while the "mixed" one- and two-particle terms may now be of two distinct types depending on whether they contain one Q-vertex (B-type) or two Q-vertices (C-type).

Again no time-reversal symmetry parameter g_i is needed in cases B and C. Considering the essentially distinct diagrams of type B shown in Fig. 24, we can write

$$M_B^{(3)} = \sum_{i=1}^{17} (\lambda_i^B + \bar{\lambda}_i^B), \tag{113}$$

where

$$\lambda_i^B(1, 2, 3, 4) = \sum_{5, 6, 7} \Lambda_i^B \kappa(\alpha_k^i; \gamma_j(l_i)), \qquad i = 1, \ldots, 12;$$

$$\lambda_i^B(1, 2, 3, 4) = \sum_{5, 6, 7, 8} \Lambda_i^B \kappa(\alpha_k^i; \gamma_j(l_i)), \qquad i = 13, \ldots, 17;$$

$$k = 1, \ldots, 6; j = 1, \ldots, 5. \tag{114}$$

Further

$$\Lambda_i^B = \langle c_1^i \mid \hat{q} \mid c_2^i \rangle \sum_{j, k=0}^{1} d_{jk}^i B_j^i A_k^i, \tag{115}$$

where the two-particle matrix elements B_j^i, A_k^i are defined analogously to (107) [cf. Eqs. (44) of PC(74)], and the parameters d_{jk}^i, c_j^i, b_j^i, and a_j^i are
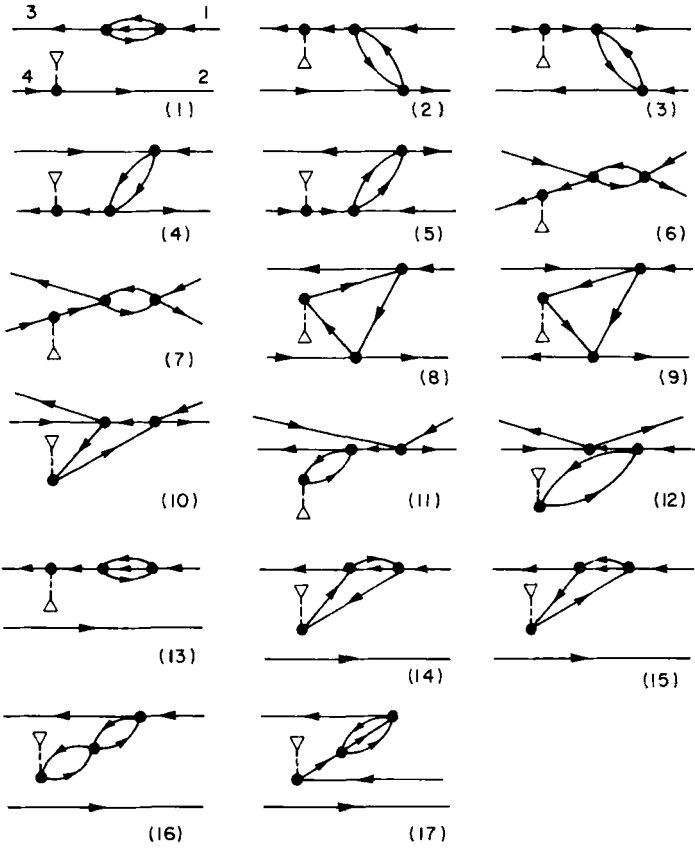
Fig. 24. Essentially distinct p-h diagrams for the mixed (type B, i.e. one Q- and two V-vertices) second-order contribution to the excitation energy.

listed in Table IVa. Finally,

$$\kappa(\alpha_k^i; \gamma_j(l_i))$$

$$= f(l_i)[\alpha_1^i(\alpha_4^i + \gamma_1(l_i)\alpha_5^i)$$

$$+ \gamma_2(l_i)\alpha_2^i(\alpha_4^i + \gamma_3(l_i)\alpha_6^i) + \gamma_4(l_i)\alpha_3^i(\alpha_5^i + \gamma_5(l_i)\alpha_6^i)], \tag{116}$$

where

$$f(k) = 1 \qquad \text{for} \qquad k = 1, 2, 3,$$

and

$$f(k) = \delta_{2,4} \qquad \text{for} \qquad k = 4, 5, 6,$$

TABLE IVa

VALUES OF PARAMETERS a_j^i, b_j^i, c_j^i, AND d_{jk}^i CHARACTERIZING THE THIRD-ORDER P–H DIAGRAMS OF TYPE B (FIG. 24) AND APPEARING IN EQS. (113)–(116)

i	Q_1^i		B_j^i				A_j^i				d_{jk}^i			
	c_1^i	c_2^i	b_1^i	b_2^i	b_3^i	b_4^i	a_1^i	a_2^i	a_3^i	a_4^i	00	10	01	11
1	2	4	3	6	7	5	5	7	6	1	$-2f$	f	0	0
2	3	7	6	7	5	1	2	5	4	6	$-2f$	f	f	$-2b$
3	7	4	2	6	7	5	3	5	1	6	$2f$	$-f$	$-f$	$2b$
4	3	7	2	7	6	5	5	6	4	1	$2b$	$-f$	0	0
5	7	4	5	6	7	1	2	3	6	5	$-2b$	f	0	0
6	3	7	6	7	5	4	2	5	1	6	$4b$	$-2b$	$-2b$	f
7	7	4	3	6	7	5	2	5	1	6	$-4b$	$2b$	$2b$	$-f$
8	6	7	2	7	4	5	3	5	1	6	$-2f$	f	f	$-2b$
9	6	5	2	3	7	6	5	7	4	1	$-2b$	f	f	$-2b$
10	6	5	3	5	4	7	2	7	1	6	$4b$	$-2b$	$-2b$	f
11	6	5	3	5	7	6	2	7	1	4	$4b$	$-2b$	$-2f$	f
12	6	5	2	3	7	4	5	7	6	1	$4b$	$-2f$	$-2b$	f
13	3	8	6	8	5	7	5	7	6	1	$2f$	$-f$	0	0
14	8	7	3	6	5	8	5	7	1	6	$-2f$	f	f	$-2f$
15	6	8	3	8	7	5	5	7	6	1	$2f$	$-f$	0	0
16	8	7	6	7	5	8	3	5	1	6	$4f$	$-2f$	$-2f$	f
17	8	1	6	7	8	5	3	5	7	6	$2f$	$-f$	0	0

TABLE IVb

VALUES OF PARAMETERS $\gamma_i(l)$ APPEARING IN (116) FOR THE SECOND-ORDER B-TYPE P–H DIAGRAMS IN FIG. 24

l	$\gamma_1(l)$	$\gamma_2(l)$	$\gamma_3(l)$	$\gamma_4(l)$	$\gamma_5(l)$
1	-1	$+1$	$+1$	-1	$+1$
2	$+1$	-1	$+1$	$+1$	-1
3	-1	-1	-1	$+1$	-1
4	-1	-1	$+1$	-1	$+1$
5	$+1$	-1	-1	-1	-1
6	$+1$	$+1$	$+1$	$+1$	$+1$

TABLE IVc

Values of the Parameters l_i and of the Sets ξ_j^i and η_j^i of Particle and Hole Indices, Respectively, Characterizing Different Time Versions of the Third-Order P-H Diagrams of Type B (Fig. 24) and Defining the Denominators α_k^i in (116)

	α_1^i		α_2^i		α_3^i		α_4^i		α_5^i		α_6^i		
i	ξ_1^i	η_1^i	ξ_2^i	η_2^i	ξ_3^i	η_3^i	ξ_4^i	η_4^i	ξ_5^i	η_5^i	ξ_6^i	η_6^i	l_i
1	3	2	5, 7	4, 6	1, 3, 6	4, 5, 7	5, 7	2, 6	1, 3, 6	2, 5, 7	1	4	1
2	7	4	1, 3, 5	4, 6, 7	3, 6	2, 5	1, 5	4, 6	6, 7	2, 5	1, 3	2, 7	2
3	3	7	3, 5, 7	2, 4, 6	1, 6	4, 5	3, 5	2, 6	1, 6	5, 7	1, 7	2, 4	2
4	7	4	3, 5, 6	2, 4, 7	1, 3	5, 6	5, 6	2, 4	1, 7	5, 6	1, 3	2, 7	2
5	3	7	1, 3, 7	4, 5, 6	5, 6	2, 4	1, 3	5, 6	5, 6	2, 7	1, 7	2, 4	2
6	7	4	3, 5	6, 7	1, 3, 6	2, 4, 5	5	6	1, 6, 7	2, 4, 5	1, 3	2, 7	2
7	3	7	5, 7	4, 6	1, 3, 6	2, 4, 5	5	6	1, 3, 6	2, 5, 7	1, 7	2, 4	2
8	3, 7	4, 6	3, 5	2, 7	1, 6	4, 5	3, 5	2, 6	1, 7	4, 5	1, 6	2, 7	3
9	3, 5	4, 6	6, 7	2, 4	1, 3	5, 7	5, 7	2, 4	1, 3	6, 7	1, 6	2, 5	3
10	3, 5	4, 6, 7	7	5	1, 3, 6	2, 4, 7	7	6	1, 3, 5	2, 4, 7	1, 6	2, 5	3
11	3, 5	4, 6	6, 7	4, 5	1, 3	2, 7	7	4	1, 3, 5	2, 6, 7	1, 6	2, 5	1
12	3, 5	4, 6	7	2	1, 3, 6	4, 5, 7	5, 7	2, 6	1, 3	4, 7	1, 6	2, 5	1
13	8	2	3, 5, 7	2, 6, 8	1, 3, 6	2, 5, 7	5, 7	2, 6	1, 6, 8	2, 5, 7	1, 3	2, 8	4
14	3, 7	2, 8	5, 8	2, 6	1, 3, 6	2, 5, 7	5, 7	2, 6	1, 3, 6	2, 5, 8	1, 8	2, 7	5
15	3, 8	2, 6	5, 7	2, 8	1, 3, 6	2, 5, 7	5, 7	2, 6	1, 3, 8	2, 5, 7	1, 6	2, 8	5
16	3, 7	2, 8	3, 5, 8	2, 6, 7	1, 6	2, 5	3, 5	2, 6	1, 6, 7	2, 5, 8	1, 8	2, 7	6
17	1, 3	2, 8	3, 5, 8	2, 6, 7	6, 7	2, 5	1, 3, 5	2, 6, 7	1, 6, 7	2, 5, 8	8	2	4

and the sign factors $\gamma_j(l_i)$ are given in Table IVb. The parameters l_i, together with the sets of hole and particle indices ξ_k^i, η_k^i defining the denominators α_k^i [Eq. (46) of PC(74)], are listed in Table IVc.

Next we consider a mixed type-C contribution, for which the essentially distinct diagrams are shown in Fig. 25. Thus

$$M_C^{(3)} = \sum_{i=1}^{10} (\lambda_i^C + \bar{\lambda}_i^C), \tag{117}$$

where

$$\lambda_i^C(1, 2, 3, 4) = \sum_{5, 6} \Lambda_i^C \kappa(\alpha_k^i; \gamma_j(l_i)), \qquad i = 1, \ldots, 7,$$

$$\lambda_i^C(1, 2, 3, 4) = \sum_{5, 6, 7} \Lambda_i^C \kappa(\alpha_k^i; \gamma_j(l_i)), \qquad i = 8, 9, 10,$$

$$k = 1, \ldots, 6; j = 1, \ldots, 5, \tag{118}$$

and

$$\Lambda_i^c = \langle c_1^i | \hat{q} | c_2^i \rangle \langle b_1^i | \hat{q} | b_2^i \rangle \sum_{j=0}^{1} d_j^i A_j^i. \tag{119}$$
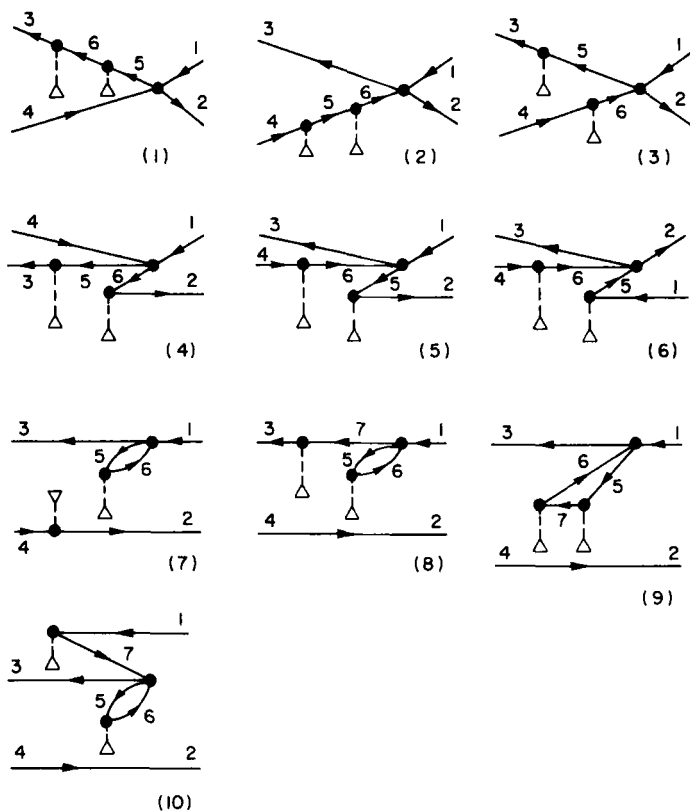
Fig. 25. Essentially distinct p–h diagrams for the mixed (type C, i.e. two Q- and one V-vertices) second-order excitation energy contributions.

The matrix elements A_j^i are defined as in (107), and the parameters d_j^i, c_j^i, b_j^i, and a_j^i are given in Table Va. The κ's are given again by (116), while the parameters $\gamma_j(l_i)$ are listed in Table Vb. The parameters l_i and the hole–particle sets ξ_k^i, η_k^i are presented in Table Vc.

Finally, the two essentially distinct diagrams of Fig. 26 for the single particle third-order contribution give

$$M_D^{(3)} = \sum_{i=1}^{2} (\lambda_i^D + \tilde{\lambda}_i^D), \tag{120}$$

where

$$\lambda_1^D(1, 2, 3, 4) = \sum_{5} \Lambda_1^D \kappa(\alpha_k^1; \gamma_j(1)),$$

$$\lambda_2^D(1, 2, 3, 4) = \sum_{5, 6} \Lambda_2^D \kappa(\alpha_k^2; \gamma_j(2)), \tag{121}$$

TABLE Va

VALUES OF THE PARAMETERS c_j^i, b_j^i, a_j^i, AND d_j^i CHARACTERIZING THE THIRD-ORDER P–H DIAGRAMS OF TYPE C (FIG. 25) AND APPEARING IN EQS. (117)–(119)

	Q_1^i		Q_2^i		A_j^i				d_j^i	
i	c_1^i	c_2^i	b_1^i	b_2^i	a_1^i	a_2^i	a_3^i	a_4^i	0	1
1	3	6	6	5	2	5	1	4	$2b$	$-f$
2	5	4	6	5	2	3	1	6	$2b$	$-f$
3	3	5	6	4	2	5	1	6	$-2b$	f
4	3	5	2	6	5	6	4	1	$2b$	$-f$
5	6	4	2	5	3	5	6	1	$-2b$	f
6	6	4	5	1	2	3	5	6	$2b$	$-f$
7	2	4	6	5	3	5	1	6	$-2f$	f
8	3	7	6	5	5	7	6	1	$2f$	$-f$
9	6	7	7	5	3	5	1	6	$2f$	$-f$
10	7	1	6	5	3	5	7	6	$-2f$	f

TABLE Vb

VALUES OF PARAMETERS $\gamma_i(l)$ APPEARING IN (116) FOR THE THIRD-ORDER P–H DIAGRAMS OF TYPE C (FIG. 25)

l	$\gamma_1(l)$	$\gamma_2(l)$	$\gamma_3(l)$	$\gamma_4(l)$	$\gamma_5(l)$
1	-1	-1	$+1$	-1	-1
2	-1	$+1$	-1	$+1$	$+1$
3	$+1$	$+1$	$+1$	$+1$	$+1$
4	$+1$	$+1$	-1	-1	$+1$
5	-1	-1	-1	$+1$	-1

and

$$\Lambda_i^D = d_i \langle c_1^i \mid \hat{q} \mid c_2^i \rangle \langle b_1^i \mid \hat{q} \mid b_2^i \rangle \langle a_1^i \mid \hat{q} \mid a_2^i \rangle. \tag{122}$$

The denominators κ are given by (116) [where now $f(1) = 1$ and $f(2) = \delta_{2,4}$] with parameters $\gamma_j(l_i)$ defined in Table VIa, while the other pertinent parameters are listed in Table VIb.

TABLE Vc

VALUES OF PARAMETERS l_i AND OF THE PARTICLE AND HOLE INDEX SETS ξ_j^i AND η_j^i, RESPECTIVELY, CHARACTERIZING DIFFERENT TIME VERSIONS OF THE THIRD-ORDER P–H DIAGRAMS OF TYPE C (FIG. 25) AND DEFINING THE DENOMINATORS α_k^i IN (116)

i	ξ_1^i	η_1^i	ξ_2^i	η_2^i	ξ_3^i	η_3^i	ξ_4^i	η_4^i	ξ_5^i	η_5^i	ξ_6^i	η_6^i	l_i
		α_1^i		α_2^i		α_3^i		α_4^i		α_5^i		α_6^i	
1	6	4	3, 5	4, 6	1, 3	2, 5	5	4	1, 6	2, 5	1, 3	2, 6	1
2	3	5	3, 5	4, 6	1, 6	2, 4	3	6	1, 6	2, 5	1, 5	2, 4	1
3	5	4	3	6	1, 3, 6	2, 4, 5	5	6	1, 6	2, 4	1, 3	2, 5	2
4	5	4	3, 6	2, 4	1, 3	5, 6	5, 6	2, 4	1	6	1, 3	2, 5	2
5	3	6	3, 5	2, 4	1, 6	4, 5	3, 5	2, 6	1	5	1, 6	2, 4	2
6	3	6	1, 3	4, 5	5, 6	2, 4	1, 3	5, 6	5	2	1, 6	2, 4	2
7	3	2	3, 5	4, 6	1, 6	4, 5	3, 5	2, 6	1, 6	2, 5	1	4	3
8	7	2	3, 5	2, 6	1, 3, 6	2, 5, 7	5, 7	2, 6	1, 6	2, 5	1, 3	2, 7	4
9	3, 7	2, 6	3, 5	2, 7	1, 6	2, 5	3, 5	2, 6	1, 7	2, 5	1, 6	2, 7	5
10	1, 3	2, 7	3, 5	2, 6	6, 7	2, 5	1, 3, 5	2, 6, 7	1, 6	2, 5	7	2	4
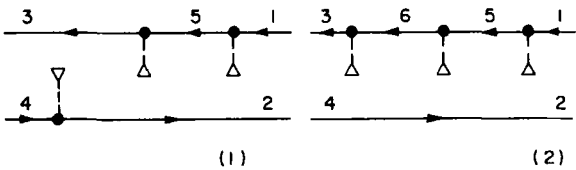
Fig. 26. Essentially distinct p–h diagrams for the one-particle (type D) second-order contribution to the excitation energy.

TABLE VIa

VALUES OF PARAMETERS $\gamma_i(l)$ APPEARING IN (116) FOR THE THIRD-ORDER P–H DIAGRAMS OF TYPE D (FIG. 26)

l	$\gamma_1(l)$	$\gamma_2(l)$	$\gamma_3(l)$	$\gamma_4(l)$	$\gamma_5(l)$
1	−1	+1	+1	−1	+1
2	−1	−1	+1	−1	−1

TABLE VIb

VALUES OF PARAMETERS a_j^i, b_j^i, c_j^i, d_i AND THE PARTICLE AND HOLE INDEX SETS ξ_j^i AND η_j^i, RESPECTIVELY, CHARACTERIZING THE THIRD-ORDER P–H DIAGRAMS OF TYPE D (FIG. 26) AND APPEARING IN EQS. (120)–(122)

	Q_3^i		Q_2^i		Q_1^i		α_1^i		α_2^i		α_3^i		α_4^i		α_5^i		α_6^i		
i	c_1^i	c_2^i	b_1^i	b_2^i	a_1^i	a_2^i	ξ_1^i	η_1^i	ξ_2^i	η_2^i	ξ_3^i	η_3^i	ξ_4^i	η_4^i	ξ_5^i	η_5^i	ξ_6^i	η_6^i	d_i
1	2	4	3	5	5	1	3	2	5	4	1, 3	4, 5	5	2	1, 3	2, 5	1	4	$-f$
2	3	6	6	5	5	1	6	2	3, 5	2, 6	1, 3	2, 5	5	2	1, 6	2, 5	1, 3	2, 6	f

VII. Perturbation Theory for the Ionization Potentials and Electron Affinities

We shall now briefly show that very much the same techniques we explained earlier may also be used when the number of particles in the system is not preserved, as occurs when one calculates the ionization potentials or electron affinities. We shall see that in fact all the necessary information needed for a calculation of these quantities is already contained in the excitation energy expressions, namely in the part corresponding to the self-energy diagrams.

Indeed, these quantities are obtained as the poles of the Fourier transform of the one-particle Green function in very much the same way as the excitation energies are obtained from the two-fermion particle–hole Green function.[22] The Green function approach to the ionization and attachment energies calculation is explained in most standard texts (cf., e.g., Raimes, 1972; Fetter and Walecka, 1971; Thouless, 1972) or in a nice exposé by Ecker and Hohlneicher (1971). A very interesting nondiagrammatic approach to the direct calculation of ionization energies using the one-particle Green function (propagator) formalism was proposed recently by Pickup and Goscinski (1973). These quantities have been calculated by a number of authors in various approximations (cf., e.g., Simons and Smith, 1973; also references in Section I). Our approach will yield the RS perturbation expansion for these quantities. One could also obtain the BW form if desired. However, we prefer to use the RS form, particularly for larger systems, since it does not mix together the various

---

[22] The other types of two-fermion Green function, i.e. the particle–particle and hole–hole ones, yield in a similar way the double ionization energies or two-electron attachment energies (Chen, 1972).

orders of the perturbation potential as does the BW form. This is essential when using model Hamiltonians, in which case we can effectively use an interpolation between the strongly and weakly correlated limits (Čížek and Paldus, 1972, 1973; Paldus et al., 1974). In fact, in many cases the perturbation theory does not even converge for physically significant values of the coupling constant (Pellégatti et al., 1974), so that even conceptually the interpolations we have suggested are preferable.

Let us now see how the same RS PT expressions given by the Green function approach may be obtained by a straightforward application of the ordinary perturbation theory to both levels, combined with a time-independent diagrammatic technique.

A. General Formulation

Consider a system with the Hamiltonian (10) and choose as the unperturbed Hamiltonian some separable operator (11). We are now interested in calculating the ionization energies or electron affinities of the system. Clearly, these quantities depend on the initial and final states of the neutral and charged systems, respectively, the most important one being associated with the ground state in both systems. In particular, the ionization potentials and electron affinities corresponding to the excited states of a neutral system are not easily accessible. We shall thus consider these quantities only for the ground state of the neutral system and some excited states of the ionized system yielding simultaneously the expressions for the higher ionization potentials.

Using the second quantization formalism the operator form of our Hamiltonian is independent of the number of particles in the system. Thus, the same Hamiltonians $\hat{H}$ and $\hat{H}_0$ apply to both neutral and charged systems. We shall again use the N-product form of these operators $\hat{K}$ and $\hat{K}_0$, Eqs. (16) and (17), respectively, defined with respect to the ground state of the *neutral* system chosen as the Fermi vacuum. The pertinent eigenstates and eigenvalues of these operators for the neutral system will be designated as before [cf. Eqs. (18) and (19)], while for the ion we shall write

$$\hat{K} \,|\, \Psi_i(A)\rangle = k_i(A) \,|\, \Psi_i(A)\rangle,$$
$$\hat{K}_0 \,|\, \Phi_i(A)\rangle = \kappa_i(A) \,|\, \Phi_i(A)\rangle, \tag{123}$$

where, for the negative ion (electron affinity calculation) we have

$$|\, \Phi_i(A'')\rangle = \hat{X}^\dagger_{A''} \,|\, \Phi_i\rangle, \tag{124}$$

while for the positive ion (ionization potential calculation) we choose

$$|\Phi_i(A')\rangle = \hat{X}_{A'}|\Phi_i\rangle, \tag{125}$$

$|\Phi_i\rangle$ being the independent particle model wavefunction of the neutral species.

As already mentioned, we shall only consider the case $i = 0$, but the orbitals A' or A'' may be any occupied or virtual orbitals. We also assume that $|\Phi_0(A)\rangle \rightarrow |\Psi_0(A)\rangle$ as the perturbation $\hat{W}$ is switched on.

Using the PT for both pertinent states we can write for the quantity $\Delta E(A)$, representing either the ionization potential or electron affinity as the case may be, the following expansion:

$$\Delta E(A) = k_0(A) - k_0 = \sum_{i=0}^{\infty} \Delta k_0^{(i)}(A) = \sum_{i=0}^{\infty} (k_0^{(i)}(A) - k_0^{(i)}). \tag{126}$$

For the first few orders of PT the ground state terms $k_0^{(i)}$ are given by Eqs. (78) and for the ionic terms we have

$$k_0^{(0)}(A) = \langle\Phi_0(A)|\hat{K}_0|\Phi_0(A)\rangle,$$
$$k_0^{(1)}(A) = \langle\Phi_0(A)|\hat{W}|\Phi_0(A)\rangle,$$
$$k_0^{(2)}(A) = \langle\Phi_0(A)|\hat{W}\hat{P}_0(A)\hat{W}|\Phi_0(A)\rangle, \text{ etc.} \tag{127}$$

The operator $\hat{P}_0(A)$ is given by Eq. (5), that is,

$$\hat{P}_0(A) = \sum_{i(\neq 0)} \frac{|\Phi_i(A)\rangle\langle\Phi_i(A)|}{\kappa_0(A) - \kappa_i(A)}, \tag{128}$$

where

$$\kappa_0(A) = k_0^{(0)}(A) = \langle\Phi_0(A)|\hat{K}_0|\Phi_0(A)\rangle$$
$$= \langle\Phi_0(A)|\hat{H}_0|\Phi_0(A)\rangle - \langle\Phi_0|\hat{H}_0|\Phi_0\rangle = \pm\omega_A, \tag{129}$$

the upper and lower signs referring to the negative and positive ion cases, respectively.

The last expression gives the zero-order energy of the ion, and since $k_0^{(0)} = 0$ for neutral species it also gives the zero order of the calculated ionization potential or electron affinity as the corresponding orbital energy of the chosen independent particle model. Choosing the Hartree–Fock basis of the neutral species as the unperturbed approximation we shall see that this result is in fact valid to the first order of PT and expresses the well-known Koopmans theorem.

Let us finally note that, as in the problem of excitation energies, we

may face the degeneracy problem of the pertinent unperturbed states (even though this will happen less often in this case, namely, only when the one-particle states of the independent particle model are degenerate). We again proceed in the same manner using the degenerate form of perturbation theory (or, simply, choosing appropriate symmetry adapted states).

Thus, assuming that states $|\Phi_0(A_i)\rangle$ $(i = 1, \ldots, s)$ are degenerate, so that

$$\omega_{A_i} = \omega_{A_1} \equiv \omega_1, \qquad i = 1, \ldots, s \qquad (130)$$

we calculate the matrix elements of the perturbations

$$k_0^{(1)}(i, j) = \langle \Phi_0(A_i) | \hat{W} | \Phi_0(A_j) \rangle, \qquad (131)$$

etc., and diagonalize the resulting $s \times s$ matrix. In order that we can easily use the results of the preceding section, we shall use the notation

$$|\Phi_0(A_j)\rangle = \hat{X}^\dagger_{A_{1''}} |\Phi_0\rangle \equiv \hat{X}^\dagger_1 |\Phi_0\rangle,$$

$$\langle \Phi_0(A_i)| = \langle \Phi_0 | \hat{X}_{A_{3''}} \equiv \langle \Phi_0 | \hat{X}_3, \qquad (132)$$

(as well as the convention of designating the spin orbitals or orbitals by subscripts only), and similarly for the corresponding positive ion case.

We see now that we can again easily evaluate the necessary quantities using the time-independent diagrammatic technique.

B. Diagrammatic Approach

Let us represent the bra and ket states (132) by the $\bar{I}$- and I-diagrams (skeletons, vertices) shown in Fig. 27a, to which we assign a scalar quantity equal to unity and the assigned operator quantity then equals the pertinent annihilation or creation operator in (132). (The weight is obviously equal to unity as well.) The operators $\hat{Q}_N$ and $\hat{V}_N$ of the perturbation potential are represented as before. We shall only consider the case of
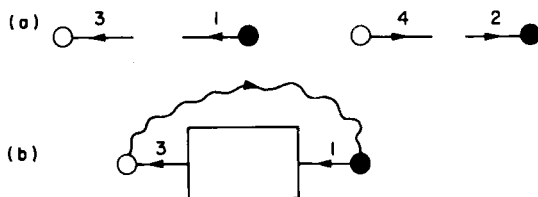
Fig. 27. (a) I- and $\bar{I}$-diagrams (skeletons, vertices) for the ionization potential and electron affinity calculation. (b) Representation of the fictitious line in the p or h diagrams.

a negative ion, yielding the electron affinities, since the calculation of corresponding ionization potentials is completely analogous. Indeed, as will be seen, both cases give the same set of diagrams differing only by the "time-reversal," i.e. obtained one from another by a reflection in the plane parallel to the interaction V-vertices. Those yielding electron affinities (having particle lines on its ends) will be called particle diagrams and, similarly, those yielding ionization potentials are called hole diagrams.

We can now calculate the necessary matrix elements (127) or, more generally, (131) using the diagrammatic technique as developed earlier with only slight changes in the rules assigning the algebraic expressions to the resulting diagrams.

The denominators will be given by the expression [cf. Eq. (128)]

$$\omega_1 + \sum_i \omega_{A_{i'}} - \sum_j \omega_{A_{j''}}, \tag{133}$$

where ω_1 is the particle orbital energy (130),[23] and the summations again extend over the hole and particle lines, respectively, crossing the interval between two given neighboring interaction vertices. In fact, we can introduce into our diagrams a fictitious wavy line (Tolmachev, 1963a), connecting the $\bar{I}$- and I-vertices as shown in Fig. 27b, to which we assign the orbital energy $\omega_1 = \omega_3$.[24] Then we get the denominator (133) in the same way as for the vacuum diagrams. Needless to say, the dangerous diagrams [yielding a vanishing denominator (133)] must be omitted.

Using the fictitious line we find that the numerical factor is again $(-1)^{l+h}$ ($w = 1$) always counting the fictitious line like any other oriented line.[25]

Finally, in going over to the spin-independent formalism, we see that we can have both spin orientations on any closed loop except one containing a fictitious line, since the external labels 1 and 3 are fixed. Thus, counting all loops as above (i.e. including the one containing a fictitious line) the additional numerical factor is again 2^{l-1}, as in the excitation energy calculation (discarding the loop with a fictitious line, the factor is 2^l).

---

[23] For hole diagrams ω_1 is replaced by the hole orbital energy $(-\omega_1)$.

[24] For hole diagrams this automatically gives $(-\omega_1)$ since the fictitious line is now a particle line.

[25] The fictitious line makes no difference for particle diagrams, where it simply introduces another hole line and an extra loop. For hole diagrams, however, it introduces a needed extra factor of (-1).

We can summarize these rules as follows:

(i) Use the self-energy diagrams and change the oriented line directly connecting $\bar{T}$- and T-vertices into a wavy fictitious line (or draw the pertinent resulting diagrams with $\bar{I}$- and I-vertices and all Q- and V-vertices to get the desired order).

(ii) Assign denominators (133) to each pair of neighboring vertices, assigning the appropriate orbital energy (130) to the fictitious line.

(iii) Assign matrix elements to Q- and V-vertices as in the ground state case.

(iv) Determine the numerical factor $(-1)^{l+h}$,[26] counting a fictitious line as an ordinary particle or hole line.

(v) In the orbital formalism use an additional factor of 2^{l-1}.

We can in fact use the same expressions as given for the excitation energies, provided that (i) we discard contributions from nonself-energy diagrams, (ii) we ignore time-reversed diagram contributions (which in fact give the ionization potential contributions), (iii) we ignore the g_i factors (they are equal to unity for self-energy diagrams anyway), and (iv) we redefine the denominators accordingly. Consequently, we shall not present these expressions here and will only illustrate the compensations occurring in our approach on low order terms.

C. Example: First- and Second-Order Terms

Let us derive the first- and second-order contributions in order to illustrate the above rules.

In the first order we have $k_0^{(1)} = 0$ and need only calculate the appropriate matrix element of $\hat{W}$ [cf. Eqs. (127) or (131)]. Since we have only two fermion lines associated with $\bar{I}$- and I-vertices, and the perturbation operator $\hat{W}$ is in the N-product form, we see immediately that the only first-order contribution comes from the one-particle part of $\hat{W}$, as shown in Fig. 28. Clearly, the first-order contribution given by this diagram vanishes completely for the Hartree–Fock basis, as mentioned earlier, and for an arbitrary potential is simply given by the appropriate $\hat{q}$ matrix element.

Fig. 28. First-order resulting diagram for the electron affinity calculation (p-Green function diagram).

[26] Notice that again the weight w_R of any resulting diagram is equal to unity.

In the second order, we shall distinguish three contributions, as in the excitation energy case, corresponding to (A) two-particle terms involving two V-vertices, (B) mixed one- and two-particle terms involving one Q- and one V-vertex, and (C) one-particle terms (two Q-vertices). The appropriate resulting diagrams for these three possibilities are easily found and are given (in the Hugenholtz form) in Fig. 29.
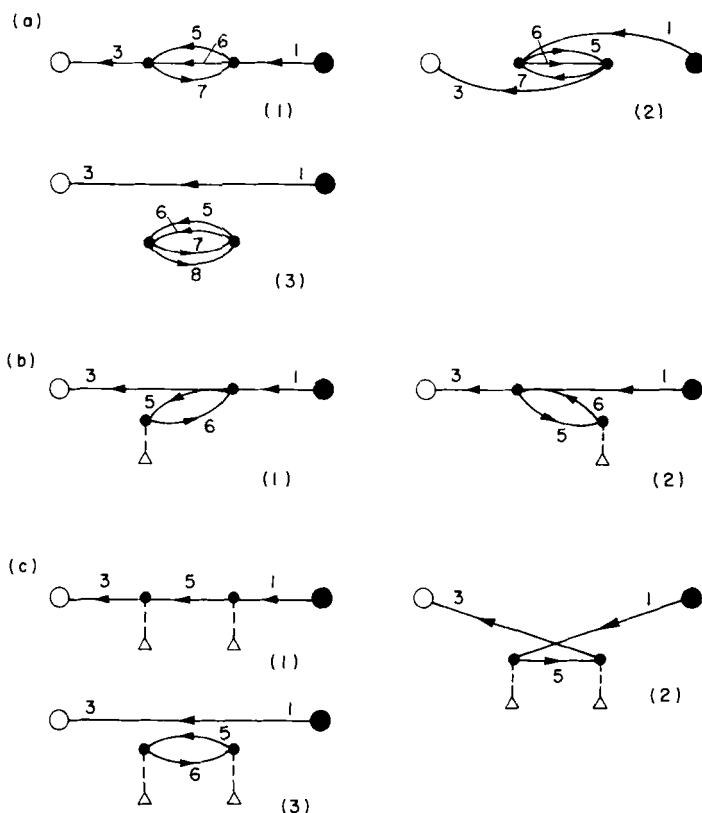
Fig. 29. Second-order resulting diagrams for the electron affinity calculations. (a) Two-particle, (b) mixed, and (c) one-particle contributions.

We see immediately that contributions from the two disconnected diagrams 29a(3) and 29c(3) will be canceled by the ground state second-order terms shown in Figs. 12 and 8b. Thus for each type A, B, and C we are left with two diagrams. The second one always represents a time

version of the first (obtained by reversing the left–right ordering of the interaction vertices). Thus, there is only one essentially distinct diagram in each group A, B, and C. We see immediately that each of these essentially distinct diagrams is in fact the corresponding self-energy diagram of the excitation energy problem [cf. Table II and Fig. 13(4) of PC(74), Figs. 22(3) and 23(1)].

Drawing corresponding Goldstone versions, we can immediately write down the final expression for $k_0^{(2)}(1, 3)$ in a similar compact form to that found in the excitation energy case, namely

$$k_0^{(2)} = k_A^{(2)} + k_B^{(2)} + k_C^{(2)}, \tag{134}$$

in complete analogy to (103). Thus

$$k_A^{(2)} = \sum_{5, 6, 7} \Theta^A(\alpha_1 - \alpha_2), \tag{135}$$

where

$$\Theta^A = \sum_{j, k = 0}^{1} d_{jk} B_j A_k,$$

$$B_0 = \langle b_1 b_2 \mid \hat{v} \mid b_3 b_4 \rangle,$$

$$B_1 = \langle b_1 b_2 \mid \hat{v} \mid b_4 b_3 \rangle,$$

$$A_0 = \langle a_1 a_2 \mid \hat{v} \mid a_3 a_4 \rangle,$$

$$A_1 = \langle a_1 a_2 \mid \hat{v} \mid a_4 a_3 \rangle. \tag{136}$$

Further,

$$\alpha_i = -\prod_{j \in \xi_i} n_j \prod_{k \in \eta_i} (1 - n_k) \left[\sum_{m \in \xi_i} \omega_m - \sum_{n \in \eta_i} \omega_n - \omega_1 \right]^{-1}, \tag{137}$$

where

$$n_j = 1 \quad \text{if} \quad j \text{ is a particle state}$$

and

$$n_j = 0 \quad \text{if} \quad j \text{ is a hole state,}$$

and ξ_i, η_i are the particle and hole index sets determined by the oriented lines passing through the interval between pertinent neighboring interaction vertices. These parameter sets are given in Table VII.

TABLE VII

VALUES OF PARAMETERS a_i, b_i, d_{ij} AND THE PARTICLE–HOLE INDEX SETS ξ_i AND η_i, RESPECTIVELY, CHARACTERIZING THE SECOND-ORDER PARTICLE DIAGRAM OF TYPE A^a AND APPEARING IN EXPRESSIONS (135)–(137)

B_i				A_i				α_1		α_2					
b_1	b_2	b_3	b_4	a_1	a_2	a_3	a_4	ξ_1	η_1	ξ_2	η_2	d_{00}	d_{01}	d_{10}	d_{11}
3	7	6	5	5	6	7	1	5, 6	7	1, 3, 7	5, 6	$2f$	$-f$	0	0

^{a} Obtained from self-energy diagram (4), Fig. 13 of Paldus and Čížek (1974).

We see immediately that this expression is identical with expression (41) of PC(74) when the above-mentioned changes are implemented, while the parameters in Table VII are immediately obtained from the last row of Table I of PC(74) by deleting label 2 (or 4) corresponding to the unperturbed hole propagator line in the corresponding particle–hole (excitation energy) self-energy diagram. Similarly

$$k_B^{(2)} = \sum_{5, 6} \Theta^B(\alpha_1 + \alpha_2), \tag{138}$$

with Θ^B given by (106), α_i's by (137), and the pertinent parameter sets are obtained from the last row of Table III (by deleting label 2).

Finally,

$$k_C^{(2)} = \sum_5 \Theta^C(\alpha_1 - \alpha_2), \tag{139}$$

with Θ^C given by (111) and the parameter sets obtained from those given in the text following (111) by deleting state 2.

This example clearly illustrates how the pertinent higher order contributions for the electron affinities (or ionization potentials) are immediately obtained from those for the excitation energies.

VIII. Conclusions

We have seen that our time-independent diagrammatic technique (Čížek, 1966, 1969; Paldus and Čížek, 1970; Paldus *et al.*, 1972a,b, 1973; Paldus, 1972) may also be directly applied to the perturbation theory and in particular to the direct perturbative calculation of excitation energies, ionization potentials, and electron affinities. We readily obtained the same expressions and diagrams as those implied by the use of the Green

function and the time-dependent S-matrix formalisms. The time-independent diagrammatic method we used clearly displays the various cancellations which result as a consequence of the direct approach. A particularly simple formulation has been achieved by using the normal product form of the operators appearing in the theory, which is a standard approach used in quantum electrodynamics. Using this formalism the explicit perturbation formulas for the excitation energy are easily obtained even for a nonHartree–Fock basis. It is also shown how the self-energy part of the excitation energy problem directly determines the pertinent ionization potentials or electron affinities.

More important, however, is the generality of the approach. Essentially the same time-independent techniques may be applied in principle to any stationary problem of quantum theory. This often yields a very simple diagrammatic representation of the various terms, which considerably simplifies both their derivation and their evaluation.

Appendix A. Bracketing Technique[2]

There are several formulas available giving the explicit form of the nth order energy term in nondegenerate Rayleigh–Schrödinger perturbation theory (Kato, 1949; Brueckner, 1955; Bloch, 1958a,b; Huby, 1961; Brandow, 1967; Salzman, 1968; Silverstone and Holloway, 1970). The most compact formulation is that of Silverstone and Holloway (1970). However, for the purposes of this paper the most convenient form is that of Brueckner (1955) and Huby (1961).

In these formulas one starts with the leading term[27]

$$\langle \Phi | \hat{W} \hat{P} \hat{W} \cdots \hat{W} \hat{P} \hat{W} | \Phi \rangle \qquad (A.1)$$

and obtains the remaining terms contributing to the nth order by inserting any number of pairs of bra-ket symbols around the inner $\hat{W}$ factors in (A.1). By an inner $\hat{W}$ factor we mean any $\hat{W}$ other than the first or the last one. The bra and ket symbols may be separated by any number of factors:

$$\hat{W} \hat{P} \hat{W} \cdots \hat{W}.$$

Furthermore, brackets may lie within brackets. Finally, a sign factor of $(-1)^l$ is assigned to each term, where l is the number of bra-ket pairs inserted. Each bra-ket pair signifies the expectation value, in the state $|\Phi\rangle$, of the operator product contained between the bra and ket symbols.

---

[27] Note that for the sake of simplicity we omit the indices referring to the given unperturbed state [cf. (9)].

The total number of terms in the nth order, including the leading one, is given by the formula (Tong, 1962)

$$\frac{(2n-2)!}{n!\,(n-1)!}.\tag{A.2}$$

Let us now illustrate this rule on several examples. In order to simplify our notation we write $\langle \hat{W}\hat{P}\hat{W}\hat{P}\cdots\hat{P}\hat{W}\rangle$ instead of $\langle \Phi\,|\,\hat{W}\hat{P}\hat{W}\hat{P}\cdots\hat{P}\hat{W}\,|\,\Phi\rangle$.

Clearly, no bracketing is possible in the second order. In the third order we have only one bracketing:

$$\langle \hat{W}\hat{P}\langle\hat{W}\rangle\hat{P}\hat{W}\rangle = -\langle\hat{W}\rangle\langle\hat{W}\hat{P}^2\hat{W}\rangle.\tag{A.3}$$

In the fourth order, four bracketings are possible, namely

$$\langle \hat{W}\hat{P}\langle\hat{W}\rangle\hat{P}\hat{W}\hat{P}\hat{W}\rangle = -\langle\hat{W}\rangle\langle\hat{W}\hat{P}^2\hat{W}\hat{P}\hat{W}\rangle,$$

$$\langle \hat{W}\hat{P}\hat{W}\hat{P}\langle\hat{W}\rangle\hat{P}\hat{W}\rangle = -\langle\hat{W}\rangle\langle\hat{W}\hat{P}\hat{W}\hat{P}^2\hat{W}\rangle,$$

$$\langle \hat{W}\hat{P}\langle\hat{W}\rangle\hat{P}\langle\hat{W}\rangle\hat{P}\hat{W}\rangle = \langle\hat{W}\rangle\langle\hat{W}\rangle\langle\hat{W}\hat{P}^3\hat{W}\rangle,$$

$$\langle \hat{W}\hat{P}\langle\hat{W}\hat{P}\hat{W}\rangle\hat{P}\hat{W}\rangle = -\langle\hat{W}\hat{P}\hat{W}\rangle\langle\hat{W}\hat{P}^2\hat{W}\rangle.\tag{A.4}$$

The reader can easily verify that in the fifth order there are already 13 bracketings. We give only a few examples

$$\langle \hat{W}\hat{P}\langle\hat{W}\hat{P}\hat{W}\rangle\hat{P}\hat{W}\hat{P}\hat{W}\rangle = -\langle\hat{W}\hat{P}\hat{W}\rangle\langle\hat{W}\hat{P}^2\hat{W}\hat{P}\hat{W}\rangle,\tag{A.5}$$

$$\langle \hat{W}\hat{P}\hat{W}\hat{P}\langle\hat{W}\hat{P}\hat{W}\rangle\hat{P}\hat{W}\rangle = -\langle\hat{W}\hat{P}\hat{W}\rangle\langle\hat{W}\hat{P}\hat{W}\hat{P}^2\hat{W}\rangle,\tag{A.6}$$

$$\langle \hat{W}\hat{P}\langle\hat{W}\hat{P}\hat{W}\hat{P}\hat{W}\rangle\hat{P}\hat{W}\rangle = -\langle\hat{W}\hat{P}^2\hat{W}\rangle\langle\hat{W}\hat{P}\hat{W}\hat{P}\hat{W}\rangle.\tag{A.7}$$

In each of these examples the bracketing gives rise to a product of a term involving two $\hat{W}$ operators by one involving three $\hat{W}$ operators. We shall use these examples in Appendix F.

We would also like to stress that in the fifth order we observe for the first time a bracketing within a bracketing:

$$\langle \hat{W}\hat{P}\langle\hat{W}\hat{P}\langle\hat{W}\rangle\hat{P}\hat{W}\rangle\hat{P}\hat{W}\rangle = \langle\hat{W}\rangle\langle\hat{W}\hat{P}^2\hat{W}\rangle\langle\hat{W}\hat{P}^2\hat{W}\rangle.\tag{A.8}$$

In the sixth order we have 41 bracketings. Once again we only give a few examples in which new qualitative features of bracketing appear for the first time. Thus, in one of the possible sixth-order terms

$$\langle \hat{W}\hat{P}\langle\hat{W}\rangle\hat{P}\langle\hat{W}\hat{P}\langle\hat{W}\rangle\hat{P}\hat{W}\rangle\hat{P}\hat{W}\rangle = -\langle\hat{W}\rangle\langle\hat{W}\rangle\langle\hat{W}\hat{P}^2\hat{W}\rangle\langle\hat{W}\hat{P}^3\hat{W}\rangle\tag{A.9}$$

there are two brackets inserted in the principal one and, moreover, in the second bracket there is inserted another bracket.

In the term

$$\langle \hat{W}\hat{P}\langle \hat{W}\hat{P}\langle \hat{W}\rangle\hat{P}\langle \hat{W}\rangle\hat{P}\hat{W}\rangle\hat{P}\hat{W}\rangle = -\langle \hat{W}\rangle\langle \hat{W}\rangle\langle \hat{W}\hat{P}^3\hat{W}\rangle\langle \hat{W}\hat{P}^2\hat{W}\rangle$$
(A.10)

we have inserted two brackets inside the bracket, which is itself already an inserted bracket in the principal one.

We see that the bracketing will become more and more complicated as the order of perturbation theory increases. However, there is a possibility of simplifying bracketing by using the recursive procedure. Namely, we can define a "superbracketing," which we shall designate by the symbol

$$\{\hat{W}\hat{P} \cdots \hat{W}\hat{P}\hat{W}\},$$
(A.11)

as the kth order contribution ΔE_k, where k is the number of $\hat{W}$ factors in the "superbracket." The rules for the superbracketing are then similar to those of the usual bracketing, with the exception that it is forbidden to insert a superbracket into another superbracket. Then ΔE_n is given by the leading term and the terms resulting from all possible "superbracketings."

As an example of a possible term appearing in the seventh order let us consider

$$\langle \hat{W}\hat{P}\{\hat{W}\hat{P}\hat{W}\hat{P}\hat{W}\hat{P}\hat{W}\}\hat{P}\{\hat{W}\}\hat{P}\hat{W}\rangle = \Delta E_1 \,\Delta E_4\langle \hat{W}\hat{P}^3\hat{W}\rangle. \quad (A.12)$$

This latter technique is perhaps the best compromise between the completely explicit rule of Brueckner (1955) and Huby (1961) and the usual implicit and asymmetric scheme.

Appendix B. Time-Independent Second Quantization Formalism

B.1. Basic Concepts

Let the spin orbitals $| A \rangle$, which are eigenstates of some one-particle Hermitian operator, form a complete orthonormal system and let us designate the antisymmetrized product of the spin orbitals $| A_{i_1} \rangle$, $| A_{i_2} \rangle$, ..., $| A_{i_N} \rangle$ by the symbol

$$| \{A_{i_1} A_{i_2} \cdots A_{i_N}\}\rangle.$$
(B.1)

Then we can define the *annihilation operator* $\hat{X}_A$ as follows:

$$\hat{X}_{A_i} | \{A_i A_{j_2} \cdots A_{j_N}\}\rangle = |\{A_{j_2} \cdots A_{j_N}\}\rangle,$$

and   (B.2)

$$\hat{X}_{A_i} | \{A_{j_1} A_{j_2} \cdots A_{j_N}\}\rangle = 0 \qquad \text{if} \quad i \neq j_1, j_2, \ldots, j_N.$$

When $N = 1$, we define

$$\hat{X}_A | A\rangle = |0\rangle,$$ (B.3)

where $|0\rangle$ is the so-called *true vacuum* state, which is also assumed to be normalized

$$\langle 0 | 0 \rangle = 1.$$ (B.4)

Finally,

$$\hat{X}_A | 0\rangle = 0.$$ (B.5)

The corresponding *creation operators* $\hat{X}_A^\dagger$ are the Hermitian conjugates of the pertinent annihilation operators, so that

$$\hat{X}_A^\dagger | 0\rangle = | A\rangle,$$

$$\hat{X}_{A_i}^\dagger | \{A_{j_1} \cdots A_{j_N}\}\rangle = |\{A_i A_{j_1} \cdots A_{j_N}\}\rangle \qquad \text{if} \quad i \neq j_1, \ldots, j_N,$$

and

$$\hat{X}_{A_i}^\dagger | \{A_{j_1} \cdots A_{j_N}\}\rangle = 0 \qquad \text{if} \qquad i = j_k \qquad \text{for some} \quad k = 1, \ldots, N.$$
(B.6)

Using these definitions we can easily derive the following anticommutation relations

$$[\hat{X}_A, \hat{X}_B]_+ = [\hat{X}_A^\dagger, \hat{X}_B^\dagger]_+ = 0$$

$$[\hat{X}_A^\dagger, \hat{X}_B]_+ = \langle A | B \rangle = \delta_{A,B}$$ (B.7)

where

$$[\hat{Y}, \hat{Z}]_+ = \hat{Y}\hat{Z} + \hat{Z}\hat{Y},$$ (B.8)

and δ_{AB} is the Kronecker symbol. These relations express the fact that fermion systems obey Fermi–Dirac statistics and automatically take care of the antisymmetry properties of the pertinent eigenstates.

The n-particle operator $\hat{Q}_n$,

$$\hat{Q}_n(x_1, \ldots, x_N) = \sum_{i_1 < \cdots < i_n} \hat{q}^{(n)}(x_{i_1}, \ldots, x_{i_n}),$$ (B.9)

is then given in this representation as follows

$$\hat{Q}_n = \frac{1}{n!} \sum_{\substack{A_1, \ldots, A_n \\ B_1, \ldots, B_n}}$$

$$\langle A_1 \cdots A_n | \hat{q}^{(n)} | B_1 \cdots B_n \rangle \hat{X}^\dagger_{A_1} \cdots \hat{X}^\dagger_{A_n} \hat{X}_{B_n} \cdots \hat{X}_{B_1}. \quad \text{(B.10)}$$

Specifically, for one- and two-particle operators, say $\hat{Z}$ and $\hat{V}$,

$$\hat{Z} = \sum_i \hat{z}(i), \qquad \hat{V} = \sum_{i<j} \hat{v}(i, j), \quad \text{(B.11)}$$

we have

$$\hat{Z} = \sum_{A, B} \langle A | \hat{z} | B \rangle \hat{X}^\dagger_A \hat{X}_B,$$

$$\hat{V} = \frac{1}{2} \sum_{A, B, C, D} \langle AB | \hat{v} | CD \rangle \hat{X}^\dagger_A \hat{X}^\dagger_B \hat{X}_D \hat{X}_C, \quad \text{(B.12)}$$

where

$$\langle A | \hat{z} | B \rangle = \int \langle A | x_i \rangle \hat{z}(x_i) \langle x_i | B \rangle \, dx_i,$$

$$\langle AB | \hat{v} | CD \rangle = \int \langle A | x_i \rangle \langle B | x_j \rangle \hat{v}(x_i, x_j)$$

$$\times \langle x_i | C \rangle \langle x_j | D \rangle dx_i dx_j. \quad \text{(B.13)}$$

If the spin orbitals $\psi_C(x_i) = \langle x_i | C \rangle$ may be written as a product of the orbital and spin functions, which is always the case for the spin-independent Hamiltonians considered here, that is

$$\langle x_i | C \rangle = \langle r_i | c \rangle \langle \eta_i | \gamma \rangle, \qquad x_i \equiv (r_i, \eta_i), \qquad \eta_i = \pm\tfrac{1}{2},$$

or

$$| C \rangle = | c \rangle | \gamma \rangle, \quad \text{(B.14)}$$

we then have

$$\langle A | \hat{z} | B \rangle = \langle a | \hat{z} | b \rangle \delta_{\alpha\beta},$$

$$\langle AB | \hat{v} | CD \rangle = \langle ab | \hat{v} | cd \rangle \delta_{\alpha\gamma} \delta_{\beta\delta}, \quad \text{(B.15)}$$

and the expressions (B.12) may be simplified accordingly by separating the spin orbital summations into the orbital and spin summations. Thus, for a typical spin-independent Hamiltonian, containing at most two-

particle interactions, we have

$$\hat{H} = \sum_{a,b} \langle a | \hat{z} | b \rangle \sum_\alpha \hat{X}^\dagger_{a\alpha} \hat{X}_{b\alpha}$$

$$+ \frac{1}{2} \sum_{a,b,c,d} \langle ab | \hat{v} | cd \rangle \sum_{\alpha,\beta} \hat{X}^\dagger_{a\alpha} \hat{X}^\dagger_{b\beta} \hat{X}_{d\beta} \hat{X}_{c\alpha} . \qquad (B.16)$$

We also know that any state $| \Psi \rangle$ may be expanded in terms of the configuration states $| \Phi_K \rangle$, $K = (A_{i_1} A_{i_2} \cdots A_{i_N})$,

$$| \Phi_K \rangle = | \{ A_{i_1} \cdots A_{i_N} \} \rangle. \qquad (B.17)$$

Ordering our spin orbitals $| A \rangle$ according to some criterion and considering only ordered configurations K, we can write (Löwdin, 1955)

$$| \Psi \rangle = \sum_K c_K | \Phi_K \rangle, \qquad (B.18)$$

where $| \Phi_K \rangle$, given by (B.17), may be expressed as follows, using (B.6)

$$| \Phi_K \rangle = \hat{X}^\dagger_{A_{i_N}} \cdots \hat{X}^\dagger_{A_{i_1}} | 0 \rangle. \qquad (B.19)$$

Thus, the calculation of an arbitrary matrix element can be reduced to the calculation of the vacuum mean value of some product of the creation and annihilation operators. This mean value is most effectively calculated using the time-independent Wick theorem. In order to formulate this theorem, we first have to define a few new concepts:

(i) A *normal product* of the operators $(\hat{M}_{B_1} \cdots \hat{M}_{B_k})$, designated $n[\hat{M}_{B_1} \cdots \hat{M}_{B_k}]$, where $\hat{M}_{B_i}$ is some creation or annihilation operator $\hat{X}^\dagger_{B_i}$ or $\hat{X}_{B_i}$, respectively, is defined as the product of these operators in which all the creation operators are to the left of all the annihilation operators, with a $(+1)$ or (-1) factor depending on whether an even or odd permutation is necessary to rearrange the operators to the desired order. Thus

$$n[\hat{M}_{B_1} \cdots \hat{M}_{B_k}] = (-1)^p \hat{X}^\dagger_{C_1} \cdots \hat{X}^\dagger_{C_r} \hat{X}_{C_{r+1}} \cdots \hat{X}_{C_k}, \qquad (B.20)$$

where p is the parity of the permutation

$$p = \begin{pmatrix} B_1 \cdots B_k \\ C_1 \cdots C_k \end{pmatrix}. \qquad (B.21)$$

This definition is not unambiguous. However, since the operators of the same kind (i.e. either the creation ones or the annihilation ones) exactly anticommute [cf. Eqs. (B.7)], this is immaterial. For the sake of completeness we also define

$$n[\varnothing] = 1, \text{ where } \varnothing \text{ is the empty set.} \qquad (B.22)$$

(ii) A *contraction* (*pairing*) of two operators $\hat{M}_1$ and $\hat{M}_2$, designated $\hat{M}_1\hat{M}_2$, is defined as

$$\underline{\hat{M}_1\hat{M}_2} = \hat{M}_1\hat{M}_2 - n[\hat{M}_1\hat{M}_2]. \qquad (B.23)$$

Thus, we find easily that all contractions vanish except the case

$$\underline{\hat{X}_A\hat{X}_B^\dagger} = \langle A \mid B \rangle, \qquad (B.24)$$

which is also equal to a c-number.

(iii) A *normal product with contractions* is then defined as follows:

$$n[\hat{M}_1\hat{M}_2 \cdots \underline{\hat{M}_{i_1} \cdots \hat{M}_{i_2}} \cdots \underline{\hat{M}_{j_2} \cdots \hat{M}_{j_1}} \cdots$$

$$\times \underline{\hat{M}_{i_3} \cdots \hat{M}_{i_4}} \cdots \underline{\hat{M}_{j_3} \cdots \hat{M}_{j_4}} \cdots \hat{M}_k]$$

$$= (-1)^p \underline{\hat{M}_{i_1}\hat{M}_{j_1}}\,\underline{\hat{M}_{i_2}\hat{M}_{j_2}} \cdots \underline{\hat{M}_{i_r}\hat{M}_{j_r}} n[\hat{M}_{s_1} \cdots$$

$$\times \hat{M}_{i_1-1}\hat{M}_{i_1+1} \cdots \hat{M}_{s_l}], $$

$$(B.25)$$

where p is the parity of the permutation

$$p = \begin{pmatrix} 1 & 2 & \cdots & 2r & (2r+1) & \cdots & k \\ i_1 & j_1 & \cdots & j_r & s_1 & \cdots & s_l \end{pmatrix}, \qquad 2r + l = k, \quad (B.26)$$

and where we have assumed that $2r$ operators are contracted. Note that while

$$n[\hat{M}_1\hat{M}_2] = -n[\hat{M}_2\hat{M}_1] \qquad (B.27)$$

we have that

$$n[\underline{\hat{M}_1\hat{M}_2}] \neq -n[\underline{\hat{M}_2\hat{M}_1}]. \qquad (B.28)$$

We can now formulate the time-independent form of *Wick's theorem* (for proofs, see, e.g., Bogoliubov and Shirkov, 1957; March *et al.*, 1967)

$$\hat{M}_1 \cdots \hat{M}_k = n[\hat{M}_1 \cdots \hat{M}_k] + \sum n[\underline{\hat{M}_1 \cdots \hat{M}_k}], \qquad (B.29)$$

where the summation extends over normal products with all possible contractions of two operators, of four operators, etc.

The importance of this theorem for the calculation of vacuum mean

values of operator products is that in view of the property (B.5), and its Hermitian conjugate, we have that

$$\langle 0 \,|\, n[\hat{M}_1 \cdots \hat{M}_i \cdots \hat{M}_j \cdots \hat{M}_k] \,|\, 0 \rangle = 0, \qquad (B.30)$$

unless all operators are contracted. Thus,

$$\langle 0 \,|\, \hat{M}_1 \cdots \hat{M}_k \,|\, 0 \rangle = \langle 0 \,|\, \sum n[\hat{M}_1 \cdots \hat{M}_k] \,|\, 0 \rangle$$

$$= \sum (-1)^P \langle A_{i_1} \,|\, A_{j_1} \rangle \cdots \langle A_{i_r} \,|\, A_{j_r} \rangle \quad (B.31)$$

i.e. the vacuum mean value of the product of the creation and annihilation operators reduces to the sum of all possible fully contracted terms, which in turn are given as a product of Kronecker delta symbols and of an appropriate sign factor.

B.2. Particle–Hole Formalism

When dealing with the ground and low excited states it is usually much more convenient to introduce a new "vacuum," containing the states occupied in the ground state, instead of the true vacuum $|0\rangle$. Clearly, this will considerably decrease the number of creation and annihilation operators in the products, which must be considered when using a true vacuum $|0\rangle$ [cf. Eq. (B.19)]. We shall refer to this new vacuum state $|\Phi_0\rangle$, $|\Phi_0\rangle \equiv |\{A_1 A_2 \cdots A_N\}\rangle$, as the *Fermi vacuum* in order to distinguish it from the *true* (or *physical*) vacuum $|0\rangle$. The states occupied in $|\Phi_0\rangle$ will be referred to as *hole states* and will be designated by singly primed letters, while the states unoccupied in $|\Phi_0\rangle$ are called *particle states* and designated by doubly primed letters. Thus, we write

$$|\Phi_0\rangle \equiv |\{A'_1 A'_2 \cdots A'_N\}\rangle \qquad (B.32)$$

and all other N-particle configurations must contain at least one particle state $|A''_j\rangle$.

We can now define a new set of creation and annihilation operators $\hat{Y}^\dagger_A$ and $\hat{Y}_A$, respectively, with respect to the Fermi vacuum $|\Phi_0\rangle$, as follows

$$\hat{Y}_{A'} = \hat{X}^\dagger_{A'}, \qquad \hat{Y}^\dagger_{A'} = \hat{X}_{A'},$$

$$\hat{Y}_{A''} = \hat{X}_{A''}, \qquad \hat{Y}^\dagger_{A''} = \hat{X}^\dagger_{A''}. \qquad (B.33)$$

Thus, the role of creation and annihilation operators is reversed for the hole states, not unlike the positron–electron theory of Dirac. It is easy to

verify that these operators satisfy the same anticommutation relations, namely

$$[\hat{Y}_A, \hat{Y}_B]_+ = [\hat{Y}_A^\dagger, \hat{Y}_B^\dagger]_+ = 0$$

$$[\hat{Y}_A^\dagger, \hat{Y}_B]_+ = \langle A | B \rangle. \tag{B.34}$$

Also, in analogy to (B.5), we have

$$\hat{Y}_A | \Phi_0 \rangle = 0. \tag{B.35}$$

Consequently, we can derive analogous relationships to all the previous ones, defining the appropriate quantities with respect to the Fermi vacuum $|\Phi_0\rangle$. In order to distinguish these quantities from those defined with respect to the true vacuum, we shall write the normal product (N-product) and contractions defined with respect to the Fermi vacuum as

$$N[\hat{M}_{B_1} \cdots \hat{M}_{B_k}] \quad \text{and} \quad \overline{\hat{M}_A \hat{M}_B},$$

respectively. In a completely analogous way, we also obtain the Wick theorem, which we can express symbolically as

$$\hat{M}_1 \cdots \hat{M}_k = N[\hat{M}_1 \cdots \hat{M}_k] + \sum N[\hat{M}_1 \overline{\cdots} \hat{M}_k]. \tag{B.36}$$

Analogously to (B.31) we now have

$$\langle \Phi_0 | \hat{M}_1 \cdots \hat{M}_k | \Phi_0 \rangle = \langle \Phi_0 | \sum N[\hat{M}_1 \overline{\cdots} \hat{M}_k] | \Phi_0 \rangle, \tag{B.37}$$

where the summation extends over all possible nonvanishing systems of pairings, in which all operators must be contracted. When all the operators $\hat{M}_i$ are Y-type operators, we have again a simple result, namely that the only nonvanishing contraction is of the type

$$\overline{\hat{Y}_A \hat{Y}_B^\dagger} = \langle A | B \rangle, \tag{B.38}$$

so that the right-hand side in (B.37) reduces again to the sum of Kronecker delta products. However, it is often convenient not to transform all the operators in the product to the Y-form, as we shall see, since we do not know *a priori* if the given state is a particle or a hole state. It is thus convenient to use the "mixed" operator representation and to derive appropriate expressions for the contractions, defined with respect to the

Fermi vacuum, in this mixed notation. Thus, we find that

$$\overset{\frown}{\hat{X}_A \hat{Y}_B} = 0 \qquad\qquad \overset{\frown}{\hat{Y}_A \hat{X}_B} = h(B)\langle A \mid B\rangle \qquad \overset{\frown}{\hat{X}_A \hat{X}_B} = 0$$

$$\overset{\frown}{\hat{X}_A^\dagger \hat{Y}_B} = 0 \qquad\qquad \overset{\frown}{\hat{Y}_A^\dagger \hat{X}_B} = 0 \qquad\qquad \overset{\frown}{\hat{X}_A^\dagger \hat{X}_B} = h(A)\langle A \mid B\rangle$$

$$\overset{\frown}{\hat{X}_A \hat{Y}_B^\dagger} = p(A)\langle A \mid B\rangle \qquad \overset{\frown}{\hat{Y}_A \hat{X}_B^\dagger} = p(B)\langle A \mid B\rangle \qquad \overset{\frown}{\hat{X}_A \hat{X}_B^\dagger} = p(A)\langle A \mid B\rangle$$

$$\overset{\frown}{\hat{X}_A^\dagger \hat{Y}_B^\dagger} = h(A)\langle A \mid B\rangle \qquad \overset{\frown}{\hat{Y}_A^\dagger \hat{X}_B^\dagger} = 0 \qquad\qquad \overset{\frown}{\hat{X}_A^\dagger \hat{X}_B^\dagger} = 0$$

$$\tag{B.39}$$

where we used the functions $p(A)$ and $h(A)$, defined on the set of spin orbital indices as

$$p(A') = 0, \qquad p(A'') = 1,$$

$$h(A') = 1, \qquad h(A'') = 0. \tag{B.40}$$

Clearly

$$h(A) + p(A) = 1, \qquad \text{for any} \qquad A, \tag{B.41}$$

and, for example,

$$\sum_A f(A)p(A) = \sum_{A''} f(A''),$$

$$\sum_A f(A)h(A) = \sum_{A'} f(A'). \tag{B.42}$$

Appendix C. The Generalized Time-Independent Wick Theorem

We need a more general form of the Wick theorem than that given in Appendix B, which can also deal with the products of operators, some of them being already in the N-product form. It may be shown that this generalized Wick theorem is very similar to that given in Appendix B, the only difference being that we must now leave out all the terms on the right-hand side containing contractions of any two operators, which appear in the same N-product on the left-hand side.

Thus, we can write symbolically (Bogoliubov and Shirkov, 1957)

$$\hat{M}_1 \cdots \hat{M}_{i_1}(N[\hat{M}_{i_1+1} \cdots \hat{M}_{i_2}])\hat{M}_{i_2+1} \cdots$$

$$\times \hat{M}_{i_3}(N[\hat{M}_{i_3+1} \cdots \hat{M}_{i_4}]) \cdots \hat{M}_{i_k}$$

$$= N[\hat{M}_1 \cdots \hat{M}_{i_k}] + \sum{}' N[\hat{M}_1 \overset{\frown\frown}{\cdots\cdots\cdots} \hat{M}_{i_k}], \tag{C.1}$$

where the prime at the summation symbol indicates that we exclude all terms in which two operators, appearing in *the same* N-product on the left-hand side, are contracted.

Appendix D. Normal Product Form of the Operators

In view of the generalized Wick theorem, it is convenient to transform the operators, whose matrix elements we calculate, to the N-product form, since the number of contraction schemes one has to consider is then considerably reduced (Čížek, 1966, 1969). Namely, one can simply ignore all systems of pairings in which the operators appearing in the same N-product are contracted (cf. Appendix C).

We shall show here how to bring the one- and two-particle operators to this form. Consider, first, some one-particle operator

$$\hat{Z} = \sum_{A, B} \langle A | \hat{z} | B \rangle \hat{X}^\dagger_A \hat{X}_B . \tag{D.1}$$

Using Wick's theorem [or, in this case, simply the definition of the contraction (B.23)], we can write the operator product appearing in (D.1) as follows:

$$\hat{X}^\dagger_A \hat{X}_B = N[\hat{X}^\dagger_A \hat{X}_B] + \overset{\frown}{\hat{X}^\dagger_A \hat{X}_B}$$
$$= N[\hat{X}^\dagger_A \hat{X}_B] + \langle A | B \rangle h(A), \tag{D.2}$$

where in the last step we have used (B.39). Thus, using this result in (D.1), we get

$$\hat{Z} = \hat{Z}_N + \sum_{A'} \langle A' | \hat{z} | A' \rangle, \tag{D.3}$$

where

$$\hat{Z}_N = \sum_{A, B} \langle A | \hat{z} | B \rangle N[\hat{X}^\dagger_A \hat{X}_B] \tag{D.4}$$

is the operator $\hat{Z}$ in the N-product form. Observing, moreover, that the last term in (D.3) is simply the Fermi vacuum mean value of $\hat{Z}$, we get, finally,

$$\hat{Z} - \langle \Phi_0 | \hat{Z} | \Phi_0 \rangle = \hat{Z}_N . \tag{D.5}$$

Thus, redefining the energy zero of this operator, we can bring it to the N-product form.

Similarly, for a two-particle operator, say

$$\hat{V} = \frac{1}{2} \sum_{A, B, C, D} \langle AB | \hat{v} | CD \rangle \hat{X}_A^\dagger \hat{X}_B^\dagger \hat{X}_D \hat{X}_C, \tag{D.6}$$

using the hole–particle form of the Wick theorem (B.29), we find

$$A^\dagger B^\dagger DC = N[A^\dagger B^\dagger DC]$$

$$+ N[\overrightarrow{A^\dagger B^\dagger D}C] + N[\overrightarrow{A^\dagger B^\dagger DC}] + N[A^\dagger \overrightarrow{B^\dagger DC}]$$

$$+ N[A^\dagger \overrightarrow{B^\dagger DC}] + N[\overrightarrow{A^\dagger B^\dagger DC}] + N[\overrightarrow{A^\dagger B^\dagger DC}]$$

$$= N[A^\dagger B^\dagger DC] + h(A)(\langle A | C \rangle N[B^\dagger D] - \langle A | D \rangle N[B^\dagger C])$$

$$+ h(B)(\langle B | D \rangle N[A^\dagger C] - \langle B | C \rangle N[A^\dagger D])$$

$$+ h(A)h(B)(\langle A | C \rangle \langle B | D \rangle - \langle A | D \rangle \langle B | C \rangle), \tag{D.7}$$

where, for the sake of simplicity, we have used the abbreviations

$$\hat{X}_A^\dagger \to A^\dagger \qquad \text{and} \qquad \hat{X}_A \to A, \tag{D.8}$$

and left out the contraction schemes containing vanishing pairings [cf. Eqs. (B.39)]. Substituting into (D.6) we get

$$\hat{V} = \hat{V}_N + \hat{G}_N + \langle \Phi_0 | \hat{V} | \Phi_0 \rangle, \tag{D.9}$$

where

$$\hat{V}_N = \frac{1}{2} \sum_{A, B, C, D} \langle AB | \hat{v} | CD \rangle N[\hat{X}_A^\dagger \hat{X}_B^\dagger \hat{X}_D \hat{X}_C], \tag{D.10}$$

$$\hat{G}_N = \sum_{A, B} \langle A | \hat{g} | B \rangle N[\hat{X}_A^\dagger \hat{X}_B], \tag{D.11}$$

$$\langle A | \hat{g} | B \rangle = \sum_{C'} \langle AC' | \hat{v} | BC' \rangle_A, \tag{D.12}$$

$$\langle \Phi_0 | \hat{V} | \Phi_0 \rangle = \frac{1}{2} \sum_{A', B'} \langle A'B' | \hat{v} | A'B' \rangle_A, \tag{D.13}$$

and

$$\langle AB | \hat{v} | CD \rangle_A = \langle AB | \hat{v} | CD \rangle - \langle AB | \hat{v} | DC \rangle. \tag{D.14}$$

Thus, we have again

$$\hat{V} - \langle \Phi_0 \mid \hat{V} \mid \Phi_0 \rangle = \hat{V}_N + \hat{G}_N , \qquad (D.15)$$

the operator in the normal product form.

Appendix E. Sign Rule

We shall show that the correct sign factor of the algebraic expression assigned to a given PT resulting diagram is given by the rule (75). In this Appendix we do not intend to present an exact proof but rather an illustration of the origin of this rule. In fact the given outline may be easily completed into a formal proof if the reader so desires.

As mentioned in the text, the correct sign of our algebraic expression is given by the parity of the permutation, which "unscrambles" a given system of pairings, corresponding to our diagram, into a simple product of contractions. Recall, however, that the order of operators in individual pairings must be preserved in this operation [cf. Eq. (B.28)].

It is easy to realize that we can first "unscramble" any system of pairings into separate factors corresponding to the individual loops of our resulting diagrams. Moreover, this may be done without bringing about any sign change, since every simple vertex is associated with a pair of operators,[28] so that only operator pairs are permuted yielding an even permutation.

Consider, next, one such factor of a system of pairings, which is associated with a single loop of a given diagram, and assume that this loop contains only one hole line. This is illustrated in Fig. 30(1), together with a corresponding system of pairings. We see immediately that any such system of pairings representing a loop containing a single hole line may be again "unscrambled" into a simple product of contractions without any sign change[29] (we permute the last operator through an even number of operators). Moreover, this result is independent of the number of particle lines in the loop. However, as soon as the number of hole lines

---

[28] Notice that for this purpose the operator belonging to each V-vertex may be written as follows $N[\hat{X}_A^\dagger \hat{X}_B^\dagger \hat{X}_D \hat{X}_C] = N[(\hat{X}_A^\dagger \hat{X}_C)(\hat{X}_B^\dagger \hat{X}_D)]$, where each operator pair is associated with one simple vertex of a given V-vertex.

[29] In these considerations it is useful to realize that the parity of a permutation is given, among many other things, by the evenness or oddness of the number of inversions (disorders) in a permutation. For a desired permutation unscrambling our system of pairings, this number may be easily shown to be given, up to multiples of a factor of 2, by the number of intersections of the contraction lines.
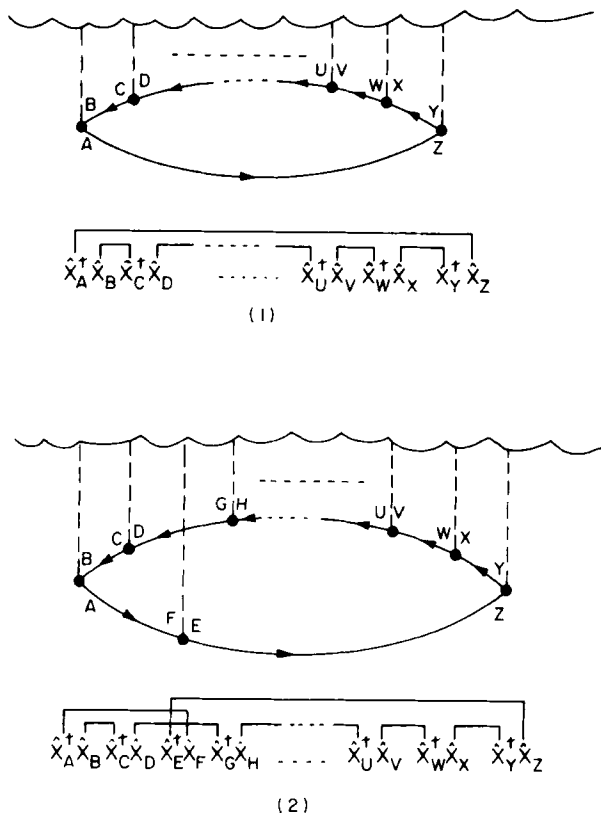
Fig. 30. Illustration of the basic (canonical) loops used for the derivation of the sign rule. Below each figure we give also that part of the system of pairings (contractions), which corresponds to a given loop.

changes we find that a factor of (-1) is introduced with each additional hole line, as Fig. 30(2) illustrates.

Thus for a single loop the desired sign factor is obviously $(-1)^{h_i+1}$, h_i designating the number of hole lines in the ith loop. Thus, for a diagram containing l loops we have

$$\prod_{i=1}^{l} (-1)^{h_i+1} = (-1)^{h+l} \tag{E.1}$$

where h is now the total number of internal hole lines.

Appendix F. Linked Cluster Theorem and EPV Diagrams

In this Appendix we show a cancellation of the unlinked terms, which result from the leading (unbracketed) term (A.1) on the one hand and, on the other hand, from the correction terms, which may be constructed by the bracketing technique of Brueckner (1955) and Huby (1961), as shown in Appendix A. In our formalism, where we have $k_0^{(1)} = 0$, this cancellation occurs for the first time in the fourth order of perturbation theory.

We shall illustrate this cancellation with a nontrivial example, which occurs in the fifth order. Consider the unlinked diagrams of the fifth order, which are composed of two linked diagrams, one of the second and one of the third order, respectively (cf. Fig. 31). Let us stress that these
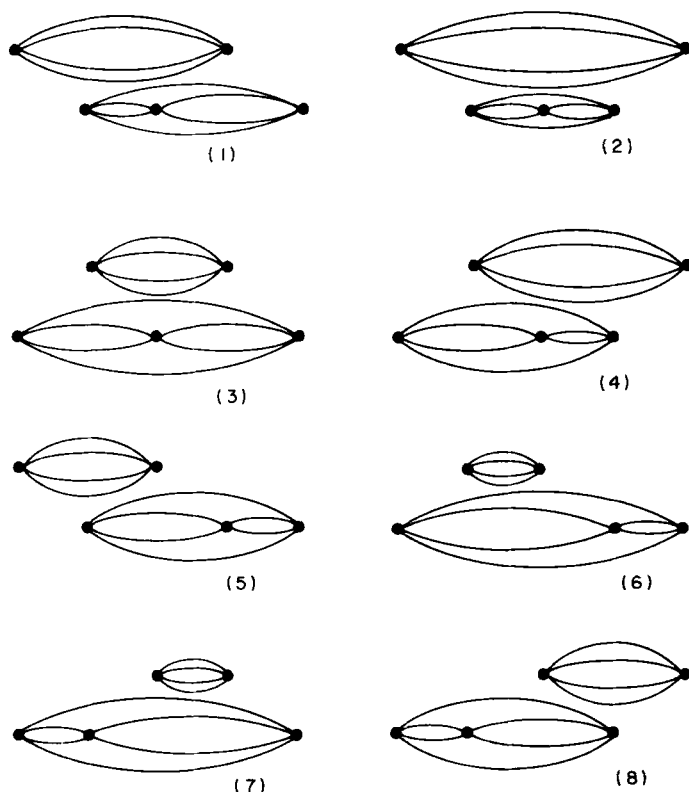
Fig. 31. All possible time versions of a given type of the fifth-order unlinked (disconnected) diagram.

diagrams result, in addition to many other linked and unlinked diagrams, when we evaluate graphically the contribution from the principal [Eq. (A.1)] fifth-order term. Notice also that in all the unlinked diagrams of Fig. 31, there is always either a biexcited or a tetraexcited configuration as the intermediate state. All lines in our diagrams are oriented particle or hole lines, but since the reasoning which follows is true for any particular consistent choice of the line orientations, we shall leave the lines unoriented. In principle there are eight possible orderings of the V-vertices in these diagrams, as shown in Fig. 31.

First, let us stress that we consider these diagrams without any restrictions on the summations over the particle and/or hole states. Consequently, the exclusion principle violating (EPV) diagrams are included among our diagrams, since in the intermediate states a given spin orbital may be included more than once. An example of such an EPV diagram is shown in Fig. 32(1). In this figure we have labeled only the particle lines. We observe, using the rules of Section IV,D, that the contribution from the diagram (1), shown in Fig. 32, is canceled by that of the linked EPV diagram (2). Clearly we are confronted with two alternatives: we can either consider both diagrams (1) and (2) of Fig. 32 or neither of them. As we already stated we adopt the first possibility, which simplifies considerably our notation as well as the theory (no summation restrictions

(1)

(2)
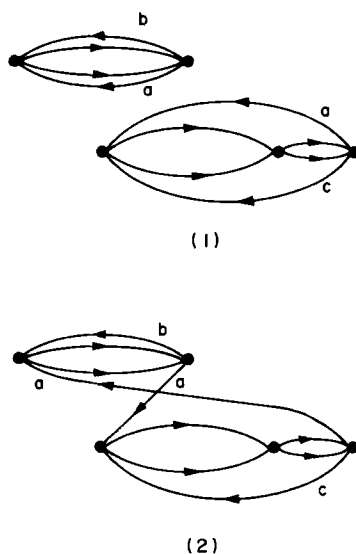
Fig. 32. An example of the EPV diagram cancellation.

and a simple cancellation of unlinked terms). This is the reason that we have to consider EPV diagrams among the linked diagrams.

Let us now return to our fifth-order example of the cancellation of unlinked terms. We designate the denominator, which corresponds to the intermediate state of the second-order diagram, by a and, similarly, the denominators corresponding to the first and the second intermediate states of the third-order diagram by b and c, respectively. Then the possible denominators which occur in the fifth-order diagrams of Fig. 31 are

$$D_1 = a(a + b)(a + c)c,$$
$$D_2 = a(a + b)(a + c)a,$$
$$D_3 = b(a + b)(a + c)c,$$
$$D_4 = b(a + b)(a + c)a,$$
$$D_5 = a(a + b)bc,$$
$$D_6 = b(a + b)bc,$$
$$D_7 = bc(a + c)c,$$
$$D_8 = bc(a + c)a. \tag{F.1}$$

The contribution from any of these diagrams is the same (cf. Section IV,D) except for these denominator parts. Thus in order to find the sum of all these contributions it is sufficient to calculate the sum of the denominator parts

$$S = \sum_{i=1}^{8} (D_i)^{-1}, \tag{F.2}$$

which we then simply multiply by the appropriate matrix elements and numerical factors. Simple algebraic manipulation yields

$$S = (a^2bc)^{-1} + (ab^2c)^{-1} + (abc^2)^{-1}. \tag{F.3}$$

It is now easy to see that the resulting contribution of the diagrams in Fig. 31 will be canceled by the renormalization (bracketed) terms which we singled out in Appendix A. Indeed, considering the expressions (A.5), (A.6), and (A.7) we can associate the denominator a with the first term appearing in (A.5) and (A.6), the denominator a^2 with the first term of (A.7), and, finally, the denominators b^2c, bc^2, and bc with the second term in expressions (A.5), (A.6), and (A.7), respectively. Thus, the denominators resulting from the bracketed terms (A.5)–(A.7) are exactly those

which appear in (F.3). The matrix elements and numerical factors associated with the first (second) terms of (A.5), (A.6), and (A.7) are identical with those associated with the corresponding second (third) order diagram from Fig. 31. However, there is an additional minus sign in expressions (A.5), (A.6), and (A.7) so that the contribution from the eight diagrams of Fig. 31 (which are associated with the leading unbracketed term) is cancelled by the terms (A.5), (A.6), and (A.7). Let us note that the contributions from the 10 remaining bracketings appearing in the fifth order are canceled by other unlinked diagrams which result from the leading term.[30]

Let us also mention that a general, purely algebraic, proof of the cancellation is given in the paper by Frantz and Mills (1960).

Finally, let us note that the linked cluster theorem is already included in the nonperturbative approach of Čížek (1966, 1969). Therefore, if we solve the equations proposed in that paper by perturbation theory, we find unlinked terms already excluded.

REFERENCES

Albat, R. (1972). *Z. Naturforsch. A* **27**, 545.
Bloch, C. (1958a). *Nucl. Phys.* **6**, 329.
Bloch, C. (1958b). *Nucl. Phys.* **7**, 451.
Bogoliubov, N. N., and Shirkov, D. V. (1957). "Introduction to the Theory of Quantized Fields." Moscow. (Engl. transl., Wiley, (Interscience), New York, 1959.)
Brandow, B. H. (1967). *Rev. Mod. Phys.* **39**, 771.
Brueckner, K. A. (1955). *Phys. Rev.* **100**, 36.

[30] In our example the unlinked parts of the resulting diagram are topologically distinct. Notice that in the case when two or more unlinked parts of the same diagram are topologically equivalent, we must take care that only nonequivalent resulting diagrams are considered.

Cederbaum, L. S., Hohlneicher, G., and Peyerimhoff, S. (1971). *Chem. Phys. Lett.* **11**, 421.
Cederbaum, L. S., Hohlneicher, G., and von Niessen, W. (1973). *Chem. Phys. Lett.* **18**, 503.
Chen. T. T. (1972). Ph.D. Thesis. Univ. of Waterloo, Waterloo, Ontario.
Čížek, J. (1966). *J. Chem. Phys.* **45**, 4256.
Čížek, J. (1969). *Advan. Chem. Phys.* **14**, 36.
Čížek, J., and Paldus, J. (1972). *Int. J. Quantum Chem., Symp.* **6**, 435.
Čížek, J., and Paldus, J. (1973). *In* "Energy, Structure and Reactivity" (D. W. Smith and W. B. McRae, eds.), p. 389. Wiley, New York.
Csanak, G., Taylor, H. S., and Yaris, R. (1971). *Advan. At. Mol. Phys.* **7**, 288.
Doll, J. D., and Reinhardt, W. P. (1972). *J. Chem. Phys.* **57**, 1169.
Ecker, F., and Hohlneicher, G. (1971). *Theor. Chim. Acta* **25**, 289.
Fetter, A. L., and Walecka, J. D. (1971). "Quantum Theory of Many-Particle Systems." McGraw-Hill, New York.
Frantz, L. M., and Mills, R. L. (1960). *Nucl. Phys.* **15**, 16.
Goldstone, J. (1957). *Proc. Roy. Soc., Ser. A* **239**, 267.
Hubač, I., Kvasnička, V., and Holubec, A. (1973). *Chem. Phys. Lett.* **24**, 381.
Hubbard, J. (1957). *Proc. Roy. Soc., Ser. A* **240**, 539.
Hubbard, J. (1958a). *Proc. Roy. Soc., Ser. A* **243**, 336.
Hubbard, J. (1958b). *Proc. Roy. Soc., Ser. A* **244**, 199.
Huby, R. (1961). *Proc. Phys. Soc., London* **78**, 529.
Hugenholtz, H. M. (1957). *Physica (Utrecht)* **23**, 481.
Kato, T. (1949). *Progr. Theor. Phys.* **4**, 514.
Kelly, H. P. (1964). *Phys. Rev. B* **136**, 896.
Kelly, H. P. (1968). *Advan. Theor. Phys.* **2**, 75.
Kelly, H. P. (1969). *Advan. Chem. Phys.* **14**, 129.
Löwdin, P.-O. (1955). *Phys. Rev.* **97**, 1474, 1490, 1509.
Löwdin, P.-O. (1966). *In* "Perturbation Theory and Its Application in Quantum Mechanics" (C. H. Wilcox, ed.), p. 255. Wiley, New York.
Malrieu, J. P. (1967). *J. Chem. Phys.* **47**, 4555.
Malrieu, J. P., Claverie, P., and Diner, S. (1967). *Theor. Chim. Acta* **8**, 606.
March, N. H., Young, W. H., and Sampanthar, S. (1967). "The Many-Body Problem in Quantum Mechanics." Cambridge Univ. Press, London and New York.
Morrison, H. L., ed. (1968). "The Quantum Theory of Many-Particle Systems." Gordon & Breach, New York.
Paldus, J. (1972). *J. Chem. Phys.* **57**, 638.
Paldus, J., and Čížek, J. (1969). *Chem. Phys. Lett.* **3**, 1.
Paldus, J., and Čížek, J. (1970). *J. Chem. Phys.* **52**, 2919.
Paldus, J., and Čížek, J. (1974). *J. Chem. Phys.* **60**, 149.
Paldus, J., and Wong, H. C. (1973). *Comput. Phys. Commun.* **6**, 1.
Paldus, J., Čížek, J., and Shavitt, I. (1972a). *Phys. Rev. A* **5**, 50.
Paldus, J., Sengupta, S., and Čížek, J. (1972b). *J. Chem. Phys.* **57**, 652.
Paldus, J., Čížek, J., and Keating, B. A. (1973). *Phys. Rev. A* **8**, 640.
Paldus, J., Čížek, J., and Hubač, I. (1974). *Int. J. Quantum Chem., Symp.* **8**, 293
Pellégatti, A., Čížek, J., and Paldus, J. (1974). *J. Chem. Phys.* **60**, 4825.
Pickup, B. T., and Goscinski, O. (1973). *Mol. Phys.* **26**, 1013.
Raimes, S. (1972). "Many-Electron Theory." North-Holland Publ., Amsterdam.
Reinhardt, W. P., and Doll, J. D. (1969). *J. Chem. Phys.* **50**, 2767.
Reinhardt, W. P., and Smith, J. B. (1973). *J. Chem. Phys.* **58**, 2148.

Roman, P. (1965). "Advanced Quantum Theory." Addison-Wesley, Reading, Massachusetts.

Salzman, W. R. (1968). *J. Chem. Phys.* **49**, 3035.

Silverstone, H. J., and Holloway, T. T. (1970). *J. Chem. Phys.* **52**, 1472.

Simons, J., and Smith, W. D. (1973). *J. Chem. Phys.* **58**, 4899.

Stell, G. (1967). *In* "Graph Theory and Theoretical Physics" (F. Harary, ed.), p. 281. Academic Press, New York.

Thouless, D. J. (1972). "The Quantum Mechanics of Many Body Systems," 2nd Ed. Academic Press, New York.

Tolmachev, V. V. (1962). *Vestn. Leningrad. Univ., Ser. Fiz., Khim.* **14**, 11.

Tolmachev, V. V. (1963a). "Field Theoretical Form of Perturbation Theory for Many Electron Atomic and Molecular Problems." Univ. of Tartu, Tartu. (In Russ.)

Tolmachev, V. V. (1963b). *Liet. Fiz. Rinkinys* 3, 47: (English transl. *in* "Three Approaches to Electron Correlation in Atoms" (O. Sinanoğlu and K. A. Brueckner, eds.), p. 327. Yale Univ. Press, New Haven, Connecticut, 1970.)

Tolmachev, V. V. (1969). *Advan. Chem. Phys.* **14**, 421, 471.

Tong, B. Y. (1962). *Proc. Phys. Soc., London* **80**, 1101.

Wong, H. C., and Paldus, J. (1973). *Comput. Phys. Commun.* **6**, 9.

Coupled-Channel Studies of Rotational and Vibrational Energy Transfer by Collision*

WILLIAM A. LESTER, JR.

IBM Research Laboratory
San Jose, California

I. Introduction

Two recent trends are having a significant impact on current activity in quantum chemistry. One is a broadening of research efforts by many quantum chemists to encompass studies of the dynamical behavior of molecular systems as an adjunct to continuing efforts to determine static (bound state) properties of individual molecules. The other is the rapid development of techniques for the measurement of cross sections for individual scattering events exemplified by the molecular beam scattering method (*Discuss. Faraday*, 1973; Toennies, 1974), and approaches using infrared chemiluminiscence (Carrington and Polanyi, 1972) and resonance fluorescence (Gordon *et al.*, 1968). For complementary theoretical

study, such experimental methods dictate the need for reliable potential energy surfaces and scattering cross sections.

At thermal and suprathermal energies, collisions of heavy particles (atoms, ions, and molecules) can generally be treated as the relative motion of the collision partners on potential energy surfaces. For a given electronic configuration of the collision system, the potential energy surface is simply the set of solutions of the electronic Schroedinger equation in the Born–Oppenheimer approximation for different nuclear geometries, with the zero of energy chosen usually as the scattered molecules infinitely separated.

For nonreactive collisions of closed-shell molecules at energies below the threshold for electronic excitation, nuclear motion is determined by a single potential energy surface. Under these conditions, the physical processes possible are elastic scattering and energy exchange between the translational (T), rotational (R), and vibrational (V) degrees of freedom.

Elastic scattering is rather well understood and will not concern us further here; see, for example, Toennies (1973) and Bernstein (1966). By comparison, inelastic scattering is in an early stage of development, particularly for processes in which information about quantum state changes is desired. For reactive scattering, much remains to be done before theory achieves a predictive capability rivaling the best measurements available.

Recent work in low energy inelastic scattering shows that it is possible with existing methods to carry through calculations of collision cross sections that have predictive content if the accuracy of the potential energy surface is "adequate" for the process of interest (Shafer and Gordon, 1973; Lester and Schaefer, 1974; Schaefer and Lester, 1975). The question of the accuracy of the potential energy surface required to yield a prescribed reliability of a collision cross section remains to be fully answered, but recent work on four-electron systems is yielding further insights. In Section II, we examine this question for the relatively well studied He–H_2 and Li^+–H_2 systems.

Before proceeding to potential energy surfaces for inelastic scattering, we comment here on the remainder of the paper. Our aim is to point out many of the crucial problems that must be dealt with in attempts to compute reliable cross sections that can serve as predictions and as a basis for new insights into the mechanism of the collision event. This goal is intimately connected, of course, with the determination of reliable potential energy surfaces and so we discuss this aspect in Section II and at appropriate places throughout; see also Takayanagi (1973). The consideration of computational methods for carrying out accurate quantum

mechanical (coupled-channel or close-coupling) scattering calculations is not covered here; for recent reviews, see Alder *et al.* (1971), Levine (1972), George and Ross (1973), Secrest (1973), and Kouri (1973). In addition, a survey of new developments in classical and semiclassical approaches to molecular collisions lies outside the intent of this paper. For a recent discussion of classical methods, see Bunker (1971); for semiclassical developments, see Miller (1973, 1974) and Marcus (1973).

II. Potential Energy Surfaces

To date almost all nonempirical potential energy surfaces determined over a range of coordinate space to be usable for scattering applications have been computed following the Hartree–Fock (HF) and configuration interaction (CI) models. These approaches in their various forms are well documented in earlier volumes of this series and will not be further discussed here; rather, attention in this paper will be directed toward problems encountered in utilizing the set of discrete energy points that define the surface. Krauss (1970) has reviewed work on potential energy surfaces, and listings of systems more recently studied are given by Certain and Bruch (1972), by Levine (1972), by Connor (1973), and by Balint-Kurti (1975).

The biggest limitation to the use of traditional *ab initio* methods for the generation of potential energy surfaces is the large number of energy points required to accurately define the surface and, concomitantly, the cost per point. Gordon and Kim (1972) have developed a method for the interaction of closed shell systems based on an electron gas model that, in comparisons involving inert gas pairs, has been shown to yield a good representation of energy surfaces in the repulsive region and in the vicinity of the well at a very considerable saving in computer time; see also Kim (1973), Kim and Gordon (1974a,b,c), Green (1974), Green and Thaddeus (1975), and Green *et al.* (1975) for applications to atom–molecule systems. Efforts to improve results in the region of intermediate overlap and at long range, where sizeable discrepancies have been noted, are reported by Rae (1973), Kim and Gordon (1974d), and by Cohen and Pack (1974).

A recurring problem that has not been dealt with adequately for potential energy surfaces defined by discrete points is the availability of general procedures for transmitting the set of energy points in a simple, compact, and accurate form for utilization in scattering calculations. Yarkony *et al.* (1974) have recently discussed this problem for the hydrogen

fluoride dimer. Alexander and Berard (1974) investigated least-squares
methods for the Gordon and Secrest (1970) He–H_2 surface. They gen-
erated least-squares fits to the *ab initio* collection of points based on
minimizing a measure of the absolute deviation between the fit function
and the known points. Criteria considered were minimization of (a) the
root-mean-square (rms) deviation, (b) the maximum deviation, and (c)
the average deviation. As noted by Secrest (1974), the differences in scat-
tering results between the original Gordon–Secrest and various
Alexander–Berard surfaces are a consequence of how the various fits
extrapolate to a region not treated in the original study. The Alexander–
Berard study clearly shows the extreme sensitivity that scattering results
can have to the form of the potential energy surface.

Sensitivity of cross sections to choice of potential energy surface was
also investigated in a recent coupled-channel study of $T \rightarrow R$ and
$T \rightarrow VR$ energy transfer in the Li^+–H_2 system. Three potential energy
surfaces were employed; two restricted HF surfaces of similar accuracy
computed using standard Gaussian (Lester, 1970, 1971, 1972) and
Gaussian-lobe (Kutzelnigg *et al.*, 1973) basis functions and a CI energy
surface determined using the Gaussian-lobe HF surface as a starting
point. For large integral cross sections which correspond to low order
$(0 \rightarrow 2,4)$ pure rotational transitions, the choice of energy surface was
unimportant. For small multiquanta $T \rightarrow R$ and $T \rightarrow VR$ transitions,
however, there were noticeable differences between integral cross sections
computed using the HF surfaces (which agreed closely with each other)
and those determined with the CI surface.

III. Coupled Equations

A method which, in principle, can yield the exact solution of the
collision dynamics on a specified potential energy surface is the "coupled
channel" or "close-coupling" (CC) method. Because almost all coupled-
channel computations have been carried out for scattering of a structure-
less projectile by a Σ-state diatomic molecule, the sketch of the following
theoretical development is limited to this case; however, see Klar (1973)
for scattering of a Π-state diatomic molecule.

The two most common formulations for the quantum mechanical
solution of the nuclear Schroedinger equation are due to Arthurs and
Dalgarno (1960), hereafter denoted AD, and to Curtiss and co-workers
(Curtiss and Adler, 1952; Curtiss, 1953, 1968; Gioumousis and Curtiss,
1961; see also Hunter and Curtiss, 1973, and references therein). CC

computations that have appeared to date have almost exclusively followed the AD formulation. An essential difference between the two developments is that AD derive scattering equations in a space-fixed frame and employ Racah algebra to simplify cross section expressions. Curtiss and co-workers transform the Hamiltonian to a body-fixed frame with resultant equations that have been shown to facilitate the use of approximate treatments in which energy transfer occurs predominantly at small distances (Lawley and Ross, 1965; Klar, 1973; McGuire and Kouri, 1974; McGuire, 1975; Pack, 1974). Because almost all attempts to compute accurate cross sections have followed the AD formalism, we briefly outline it here to facilitate discussion in Section IV.

A. Coupled Channel

In the AD formalism the nuclear Schroedinger equation in a center-of-mass (c.m.) frame may be written,

$$[-(\hbar^2/2\mu)\nabla^2 - H_{int}(\mathbf{r}) + V(\mathbf{r}, \mathbf{R}) - E_{vj}]\Psi_{vj}(\mathbf{r}, \mathbf{R}) = 0 \qquad (1)$$

where the terms in the brackets are, from the left, the kinetic energy operator for relative motion, the Hamiltonian for internal (rotational and vibrational) motion, the potential energy surface, and the total energy of the system with the diatomic initially in the vjth vibrational-rotational state. Here μ is the reduced mass of the atom–molecule system, $\mathbf{r}$ specifies the relative coordinates of the diatomic molecule with respect to a space-fixed origin, and $\mathbf{R}$ is the atom-to-molecule c.m. distance.

Since the total angular momentum $\mathbf{J}(= \mathbf{j} + \mathbf{L})$ and z projection M are good quantum numbers, AD find it convenient to form eigenfunctions of $\mathbf{J}^2$, J_z, $\mathbf{j}^2$, and $\mathbf{L}^2$,

$$\mathscr{Y}_{jl}^{JM}(\hat{r}, \hat{R}) = \sum_{m_j m_l} (jlm_j m_l \mid jlJM) Y_{jm_j}(\hat{r}) Y_{lm_l}(\hat{R}) \qquad (2)$$

where $(jlm_j m_l \mid jlJM)$ is Clebsch–Gordan coefficient, $\mathbf{j}$ is the rotational angular momentum and $\mathbf{L}$ is the orbital angular momentum. Using Eq. (2), the total wavefunction is written,

$$\Psi_{vj}(\mathbf{r}, \mathbf{R}) = \sum_{JM\gamma} \Psi_{\gamma}^{JM}(\mathbf{r}, \mathbf{R}) \qquad (3)$$

where

$$\Psi_{\gamma}^{JM}(\mathbf{r}, \mathbf{R}) = \sum_{\gamma'} (rR)^{-1} \chi_{v'j'}(r) \mathscr{Y}_{j'l'}^{JM}(\hat{r}, \hat{R}) u_{\gamma' \leftarrow \gamma}^{J}(R) \qquad (4)$$

and $\gamma \equiv vjl$ is the channel index. Here $\chi_{vj}(r)$ are eigenfunctions of a radial Schroedinger equation for nuclear motion of the molecule.

Substituting Eq. (3) into Eq. (1) leads to

$$\left(\frac{d^2}{dR^2} + k_{v'j'}^2 - \frac{l'(l'+1)}{R^2}\right)u_{\gamma'\leftarrow\gamma}^J(R)$$

$$= \left(\frac{2\mu}{\hbar^2}\right)\sum_{\gamma''} V_{\gamma'\gamma''}^J(R)u_{\gamma''\leftarrow\gamma}^J(R), \qquad (5)$$

where

$$k_{v'j'}^2 = (2\mu/\hbar^2)(E_{vj} - \varepsilon_{v'j'})$$

and

$$V_{\gamma'\gamma''}^J(R) = \int \chi_{v'j'}^*(r)\mathscr{Y}_{j'l'}^{JM*}(\hat{r}, \hat{R})V(\mathbf{r}, \mathbf{R})\chi_{v''j''}(r)\mathscr{Y}_{j''l''}^{JM}(\hat{r}, \hat{R}) \, d\hat{r} \, d\hat{R}. \qquad (6)$$

V can be expanded,

$$V(\mathbf{r}, \mathbf{R}) = \sum_\lambda v_\lambda(r, R)P_\lambda(\cos\theta) \qquad (7)$$

where P_λ is a Legendre polynomial of order λ and θ is the angle formed by $\mathbf{r}$ and $\mathbf{R}$. Use of Eq. (7) in Eq. (6) leads to

$$V_{\gamma'\gamma''}^J(R) = \sum_\lambda f_\lambda(j'l', j''l''; J)\int_0^\infty \chi_{v'j'}^*(r)v_\lambda(r, R)\chi_{v''j''}(r) \, dr, \qquad (8)$$

where

$$f_\lambda(j'l', j''l''; J)$$

$$= (-1)^{j''+J'-J}[(2j'+1)(2l'+1)(2j''+1)(2l''+1)]^{1/2}$$

$$\times \begin{pmatrix} l' & l'' & \lambda \\ 0 & 0 & 0 \end{pmatrix}\begin{pmatrix} j' & j'' & \lambda \\ 0 & 0 & 0 \end{pmatrix}\begin{Bmatrix} j' & l' & J \\ l'' & j'' & \lambda \end{Bmatrix}. \qquad (9)$$

The $\begin{pmatrix} \cdot & \cdot & \cdot \\ \cdot & \cdot & \cdot \end{pmatrix}$ are 3-j symbols and the $\begin{Bmatrix} \cdot & \cdot & \cdot \\ \cdot & \cdot & \cdot \end{Bmatrix}$ is a 6-j symbol.

The S-matrix is defined by the requirement that asymptotically

$$u_{\gamma'\leftarrow\gamma}^J(R) \rightarrow \delta_{j'j}\delta_{l'l} \exp\left[-i\left(k_j r - \frac{l\pi}{2}\right)\right]$$

$$- \left(\frac{k_j}{k_{j'}}\right)^{1/2}S_{\gamma'\gamma}^J \exp\left[i\left(k_{j'} r - \frac{l'\pi}{2}\right)\right]. \qquad (10)$$

Differential cross sections $d\sigma/d\omega$ for the $(vjm_j) \rightarrow (v'j'm_{j'})$ transition can be obtained by taking appropriate linear combinations of the functions Ψ_γ^{JM}. Averaging over m_j and summing over $m_{j'}$ yields the cross section for the $(vj) \rightarrow (v'j')$ transition, the so-called "degeneracy-averaged" cross section. It is computationally convenient to employ the helicity representation (Jacob and Wick, 1959; Miller, 1969) to evaluate the differential cross section which has the form

$$\frac{d\sigma_{v'j'\leftarrow vj}}{d\omega} = (2j + 1)^{-1} \sum_{m_j} \sum_{m_{j'}} |f_{v'j'm_{j'},\leftarrow vjm_j}|^2, \tag{11}$$

where

$$f_{v'j'm_{j'},\leftarrow vjm_j}(\theta) = (-)^{j+j'}(2ik_{vj})^{-1} \sum_J (2J + 1) d_{m_{j'}m_j}^J(\theta)$$

$$\times \sum_{ll'} i^{l-l'} \begin{pmatrix} j' & J & l' \\ m_{j'} & -m_{j'} & 0 \end{pmatrix} \begin{pmatrix} j & J & l \\ m_j & -m_j & 0 \end{pmatrix}$$

$$\times [(2l' + 1)(2l + 1)]^{1/2}(S_{\gamma'\gamma}^J - \delta_{vv'}\delta_{jj'}\delta_{ll'}). \tag{12}$$

Here $d_{m_{j'}m_j}^J(\theta)$ is the usual reduced rotation matrix. The integral cross section is simply

$$\sigma_{v'j'\leftarrow vj} = \left[\frac{\pi}{k_{vj}^2(2j + 1)}\right] \sum_J (2J + 1) \sum_{ll'} |T_{\gamma'\gamma}^J|^2, \tag{13}$$

where $T = I - S$.

It is noted that using the functions $Y_{jm_j}(\hat{r})Y_{lm_l}(\hat{R})$ directly, the uncoupled representation can, in principle, lead to an exact solution of the collision problem. It is less convenient, however, because unlike the AD treatment, S is not diagonal in J and M.

B. Effective Potential

A major limitation to the applicability of the CC method is the large number of terms that must be retained in Eq. (4) due to the $2j + 1$ degeneracy of the jth rotational level. To avoid this difficulty, Rabitz (1972) has proposed the effective potential (EP) method which retains the coupling between vj states but averages over the projection quantum numbers m_j before carrying out the dynamics. In Section IV, we discuss cross sections obtained with CC equations in the EP formulation for rigid rotator scattering and computed following the AD total angular momentum representation. Therefore, we briefly describe the essential differences in the treatments.

The effective potential derived from Eq. (7) has the form (Zarur and Rabitz, 1973)

$$V^{\text{eff}}_{\Gamma\Gamma'}(R) = (-)^{\eta}[(2j + 1)(2j' + 1)]^{1/4} \sum_{\lambda} \langle v' | v_{\lambda}(R) | v \rangle$$

$$\times (2\lambda + 1)^{-1/2} \begin{pmatrix} j' & \lambda & j \\ 0 & 0 & 0 \end{pmatrix}, \tag{14}$$

where $\eta = \frac{1}{2}(|j - j'| + j + j')$, $\Gamma \equiv (vj)$, and $|vj\rangle$ are "effective" states of H_{int}. In place of Eq. (3), we have

$$\Psi_{\Gamma}(R) = R^{-1} \sum_{l} U^{l}_{\Gamma}(R) P_{l}(\cos\theta) \tag{15}$$

which eventually leads to, in lieu of Eq. (5),

$$\left(\frac{d^2}{dR^2} + k^2_{\Gamma} - \frac{l'(l' + 1)}{R^2} \right) U^{l}_{\Gamma}(R) = (2\mu/\hbar^2) \sum_{\Gamma'} V^{\text{eff}}_{\Gamma\Gamma'}(R) U^{l}_{\Gamma'}(R). \tag{16}$$

The wavefunction $\Psi_{\Gamma'}(\mathbf{R})$ has the asymptotic form

$$\Psi_{\Gamma'}(\mathbf{R}) \sim [(2\pi)^{3/2}]^{-1} \left[\delta_{vv'} \delta_{jj'} \exp(ik_{\Gamma} R \cos\theta) + f_{\Gamma\Gamma'}(\theta) \frac{\exp(ik_{\Gamma'} R)}{R} \right], \tag{17}$$

where $f_{\Gamma\Gamma'}(\theta)$ is the scattering amplitude connecting the intial $\Gamma \equiv vj$ state to the final $\Gamma' \equiv v'j'$ state. It is important to note all references here are to states (vj) unlike the AD formulation which refers to channels (vjl). One may define an effective scattering matrix S by the relation

$$f_{\Gamma\Gamma'}(\theta) = -\frac{1}{2i(k_{\Gamma} k_{\Gamma'})^{1/2}} \sum_{l} (2l + 1)(\delta_{vv'} \delta_{jj'} - S^{l}_{\Gamma\Gamma'}) P_{l}(\cos\theta) \tag{18}$$

which leads to the standard expression for the differential cross section, cf. Eq. (11),

$$d\sigma_{\Gamma' \leftarrow \Gamma}/d\omega = (k_{\Gamma'}/k_{\Gamma})[(2j' + 1)/(2j + 1)]^{1/2} | f_{\Gamma\Gamma'}(\theta)|^2 \tag{19}$$

and integral cross section, cf. Eq. (13),

$$\sigma_{\Gamma' \leftarrow \Gamma} = (\pi/k^2_{\Gamma})[(2j' + 1)/(2j + 1)]^{1/2} \sum_{l} (2l + 1) | T^{l}_{\Gamma\Gamma'} |^2. \tag{20}$$

Comparison of the EP and CC equations shows that EP leads to fewer summations, simpler angular momentum algebra (l is a good quantum number), and fewer coupled equations. In addition, it has been shown (Rabitz, 1972) that if N is the dimension of the CC equations, the

EP equations are of dimension $\sqrt{N}$. The use of V^{eff} results in a partial decoupling of the internal and orbital angular momenta.

C. Coupled States

McGuire (1973) has developed and applied what is now called the "coupled states" (CS) method which is also a procedure for reducing the dimensionality of the CC equations through decoupling of j and l. The theory has been presented and applied by McGuire and Kouri (1974), and separately reported by Pack (1974). In this approach, one employs the exact set of coupled equations in the "rotating" or "body-fixed" system developed so fully by Curtis and associates (1952, 1953, 1968; Hunter and Curtiss, 1973). They are obtained from the transformed Schroedinger equation (McGuire, 1975ab)

$$(\mathscr{R}H\mathscr{R})\mathscr{R}^{-1}\Psi_{vjm_j} = E\mathscr{R}^{-1}\Psi_{vjm_j} \tag{21}$$

where $\mathscr{R}$ is the rotation that makes the space-fixed z axis coincident with $\mathbf{R}$ and the rotated y axis lie in the space-fixed x–y plane. The Euler angles (α, β, γ) which accomplish this transformation are $(\Phi, \vartheta, 0)$ so that

$$\Psi_{vj\Omega} = \mathscr{R}^{-1}\Psi_{vjm_j}$$

$$= \sum_{m_j=-j}^{j} D^{j}_{m_j\Omega}(\Phi, \vartheta, 0)\Psi_{vjm_j} \tag{22}$$

where $D^{j}_{m_j\Omega}$ are the matrix elements of the irreducible representation of the rotation operator (Brink and Satchler, 1962) and Ω is the projection of $\mathbf{j}$ on the body-fixed z axis. The transformed Hamiltonian $H' \equiv (\mathscr{R}^{-1}H\mathscr{R})$ is

$$H' = -\frac{\hbar^2}{2\mu R}\frac{\partial^2}{\partial R^2}R + \frac{\hat{l}^2}{2\mu R^2} - \frac{\hbar^2}{2m}\nabla_r^2 + V(\mathbf{r}, R) \tag{23}$$

where $\hat{l} = (\hat{J} - \hat{j})$ and $\hat{l}^2$ operates on the angular part of $\Psi_{vj\Omega}$. Matrix elements of $\hat{l}^2$ have a contribution diagonal in Ω,

$$[\hat{l}^2]_{\Omega\Omega} = \hbar^2[J(J+1) + j(j+1) - 2\Omega^2] \tag{24}$$

and a nondiagonal part,

$$[\hat{l}^2]_{\Omega\Omega'} = -\hbar^2 \delta_{\Omega',\Omega\pm1}[(J\pm\Omega+1)(J\mp\Omega)]^{1/2}j^{\mp} \tag{25}$$

where $j^{\mp}$ are the raising and lowering operators for the rotator.

To obtain the coupled states approximation requires (1) neglecting the off-diagonal coupling in Ω which amounts to ignoring coriolis

coupling and (2) approximating the centrifugal potential matrix elements, cf. Eq. (24), by $\hbar^2 l(l + 1)$. In previous CC studies of rotational excitation in weakly coupled He–H_2 (McGuire and Micha, 1972; Eastes and Secrest, 1972), each l contribution, consistent with the requirement $|J - j| \leq l \leq J + j$, gives approximately the same contribution to the cross sections. In such cases $l = J$ which is roughly the average of values between $J - j$ and $J + j$. Kouri and McGuire (1975) have found for the more strongly coupled Li^+–H_2 system that the value $l = J - j$ is most appropriate. Further study to refine the specification of l for other systems will be useful.

With the above two approximations, the CS equations take the form (McGuire, 1975ab)

$$(d^2/dR^2 + k_\Gamma^2 - l(l + 1)/R^2)F^l_{\xi'\Omega' \leftarrow \xi\Omega}(R)$$
$$= (2\mu/\hbar^2) \sum_{\xi''} V^l_{\xi'\xi''}(R)F^l_{\xi''\Omega \leftarrow \xi\Omega}(R) \qquad (26)$$

where $\xi \equiv (vj)$,

$$V^l_{\xi'\xi''}(R) = \sum_\lambda G^\lambda(j'\Omega', j''\Omega'') \int \chi^*_{\xi'}(r)v_\lambda(r, R)\chi_{\xi''}(r) \, dr. \qquad (27)$$

and

$$G^\lambda \equiv \langle j'\Omega' \,|\, P_\lambda \,|\, j''\Omega'' \rangle = \delta_{\Omega\Omega'}(-)^\Omega \begin{pmatrix} j & \lambda & j' \\ 0 & 0 & 0 \end{pmatrix} \begin{pmatrix} j & \lambda & j' \\ -\Omega & 0 & \Omega' \end{pmatrix} \qquad (28)$$
$$\times [(2j + 1)(2j' + 1)]^{1/2}$$

Note in Eq. (28) that the coupling between states of different Ω vanishes. However, Δm_j transitions are obtainable, which is not possible in the EP method, through use of Eq. (22). By neglecting effects of rotation on the body fixed wavefunctions, standard expressions for differential and integral cross sections can be used (McGuire and Kuori, 1974; McGuire, 1975ab).

IV. Cross Sections

Applications of CC methods have been restricted almost exclusively to collisions of H, He, and Li^+ with H_2 because of the lack of availability of accurate *ab initio* and reliable semiempirical potential energy surfaces for larger systems. The H_2 molecule provides a particularly useful scatter-

ing target because of its large energy level spacing which greatly reduces the range of excitations possible at a specified collision energy. In this section, we examine the dependence of computed cross sections on selected computational and physical parameters.

A. Convergence

Once the potential energy surface has been specified, the usual procedure in CC studies is to carry out calculations with succeedingly larger target state expansions, Eq. (4) or its EP and CS analog, until the cross section or S-matrix ceases to change beyond some desired limit. Experience with model systems (Lester and Bernstein, 1967) indicated that a good rule of thumb is to retain channels corresponding to the $(n + 1)$th order transition in order to obtain reliable nth-order excitation cross sections. This rule was found to hold well for rotational excitation studies of $H-H_2$ (Wolken *et al.*, 1972) and $He-H_2$ (Eastes and Secrest, 1971, 1972), but is violated for the Li^+-H_2 system (Lester and Schaefer, 1973; McGuire, 1974). This distinguishing behavior of the latter system has its origin in ion-molecule interactions at long range and a relatively large (compared to v_0) nonspherical potential term v_2 at smaller distances that is not shielded by v_0 as is found for $H-H_2$ (and noted by Wolken *et al.*, 1972) and $He-H_2$ (Krauss and Mies, 1965; Gordon and Secrest, 1970).

Convergence behaviour of EP and CS cross sections is emerging from recent studies of H_2 scattered by He, H_2, and Li^+. Comparison of EP and CC two($j = 0, 2$)- and three($j = 0, 2, 4$)-state calculations of integral cross sections for rotational excitation of H_2 by He impact using the Roberts (1963) potential show similar convergence behavior (Zarur and Rabitz, 1973). Note that the EP cross sections are in semiquantitative agreement with those calculated by CC methods.

Green (1975) has computed CC integral cross sections for rotational transitions in the H_2-H_2 system for many of the same transitions and using the same potential that Zarur and Rabitz (1974) employed in an EP study. Green finds a faster rate of convergence for CC cross sections, but due to the reduction of the number of equations realizable in the EP method, the largest basis set EP calculations require less computer time than the converged CC ones. In addition, for the dominant inelastic processes, EP cross sections are seen to be typically 20–30% larger than those computed in the CC formalism. A weakness of the EP method noted in this study was the inability to reliably predict cross sections for near-resonant transitions which, contrary to the general conclusion just stated, were anomalously small. Despite these quantitative shortcomings,

Green (1975) finds that the EP method appears to mimick the true dynamics rather closely and therefore we expect considerable application of the method to larger systems where CC computations are currently prohibitive.

McGuire (1975b) has recently compared convergence patterns of CC and CS cross sections for scattering of H_2 by He. As in the EP–CC comparison just discussed, elastic and rotational excitation cross sections are found to converge similarly. For vibrational excitation, CS and CC cross sections again display similar convergence trends, but trends that are decidedly irregular by comparison with elastic and rotational excitation results. In general, the CS result in best accord with converged CC cross sections is the fully converged one.

Clearly from the limited comparisons available to date, the preferred approach in applying approximate coupled equations methods is to compute converged cross sections for the transitions of interest. Based on the convergence patterns discussed, this would likely result in larger basis sets in EP and to some extent in CS calculations (McGuire, 1975b) than those required for converged CC results. The computational savings arising from the use of such approximate quantum methods, if the findings of recent study are maintained in subsequent applications, should hold the computational effort below that required for a converged CC cross section. Thus the EP and CC methods should be useful for gaining insight on the collision dynamics of systems currently intractable by rigorous CC methods.

B. Energy Level Spacing

The energy level spacing plays a fundamental role in determining collision cross sections through the definition of the scattering wavevector; see Eq. (5). In rigid rotator CC studies on the Li^+-H_2 system (Lester and Schaefer, 1973), integral cross sections were computed using H_2 energy level spacings determined by the usual rigid rotator (RR) expression for H_{int} using an experimental rotational constant B_0, and by the addition of the centrifugal distortion term to the standard RR energy level expression again employing experimental rotation constants. The latter procedure, denoted ECRR (energy corrected rigid rotator), produced integral cross sections for pure rotational excitation within a few percent of cross sections computed using a H_{int}, Eq. (1), which properly takes into account vibrational as well as rotational motion and employed the Kolos and Wolniewicz (KW) H_2 potential, including adiabatic correction (Kolos and Wolniewicz, 1964).

C. Expansion Functions

Because previous CC computations have been based on target state expansions, the choice of expansion functions for diatomic molecule collisions reduces to the selection of vibrational–rotational eigenfunctions $\chi_{vj}(r)$ of Eq. (4) to go with spherical harmonics and, of course, only spherical harmonics for RR scattering. For vibration this has usually amounted to a choice between harmonic and Morse oscillator functions (Taylor and Gianturco, 1969; Kouri and Wells, 1974). Differences in cross sections obtained using the two sets of functions can arise from two sources. One is the energy level spacing (Section IV,B) as it enters the CC formalism in the specification of k_{vj}^2, Eq. (5), and the other is the form of the wavefunctions *per se*.

Recent CC calculations (Schaefer *et al.*, 1974) carried out using harmonic oscillator, Morse oscillator, and numerical KW functions in which the scattering wavevectors were constrained to be the same for each choice of χ_{vj} resulted in essentially the *same* integral cross sections for one to five quantum pure rotational transitions. For $0 \to 1$ vibrational cross sections, however, cross sections obtained using harmonic oscillator wavefunctions were found to differ significantly from those computed utilizing Morse and KW functions which were in excellent agreement with each other.

D. Multiquanta Transitions

Cross sections for a variety of multiquanta transitions have been computed by the EP version (Section III,B) for $He-H_2$ (Zarur and Rabitz, 1973, 1974; Alexander, 1974) and by the CC method (Section II,A) for Li^+-H_2 (Schaefer and Lester, 1973, 1975). As may be anticipated based on the larger anisotropy of the potential energy surface, cross sections for multiquanta transitions for Li^+-H_2 are considerably larger than the corresponding transitions in $He-H_2$ and decrease less rapidly with increasing order of the transition.

E. Initial *j*-Dependence

Computations of integral cross sections have been carried out at a fixed total energy (relative translational plus internal) for excitation to the $v = 1, j = 0$ state as a function of the initial *j*-state in the Li^+-H_2 system (Schaefer and Lester, 1973). These studies show that the magnitude of the excitation cross sections lie in the order [denoting initial (vj) state only], $(0, 2) > (0, 4) > (0, 6) > (0, 0)$. The ratio of the $(0, 2) \to (1, 0)$ to $(0, 0) \to (1, 0)$ integral cross sections is approximately 4 to 1. Such a

pronounced dependence on the initial state is likely due to the large anisotropy of the potential energy surface and the coordinate dependence of the radial coupling. Direct 0 to 2, predominantly indirect 0 to 4, and indirect 0 to 6 couplings serve to "drive" excitation to the (1, 0) state which is not available for 0 to 0.

V. Concluding Remarks

Coupled equations methods can contribute valuable insights regarding the dynamics of transitions between individual quantum states. In addition, CC calculations continue to serve as standards to test other methods (e.g., La Budde and Bernstein, 1973; Miller and Raczkowski, 1974). Finally, it has now been demonstrated that reliable theoretical predictions are obtainable of sufficient accuracy to test the quality of molecular beam scattering experiments (Schaefer and Lester, 1975).

REFERENCES

Alder, B., Fernbach, S., and Rotenberg, M., eds. (1971). *Methods Comput. Phys.* **10**.
Alexander, M. H. (1974). *J. Chem. Phys.* **61**, 5167.
Alexander, M. H., and Berard, E. V. (1974). *J. Chem. Phys.* **60**, 3950.
Arthurs, A. M., and Dalgarno, A. (1960). *Proc. Roy. Soc., Ser. A* **256**, 540.
Balint-Kurti, G. G. (1975). *In* "Advances in Molecular Beams" (K. P. Lawley, ed.) (to be published).
Bernstein, R. B. (1966). *Advan. Chem. Phys.* **10**, 75.
Brink, D. M., and Satchler, G. R. (1962). "Angular Momentum," pp. 19–25. Clarendon, Oxford, England.
Bunker, D. L. (1971). *Methods Comput. Phys.* **10**, 287.
Carrington, T., and Polanyi, J. (1972). *In* "MTP International Review of Science" (J. C. Polanyi, ed.), Vol. 9, p. 135. Univ. Park Press, Baltimore, Maryland.
Certain, P. R., and Bruch, L. W. (1972). *In* "MTP International Review of Science" (W. Byers Brown, ed.), Vol. 1, p. 113. Univ. Park Press, Baltimore, Maryland.
Cohen, J. S., and Pack, R. T. (1974). *J. Chem. Phys.* **61**, 2372.
Connor, J. N. L. (1973). *Annu. Rep. Chem. Soc.* **70A**, 5.

Curtiss, C. F. (1953). *J. Chem. Phys.* **21**, 2045.

Curtiss, C. F. (1968). *J. Chem. Phys.* **49**, 1952.

Curtiss, C. F., and Adler, F. T. (1952). *J. Chem. Phys.* **20**, 249.

Eastes, W., and Secrest, D. (1971). *Chem. Phys. Lett.* **9**, 508.

Eastes, W., and Secrest, D. (1972). *J. Chem. Phys.* **56**, 640.

Discuss. Faraday Soc. (1973). **55**.

George, T. F., and Ross, J. (1973). *Annu. Rev. Phys. Chem.* **24**, 263.

Gioumousis, G., and Curtiss, C. F. (1961). *J. Math. Phys.* **2**, 96.

Gordon, M. D., and Secrest, D. (1970). *J. Chem. Phys.* **52**, 120.

Gordon, R. G., and Kim, Y. S. (1972). *J. Chem. Phys.* **56**, 3122.

Gordon, R. G., Klemperer, W., and Steinfeld, J. I. (1968). *Annu. Rev. Phys. Chem.* **19**, 215.

Green, S. (1974). *J. Chem. Phys.* **60**, 2654.

Green, S. (1975). *J. Chem. Phys.* **62**, 2271.

Green, S., and Thaddeus, P. (1974). *Astrophys. J.* **191**, 653.

Green, S., and Thaddeus, P. (1975). (Private communication).

Green, S., Garrison, B. J., and Lester, W. A., Jr. (1975). "Hartree-Fock and Gordon-Kim Interaction Potentials for Scattering of Closed-Shell Molecules and Atoms: (H_2CO, He) and (H_2, Li^+)" (to be published).

Hunter, L. W., and Curtiss, C. F. (1973). *J. Chem. Phys.* **58**, 3884.

Jacob, M., and Wick, G. C. (1959). *Ann. Phys. (New York)* **7**, 404.

Kim, Y. S. (1973). Thesis, Harvard University (unpublished).

Kim, Y. S., and Gordon, R. G. (1974a). *J. Chem. Phys.* **60**, 1842.

Kim, Y. S., and Gordon, R. G. (1974b). *J. Chem. Phys.* **60**, 4323.

Kim, Y. S., and Gordon, R. G. (1974c). *J. Chem. Phys.* **60**, 4332.

Kim, Y. S., and Gordon, R. G. (1974d). *J. Chem. Phys.* **61**, 1.

Klar, H. (1973). *J. Phys. B* **6**, 2139.

Kolos, W., and Wolniewicz, L. (1964). *J. Chem. Phys.* **41**, 3663.

Kouri, D. (1973). *In* "The physics of Electronic and Atomic Collisions" (B. C. Cobic and M. V. Kurepa, eds.), p. 529, Buducnost, Zrenjanin, Belgrade.

Kouri, D., and McGuire, P. (1975). *Chem. Phys. Lett.* **29**, 414.

Kouri, D., and Wells, C. A. (1974). *J. Chem. Phys.* **60**, 2296.

Krauss, M. (1970). *Annu. Rev. Phys. Chem.* **21**, 39.

Krauss, M., and Mies, F. (1965). *J. Chem. Phys.* **42**, 2703.

Kutzelnigg, W., Staemmler, V., and Hoheisel, K. (1973). *Chem. Phys.* **1**, 27.

La Budde, R., and Bernstein, R. B. (1973). *J. Chem. Phys.* **59**, 3687.

Lawley, K. P., and Ross, J. (1965). *J. Chem. Phys.* **43**, 2930.

Lester, W. A., Jr. (1970). *J. Chem. Phys.* **53**, 1511.

Lester, W. A., Jr. (1971). *J. Chem. Phys.* **54**, 3171.

Lester, W. A., Jr. (1972). *J. Chem. Phys.* **57**, 3028.

Lester, W. A., Jr., and Bernstein, R. B. (1967). *Chem. Phys. Lett.* **1**, 207, 347.

Lester, W. A., Jr., and Schaefer, J. (1973). *J. Chem. Phys.* **59**, 3676.

Lester, W. A., Jr., and Schaefer, J. (1974). *J. Chem. Phys.* **60**, 1672.

Levine, R. D. (1972). *In* "MTP International Review of Science" (W. Byers Brown, ed.), Vol. 1, p. 229. Univ. Park Press, Baltimore, Maryland.

McGuire, P. (1973). *Chem. Phys. Lett.* **23**, 575.

McGuire, P. (1974). *Chem. Phys.* **4**, 29.

McGuire, P., and Kouri, D. J. (1974). *J. Chem. Phys.* **60**, 2488.

McGuire, P. (1975a). *J. Chem. Phys.* **62**, 525.

McGuire, P. (1975b). "Convergence of the Elastic and Inelastic Collision Cross Sections in the Coupled States and the Close-Coupling Methods" (to be published).

McGuire, P., and Micha, D. (1972). *Int. J. Quant. Chem., Symp.* No. 6, 111.

Marcus, R. A. (1973). *Discuss. Faraday Soc.* **55**, 9.

Miller, W. H. (1969). *J. Chem. Phys.* **50**, 407.

Miller, W. H. (1973). *In* "The Physics of Electronic and Atomic Collisions" (B. C. Cobic and M. V. Kurepa, eds.), p. 503. Buducnost, Zrenjanin, Belgrade.

Miller, W. H. (1974). *Advan. Chem. Phys.* **25**, 69.

Miller, W. H., and Raczkowski, A. W. (1974). *J. Chem. Phys.* **61**, 5413.

Pack, R. T. (1974). *J. Chem. Phys.* **60**, 633.

Rabitz, H. (1972). *J. Chem. Phys.* **57**, 1718.

Rae, A. I. M. (1973). *Chem. Phys. Lett.* **18**, 574.

Roberts, C. S. (1963). *Phys. Rev.* **131**, 203.

Schaefer, J., and Lester, W. A., Jr. (1973). *Chem. Phys. Lett.* **20**, 575.

Schaefer, J., and Lester, W. A., Jr. (1975). *J. Chem. Phys.* **62**, 1913.

Schaefer, J., Lester, W. A., Jr., Kouri, D., and Wells, C. A. (1974). *Chem. Phys. Lett.* **24**, 185.

Secrest, D. (1973). *Annu. Rev. Phys. Chem.* **24**, 379.

Secrest, D. (1974). *J. Chem. Phys.* **61**, 3867.

Shafer, R., and Gordon, R. G. (1973). *J. Chem. Phys.* **58**, 5422.

Takayanagi, K. (1973). *Comments At. Mol. Phys.* **4**, 59.

Taylor, A. J., and Gianturco, F. A. (1969). *Chem. Phys. Lett.* **4**, 376.

Toennies, J. P. (1973). *Discuss. Faraday Soc.* **55**, 129.

Toennies, J. P. (1974). *In* "Physical Chemistry, An Advanced Treatise, Kinetics of Gas Reactions," Vol. 6A, p. 227. Academic Press, New York.

Wolken, G., Jr., Miller, W. H., and Karplus, M. (1972). *J. Chem. Phys.* **56**, 4930.

Yarkony, D. R., O'Neil, S. V., Schaefer, H. F., III, Baskin, C. P., and Bender, C. F. (1974). *J. Chem. Phys.* **60**, 855.

Zarur, G., and Rabitz, H. (1973). *J. Chem. Phys.* **59**, 943.

Zarur, G., and Rabitz, H. (1974). *J. Chem. Phys.* **60**, 2057.

Theory of Low Energy Electron Scattering by Complex Atoms

R. K. NESBET

IBM Research Laboratory
San Jose, California

I. Introduction

This article is concerned with theoretical methods that have the promise of providing a quantitative description of electron scattering by atoms with more than one electron, in the low energy region where ionization is either energetically impossible or unimportant. The principal scattering processes are elastic scattering and excitation of discrete target atom states. Only neutral target atoms will be considered here.

The quantitative description of electron scattering by a complex atom presents a formidable challenge to theory. At short range, the incident electron essentially becomes part of a transient negative ion, requiring detailed treatment of electronic interactions. At long range, the incident

electron distorts the target atom, and responds to the perturbed potential due to this distortion. The target atom may undergo a transition between different states, leading to energy loss or gain by the incident electron.

The Born approximation is valid in the limits of high impact energy (keV) and small scattering angle. In this approximation, the elastic scattering cross section is determined by the static charge density of the target atom. In the low energy region considered here, scattering is strongly influenced by the mutually induced polarization of the target atom and incident electron. The polarization potential due to this interaction is the dominant long-range term in the interaction potential for an electron scattered by a spherically symmetrical but polarizable neutral target atom.

This polarization potential, attractive for induced dipole polarization, can combine with the centrifugal potential of the incident electron to form an effective potential well, enclosed by a finite barrier. States inside this barrier may be bound, producing a stable negative ion, or may lie above the asymptotic limit but below the top of the potential barrier. This latter situation leads to metastable states, or scattering resonances, which can trap an electron from the continuum. The lifetime or energy width of such resonances is a subject of considerable experimental and theoretical interest. Resonances are of special importance in the low energy region, since polarization potentials are strong enough to counteract the centrifugal potential barrier in low angular momentum states of the incident electron.

Typically, only a small number of incident electron angular momentum states (partial waves) contribute significantly to low energy electron scattering. This number increases with impact energy and with the strength of the dominant long-range interaction potential (static quadrupole or polarization potential). The methods to be considered here are all based on a partial wave representation of the electronic wavefunction. Independent calculations must be carried out for each distinct angular momentum component of the total electronic wavefunction. For this reason, these methods can be extended into the intermediate energy or high energy ranges only by introducing systematic approximations. These methods are inapplicable in principle above the ionization threshold, since the number of open channels becomes formally infinite.

A critical review of experimental measurements of total electron–atom scattering cross sections at low energies has recently been published by Bederson and Kieffer (1971). Experimental work on differential elastic cross sections has been reviewed by Andrick (1973).

Although there has been a great deal of theoretical work on electron scattering by atomic hydrogen, only a very small number of experimental studies have been carried out in the low energy range. The need for a high temperature oven or discharge excitation to dissociate H_2 into atoms precludes effective use of the most accurate experimental scattering techniques. According to Bederson and Kieffer, none of the available e–H cross section measurements has accuracy comparable to recent calculations.

Accurate experiments on electron scattering by rare gas atoms can be carried out in the low energy range. In the case of He, which will be considered in the present article, theory and experiment can both be carried to high accuracy. The current status of work on the e–He elastic scattering cross section at low energies is reviewed by Bederson and Kieffer. The cross sections for excitation of the $n = 2$ excited states of He (configurations 1s2s and 1s2p) are also of great current experimental interest. Excitation cross sections have considerable detailed structure as functions of either impact energy or scattering angle. This structure has been reproducibly resolved by recent experiments. The relevant theory and experimental results will be reviewed here. Recent theoretical computations of excitation cross sections in both high and low energy ranges have been reviewed by Rudge (1973). Much of the observed energy-dependent structure in e–He cross sections arises from resonances, which can be thought of as transient states of He^-. The present experimental and theoretical understanding of these transient states is reviewed by Schulz (1973), in a general study of electron–atom scattering resonances.

Because there is only one valence electron, electron scattering by alkali metal atoms can be treated in certain approximations by theoretical methods no more complicated than those applicable to atomic hydrogen. These atoms (with the exception of Li) can be produced in a stable vapor at reasonably low temperatures. The current state of experimental cross section measurements is reviewed by Bederson and Kieffer (1971), and the comparison of experiment and theory for elastic cross sections has been surveyed by Bederson (1970a,b). More recent theoretical calculations will be discussed here.

Despite their great importance as constituents of planetary and stellar atmospheres, the light open-shell atoms C, N, and O have received much less attention both from theory and experiment than the rare gas and alkali metal atoms. Because molecular dissociation is required, accurate low energy electron scattering experiments are difficult. The open valence shell structure precludes the application of simplified one-electron theory.

New developments of computational theory, which have recently made possible the quantitative study of electron scattering by these atoms, will be reviewed in the present article.

Early developments and applications of the theory of electron–atom scattering are reviewed by Mott and Massey (1965). A more recent review of the general subject has been given by Burke (1972). Brandsden (1970) and Geltman (1969) cover basic scattering theory relevant to electron–atom collisions. Newton (1966) gives a thorough treatment of formal scattering theory. Several review articles or monographs present the formalism and practical computational techniques of close-coupling theory, which has been applied extensively to electron–atom scattering (Burke, 1965, 1968; Burke and Seaton, 1971; Smith, 1971). Theory and applications of the polarized orbital method have recently been reviewed by Drachman and Temkin (1972). The matrix variational method, which is currently being developed as a general computational technique for electron–atom scattering, was reviewed by Harris and Michels (1971). A survey of earlier work on variational bounds in scattering theory is contained in a paper by Hahn and Spruch (1967). Theory and experimental results for resonances in electron–atom scattering have been reviewed by Schulz (1973) and by Taylor (1970). A collection of papers reviewing various computational methods relevant to low energy electron–atom scattering has recently been published (Van Regemorter, 1973).

Sections II and III of this article are concerned with the structure and interpretation of the electronic wavefunction appropriate to continuum states of the system consisting of an N-electron target atom and an external electron. Variational formalism appropriate for the construction and analysis of such wavefunctions is described in Section IV. A detailed discussion of the theory of resonances and threshold effects is given in Section V. A survey of theoretical methods relevant to low energy electron scattering is given in Section VI. Applications of these methods and comparison with experimental data for electron scattering by He, alkali metal atoms, O, N, and C are reviewed in Section VII.

II. Structure of the Wavefunction

Scattering of an electron by an N-electron atom can be described by a stationary state wavefunction of the form

$$\Psi = \sum_p \mathscr{A}\vartheta_p \psi_p + \sum_\mu \Phi_\mu c_\mu \,. \tag{1}$$

Here ϑ_p is a normalized N-electron wavefunction for the electronic stationary state of the target atom corresponding to open scattering channel p; ψ_p is the one-electron *open-channel orbital* wavefunction for a channel with angular momentum l_p and wavevector of magnitude k_p (kinetic energy $\frac{1}{2}k_p^2$ in Hartree atomic units); Φ_μ is one of an assumed orthonormal set of $N + 1$-electron Slater determinants. The quadratically integrable function

$$\Psi_H = \sum_\mu \Phi_\mu c_\mu \qquad (2)$$

is the *Hilbert space component* of Ψ. The functions ψ_p are not quadratically integrable. The operator $\mathscr{A}$ antisymmetrizes $\vartheta_p \psi_p$, and is assumed here to include the factor $(N + 1)^{-1/2}$ required to give this antisymmetrized function the same relative normalization as an $N + 1$-electron Slater determinant.

The wavefunction Ψ can be taken to be an eigenfunction of $\mathbf{L}^2$, $\mathbf{S}^2$, and of parity π. Then instead of simple Slater determinants, the Hilbert space wavefunction Ψ_H can be expanded in antisymmetrized LS-eigenfunctions. Since these in turn can be expressed as linear combinations of Slater determinants, the expansion indicated in Eq. (2) is completely general. The *a priori* construction of LS-eigenfunctions can be considered to be a matter of computational convenience. For these reasons, the discussion here will be based on the use of simple Slater determinants as a basis for the $N + 1$-electron Hilbert space. The wavefunction Ψ will have well-defined values of M_L, M_S, and parity, but in general can be a superposition of noninteracting LS-components.

The open-channel orbital wavefunctions are of the form

$$\psi_p = f_p(r) Y_{l_p m_{l_p}}(\theta, \phi) v_{m_{s_p}}, \qquad (3)$$

where f_p satisfies the usual bound state boundary condition at $r = 0$, is orthogonal (by construction) to all radial functions for Hilbert space orbitals (one-electron functions) with the same angular and spin quantum numbers, and has the asymptotic form

$$f_p(r) \sim k_p^{-1/2} r^{-1} \sin(k_p r - \tfrac{1}{2} l_p \pi + \delta_p) \qquad (4)$$

for scattering by a neutral atom in a state of definite parity. This functional form must be suitably modified for scattering by a Coulomb or dipole potential. For multichannel scattering f_p can be written in the form

$$f_p = \sum_{i=0, 1} F_{ip} \alpha_{ip}, \qquad (5)$$

where

$$F_{0p} = S_p \sim k_p^{-1/2} r^{-1} \sin(k_p r - \tfrac{1}{2} l_p \pi),$$

$$F_{1p} = C_p \sim k_p^{-1/2} r^{-1} \cos(k_p r - \tfrac{1}{2} l_p \pi). \tag{6}$$

These functions are required to satisfy the same boundary condition at $r = 0$ and the same orthogonality conditions as f_p. This ensures that the open-channel part of Ψ, given by the first term in Eq. (1), is orthogonal to the Hilbert space $\{\Phi_\mu\}$.

A target atom wavefunction ϑ_p can be expressed in the form

$$\vartheta_p = \sum_\sigma \Phi_\sigma c_\sigma^p \tag{7}$$

where each Φ_σ is a normalized N-electron Slater determinant. The coefficients c_σ^p can be obtained as a normalized eigenvector of the N-electron Hamiltonian matrix $H_{\sigma\sigma'}$, corresponding to energy eigenvalue E_p. If E is the total energy of the system, an open-channel k value is defined by

$$\tfrac{1}{2} k_p^2 = E - E_p, \tag{8}$$

for energies in Hartree atomic units, if $E - E_p$ is non negative. Target atom wavefunctions ϑ_p can be taken to be eigenfunctions of the N-electron operators $\mathbf{L}^2$, $\mathbf{S}^2$, and parity. This is ensured in a variational calculation if all Slater determinants from a given electronic configuration are always included together in the basis $\{\Phi_\sigma\}$ for the expansion of ϑ_p. As in the case of the $N + 1$-electron wavefunction Ψ, *a priori* construction of LS-eigenfunctions is a matter of computational convenience, not essential for the formal theory.

The Slater determinants Φ_μ in Eq. (2) can be defined in terms of virtual excitations of an N-electron reference determinant Φ_0, itself defined as an antisymmetrized product of N orthonormal *occupied* orbital functions $\phi_i, \phi_j, \dots$. Virtual excitations are defined by replacing some n specified occupied orbitals of Φ_0 by $n + 1$ one-electron functions drawn from a set of *unoccupied* orbitals $\phi_a, \phi_b, \dots$ that are mutually orthonormal and orthogonal to the occupied set. These orbitals are quadratically integrable functions of space and spin variables. An assumed countable complete set of normalizable orbitals $\{\phi_i; \phi_a\}$ generates a uniquely defined basis $\{\Phi_\mu\}$ for the $N + 1$-electron Hilbert space. A typical Slater determinant Φ_μ can be denoted by

$$\Phi_{ij\dots}^{abc\dots}, \qquad i < j < \dots \leqq N < a < b < c < \dots, \tag{9}$$

where the notation implies that $(\phi_a, \phi_b, \phi_c, \ldots)$ replace $(\phi_i, \phi_j, \ldots)$ in reference determinant Φ_0, in the order specified. Appropriate normalization of Φ_μ is implied. As examples of this notation,

$$\Phi^a = \det \phi_1(1) \cdots \phi_i(i) \cdots \phi_N(N)\phi_a(N + 1),$$

$$\Phi_i^{ab} = \det \phi_i(1) \cdots \phi_a(i) \cdots \phi_N(N)\phi_b(N + 1), \tag{10}$$

The notation *det* implies antisymmetrization and normalization appropriate to the number of electrons.

Obviously an oscillatory function of nonvanishing asymptotic amplitude cannot be represented as a superposition of the Hilbert space orbitals $\{\phi_i; \phi_a\}$. The part of Ψ containing the open-channel orbitals ψ_p remains distinct from the Hilbert space component, as indicated in Eq. (1), for any calculation using a finite set of Hilbert space orbitals.

In *close-coupling* theory, part of Ψ_H is represented in the form

$$\sum_\gamma \mathcal{A} \vartheta_\gamma \psi_\gamma, \tag{11}$$

analogous to the open-channel part of Eq. (1), except that the functions ϑ_γ represent target states with E_γ greater than E, corresponding to *closed channels*. The closed-channel orbital functions ψ_γ are quadratically integrable. The coupled functions $\mathcal{A}\vartheta_\gamma\psi_\gamma$ can be represented as in Eq. (1) as linear combinations of the Hilbert space Slater determinants Φ_μ.

The target atom functions ϑ_γ need not correspond to specific stationary states, although they should be orthogonal to the open-channel states $\{\vartheta_p\}$. In close-coupling theory polarization effects are represented by using *pseudostates* $\vartheta_{\gamma(p)}$ that correspond to the first-order perturbation of ϑ_p by a polarizing field. In the *polarized orbital* method, the closed-channel orbital $\psi_\gamma(N + 1)$ to be combined with a pseudostate $\vartheta_{\gamma(p)}$ is replaced by a function $\chi_{(i)}\psi_p$, where $\chi(i, N + 1)$ describes the modulation of ψ_p due to induced polarization of the target atom. The antisymmetrized function

$$\mathcal{A} \sum_i \vartheta_{\gamma(p)}\chi_{(i)}\psi_p \tag{12}$$

is part of Ψ_H because $\chi\psi_p$ is quadratically integrable.

Equation (1) can be expressed in the form

$$\Psi = \sum_i \sum_p (\vartheta_{ip} + \sum_\mu \Phi_\mu c_\mu^{ip})\alpha_{ip}, \tag{13}$$

with

$$\vartheta_{ip} = \sum_\sigma \Phi_\sigma^{ip} c_\sigma^p, \tag{14}$$

where the coefficients c_σ^p are the target state eigenvector coefficients of Eq. (7), and the coefficients α_{ip}, with $i = 0, 1$, are defined in terms of the asymptotic open-channel orbitals by Eq. (5). The functions Φ_σ^{ip} are un-normalized (not quadratically integrable) $N + 1$-electron Slater determinants

$$\Phi_\sigma^{ip} = \mathscr{A}\Phi_\sigma F_{ip},\qquad(15)$$

defined in terms of the functions S_p, C_p of Eq. (6).

In the *matrix variational* method, the coefficients c_μ^{ip} of Eq. (13) are obtained separately for each set of indices i, p from the matrix equations

$$\left(\Phi_\mu \mid H - E \mid \vartheta_{jq} + \sum_\nu \Phi_\nu c_\nu^{jq}\right) = 0,\qquad \text{all}\qquad \mu, j, q.\qquad(16)$$

Index q here refers to open channels only, and H is the $N + 1$-electron Hamiltonian operator. These equations follow from the variational condition

$$\partial\Xi/\partial c_\mu^{ip*} = 0,\qquad \text{all}\qquad \mu, i, p, \alpha_{jq},\qquad(17)$$

where the variational functional is

$$\Xi = (\Psi \mid H - E \mid \Psi).\qquad(18)$$

When Eq. (16) is satisfied, the variational functional becomes an explicit quadratic function of the coefficients α_{ip}:

$$\Xi = \sum_{ip}\sum_{jq} \alpha_{ip}^* m_{ij}^{pq} \alpha_{jq},\qquad(19)$$

where, in consequence of Eq. (16),

$$m_{ij}^{pq} = M_{ij}^{pq} - \sum_\mu\sum_\nu M_{ip,\,\mu}(M^{-1})_{\mu\nu} M_{\nu,\,jq}.\qquad(20)$$

The matrices combined in Eq. (20) are the *bound–bound matrix* (Hermitian)

$$M_{\mu\nu} = (\Phi_\mu \mid H - E \mid \Phi_\nu);\qquad(21)$$

the *bound–free matrix*

$$M_{\mu,\,ip} = (\Phi_\mu \mid H - E \mid \vartheta_{ip});\qquad(22)$$

and the *free–free matrix* (nonHermitian)

$$M_{ij}^{pq} = (\vartheta_{ip} \mid H - E \mid \vartheta_{jq}).\qquad(23)$$

If Ψ is an exact solution of the Schrödinger equation,

$$(H - E)\Psi = 0,$$

the coefficients α must satisfy the matrix equations

$$\sum_{jq} m_{ij}^{pq}\alpha_{jq} = 0, \qquad \text{all} \qquad i, p. \tag{24}$$

For N_C open channels, these equations have N_C linearly independent solutions, each defined by a column vector α_{jq} with $2N_C$ components. Since the asymptotic wavefunction is specified through Eqs. (5) and (6) entirely by the coefficients α, these coefficients determine physical scattering cross sections.

It is convenient to use a matrix notation in which open-channel indices p, q are suppressed but matrices and vectors are segmented according to the indices $i, j = 0, 1$. In this notation the matrix generalization of Eq. (19) is

$$\Xi = \alpha^\dagger m\alpha$$

$$= \alpha_0^\dagger(m_{00}\alpha_0 + m_{01}\alpha_1) + \alpha_1^\dagger(m_{10}\alpha_0 + m_{11}\alpha_1), \tag{25}$$

and Eqs. (24), for an exact scattering solution, are

$$m\alpha = \begin{pmatrix} m_{00} & m_{01} \\ m_{10} & m_{11} \end{pmatrix}\begin{pmatrix} \alpha_0 \\ \alpha_1 \end{pmatrix} = 0. \tag{26}$$

Here α denotes the $2N_C \times N_C$ rectangular matrix consisting of N_C linearly independent column vector solutions of Eqs. (26). The symbol ($\dagger$) denotes an Hermitian adjoint, or transpose of a real matrix.

In general, for approximate wavefunctions, the homogeneous system of Eqs. (26) has no nontrivial solutions. Variational methods are used to obtain an approximate solution matrix α in the matrix variational method. Equations (5) and (6) can be used to define the matrix α in terms of the asymptotic open-channel orbital solutions of the coupled integro-differential equations solved in the close-coupling method.

The reactance matrix K is defined by a matrix solution of Eqs. (26) in the form (Mott and Massey, 1965)

$$\alpha_0 = I, \qquad \alpha_1 = K, \tag{27}$$

where I is the $N_C \times N_C$ unit matrix. An arbitrary solution matrix α can be reduced to this form by multiplying on the right by α_0^{-1}, if α_0 is not singular.

Then, in general,

$$K = \alpha_1 \alpha_0^{-1}. \tag{28}$$

Alternatively, if α_1 is not singular,

$$K^{-1} = \alpha_0 \alpha_1^{-1}. \tag{29}$$

For exact scattering solutions the matrix K is real and symmetric. It can be diagonalized by an orthogonal transformation that constructs "eigen-channels" as linear combinations of the physical open channels. The eigenvalues of K are tangents of the "eigenphases" corresponding to these eigenchannels. Matrix functions of K are most easily computed by applying the inverse orthogonal transformation defined by the eigenchannel vectors to the diagonal matrix defined by the required function of the eigenphases.

The scattering and transition matrices (Mott and Massey, 1965) can be expressed in terms of the reactance matrix by

$$S = (I + iK)(I - iK)^{-1},$$
$$T = S - I = 2iK(I - iK)^{-1}, \tag{30}$$

respectively. The partial cross section for scattering from channel p to channel q is, in units a_0^2,

$$Q_{pq} = (\pi/k_p^2)\,|\,T_{pq}\,|^2$$
$$= (4\pi/k_p^2)\,|\,[K(I - iK)^{-1}]_{pq}\,|^2. \tag{31}$$

In terms of eigenchannels, indexed by α, this is

$$Q_{pq} = (4\pi/k_p^2)\left|\sum_\alpha x_{p\alpha} x_{q\alpha} e^{i\delta_\alpha} \sin \delta_\alpha\right|^2, \tag{32}$$

where δ_α is an eigenphase and $x_{p\alpha}$ is a component of a normalized eigenchannel column eigenvector.

In the case of electron scattering by a complex atom, initial and final states of the collision process are in general multiply degenerate. The total cross section for random polarization of electron beam and target atom is obtained by summing Q_{pq} over degenerate final states and averaging over initial states. This is equivalent to a properly weighted sum over all states of the $N + 1$-electron system that connect given initial and final target states. Since the T-matrix is diagonal in the total quantum numbers $(LS\pi)$ and independent of total M_L and M_S, this sum is over $(LS\pi)$ only.

If target atom quantum numbers are denoted by $(LS\pi)_\gamma$, the total cross section for the transition $\gamma \to \gamma'$ is

$$Q_{\gamma\gamma'} = \frac{\pi}{k_\gamma^2} \sum_{L, S, \pi} \frac{(2L + 1)(2S + 1)}{2(2L_\gamma + 1)(2S_\gamma + 1)} \sum_{l, l'} | T_{\gamma'l', \gamma l}^{LS\pi} |^2, \tag{33}$$

where l, l' are orbital angular momentum quantum numbers of the incident and scattered electron, respectively. They assume all values that can couple with the target atom quantum numbers to give total quantum numbers $(LS\pi)$. In Eq. (33), the factor $(2L + 1)(2S + 1)$ arises from summation of equal values of $| T |^2$ over degenerate substates of the total angular momenta. The factor $2(2L_\gamma + 1)(2S_\gamma + 1)$ in the denominator is the degeneracy of the initial state γ, including spin degeneracy of the incident electron. This is the weight factor required in averaging over initial state degeneracy.

Equation (33) is a special case of general formulas for total cross sections in the theory of collisions of systems with internal angular momenta (Blatt and Biedenharn, 1952; Jacob and Wick, 1959). These references give formulas for differential cross sections (cross section as a function of scattering angle) and for cross sections relevant to experiments that select angular momentum sublevels (polarized electrons, polarized target, or recoil atom).

The differential cross section for scattering from state $\gamma\mu$ (where μ denotes M_L, M_S, m_s) to state $\gamma'\mu'$, for electron deflection angles (θ, ϕ), is

$$d\sigma_{\gamma'\mu', \gamma\mu}/d\Omega = | (\gamma'\mu' | f(\theta, \phi) | \gamma\mu) |^2, \tag{34}$$

where (Blatt and Biedenharm, 1952, Eq. (3.14))

$$(\gamma'\mu' | f | \gamma\mu) = \sum_{LS} \sum_{ll'} [(2l' + 1)(2l + 1)]^{1/2} i^{l - l'} d_{m'0}^{l'}(\theta) e^{im'\phi}$$
$$\times (T_{\gamma'l', \gamma l}^{LS}/2ik_\gamma)$$
$$\times (L_{\gamma'} M_{L\gamma'} l'm' | LM_L)(L_\gamma M_{L\gamma} l0 | LM_L)$$
$$\times (S_{\gamma'} M_{S\gamma'} \tfrac{1}{2}m_s' | SM_S)(S_\gamma M_{S\gamma} \tfrac{1}{2}m_s | SM_S),$$
$$d_{m'0}^{l'}(\theta) e^{im'\phi} = (4\pi/2l' + 1)^{1/2} Y_{l'm'}(\theta\phi),$$

and

$$M_L = M_{L\gamma} = M_{L\gamma'} + m', \qquad M_S = M_{S\gamma} + m_s = M_{S\gamma'} + m_s'.$$

The total differential cross section for the process $\gamma \rightarrow \gamma'$ is

$$\frac{d\sigma}{d\Omega} = \frac{1}{2(2L_\gamma + 1)(2S_\gamma + 1)} \sum_{\mu'} \sum_\mu |(\gamma'\mu' | f | \gamma\mu)|^2. \qquad (35)$$

Specialized derivations of cross section formulas for electron–atom scattering are given in several references (Percival and Seaton, 1957; Burke and Schey, 1962b). Miller (1969) and Klar (1969, 1971) have applied the helicity representation formalism of Jacob and Wick (1959) to differential cross sections for atom–molecule and molecular collisions. In the helicity representation, final state angular momenta are quantized about the direction ($\theta\phi$) of the scattered electron, while initial state angular momenta are quantized about the incident direction (00), defined by the z-axis. In Eq. (34), both initial and final states are quantized about the fixed z-axis.

Explicit formulas for the sums appearing in Eq. (35), expressed in compact form in terms of angular momentum recoupling coefficients (6-j symbols or Racah coefficients) are given by Blatt and Biedenharn (1952). When contributions of a large number of partial waves must be combined, it may be more efficient to compute the amplitudes $(\gamma'\mu' | f | \gamma\mu)$ of Eq. (35), or the corresponding helicity amplitudes given by Miller (1969), than to use the summed cross section formulas of Blatt and Biedenharn.

III. Interpretation of the Wavefunction

The Hilbert space component of Ψ, given by Eq. (2), can be expressed in terms of the operator Q for projection onto the Hilbert space $\{\Phi_\mu\}$, such that

$$\Psi_H = Q\Psi = \Psi_Q = \sum_\mu \Phi_\mu(\Phi_\mu | \Psi). \qquad (36)$$

If a projection operator P is defined as the orthogonal complement of Q, such that

$$\Psi = \Psi_P + \Psi_Q,$$

then the Schrödinger equation can be partitioned as

$$M_{PP}\Psi_P + M_{PQ}\Psi_Q = 0$$
$$M_{QP}\Psi_P + M_{QQ}\Psi_Q = 0 \qquad (37)$$

in an obvious notation, where M denotes $H - E$. If the second equation is solved for Ψ_Q, and the result substituted into the first equation, an effective equation for Ψ_P is derived in the form

$$M'_{PP}\Psi_P = 0, \tag{38}$$

where

$$M'_{PP} = M_{PP} - M_{PQ}(M_{QQ})^{-1}M_{QP}. \tag{39}$$

This partitioning technique is used in the resonance theory of Feshbach (1958, 1962). The operator $(M_{QQ})^{-1}$ here is a linear integral operator in the coordinates of $N + 1$ electrons, defined by the kernel

$$\sum_\mu \sum_\nu \Phi_\mu (H - E)_{\mu\nu}^{-1}\Phi_\nu^*, \tag{40}$$

in terms of the inverse of the bound–bound matrix $H_{\mu\nu} - E\delta_{\mu\nu}$.

Effective one-electron equations can be derived by taking components of the wavefunction Ψ_P and effective Hamiltonian H'_{PP} with respect to the target atom states ϑ_p, and with respect to spin and angular momentum factors of the open-channel orbitals ψ_p. When suitable normalizing factors are included

$$(\vartheta_p \,|\, \Psi_P) = \psi_p, \tag{41}$$

from Eq. (1). The matrix operator acting on open-channel orbitals is

$$m^{pq} = (\vartheta_p \,|\, M'_{PP} \,|\, \mathscr{A}\vartheta_q). \tag{42}$$

Orbitals with different angular or spin quantum numbers are assumed here to correspond to different values of the open-channel index (p, q).

The modified Hamiltonian operator m^{pq} acts on open-channel orbitals ψ_p that are constrained to be orthogonal to the orbital Hilbert space $\{\phi_i; \phi_a\}$. As this Hilbert space becomes complete, only two linearly independent functions are required for each open scattering channel, since the asymptotic scattering equation has only two linearly independent solutions. These functions are represented by the functions S_p, C_p of Eq. (6). The matrix elements m_{ij}^{pq} defined by Eq. (20) are matrix elements of m with respect to these functions.

The terms in Eqs. (20) and (39) arising from $(M_{QQ})^{-1}$ define a matrix *optical potential* that acts on the open-channel orbital wavefunctions. In its full form this is an energy-dependent integral operator. Detailed analysis shows that in the limit of large radial coordinate r this operator is equivalent to a "polarization potential" of the form $-\alpha/2r^4$ for the terms

arising from dipole virtual excitations. The parameter α is the electric dipole polarizability of the target atom. In general, virtual excitations of the target atom of multipole index l produce a multipole polarization potential of the asymptotic form $-\alpha_l/2r^{2l+2}$, where α_l is a generalized multipole polarizability.

For a neutral atom in a spherically symmetrical state (S-state), the dipole polarization potential is the term of longest range in the scattering potential. This term dominates low-energy scattering behavior. The polarization potential can be derived most directly by writing the wavefunction in the form used in close-coupling theory,

$$\Psi = \sum_p \mathscr{A}\vartheta_p \psi_p + \sum_\gamma \mathscr{A}\vartheta_\gamma \psi_\gamma, \qquad (43)$$

where the functions $(\vartheta_p; \vartheta_\gamma)$ represent, in principle, a complete set of target atom eigenfunctions. Here index p is used for open channels and index γ for closed channels.

In practice, only a few functions ϑ_γ are included in close-coupling calculations. Polarizability is taken into account by introducing pseudostate functions ϑ_γ that represent the first-order polarization corrections to open-channel functions ϑ_p (Damburg and Karule, 1967; Damburg and Geltman, 1968; Burke *et al.*, 1969b; Geltman and Burke, 1970). Integrodifferential equations for both open-channel orbitals ψ_p and closed-channel orbitals ψ_γ are obtained with the matrix Hamiltonian operator given as in Eq. (42) by taking components of the Schrödinger equation with respect to all functions $(\vartheta_p; \vartheta_\gamma)$. These coupled equations are solved for both open- and closed-channel orbitals (Burke and Seaton, 1971; Smith, 1971).

When expanded in spherical polar coordinates of two electrons, the Coulomb interaction potential $1/r_{12}$ depends on the radial coordinates through a factor

$$r_<^\lambda/r_>^{\lambda+1}, \qquad (44)$$

multiplying spherical harmonics of degree λ in the angular variables. Here $r_<$ is the lesser of r_1, r_2 and $r_>$ is the greater. For a neutral target atom, terms with $\lambda = 0$ from the electronic Coulomb interaction cancel against the Coulomb potential of the nucleus. If the atom is in a nonspherical state ($L > 0$), diagonal matrix elements of the electronic Coulomb interaction occur for even λ such that $0 < \lambda \leqq 2L$. From Eq. (44), this produces static external multipole potential terms proportional to $1/r^{\lambda+1}$. When L is not zero, the dominant term is the electric quadrupole potential, proportional to r^{-3}.

Off-diagonal matrix elements of spherical harmonic λ connect a target atom open-channel state of given L to pseudostates with

$$L' = |L - \lambda|, \; |L - \lambda| + 2, \ldots, L + \lambda. \tag{45}$$

Such matrix elements in the close-coupling equations produce an effective asymptotic off-diagonal potential proportional to $1/r^{\lambda+1}$, connecting the external closed-channel and open-channel orbitals. By the transformation of these equations symbolized in Eq. (39), this off-diagonal matrix element contributes quadratically to an effective polarization potential in the open channel, asymptotically proportional to $1/r^{2\lambda+2}$. When $\lambda = 1$, this effective potential is the electric dipole polarization potential. The argument given here can be made more precise by considering the explicit asymptotic expansion of the close-coupling equations (Burke and Schey, 1962a).

For a one-electron target atom or ion, the target wavefunctions are known, and pseudostates appropriate to a given multipole polarization are obtained in closed form as solutions of a first-order perturbation equation. The perturbing field is taken to be a static multipole field. Use of such pseudostates neglects both the velocity of the scattered electron and the effect of its penetration within the charge cloud of the target atom. The penetration effect can be taken into account more fully by use of the polarized orbital method (Temkin, 1957; Temkin and Lamkin, 1961; Drachman and Temkin, 1972). In this method, the first-order perturbation of the target wavefunction is computed as a function of the radial coordinate of an incident electron. If this electron is completely external to the target atom, the perturbation is of the form (omitting vector-coupling coefficients)

$$\vartheta_{\gamma(p)} Y_L(\theta, \phi) r^{-L-1}, \tag{46}$$

where $\vartheta_{\gamma(p)}$ is the pseudostate appropriate to perturbation of target state ϑ_p by a multipole field of order L, and $Y_L(\theta, \phi)$ is a spherical harmonic. The asymptotic effect of this perturbation is to approximate the external closed-channel orbital ψ_γ by

$$Y_L(\theta, \phi) r^{-L-1} \psi_p(r, \theta, \phi). \tag{47}$$

Analysis of the close-coupling equations shows that this is the correct asymptotic functional form (Burke and Schey, 1962a; Damburg and Karule, 1967), and that it leads to the correct asymptotic multipole polarization potential.

In the polarized orbital method, if the external electron penetrates the

charge cloud of the target atom, the interchange of internal and external radial coordinates indicated in Eq. (44) changes the functional form of Eq. (46). This implies that the closed-channel wavefunction cannot be expressed as a single separable function, the form assumed in the close-coupling expansion when a single pseudostate is used to represent a given multipole polarizability of the target atom. This amounts to a short range modification of the effective polarization potential.

In deriving an effective equation for the open-channel orbital ψ_p in the polarized orbital method, terms occur that arise from the action of the open-channel orbital kinetic energy operator on the perturbed target wavefunction, since the latter is a function of the open-channel radial coordinate. These terms give an effective "distortion potential." Taken together, the polarization and distortion potentials define an "extended polarization potential" whose use in the case of electron–helium scattering gives a computed elastic cross section in good agreement with experiment (Callaway *et al.*, 1968). The distortion potential greatly reduces the magnitude of the net effective potential from that given by the polarization potential alone. Because the distortion potential for electric dipole interactions vanishes as r^{-6} at large r, it does not alter the asymptotic r^{-4} polarization potential.

The effect of the velocity of the incident electron appears both explicitly in the energy denominators of the generalized optical potential operator of Eq. (39) and implicitly in the dependence of matrix elements on the wavenumber parameter k. In general, as k increases, matrix elements between quadratically integrable orbitals and an oscillatory function of kr tend to zero, because of the cancellation of equal but opposite contributions to matrix element integrands from each full period of the oscillatory function. Matrix elements of the bound–free operator M_{QP} of Eq. (39) are of this kind, but they do not vanish in the limit of large k because of the special form of the external closed-channel orbitals ψ_γ, indicated in Eq. (47). Because ψ_γ contains the radial part of the corresponding open-channel orbital ψ_p as an explicit asymptotic factor, radial integrals contain factors $\sin^2(kr + \delta)$, which average over a wavelength to $\frac{1}{2}$ rather than to zero. The fact that only oscillatory integrands of this form fail to integrate to zero is the essential reason for the occurrence of ψ_p as a factor in the asymptotic form of an external closed-channel orbital that describes a virtual excitation or polarization of ψ_p.

From the analysis given above, the principal energy dependence of the generalized optical potential is expected to arise from the energy denominators $(H - E)^{-1}$. Since the coupled equations solved in the close-

coupling method are of the same structure as Eqs. (37), this energy dependence is properly incorporated in the close-coupling formalism. In contrast, the polarizability, computed in the static limit in the polarized orbital method, would have to be generalized to a frequency or energy dependent polarizability in order to represent the energy dependence of the optical potential.

The physical significance of individual Slater determinants Φ_μ in the Hilbert space component of the total wavefunction can be understood in terms of the discussion given above. For elastic scattering, if the target atom ground state is approximated by a single Hartree–Fock Slater determinant Φ_0, the determinants Φ^a of Eq. (10) contribute only to the interacting inner part of the open-channel orbital ψ_p. As indicated in Eqs. (10), each Φ^a is constructed by antisymmetrizing a normalizable orbital ϕ_a into the unmodified target atom Φ_0. Obviously, a calculation with Hilbert space component restricted to expansion in the basis $\{\Phi^a\}$ corresponds to the *static exchange* approximation, with no virtual excitations of the target and no polarization potential.

A Slater determinant Φ_i^{ab} of Eqs. (10) represents a one-electron virtual excitation (a/i) of the target atom, coupled to an additional quadratically integrable orbital ϕ_b. This is exactly the structure of the closed-channel functions $\mathscr{A}\vartheta_\gamma\psi_\gamma$ in the close-coupling expansion of Ψ, Eq. (43). Multipole polarizabilities of a closed-shell target state are described by a first-order perturbed wavefunction that can be expressed as a linear combination of one-electron virtual excitations (a/i). A closed-channel pseudostate ϑ_γ represents such a perturbed wavefunction. With this interpretation, the additional orbital ϕ_b in Φ_i^{ab} represents an external closed-channel orbital, or a basis function for the linear expansion of such an orbital.

In the formalism of the polarized orbital method, closed-channel terms in Ψ cannot be expressed in the separable form assumed in Eq. (43). The general form of the Hilbert space component of Ψ, in Eqs. (1) or (2), takes this failure of separability into account, by allowing for a linear combination of determinants Φ_i^{ab}. The coefficients in this expansion are directly energy-dependent through the solution of Eqs. (14), and indirectly through the dependence of matrix elements on k.

If the target atom state belongs to an open-shell configuration, virtual excitations must be considered in terms of configurations rather than of individual orbitals. Then Φ_0 is replaced by a linear space of Slater determinants spanning those configurations used to represent the target state, and each virtually excited determinant such as Φ^a or Φ_i^{ab} is accompanied

by other determinants of the same configuration. The specific linear combinations of Slater determinants that occur in the theory are symmetry-adapted LS-eigenfunctions for $N + 1$ electrons.

From the analysis given here, it is clear that for a single configuration target state the physical effects of a generalized multipole polarization potential can be described by a wavefunction constructed from Slater determinants of the form Φ^a and Φ_i^{ab}, or from the corresponding configurations. Assuming a Hartree–Fock target state (single configuration), the functions $\{\Phi^a\}$ give the static-exchange expansion of an open-channel orbital for elastic scattering, and the functions $\{\Phi_i^{ab}\}$ describe the coupling of a multipole polarization or virtual excitation of the target atom to a virtual excitation of the incident electron, represented by an external closed-channel orbital. When the representation of the target state is extended, either to describe additional target states for other open scattering channels, or to include target atom correlation effects, the Hilbert space of the scattering problem must be suitably augmented.

IV. Variational Formalism

The principal theoretical methods relevant to low-energy electron scattering rely on variational principles. Variational theory appropriate to representation of the electronic wavefunction in the form of Eq. (1) will be presented here. Direct computational application of this formalism is referred to here as the *matrix variational method*. Since it has been shown in the preceding sections how the widely applied close-coupling and polarized orbital methods can be described by Eq. (1), the general variational argument to be given also applies to these methods, with some modifications of detail.

In Section III, it was shown that the effects of the Hilbert space component of the $N + 1$-electron scattering wavefunction Ψ can be condensed into an effective matrix operator m^{pq}, defined by Eq. (42), which acts only on open-channel orbitals. This operator contains a generalized matrix optical potential as a nonlocal potential operator, whose asymptotic form is that of a sum of multipole polarization potentials. The open-channel orbitals ψ_p are orthogonal (by constraint or projection) to all orbitals used to construct the Hilbert space component Ψ_H of Ψ. Acting on such orbitals, the operator m^{pq} gives generalized close-coupling equations

$$\sum_q m^{pq}\psi_q = 0. \tag{48}$$

In the limit of completeness of the Hilbert space, Eqs. (24) of the matrix variational method, symbolized in matrix notation by Eqs. (26), become equivalent to these close-coupling equations. The corresponding matrix notation for Eq. (48) is

$$m\psi = 0. \tag{49}$$

The variational functional defined by Eq. (19) becomes

$$\Xi = \psi^\dagger m\psi \tag{50}$$

in matrix notation or explicitly

$$\Xi_{\sigma\tau} = \sum_p \sum_q \int \psi^\dagger_{\sigma p} m^{pq} \psi_{q\tau} \, d\tau, \tag{51}$$

where for N_C open channels $\psi_{q\tau}$ is the component in channel q of the independent solution indexed by τ. Both indices have N_C values.

An infinitesimal variation of ψ induces a variation of Ξ of the form

$$\delta\Xi = \delta\psi^\dagger m\psi + (m\psi)^\dagger \, \delta\psi + \psi^\dagger(m - m^\dagger) \, \delta\psi. \tag{52}$$

The last term here is a formal notation for a surface integral, to be evaluated in the limit of large radial coordinate r. Its value can be found from the corresponding equation of the matrix variational method, Eq. (25),

$$\delta\Xi = \delta\alpha^\dagger m\alpha + (m\alpha)^\dagger \, \delta\alpha + \alpha^\dagger(m - m^\dagger) \, \delta\alpha. \tag{53}$$

This can be put in a more useful form by observing that the nonHermitian part of the free–free matrix, Eq. (23), is given by

$$M^{pq}_{ij} - M^{qp}_{ji} = \tfrac{1}{2}\delta_{pq}(\delta_{i0}\delta_{j1} - \delta_{i1}\delta_{j0}). \tag{54}$$

This formula expresses the surface integral resulting from the action of the kinetic energy operator in H on open channel orbitals with asymptotic form specified by Eqs. (6). Since the other terms in Eq. (20) are Hermitian, the same formula holds for m^{pq}_{ij}. In matrix notation this is

$$m_{01} - m^\dagger_{10} = \tfrac{1}{2}I. \tag{55}$$

When substituted into Eq. (53) this gives

$$\delta\Xi = \delta\alpha^\dagger m\alpha + (m\alpha)^\dagger \, \delta\alpha + \tfrac{1}{2}(\alpha^\dagger_0 \, \delta\alpha_1 - \alpha^\dagger_1 \, \delta\alpha_0). \tag{56}$$

Since the asymptotic form of ψ is completely defined by the matrices α_0 and α_1, the final terms in Eqs. (52) and (56) are identical, and Eq. (52) becomes

$$\delta\Xi = \delta\psi^\dagger m\psi + (m\psi)^\dagger \, \delta\psi + \tfrac{1}{2}(\alpha^\dagger_0 \, \delta\alpha_1 - \alpha^\dagger_1 \, \delta\alpha_0). \tag{57}$$

Equations (56) and (57) lead to various multichannel forms of the variational principle originally derived by Kohn (1948). If the reactance matrix K is defined as in Eqs. (27), and the matrix elements of K are treated as variational parameters, then

$$\delta\alpha_0 = 0, \qquad \delta\alpha_1 = \delta K. \tag{58}$$

From Eqs. (25) and (56), in the matrix variational formalism,

$$\delta\Xi = \delta K^\dagger(m_{10} + m_{11}K) + (m_{10} + m_{11}K)^\dagger\, \delta K + \tfrac{1}{2}\,\delta K, \tag{59}$$

or from Eq. (57), in the close-coupling formalism,

$$\delta\Xi = \delta\psi^\dagger m\psi + (m\psi)^\dagger\, \delta\psi + \tfrac{1}{2}\,\delta K. \tag{60}$$

In the Kohn method, this equation is used in the form

$$\delta[K] = \delta(K - 2\Xi) = -2(\delta\psi^\dagger m\psi + (m\psi)^\dagger\, \delta\psi) = 0 \tag{61}$$

if and only if the open-channel wavefunction satisfies Eq. (49). Thus

$$[K] = K_t - 2\Xi_t, \tag{62}$$

the Kohn variational estimate of the reactance matrix, is stationary under variations of a trial wavefunction ψ_t about an exact solution of the scattering equations.

In the variational analysis of Kato (1951), the second-order terms are retained in Eq. (61) to give

$$\delta[K] = -2(\delta\psi^\dagger m\psi + (m\psi)^\dagger\, \delta\psi) - 2\,\delta\psi^\dagger m\, \delta\psi. \tag{63}$$

If m is positive definite, the second-order error in $[K]$ for variations about an exact scattering solution is a negative-definite matrix. This result is the basis for theories of variational bounds for eigenphase shifts or for elements of the K-matrix (Hahn et al., 1962, 1963, 1964a,b; Sugar and Blankenbecler, 1964; Gailitis, 1964; Hahn and Spruch, 1967). Such theories are most useful in the close-coupling method, when Eqs. (49) are solved exactly, but m is approximated by a truncated closed-channel expansion. When exact target atom wavefunctions are used in the close-coupling expansion, these theories establish lower bounds to phase shifts or upper bounds to elements of K^{-1}, the inverse of the reaction matrix (Hahn and Spruch, 1967). Since exact target wavefunctions are available only for hydrogen, these theories cannot be applied rigorously to the subject of the present article—electron scattering by complex atoms. Hahn (1971) has formulated a "quasi-minimum" variational principle which relaxes the rigorous bound argument in order to allow variational

approximation to the solutions of the open-channel equations. In practice, it is found that computed K-matrix elements or phase shifts show stationary behavior as functions of variational parameters when the overall scattering wavefunction is of sufficient accuracy to make Eq. (63) valid for the residual error in K.

In the matrix variational formalism, Eq. (59) shows that $[K]$ is stationary for variations about a trial matrix K_t chosen so that

$$m_{10} + m_{11} K_t = 0 \tag{64}$$

or

$$K_t = -m_{11}^{-1} m_{10}. \tag{65}$$

Substitution of this expression for K_t into Eq. (25), the definition of Ξ, with Eq. (55) used to express m_{01} in terms of $m_{10}^\dagger$, gives the Kohn formula

$$[K] = -2(m_{00} - m_{10}^\dagger m_{11}^{-1} m_{10}). \tag{66}$$

Since m_{00} and m_{11} are symmetric (real) matrices, this is obviously a real symmetric matrix. Anomalous singularities of $[K]$ are inherent in this formula, occurring at singular points of the matrix m_{11} as a function of E or k or of other parameters in the variational wavefunction (Nesbet, 1968, 1969a).

Analogous formulas ("inverse Kohn") for the matrix K^{-1} are given by the equations

$$\alpha_0 = K^{-1}, \qquad \alpha_1 = I \tag{67}$$

$$\delta\Xi = \delta K^{-1\dagger}(m_{00} K^{-1} + m_{01}) + (m_{00} K^{-1} + m_{01})^\dagger \delta K^{-1} - \tfrac{1}{2}\delta K^{-1} \tag{68}$$

$$m_{00} K_t^{-1} + m_{01} = 0 \tag{69}$$

$$K_t^{-1} = -m_{00}^{-1} m_{01} \tag{70}$$

$$[K^{-1}] = K_t^{-1} + 2\Xi_t = 2(m_{11} - m_{01}^\dagger m_{00}^{-1} m_{01}). \tag{71}$$

In the inverse Kohn case, anomalous singularities occur at singular points of the matrix m_{00} (Nesbet, 1968, 1969a).

The anomalous singularities in the Kohn formula were first considered by Schwartz (1961a,b), who encountered these anomalies in variational calculations of electron–hydrogen scattering. The s-wave phase shift obtained by Schwartz, after empirically smoothing the variationally computed numbers, still stands as the most accurate work available. The anomalies were originally attributed to the effect of eigenvalues of the

bound–bound matrix, causing singularities in the effective optical potential through zeroes of the energy denominator in Eq. (40). More detailed analysis (Nesbet, 1968, 1969a) shows that these zeroes exactly cancel out of the Kohn and inverse Kohn formulas. The observed anomalies arise instead from the singular points of m_{00} or m_{11}, as stated above. This fact is of great practical importance, since singularities of the optical potential would be common to all variational methods, whereas in practice the singular points of matrices m_{00} and m_{11} do not coincide. Hence anomalies can be avoided by a suitable choice of variational formalism.

The *anomaly-free* (AF) multichannel variational method (Nesbet, 1969a) uses the ratio of determinants

$$|\det m_{00}/\det m_{11}| \tag{72}$$

as a criterion: if this ratio is less than unity the Kohn formula should be used to compute $[K]$; if this ratio is greater than unity, the inverse Kohn formula should be used to compute $[K^{-1}]$. This simple procedure leads to discontinuities of results as functions of total energy or of k. These discontinuities disappear as the Hilbert space becomes complete, but they make the AF method unsatisfactory for extrapolation to completeness or for interpolation or analytic continuation of K-matrix elements as functions of E or k.

Since the homogeneous matrix equations for α, Eq. (26), in general have no nontrivial solutions, Harris and Michels (1969a) have proposed that a trial matrix α_t should be determined by minimizing the norm of these equations. With the normalization conditions used here, this *minimum-norm* method would obtain α_t by minimizing the trace of the quadratic form

$$(m\alpha)^\dagger m\alpha = \alpha^\dagger m^\dagger m\alpha. \tag{73}$$

Then α_t is the $2N_C \times N_C$ matrix of those column eigenvectors of $m^\dagger m$ that correspond to the N_C smallest eigenvalues. Since $m^\dagger m$ is a real symmetric, positive definite matrix, these eigenvalues are nonnegative real numbers and the eigenvectors are orthonormal real vectors. A trial matrix K_t is obtained from α_t in the form

$$K_t = \alpha_{t1}\alpha_{t0}^{-1}, \tag{74}$$

and this estimate is used in the Kohn formula, Eq. (62). Alternatively, a trial matrix

$$K_t^{-1} = \alpha_{t0}\alpha_{t1}^{-1} \tag{75}$$

can be used in the inverse Kohn formula, Eq. (71).

The minimum-norm method does not provide a unique prescription for refining the trial matrix α_t. In fact, use of the Kohn formula with K_t defined by Eq. (74) is not really justified, since $[K]$ is stationary with respect to variations of K_t only if K_t is given by Eq. (65), so that Eq. (64) is satisfied. In general Eqs. (65) and (74) are not compatible. A similar remark holds for use of the inverse Kohn formula, with K_t^{-1} given by Eq. (75).

Defining a trial matrix α_t by minimizing the norm of $m\alpha$, which must vanish for an exact scattering solution, is an intuitively reasonable procedure. The problem that remains is to define a stationary matrix $[\alpha]$ that is equal to α_t in the limit of an exact solution. A matrix with these properties is defined in the *optimized minimum-norm* (OMN) method (Nesbet and Oberoi, 1972) by introducing an additional approximation that itself becomes exact in the limit of exact scattering solutions. Consider an arbitrary unitary transformation of the $2N_C$-dimensional linear space of the asymptotic wavefunctions for open channels. Such a transformation is of the form

$$u = (\alpha\beta), \tag{76}$$

where α and β are both $2N_C \times N_C$ matrices, each representing N_C orthonormal column vectors. The orthonormality conditions are

$$\alpha^\dagger\alpha = \beta^\dagger\beta = I; \alpha^\dagger\beta = \beta^\dagger\alpha = 0. \tag{77}$$

The transformed matrix m is

$$m' = u^\dagger m u = \begin{pmatrix} m'_{00} & m'_{01} \\ m'_{10} & m'_{11} \end{pmatrix} = \begin{pmatrix} \alpha^\dagger m\alpha & \alpha^\dagger m\beta \\ \beta^\dagger m\alpha & \beta^\dagger m\beta \end{pmatrix}. \tag{78}$$

In the minimum-norm method, α and β consist of column eigenvectors corresponding, respectively, to the N_C least and greatest eigenvalues of $m^\dagger m$. Since m is not symmetrical, these eigenvectors do not diagonalize m and $m^\dagger$ separately. Hence m'_{00} and m'_{11} are not diagonal and cannot in general be assumed to be symmetric. Equation (55) is not true in general for the transformed matrices. If it were true, the Kohn formula, Eq. (66), would define a stationary matrix $[K']$ in terms of the transformed matrices m'_{ij}.

In the limit of an exact scattering solution, the matrix defined by Eq. (74) becomes the exact reactance matrix, which is real and symmetric. In the OMN method, the symmetric part of this matrix is used to define an orthogonal transformation of the asymptotic open channels that *does*

preserve Eq. (55). Then a stationary matrix $[\alpha]$ is constructed with the use of Eq. (66) for a matrix $[K']$ such that

$$[\alpha] = \alpha + \beta[K'].\tag{79}$$

The crucial step in this method is to approximate Eq. (74) by a real symmetric matrix

$$K_t = \tan \Delta = \tfrac{1}{2}[\alpha_{t1}\alpha_{t0}^{-1} + (\alpha_{t1}\alpha_{t0}^{-1})^\dagger].\tag{80}$$

The transformation matrix of Eq. (76) is replaced by

$$u = \begin{pmatrix} \cos \Delta & -\sin \Delta \\ \sin \Delta & \cos \Delta \end{pmatrix},\tag{81}$$

where $\cos \Delta$ and $\sin \Delta$ are real symmetric matrices defined as matrix functions of $\tan \Delta$. Obviously u is an orthogonal matrix, but of a specialized form, since the submatrices are such that

$$(\cos \Delta)^2 + (\sin \Delta)^2 = I,\tag{82}$$

$$\cos \Delta \sin \Delta = \sin \Delta \cos \Delta.\tag{83}$$

Because of these properties, the transformed matrices m'_{00} and m'_{11} are real and symmetric, and Eq. (55) is preserved in the form,

$$m'_{01} - m'_{10}{}^\dagger = \tfrac{1}{2}I.\tag{84}$$

Because this equation is valid for the transformed matrix m', the Kohn variational formula can be used to give stationary matrices

$$[K'] = -2(m'_{00} - m'_{10}{}^\dagger(m'_{11})^{-1}m_{10})\tag{85}$$

$$[\alpha] = \begin{pmatrix} \cos \Delta - (\sin \Delta)[K'] \\ \sin \Delta + (\cos \Delta)[K'] \end{pmatrix},\tag{86}$$

from Eqs. (72) and (85). The general definition of the reactance matrix as $\alpha_1 \alpha_0^{-1}$ implies that

$$[K] = (\sin \Delta + \cos \Delta[K'])(\cos \Delta - \sin \Delta[K'])^{-1}\tag{87}$$

in this case. These equations define the OMN method.

   The OMN method is an extension of earlier work by Seaton (1966), who considered a preliminary transformation of open scattering channels in the specialized form given here by Eq. (81). Equation (87) is given by Seaton. In the calculations of Saraph *et al.* (1969) on electron–ion scattering, this preliminary transformation of open channels takes the form of a

distorted-wave approximation, defining a background phase shift in each physical open channel but not mixing different channels.

In the minimum-norm method the transformation u is constructed so that $\alpha^\dagger m^\dagger m\alpha$ has minimum eigenvalues and $\beta^\dagger m^\dagger m\beta$ has maximum eigenvalues. This might be expected generally to imply that $|m'_{00}|$ is smaller than $|m'_{11}|$, which would justify use of the Kohn formula for $[K']$ rather than the inverse Kohn formula. In practice this is not always true. Model calculations with this method show that m'_{11} can be singular, introducing spurious anomalies. As in the Kohn method without a preliminary transformation, a choice of formula could be made using $|m'_{00}|/|m'_{11}|$ as a criterion, but this would give discontinuous results as E or parameters vary.

These difficulties with the OMN method have led to consideration of general unitary transformations of the unsymmetric matrix m, in the *optimized anomaly-free* (OAF) method (Nesbet and Oberoi, 1972). An unsymmetric real matrix can be transformed to real upper triangular form by an orthogonal transformation unless it has complex eigenvalues. In the latter case, a unitary transformation is required. Hence complex column vector matrices α and β can be found such that

$$m'_{10} = \beta^\dagger m\alpha = 0. \tag{88}$$

In general, the transformation for which m'_{10} vanishes does not preserve $m_{01} - m^\dagger_{10}$, but the variational formalism can nevertheless be generalized to give a method based on Eq. (88). This method is anomaly-free because the term containing $(m'_{11})^{-1}$ in Eq. (85) is absent when m'_{10} vanishes.

Given complex matrices α, β that define a preliminary unitary transformation of m, the effective reactance matrix $\delta K'$ in the transformed linear space gives the infinitesimal variation of α as $\beta\,\delta K'$, from Eq. (79), or

$$\delta\alpha_0 = \beta_0\,\delta K', \qquad \delta\alpha_1 = \beta_1\,\delta K'. \tag{89}$$

The variational functional is

$$\Xi = \alpha^\dagger m\alpha = m'_{00} \tag{90}$$

and the variation of Ξ is

$$\delta\Xi = \delta K'^\dagger m'_{10} + m'_{10}{}^\dagger\,\delta K' + (m'_{01} - m'_{10}{}^\dagger)\,\delta K', \tag{91}$$

since $K'_t = 0$. If Eq. (88) is satisfied by matrices α, β, this implies

$$\delta(K' - (m'_{01})^{-1}\Xi) = \delta(K' - (m'_{01})^{-1}m'_{00}) = 0. \tag{92}$$

Since K'_t is zero, a stationary matrix that reduces to K' for an exact scattering solution is

$$[K'] = -(m'_{01})^{-1} m'_{00} . \qquad (93)$$

This determines a stationary matrix $[\alpha]$ from Eq. (79) and the reactance matrix is

$$[K] = (\alpha_1 + \beta_1[K'])(\alpha_0 + \beta_0[K'])^{-1}. \qquad (94)$$

The matrices α, β are to be constructed so that they transform m to upper triangular form, subject to the condition that the residual diagonal elements of m'_{00} should all be smaller in magnitude than those of m'_{11}. This condition ensures that the column vectors α are correct in the limit of exact scattering solutions, when all elements of m'_{00} would vanish. This procedure, using Eqs. (93) and (94), defines the OAF method.

The matrix $[K]$ in the OAF method is not symmetric except in the limit of exact solutions. The symmetric part of this matrix is used to define a real symmetric K-matrix.

Results of model calculations using the various multichannel variational methods described here indicate that the OAF method converges somewhat more rapidly to exact results than do any of the other methods (Nesbet and Oberoi, 1972).

V. Resonances and Threshold Effects

Much of the energy-dependent structure observed in low energy electron scattering is due to resonances and threshold effects. The latter occur at the threshold for excitation of each successive target atom stationary state, since distinct electronic continua arise from each energetically accessible target state.

A *resonance* occurs as a rapid increase through π radians of a partial wave phase shift δ_l in a small energy interval of magnitude $2\Gamma_r$, where Γ_r is the *width* of the resonance. In multichannel scattering, all coupled open scattering channels experience this rapid variation in the same energy interval. The sum of eigenphases increases through π radians. This causes a rapid variation of elastic and inelastic cross sections. Reviews of theory and experimental data have been given recently by Burke (1968), Taylor (1970), and Schulz (1973).

The physical origin of scattering resonances is the occurrence of a metastable state that interacts weakly with an adjacent continuum, implying a finite lifetime in a time-dependent formalism. The simplest example

of such a resonance is provided by a one-dimensional potential well enclosed by a barrier of finite height. For a particle in the potential well, stationary states defined for infinite barrier height interact with the continuum of states outside the barrier as its height is reduced, and become metastable. Resonances of this kind are known as *shape resonances*. The resonant energy E_r is approximated by the unperturbed metastable energy level, and the width Γ_r (inversely proportional to the lifetime) is determined by the matrix element of the Hamiltonian operator connecting this unperturbed state with the adjacent continuum.

In electron–atom scattering, excited states of the target atom are degenerate with the kinetic energy continuum of an external electron incident on the target atom in any lower stationary state. An attractive interaction between the excited target state and an external electron can lead to a metastable compound state with energy below the excitation threshold. Because the adjacent scattering continuum arises from lower states of the target atom, the interaction matrix elements are small, and Γ_r is relatively small. Such narrow resonances immediately below an excitation threshold are referred to as *closed channel* resonances (Burke, 1968) or as core-excited resonances of type 1 (CE1) (Taylor, 1970).

If the external electron has orbital angular momentum greater than zero, an effective rotational barrier can cause a compound state to be metastable even though it lies above the corresponding excitation threshold of the target atom. Because the adjacent scattering continuum contains states arising from the same excited target state, interaction matrix elements are greater than in the case of CE1 resonances, and the resonance width is greater. Such resonances, analogous to shape resonances, are referred to as core-excited resonances of type 2 (CE2) (Taylor, 1970).

For a single open channel, an isolated resonance can be parametrized by the phase shift formula

$$\delta(E) = \delta_0(E) + \tan^{-1}[\tfrac{1}{2}\Gamma_r/(E_r - E)], \qquad (95)$$

where $\delta_0(E)$, the background or potential scattering phase shift, is a slowly varying function of E near E_r. This Breit–Wigner formula for an isolated resonance follows from the general resonance theory of Feshbach (1958, 1962). Since the partial wave contribution to the total scattering cross section is proportional to $\sin^2 \delta$, the relative modification of the background partial cross section due to a resonance is given by

$$\sigma_r/\sigma_0 = \sin^2(\delta_0 + \delta_r)/\sin^2 \delta_0, \qquad (96)$$

where δ_r is the last term of Eq. (95). If $\delta_0(E)$ is taken to be constant over

the width of the resonance, Eq. (96) gives the resonant lineshape formula (Fano, 1961; Fano and Cooper, 1965)

$$\sigma_r/\sigma_0 = (\varepsilon + q)^2/(1 + \varepsilon^2), \tag{97}$$

where

$$\varepsilon = -\cot \delta_r = (E - E_r)/\tfrac{1}{2}\Gamma_r,$$

$$q = -\cot \delta_0. \tag{98}$$

Equation (97) gives a characteristically unsymmetrical lineshape that goes to zero when $\varepsilon = -q$. This leads to sharp resonance peaks in electron transmission experiments. The observed structure must be fitted to Eq. (97) to obtain the three independent parameters E_r, Γ_r, and δ_0 or q.

A derivation of Eq. (95) relevant to electron–atom scattering, using the Feshbach formalism, has been given by O'Malley and Geltman (1965). The essential idea of the Feshbach theory is that a resonance can be characterized by an eigenstate of the Hilbert-space Hamiltonian H_{QQ} defined by partitioning, as in Eq. (37) here. A background scattering problem can be defined by solving the continuum Schrödinger equation subject to the constraint of orthogonality of the continuum wavefunction to the selected eigenfunction of H_{QQ}. Then Eq. (95) follows from consideration of the perturbing effect of this eigenfunction on the background continuum state.

The simplest possible application of this formalism is to the case of a shape resonance in scattering by a one-dimensional potential function, assumed to consist of a potential well inside a finite barrier. H_{QQ} is defined by the matrix representation of the one-dimensional Hamiltonian

$$H = -\frac{1}{2}\frac{d^2}{dr^2} + V(r), \tag{99}$$

in a finite basis of quadratically integrable functions. An eigenvector of this matrix defines a quadratically integrable function ϕ_α corresponding to the matrix eigenvalue

$$E_\alpha = (\alpha \,|\, H \,|\, \alpha). \tag{100}$$

The background continuum wavefunction w_0 is obtained by solving the Schrödinger equation, at an arbitrary energy $E = \tfrac{1}{2}k^2$ in the scattering continuum, subject to the constraint of orthogonality to ϕ_α. Then w_0 satisfies the integro-differential equation

$$(H - E)w_0 - \phi_\alpha(\alpha \,|\, H - E \,|\, w_0) = 0. \tag{101}$$

It is convenient to define an irregular solution w_1 of the same equation. The asymptotic normalization

$$w_0 \sim k^{-1/2} \sin(kr + \delta_0)$$

$$w_1 \sim k^{-1/2} \cos(kr + \delta_0) \tag{102}$$

is chosen so that the Wronskian $w_0' w_1 - w_1' w_0$ is unity.

A regular solution of the full Schrödinger equation can be expressed in the form

$$\psi = u + \phi_\alpha c_\alpha \tag{103}$$

where u is orthogonal to ϕ_α and

$$(H - E)u - \phi_\alpha(\alpha \mid H - E \mid u) = -(H - E_\alpha)\phi_\alpha c_\alpha. \tag{104}$$

This equation has the formal solution

$$u = w_0 + 2[G(H - E_\alpha)\phi_\alpha - \phi_\alpha(\alpha \mid G(H - E_\alpha) \mid \alpha)]c_\alpha, \tag{105}$$

where the one-dimensional Green's function operator is

$$G = -w_0 \int_r^\infty w_1 \, dr' - w_1 \int_0^r w_0 \, dr'. \tag{106}$$

The coefficient c_α is determined by the condition

$$(\alpha \mid H - E \mid \psi) = 0 \tag{107}$$

or

$$c_\alpha = (E - E_\alpha)^{-1}(\alpha \mid H - E \mid u) = (E - E_\alpha)^{-1}(\alpha \mid H \mid u). \tag{108}$$

From Eqs. (102), (105), (106), and (108) the asymptotic value of the coefficient of w_1 in $u(r)$ is

$$\tan \delta_r = -2(w_0 \mid H \mid \alpha)(E - E_\alpha)^{-1}(\alpha \mid H \mid u). \tag{109}$$

From Eq. (105),

$$(\alpha \mid H \mid u) = (\alpha \mid H \mid w_0) + 2(\alpha \mid (H - E_\alpha)G(H - E_\alpha) \mid \alpha)c_\alpha. \tag{110}$$

If c_α is taken from Eq. (108), this can be solved for

$$(\alpha \mid H \mid u) = (E - E_\alpha)(\alpha \mid H \mid w_0)/E - E_\alpha - \Delta_\alpha \tag{111}$$

where

$$\Delta_\alpha = 2(\alpha \mid (H - E_\alpha)G(H - E_\alpha) \mid \alpha). \tag{112}$$

When Eq. (111) is substituted into Eq. (109),

$$\tan \delta_r = -\tfrac{1}{2}\Gamma_r/(E - E_r) \tag{113}$$

with

$$\tfrac{1}{2}\Gamma_r = 2\,|\,(w_0\,|\,H\,|\,\alpha)\,|^2, \tag{114}$$

$$E_r = E_\alpha + \Delta_\alpha. \tag{115}$$

The asymptotic form of $\psi(r)$ or $u(r)$, since ϕ_α is quadratically integrable, is

$$\psi \sim u \sim k^{-1/2}[\sin(kr + \delta_0) + \cos(kr + \delta_0)\tan \delta_r]$$

$$= \frac{k^{-1/2}}{\cos \delta_r}\sin(kr + \delta_0 + \delta_r). \tag{116}$$

Equation (113) gives δ_r in the form assumed in Eq. (95).

The asymptotic behavior of the continuum wavefunction affects any inelastic process involving transitions into the continuum, such as photodetachment of an electron from a bound negative ion. Fano (1961) and O'Malley and Geltman (1965) show that this leads to intensity variations described by the Fano formula, Eq. (97).

Equation (114) can be recognized as a form of the quantum mechanical "golden rule"

$$\Gamma = 2\pi\rho\,|\,(f\,|\,H\,|\,i)\,|^2 \tag{117}$$

for transitions into continuum states. The initial state (i) is normalized to unity and the final continuum state (f) is normalized so that the energy density of states is given by ρ, equal to $2/\pi$ in atomic units for the normalization implied by Eqs. (102). Miller (1966, 1970), who emphasizes this relationship to continuum perturbation theory, shows that Γ_r can be computed in the limit of completeness of the Hilbert space basis for ϕ_α in the range of the interaction potential, without explicit solution of the background scattering problem. If Eq. (114) is written in the form

$$\Gamma_r = 4\,|\,(w_0\,|\,H - E_\alpha\,|\,\alpha)\,|^2, \tag{118}$$

it is clear that the functional form of w_0 is irrelevant in the range of completeness of the Hilbert space basis, since $(H - E_\alpha)\phi_\alpha$ effectively vanishes in this range. Hence if this completeness range extends over the full range of the interaction potential, w_0 can be replaced by its asymptotic form given by the first of Eqs. (102), for the purpose of evaluating Γ_r. This form depends only on the background phase shift δ_0.

The problem of obtaining the correct value of δ_0 for use in Miller's golden-rule formula has been considered by Hazi and Fels (1971), in the context of the *stabilization method* for resonance calculations (Taylor, 1970; Hazi and Taylor, 1970; Fels and Hazi, 1971, 1972). This method provides a great deal of insight into practical implications of the general theory of resonances. It is applied to several very illuminating model problems in the references cited.

In the stabilization method, bound state methods are used to compute a quadratically integrable wavefunction ϕ_α, whose energy mean value E_α lies in the scattering continuum. In general, such a state, defined by an eigenvector of the Hamiltonian matrix in a finite Hilbert space basis, is not associated with a resonance. Such an association is established only if the eigenvalue E_α is insensitive to augmentation of the Hilbert space basis, and if ϕ_α continues to represent essentially the same function as the basis is augmented. The number of eigenvalues *below* E_α increases without limit, so ϕ_α must be identified by its persistent or *stabilized* character (Taylor, 1970). In electron–atom scattering, resonances are usually associated with well-defined configurations and quantum states of the negative ion.

A stabilized energy eigenvalue E_α cannot itself be identified as the resonance energy E_r, because the energy shift Δ_α, Eq. (112), depends on the residual interaction with the continuum. If two or more stabilized states associated with the same resonance are available, perhaps corresponding to different basis expansions, Hazi and Fels (1971) show that the resonance parameters $(E_r, \delta_0, \Gamma_r)$ can be obtained from ϕ_α and the bound–free matrix elements

$$M_{\alpha S} = (\alpha \,|\, H - E_\alpha \,|\, S_\alpha)$$
$$M_{\alpha C} = (\alpha \,|\, H - E_\alpha \,|\, C_\alpha), \tag{119}$$

where the oscillatory functions S_α and C_α are defined as in Eqs. (6). Since E_α is an eigenvalue of the bound–bound matrix, Eqs. (16) of the matrix variational method have finite solutions at E_α only if

$$M_{\alpha S} + M_{\alpha C} \tan \delta_\alpha = 0. \tag{120}$$

This condition is used to determine the phase shift δ_α, at eigenvalues E_α, in the single channel variational method of Harris (1967). Then if E_α is associated with a resonance at E_r, Eq. (95) gives

$$\delta_\alpha = -\tan^{-1}(M_{\alpha S}/M_{\alpha C}) = \delta_0 + \tan^{-1}[\tfrac{1}{2}\Gamma_r/(E_r - E_\alpha)]. \tag{121}$$

When w_0 is replaced by its asymptotic form (Miller, 1970), in terms of S_α and C_α, Eq. (114) becomes

$$\Gamma_r = 4 \cos^2\delta_0(M_{\alpha S} + M_{\alpha C} \tan \delta_0)^2. \tag{122}$$

Both Γ_r and δ_0 are determined by the intersection of graphs $\Gamma_r(\delta_0)$ of Eq. (122), for two or more stabilized states α. Hazi and Fels (1971) give a model example in which three such curves intersect at a common point. Given Γ_r and δ_0, E_r is determined by Eq. (121). An extension of these ideas to multichannel resonances has been given by Fels and Hazi (1972). Positions and widths of autoionization states in He and H$^-$ have been computed by this method (Bhatia, 1974).

Multiconfiguration bound state methods have been used for calculations of autoionizing states (Holøien, 1958a,b, 1961; Holøien and Midtdal, 1970, 1971), and there have been many applications of the Feshbach formalism, using explicit projection operators. Most applications have been to autoionizing states rather than to negative ion resonances associated with electron–neutral scattering, the subject of the present article.

In multichannel scattering, a resonance affecting n coupled channels is described by the n solutions $\delta_j(E)$ of the equation (Macek, 1970)

$$E - E_r = \tfrac{1}{2}\Gamma_r \sum_{i=1}^{n} y_i^2 \cot[\delta_{0i}(E) - \delta_j(E)]. \tag{123}$$

It follows from this equation that the eigenphases are continuous and that their sum increases by π radians in passing through the resonance. The coefficients y_i^2, whose sum is unity, determine partial widths with respect to the asymptotic eigenchannels. Typical behavior of eigenphases for a narrow resonance is shown in Fig. 1, from calculations by Oberoi and Nesbet (1973b) on e–He inelastic scattering below the $n = 3$ threshold. Each curve $\delta_j(E)$ increases monotonically with energy, and connects an initial asymptotic eigenchannel with that next above it in order of increasing δ_{0i}. Since the eigenphases are obtained by diagonalizing a matrix for each value of E, a noncrossing rule holds.

It is found in detailed calculations of multichannel resonances, for a narrow resonance unperturbed by other structure, that the sum of eigenphases $\sum_j \delta_j(E)$ can be fitted with high accuracy to the single-channel formula, Eq. (95). The detailed structure of the curves $\delta_j(E)$, shown in Fig. 1, is due primarily to avoided crossings among the eigenphases. The multichannel resonance can be described as a resonance in any one of the background eigenchannels (δ_i^0 increasing by π radians), perturbed by the other eigenchannels through the effect of the noncrossing rule.
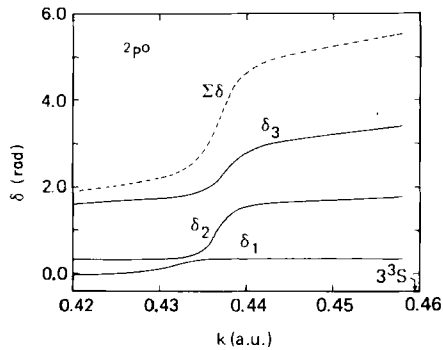
Fig. 1. e–He. ^{2}P^o eigenphases and their sum in the vicinity of a Feshbach resonance. k is defined relative to the 2 ^{3}S threshold.

The original eigenchannel can be traced through the resonance by the approximate continuity of the eigenchannel vector, jumping from one branch of $\delta_j(E)$ to another at the avoided crossing. Macek (1970) shows that the extent of the gap at any crossing point is proportional to the partial width $y_i \Gamma^{1/2}$, where index i denotes the asymptotic eigenchannel associated with the crossing point.

In close-coupling calculations (Burke, 1968) a resonance is found essentially as it would be observed experimentally, by scanning a range of incident energy E or wavevector k for the characteristic resonant behavior of a phase shift. In the case of a typically narrow closed-channel resonance this may require a search with very small increments of k. Once a resonance is located on a sufficiently small scale of k increments, the resonance parameters are obtained by a least-squares fit to Eq. (95) or to Eq. (123) for multichannel resonances.

In the matrix variational method, an automatic resonance search procedure (Nesbet and Lyons, 1971) is used to locate single or multichannel resonances and to compute accurate values of the resonance parameters. Since a bound–bound matrix is constructed, its eigenvalues can be used to locate possible resonances, as in the stabilization method. The modified Cholesky algorithm (Nesbet, 1971), used for triangular decomposition of the bound–bound matrix $(H-E)_{\mu\nu}$, provides an index that counts the negative eigenvalues of this matrix. This fact is used to bracket an eigenvalue, which is then located more precisely by interpolating to a common pole of the elements and determinant of the matrix m_{ij}^{pq} defined by Eq. (20). Residues at this eigenvalue pole define an effective resonant channel (as a linear combination of the open channels), and provide

values of bound–free matrix elements for this effective channel that can be used to estimate the location of the nearest zeroes of the tangent and cotangent of the sum of eigenphases. The energy separation between these two points, where the eigenphase sum differs by $\pi/2$, is a useful estimate of the resonance width Γ_r. With this information, a rapidly convergent iteration, using a three-point formula to fit the sum of eigenphases to Eq. (95), is used to locate the resonance position E_r or k_r. If there is no relatively narrow resonance in the eigenchannels associated with a given bound–bound eigenvalue, the resonance search is found to diverge rapidly, and is terminated by testing the extrapolated interval Δk against an upper limit.

Examples of calculations with this resonance search procedure (Nesbet and Lyons, 1971) are illustrated in Figs. 2–4. Figure 2 shows the $^1S^e$ phase shift for e–H elastic scattering computed over the indicated
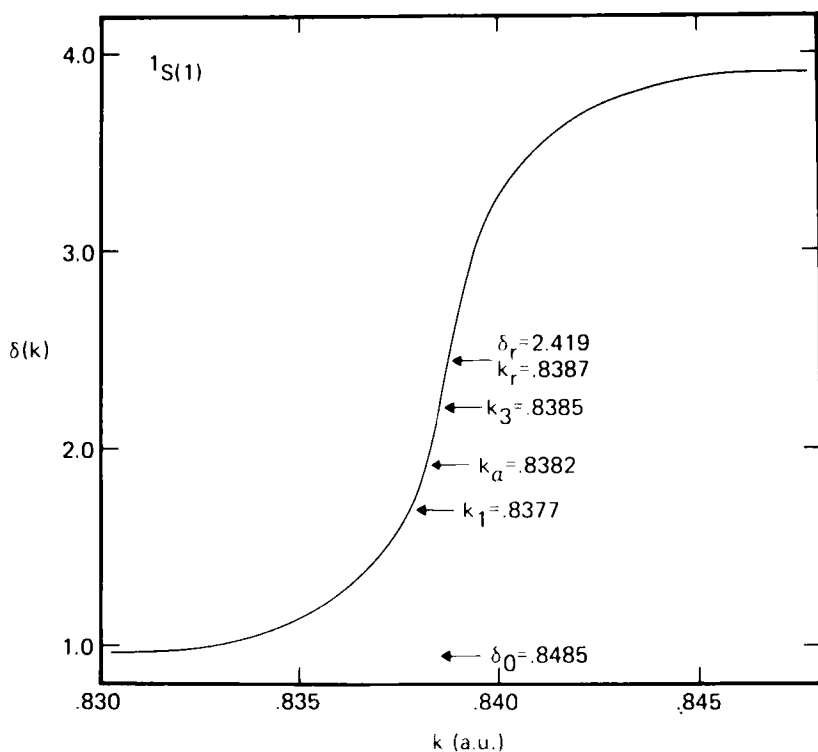
Fig. 2. e–H. Phase shift for ^1S (1) resonance.
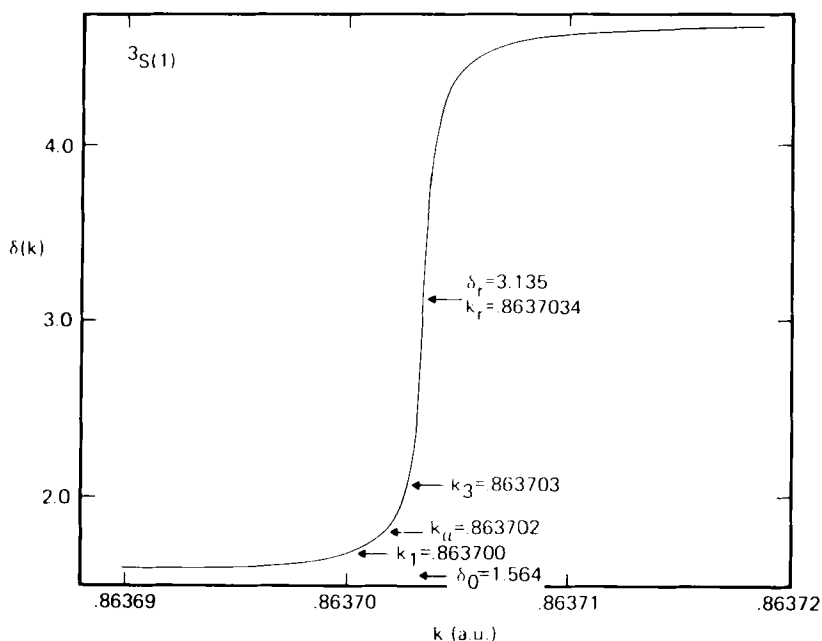
Fig. 3. e–H. Phase shift for ^{3}S (1) resonance.

range. The resonance search, which proceeds without prior knowledge of the resonance curve shown, first locates eigenvalue E_α, corresponding to k_α, then computes k_1 and k_3 as estimates of the neighboring zeroes of $\tan \delta$ and $\cot \delta$. After several iterations, narrowing to a scale not visible on the graph, the resonance is located at k_r, with phase shift $\delta_r(k_r)$ as shown. The background phase shift is $\delta_r(k_r) - (\pi/2)$. The full phase shift curve shown in Fig. 2, computed independently of the resonance search, shows that the computed resonance parameters agree with those appropriate to the full resonance curve. The computed Γ_r is 4.918×10^{-2} eV.

Figure 3 shows the lowest ^{3}S^e resonance for e–H scattering, much narrower than the singlet resonance of the previous figure. Parameters obtained by the resonance search are shown together with the full resonance curve obtained by separate calculations. The computed width is 1.949×10^{-5} eV.

Similar results for a multichannel resonance are shown in Fig. 4. This represents an approximate calculation, used only to illustrate the method, of a ^{3}S^e resonance below the $n = 3$ threshold in hydrogen. The open channel $(2pkp)^3$S has been omitted, to simplify the calculations. This
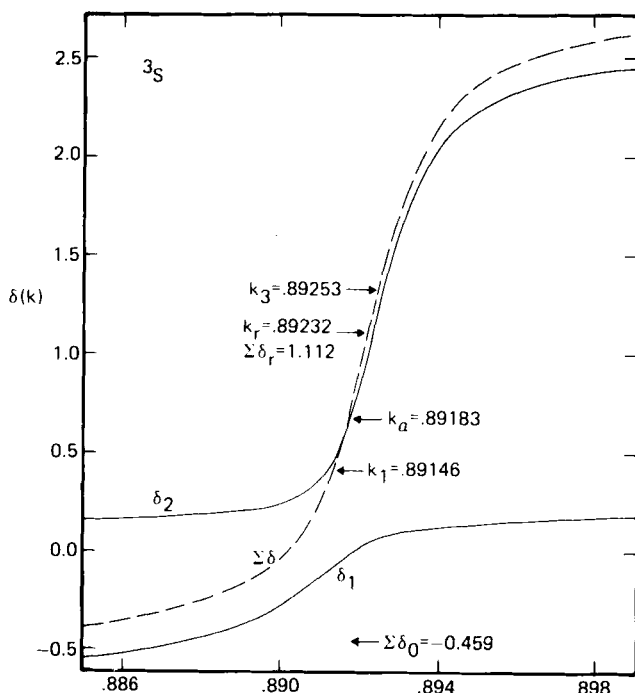
Fig. 4. e–H. Eigenphase shift for ^{3}S resonance.

calculation shows that the search procedure using the sum of eigenphases gives qualitatively correct results.

The formal mathematical theory of scattering can be very helpful in interpreting structural features of collision cross sections. Geltman (1969) applies this theory to resonance and threshold effects, including the effects of the long range potentials typical of electron–atom scattering. McVoy (1967) has reviewed this subject, as developed in the theory of nuclear resonances, with many illustrative examples from model calculations.

The discussion here, which uses the notation and definitions of McVoy, will be limited to single-channel or potential scattering. The S-matrix reduces to its partial wave form

$$S_l = e^{2i\delta_l}, \tag{124}$$

where δ_l is a partial wave phase shift. It is convenient to define the *Jost function* $f_l(k)$ such that

$$S_l(k) = f_l(-k)/f_l(k), \tag{125}$$

with the fundamental analytic property, for complex k,

$$(f_l(k^*))^* = f_l(-k). \tag{126}$$

This property ensures that $S(k)$ is a unitary matrix for real k, reducing to Eq. (124) with real δ_l for a single partial wave. For a scattering potential $V(r)$ that vanishes more rapidly than r^{-2} for large r, the asymptotic form of a radial wavefunction regular at $r = 0$ and normalized by the k-independent condition

$$\lim_{r \to 0} r^{-l-1} \phi_l(k, r) = 1 \tag{127}$$

is

$$\phi_l(k, r) \sim \frac{1}{2} \left(\frac{i}{k}\right)^{l+1} [f_l(k)e^{-ikr} - (-1)^l f_l(-k)e^{ikr}]. \tag{128}$$

For fixed r, $\phi_l(k, r)$ is an entire function of complex k, and $f_l(k)$ is regular in the open upper half-plane of k (Newton, 1966). Zeroes of $f_l(k)$, which correspond to poles of $S_l(k)$, must either lie on the imaginary axis or occur in pairs symmetrically displaced from this axis.

Zeroes of $f_l(k)$ in the upper half-plane are confined to the positive imaginary axis,

$$k_b = +i\kappa, \tag{129}$$

and correspond to bound states since

$$e^{ik_b r} = e^{-\kappa r}$$

is the only term remaining in $\phi_l(k_b, r)$. Zeroes of f_l in the lower half-plane occur either as pairs

$$k_\rho = \alpha - i\beta, \qquad -k_\rho^* = -\alpha - i\beta \tag{130}$$

corresponding to a resonance at the real value $|k_\rho|$, or occur as single points on the negative imaginary axis

$$k_v = -i\kappa, \tag{131}$$

which corresponds to a *virtual state*. Since energy E above the scattering threshold is given by $k^2/2$, the upper half-plane of complex k is mapped conventionally onto the entire complex E-plane, with a branch cut extending from $E = 0$ to infinity on the positive E-axis. The lower half-plane of k is mapped onto a second Riemann surface of complex E, the "nonphysical sheet." Resonance and virtual state zeroes of f_l correspond

to values of E on this nonphysical sheet. They influence scattering cross sections in proportion to their proximity to the real k-axis, mapped onto the branch cut in the E-plane.

When f_l has resonance zeroes as in Eq. (130), S_l can be expressed in the form

$$S_l(k) = \exp[2i(\delta_0 + \delta_r)] \tag{132}$$

where

$$\exp(2i\delta_r) = \frac{1 + i \tan \delta_r}{1 - i \tan \delta_r} = \left(\frac{k - k_\rho^*}{k - k_\rho}\right)\left(\frac{k + k_\rho}{k + k_\rho^*}\right). \tag{133}$$

This can be solved for $\tan \delta_r$ in terms of the parameters of Eq. (130),

$$\tan \delta_r = \frac{2k\beta}{k_r^2 - k^2} \tag{134}$$

where

$$k_r^2 = \alpha^2 + \beta^2.$$

If $k_r \gg \beta$, k can be replaced in the numerator of Eq. (134) by k_r, and this formula reduces to Eq. (95) with $\Gamma_r = 2k_r\beta$. If the scattering potential is varied so that a resonance approaches the threshold, β must vanish at least as rapidly as k_r, and this analysis shows that Γ_r must vanish at least quadratically with k_r. For potentials of finite range, Γ_r vanishes as k_r^{2l+1} for a resonance due to the centrifugal barrier in partial wave l (McVoy, 1967). Such a resonance becomes a bound state as a zero of $f_l(k)$ passes through the origin onto the positive imaginary axis. The paired resonance zeroes can be pictured as colliding at the origin, then separating as paired bound and virtual states.

When there is no potential barrier, as for s-states $(l = 0)$ in an attractive potential, zeroes of $f_l(k)$ remain single as they pass through the origin under variations of the scattering potential. Hence a virtual state, with k_v given by Eq. (131), is the precursor of a true bound state with no potential barrier. The phase shift is given as in Eqs. (132) and (133) by $\delta_0 + \delta_v$, with

$$\exp(2i\delta_v) = \frac{1 + i \tan \delta_v}{1 - i \tan \delta_v} = \frac{-k - k_v}{k - k_v}, \tag{135}$$

or

$$\tan \delta_v = k/\kappa. \tag{136}$$

This formula shows that a virtual state is characterized by a phase shift (usually s-wave) that rises rapidly above threshold, but with total increase limited to $\pi/2$ radians. The partial cross section for an s-wave, from Eq. (32) with $\tan \delta_v$ given by Eq. (136), is

$$\sigma = \frac{4\pi}{k^2 + \kappa^2},$$
(137)

so the cross section starts from a finite value at threshold. From Eq. (129), the partial cross section due to a true bound state close to threshold is also given by Eq. (137). Thus the scattering effect of a virtual state at "energy" $\kappa^2/2$ below threshold is the same as a true bound state at the same energy, but the virtual state is displaced onto the nonphysical sheet of the complex E-plane.

Geltman (1969) reviews the theory of threshold behavior of cross sections and gives rules for the variation of $\tan \delta_l$ near threshold for long-range potentials. The effects of such potentials in single-channel scattering were studied by O'Malley *et al.* (1961) and by Levy and Keller (1963). This analysis has recently been extended to multichannel scattering by Bardsley and Nesbet (1973).

Formal solutions to the scattering equations for coupled open channels can be expressed in terms of the Green's function of Eq. (106), for comparison functions w_0 and w_1 defined by Eqs. (102) with $\delta_0(r)$ suitably chosen. NonCoulombic phase shifts are defined with reference to the centrifugal barrier as comparison potential, spherical Bessel functions (regular and irregular) as comparison functions, and background phase shifts that approach $-l\pi/2$ for large r. The asymptotic limit of these formal solutions gives a formula for the K-matrix, expressed as an integral involving the scattering potential and an exact solution of the equations. The derivation given here of Eq. (109) is an application of this argument. Since all K-matrix elements indexed by the new channels that open at a given threshold must vanish at this threshold, and these matrix elements are the coefficients of the irregular functions w_1 in the wavefunction, these coefficients can be neglected in the neighborhood of the threshold. The formula for the K-matrix then takes the form of the partial wave Born approximation (Seaton, 1961),

$$K_{\alpha\beta} = -2k_\alpha^{1/2}k_\beta^{1/2} \int_0^\infty V_{\alpha\beta}(r)j_{l\alpha}(k_\alpha r)j_{l\beta}(k_\beta r)r^2 \, dr.$$
(138)

As shown for single-channel scattering by Levy and Keller (1963), the dominant term in the threshold behavior is given by Eq. (138).

Assume that there are one or more old channels labeled α, β, ..., and one or more new channels, opening at the specified threshold, labeled p, q, ... The new channels have $k_p = k_q = \cdots$, and the dependence of elements of K on k_p is to be determined. First consider K_{pq}, which corresponds to elastic scattering in the new channels. For any short-range interaction the integral is dominated as $k_p \to 0$ by small r, and

$$K_{pq}^S = -2k_p^{l_p + l_q + 1} \left[\int_0^\infty V_{pq}(r) r^{l_p + l_q + 2} \, dr + O(k_p^2) \right], \qquad (139)$$

from the power series expansion of the spherical Bessel functions. However, if the interaction contains a long-range component of the form Cr^{-s}, this leads to a contribution of the form

$$K_{pq}^L = -2Ck_p \int_0^\infty r^{2-s} j_{l_p}(k_p r) j_{l_q}(k_q r) \, dr. \qquad (140)$$

If $s < (l_p + l_q + 3)$ this integral is well-defined and gives

$$K_{pq}^L = \frac{-\pi C}{2^{s-1}} k_p^{s-2}$$

$$\times \frac{\Gamma(s-1)\Gamma[\tfrac{1}{2}(l_p + l_q - s + 3)]}{\Gamma[\tfrac{1}{2}(l_p - l_q + s)]\Gamma[\tfrac{1}{2}(l_p + l_q + s + 1)]\Gamma[\tfrac{1}{2}(l_q - l_p + s)]}. \qquad (141)$$

Given the inequality above, $(s - 2) < (l_p + l_q + 1)$, and this term is dominant for small k. This shows for elastic scattering that threshold behavior of K_{pq} is modified by long-range potentials. However, if $s \geq (l_p + l_q + 3)$, the potential will be modified at small r, since the integral is made finite by the short-range behavior of the potential. The dominant term remains $k_p^{l_p + l_q + 1}$ in this case.

Next consider $K_{\alpha p}$, which corresponds to inelastic scattering. For any short-range interaction, power series expansion, as in Eq. (139), gives a dominant term proportional to $k_p^{l_p + 1/2}$. This argument requires use of the Born approximation only for the radial function $u_p(r)$, since $u_\alpha(r)$ and $j_{l_\alpha}(r)$ have the same leading power of r when expanded about $r = 0$. For a long-range potential Cr^{-s}, if $s < (l_\alpha + l_p + 3)$, and u_α is approximated by j_{l_α},

$$K_{\alpha p}^L = -2Ck_\alpha^{1/2} k_p^{1/2} \int_0^\infty r^{2-s} j_{l_\alpha}(k_\alpha r) j_{l_p}(k_p r) \, dr$$

$$= -\frac{\pi C}{2^{s-1}} k_\alpha^{s - l_p - 5/2} k_p^{l_p + 1/2}$$

$$\times \frac{\Gamma[\tfrac{1}{2}(l_\alpha + l_p - s + 3)]}{\Gamma(l_p + \tfrac{3}{2})\Gamma[\tfrac{1}{2}(l_\alpha - l_p + s)]} \left[1 + O\left(\frac{k_p^2}{k_\alpha^2}\right) \right]. \qquad (142)$$

For small k_p, this has the same form as $K_{\alpha p}^S$. Since this result depends only on the series expansion of j_{l_p}, it is altered only by a change of numerical coefficient if u_α is used instead of j_{l_α} in the integrand. Thus it can be concluded that long-range interactions do not change the dominant power of k_p for K-matrix elements that connect two open channels with different values of k.

From Eqs. (31) and (142), the inelastic cross section for the excitation process $\alpha \to p$ varies as $k_p^{2l_p + 1}$ at the excitation threshold. An abrupt onset occurs only for $l_p = 0$, when the excitation cross section is proportional to k_p or $(E - E_{\text{th}})^{1/2}$, where E_{th} is the threshold energy, so that the initial slope is infinite. As a consequence of conservation of flux, this behavior is mirrored in the partial wave elastic cross section $\sigma_{\alpha\alpha}$, which can have infinite slope at the threshold (Wigner, 1948; Baz, 1957). The resulting structure in the elastic cross section is a *Wigner cusp*, or an apparent abrupt step or point of inflection. The analytic description of this structure can be obtained by analytic continuation of the K-matrix below the inelastic threshold. A convenient formalism for such analysis has been proposed by Ross and Shaw (1961).

From the argument given here, abrupt threshold structures (Wigner cusps or steps) should occur only if $l_p = 0$ for the electron in the threshold channel. If $(L, S, \pi)_p$ are the target atom quantum numbers defining this channel, this implies that such structure is possible only for partial wave states with total quantum numbers $(L_p, S_p \pm \frac{1}{2}, \pi_p)$. For example, in the case of electron scattering by alkali metal atoms in the ^{2}S ground state, the first excitation threshold is ^{2}P$^{\circ}$. For collisions in which the ^{2}P$^{\circ}$ state is excited, the initial and final values of the angular momentum of the scattered electron, l_α and l_p, are linked by the selection rule

$$l_p = l_\alpha \pm 1. \tag{143}$$

Thus l_p can be zero only if $l_\alpha = 1$, so that cusps can appear at the excitation threshold only for incident p-waves, for elastic scattering in total states ^{1}P$^{\circ}$ or ^{3}P$^{\circ}$.

This expected threshold behavior is illustrated in Fig. 5, which shows partial wave elastic cross sections for e–Li scattering, near the 2^2P$^{\circ}$ threshold, computed by the matrix variational method (Bardsley and Nesbet, 1973). The s- and d-wave cross sections pass smoothly through the threshold. There is a very clear cusp in the ^{1}P$^{\circ}$ cross section, and the ^{3}P$^{\circ}$ cross section shows a small but real step at threshold. In this work, the ^{1}P$^{\circ}$ cross section fails to reach infinite slope approaching the threshold from below. This is attributed to approximations in the variational trial function used in these calculations. The basis set does not contain functions
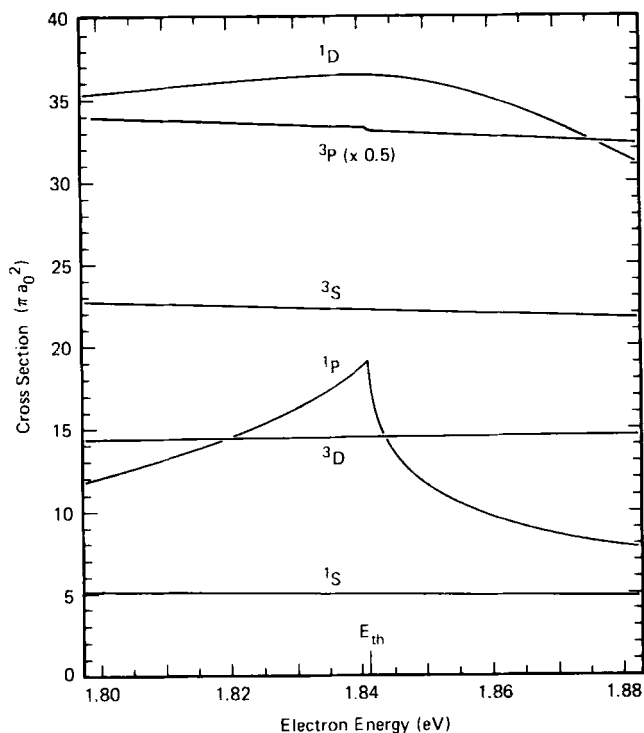
Fig. 5. e–Li. Partial wave components of elastic cross section at 2 ^{2}P° threshold.

with exactly correct asymptotic form for closed channels very near threshold, although the corresponding open channel functions are correctly represented.

VI. Theoretical Methods

A. Close-Coupling

The close-coupling method has been discussed here in terms of the explicit closed-channel expansion of the Hilbert space component of the scattering wavefunction as indicated in Eq. (11). Coupled integrodifferential equations are solved for both open-channel orbitals ψ_p and external closed-channel orbitals ψ_γ. The general procedure of expansion in target eigenstates was originally proposed by Massey and Mohr (1932). The method was implemented for practical computations by Seaton (1953a,b, 1955), and has become the principal computational method of

low energy electron scattering theory. Details of computational procedure have been given in several review articles or monographs (Burke and Smith, 1962; Burke and Seaton, 1971; Smith, 1971). The original method has been significantly improved by the inclusion of closed-channel pseudostates, discussed in Section III above, to account for the effect of target atom polarizability. Pseudostates have also been introduced to allow for perturbing effects of highly excited and continuum (ionization) channels, which cannot be included directly in the formalism (Burke and Webb, 1970; Burke and Mitchell, 1973). Explicit "correlation functions" of the form indicated in Eq. (2) can be included in addition to closed-channel functions or pseudostates. When the continuum orbitals are orthogonalized to the set of bound state orbitals used to construct target atom states, correlation functions constructed from these bound state orbitals must be included in the full wavefunction (Burke and Seaton, 1971). As shown in Eqs. (39) and (42), these terms contribute to a matrix optical potential in the close-coupling equations. When correlation functions are included, the close-coupling method becomes fully general, and can be applied in principal to calculations of arbitrary accuracy.

B. Polarized Orbital Method

The polarized orbital method is characterized by a description of the polarization response of the target atom to the external electron through inclusion of functions of the form indicated in Eqs. (12), (46), and (47) in the Hilbert space component of the scattering wavefunction. This method was originally proposed by Temkin (1957). Formalism and applications have recently been reviewed by Drachman and Temkin (1972) and by Callaway (1973). The target atom polarization functions introduced by Temkin are essentially the same as the pseudostates introduced subsequently in the close-coupling theory (Damburg and Karule, 1967). The principal difference between these methods is that the external closed-channel orbital ψ_γ of the close-coupling expansion, Eq. (11), is replaced by the functional form $\chi\psi_p$ in the polarized orbital method. Here ψ_p is an open-channel orbital, and χ is a modulating factor that can depend on the coordinates of two electrons, the external electron coordinate and an internal target coordinate to be antisymmetrized into the polarization function $\vartheta_{\gamma(p)}$. In its simplest form (Temkin and Lamkin, 1961) the modulating factor contains the multipole interaction factor $Y_L r^{-L-1}$, indicated in Eqs. (46) and (47), and a cutoff factor $\varepsilon(x, r)$ which vanishes when r is less than the internal coordinate x. This functional Ansatz leads through

analysis equivalent to the general derivation of an optical potential, Eqs. (39) and (42) here, to a polarization potential of the correct asymptotic form in an effective open-channel orbital Schrödinger equation (Temkin, 1957, 1959; Sloan, 1964). For a properly antisymmetrized wavefunction, the original derivation leads to both a local polarization potential and a nonlocal (integral operator) exchange polarization potential. Calculations in which this exchange potential is dropped are comparable to static exchange calculations, corrected for target atom polarization, and have been extensively applied to electron–atom scattering. Drachman and Temkin (1972) recommend that the terminology *adiabatic exchange* approximation be used for such calculations, which involve *ad hoc* approximations not required in the full *polarized orbital* formalism.

The adiabatic exchange approximation, because of its relative computational simplicity, lends itself to modifications intended to include additional physical effects. The "extended polarized orbital" method (EPOM) introduces a distortion potential that corrects for short-range penetration effects (LaBahn and Callaway, 1966; Callaway *et al.*, 1968). This distortion potential vanishes asymptotically as r^{-6} but greatly reduces the inner part of the adiabatic polarization potential.

Drachman and Temkin (1972) provide a critical review of the various approximate and modified versions of the polarized orbital method that have been proposed. Drachman and Temkin point out the close relationship between the close-coupling theory with polarization pseudostates and the variationally derived version of the polarized orbital method (Drachman, 1968). A close-coupling polarized orbital formalism suitable for complex target atoms has recently been proposed by Feautrier *et al.* (1971), and applied to e–O scattering (Vo Ky Lan *et al.*, 1972).

C. Matrix Variational Method

The method considered under this heading is an extension to electronic continuum states of matrix computational techniques that have been found to be very useful in applications to bound states of complex atoms. Coupled continuum equations for external open-channel orbitals are solved not as numerical integro-differential equations but as matrix equations for the asymptotic coefficients α defined by Eq. (5). The variational algorithms discussed in detail in Section IV are used, all involving manipulations of the fundamental matrix m_{ij}^{pq} defined by Eq. (20). This is the matrix of an effective multichannel Schrödinger equation coupling open scattering channels, in which all effects of the Hilbert space component of the full wavefunction have been condensed by partitioning, through

Eqs. (37) and (39), into a generalized optical potential. All integrations reduce to quadratures, but algebraic procedures are required for matrices that can be of very large dimension.

The review by Harris and Michels (1971) gives some of the background of this method, which is currently in a rapid state of evolution. Details of the algebraic algorithms required in applications to complex target atoms have been given by Lyons *et al.* (1973). A description of the method in its current form and a review of applications is given by Nesbet (1973). Special methods have been developed for the required integrals over asymptotic continuum functions (Lyons and Nesbet, 1969, 1973; Harris and Michels, 1969b). Computation of Eq. (20) makes use of a special algorithm (Nesbet, 1971) that avoids direct inversion of the very large bound–bound matrix $M_{\mu\nu}$.

Schwartz (1961a,b), who used a Hyleraas correlation expansion (functions of relative coordinates) for the Hilbert space wavefunction component in calculations of the e–H s-wave elastic phase shift, first recognized the computational significance of decomposing the wavefunction as indicated in Eq. (13). The bound–bound and bound–free matrices can be very large, compared with m_{ij}^{pq} which is indexed only by the number of open scattering channels. All manipulations of these large matrices are completed to high numerical accuracy when m_{ij}^{pq} is constructed. Subsequent application of any of the continuum variational methods considered in Section IV involves computations of relatively negligible weight. Thus alternative methods can easily be used and compared, and the complexity of any particular method is not a practical argument against its use.

In close-coupling theory, the number of coupled integro-differential equations to be solved increases with the number of closed-channel functions included in the Hilbert space component of the scattering wavefunction. In practice, this severely limits the capability of the theory to represent electronic correlation and polarization effects. In the matrix variational method this practical limitation is very greatly relaxed, since algebraic methods can be applied to very large matrices, using sophisticated data handling techniques if necessary.

D. Continuum Bethe–Goldstone Equations

The number of possible Slater determinants $\{\Phi_\mu\}$ in the Hilbert space basis increases very rapidly with the number of target atom electrons and with the number of basis orbital functions. Except for the lightest atoms, this implies that calculations requiring a full configuration interaction

expansion of the scattering wavefunction cannot be carried to conver-
gence in terms of basis orbitals unless some systematic simplifications are
introduced. A particular approach to this problem, using a hierarchy of
Bethe–Golstone equations in matrix variational form, has been applied
successfully to bound state calculations of energies and hyperfine struc-
ture parameters (Nesbet, 1969b). The generalization of this method
appropriate to the scattering problem will be described here (Nesbet,
1967).

The Bethe–Goldstone equation, which originated in nuclear many-
body theory (Brueckner, 1959; Bethe and Goldstone, 1957), is the time-
independent Schrödinger equation for a pair of particles embedded in the
Fermi sea of the remaining N-2 particles of an N-particle system. The
two-particle Bethe–Goldstone wavefunction is constrained to be ortho-
gonal to N-2 specified occupied orbitals of the Fermi sea. Solution of
the Bethe–Goldstone equation corresponds to an "independent pair"
model, in which the correlation energy of each pair of particles is
computed exactly. These pair correlation energies are added to give an
estimate of the total correlation energy (Gomes *et al.*, 1958). Mittleman
(1966) proposed that the same approach could be used in scattering
theory. In particular, scattering of an electron by an alkali atom can be
approximated by a continuum Bethe–Goldstone electron pair wavefunc-
tion for the external and series electrons, constrained by orthogonality to
the occupied orbitals of the closed shell ion core. This wavefunction
satisfies boundary conditions appropriate to one bound electron and one
free electron of specified momentum.

For an N-electron alkali atom the Hilbert space component of the
$N + 1$-electron scattering wavefunction considered by Mittleman can be
expanded as a linear combination of Slater determinants $\{\Phi^a, \Phi_i^{ab}\}$ in the
notation of Eqs. (10). Here index i has a specific value, referring to the
series electron of the target atom. The *variational subspace* of the
$N + 1$-electron Hilbert space $[\Psi_H]$ defined by this set of Slater determi-
nants will be denoted here by $[i]$. In terms of configurational virtual excita-
tions (Nesbet, 1970) the index i specifies the quantum numbers (nl) of
the series electron. As the orbital set $\{\phi_i; \phi_a\}$ becomes complete, a varia-
tional scattering calculation using the Hilbert space $[i]$ becomes equiva-
lent to solution of the continuum two-electron Bethe–Goldstone
equation considered by Mittleman. The analysis given in Section III
indicates that the resulting wavefunction describes the full energy-
dependent effect of multipole polarization potentials associated with vir-
tual excitation of the series electron, while neglecting the polarizability of
the ion core.

These concepts can be generalized to provide a step-by-step computational procedure which converges in a finite number of steps to exact results for scattering by any N-electron atom (Nesbet, 1967, 1970). Each computational step involves the solution of generalized continuum Bethe–Goldstone equations of order n, defined to be equivalent to a variational calculation in which all possible configurational excitations of n orbitals ϕ_i, ϕ_i, ..., specified by their (nl) quantum numbers, are represented in the wavefunction. The corresponding variational Hilbert space will be denoted by $[ij\cdots]$, specifying the n indices $i, j, \ldots$. This Hilbert space is a direct sum of *disjoint* subspaces $(ij\cdots)$, where this notation indicates the linear space spanned by all Slater determinants obtained from the reference configuration (0) by virtual excitation of occupied orbitals with the specified indices $i, j, \ldots$, to one-particle states represented by $n + 1$ unoccupied orbitals with all possible indices. A *variational* Hilbert space $[ijk\cdots]$ is defined as the direct sum of all disjoint subspaces whose indices form a subset of $ijk\cdots$. For example

$$[ij] = (0) + (i) + (j) + (ij). \tag{144}$$

The complete Hilbert space of $N + 1$-electron Slater determinants is the direct sum of all disjoint subspaces,

$$[\Psi_H] = (0) + \sum_i (i) + \sum_{ij} (ij) + \sum_{ijk} (ijk) + \cdots. \tag{145}$$

The variational subspaces form a *lattice* in the technical sense that

$$[0] \subseteq [ijk\cdots] \subseteq [\Psi_H] \tag{146}$$

for any $[ijk\cdots]$. Simple ordering holds for variational subspaces with nested indices,

$$[0] \subset [i] \subset [ij] \subset [ijk\cdots], \tag{147}$$

but no ordering relation is defined otherwise.

This lattice structure of Hilbert spaces defines a hierarchy of variational calculations, to be carried out independently for each different variational subspace corresponding to a node on the lattice diagram. The useful information gained by each such calculation is defined inductively in terms of *net increments* of properties of the variational wavefunction. Values of such properties computed directly for a given variational Hilbert space $[ij\cdots]$ are referred to as *gross increments* $\Delta F_{ij\ldots}$, usually obtained as corrections to properties of the reference state, or of a static-exchange calculation in scattering theory. A *net increment* $f_{ij\ldots}$ is

defined as the difference between the corresponding gross increment and the sum of all net increments of lower order whose indices form a proper subset of the given set $ij \cdots$.

In the case of bound states, this definition of gross and net increments in terms of a lattice decomposition of the N-electron Hilbert space ensures that when each variational calculation is carried to convergence a given physical property is expressed exactly by the finite sum of all net increments up to order N. In practice, correlation energies are usually obtained to satisfactory accuracy by terminating this summation at order two, corresponding to the independent-pair approximation (Nesbet, 1969b). In scattering theory, the situation is more complicated. Convergence of the Hilbert space component ψ_H of the wavefunction does not affect the asymptotic target states, denoted by ϑ_p in Eq. (1). Ultimate convergence of the theory requires systematic correlation corrections to ϑ_p as well as to Ψ_H. Formally this could be carried out by a lattice decomposition of the direct product of the N-electron Hilbert space for ϑ_p with the $N + 1$-electron Hilbert space for Ψ_H. Each gross and net increment would carry two sets of indices, one for each lattice. While this procedure provides justification for the theory, it could not be carried out in practice for most atoms.

As a working compromise, the zero-order variational Hilbert space [0] can be extended to include those target configurations that contribute most strongly to the target atom open-channel states. Since the definition of continuum Bethe–Goldstone equations given here depends fundamentally only on the definition of a lattice structure of nested subspaces of the full Hilbert space, such an extension of definition of the variational subspaces does not change the formal structure of the theory.

If the hierarchy of variational calculations is truncated at the level of single subshell excitations [i], this corresponds to solution of two-particle continuum Bethe–Goldstone equations, independently for each subshell, adding the incremental contributions to computed quantities such as K-matrix elements. The essential approximation, following the discussion in Section III, is that polarizability contributions of different subshells are assumed to be independent and additive. Since essentially this approximation is involved in the usual perturbation theory of static polarizabilities, it can be expected to give results of useful accuracy in scattering theory. This approximation is inherent in the polarized orbital method and in the use of polarization pseudostates in close-coupling calculations. No calculations to date with the continuum Bethe–Goldstone formalism have gone beyond this level of approximation. Inclusion of higher order

terms would allow for systematic correction of the assumption of additive polarizabilities.

The hierarchy of continuum Bethe–Goldstone equations can be solved either by matrix variational methods or by numerical integration of the generalized close-coupling equations indicated in Eq. (48). The method was originally formulated in terms of such coupled open-channel equations (Mittleman, 1966; Nesbet, 1967), but actual calculations have used the matrix variational method.

E. Separation of Open- and Closed-Channel Components

In the Feshbach partitioning scheme, Eqs. (36) and (37), any basis subset of the Hilbert space functions $\{\Phi_\mu\}$ can be included in Ψ_P rather than Ψ_Q. Since the system of equations is linear any such decomposition must ultimately be equivalent to the extreme case considered in the analysis of Section III, where the entire Hilbert space basis is included in Ψ_Q. Since this analysis shows that spurious anomalies in the Kohn and inverse Kohn variational methods arise from the singularities of the matrix m_{ij}^{pq}, defined by Eq. (20), this continues to be true for any intermediate partitioning scheme. This fact can be obscured by analysis that does not explicitly construct m_{ij}^{pq}, but the matrix equations of any linear variational method can be transformed into the form considered in Section III, and are computationally equivalent. Anomalies can be avoided either by use of an anomaly-free method, considered in Section IV, or by solving the open-channel equations by numerical integration.

Intermediate partitioning of the Hilbert space basis has been proposed by Hahn (1971), who uses this formalism to justify a "quasi-minimum principle," and by Chung and Chen (1971, 1972), who use this method for accurate calculations of e–H elastic phase shifts and resonances. In the latter work, anomalies are avoided in the Kohn formalism apparently by judicious choice of a nonlinear parameter. The practical validity of the quasi-minimum principle has been examined in a series of variational calculations by Truhlar and Smith (1972). They find, in accord with the analysis of Hahn (1971), that phase shifts increase monotonically with closed-channel basis size after the open-channel quadratically integrable basis has been made large enough to provide a good approximation to open-channel orbitals. Under these circumstances, e–H elastic phase shifts computed variationally are found to be true lower bounds to their accurately known values (Truhlar and Smith, 1972).

Numerical integration of the open-channel equations, obtained as in Eq. (48) here by Feshbach partitioning, treating closed channels alge-

braically by a basis expansion, has been proposed (Chen and Chung, 1970) as a practical alternative to the close-coupling procedure of numerical integration of both open- and closed-channel equations. This method was used for a study of e–H resonances (Chen *et al.*, 1971).

By selecting appropriate basis states for the Hilbert space component of the scattering wavefunction, matrix variational calculations can be made equivalent to close-coupling calculations with a specified set of target atom states. Algebraic close-coupling calculations of this kind have been carried out for e–H scattering by Seiler *et al.* (1971). In this work, it was found necessary to include orbital basis functions of the kind indicated in Eq. (47), oscillatory functions divided by powers of r, in order to obtain adequate convergence of the variational calculations. This was attributed to the nature of the external closed-channel orbitals suitable for the r^{-2} potential arising from the degenerate 2s and 2p states of atomic hydrogen. These functions are quadratically integrable, but of much longer range than the exponential basis functions commonly used in atomic wavefunction calculations. Since the asymptotic form of external closed-channel orbitals is given in general by Eq. (47), it is clear that convergence of the matrix variational method for strong polarization potentials can be facilitated by including functions of this form in the orbital basis set.

F. *R*-Matrix Method

This method combines matrix techniques for expansion of the wavefunction within a boundary radius r_0 and numerical solution of coupled differential equations outside r_0 (Burke *et al.*, 1971; Burke and Robb, 1972; Fano and Lee, 1973; Burke, 1973). Such a " hybrid " method gains the advantage of matrix manipulation of algebraic equations containing a nonlocal optical potential within r_0, while exploiting the simple form of asymptotic polarization potentials by direct integration outside r_0. The *R*-matrix method was developed in nuclear physics (Wigner and Eisenbud, 1947; Lane and Thomas, 1958). It must be modified for electron–atom scattering to take into account the long range potentials due to target atom polarizabilities and static moments. This is done by solving close-coupling equations (without exchange) for open- and closed-channel orbitals outside r_0 (Burke *et al.*, 1971).

The *R*-matrix theory, as usually presented, makes use of Green's theorem to relate value and slope of the channel orbitals at boundary radius r_0, using an expansion of these functions as linear combinations of basis functions satisfying fixed boundary conditions at r_0. The true logar-

ithmic derivative at r_0 is computed from Green's theorem, despite the use of basis functions with a fixed but arbitrary value of this parameter. This expansion tends to converge slowly, because of the inherent discontinuity of the boundary derivative, but this can be corrected by an approximate method due to Buttle (1967). The method can be reformulated as a variational procedure, using trial functions with discontinuous derivative at r_0 (Oberoi and Nesbet, 1973a, 1974). This reformulation makes it possible to use basis functions within r_0 that are not constrained by a particular boundary condition. Model calculations show that convergence is greatly improved by dropping this constraint, and very simple basis functions can be used without the Buttle correction.

Preliminary results reported by Burke (1973), of applications of this method to electron scattering by complex atoms, indicate that it may develop into one of the most efficient and most widely applicable of the available computational methods.

G. Many-Body Green's Function Methods

Formal methods of quantum field theory can be applied to the problem of electron scattering by a complex atom. The diagrammatic perturbation theory of Feynman, Brueckner, and Goldstone can be used to define a perturbation expansion of an effective optical potential. In the formal theory, this optical potential appears as the self-energy operator of the one-particle Green's function. The second-order optical potential was computed by Pu and Chang (1966) and used to obtain s- and p-wave e–He elastic scattering phase shifts. Similar calculations were carried out by Kelly (1967, 1968) for singlet and triplet s-wave e–H elastic phase shifts. Kelly included corrections for effects higher than second order, and obtained results in very good agreement with the accurate variational values of Schwartz (1961a). Knowles and McDowell (1973) have corrected the e–He work of Pu and Chang for some important omitted effects (EPV diagrams) and have computed d-wave phase shifts. The optical potential computed in these applications is formally equivalent to that defined here by Eqs. (39) and (42), except that the Hilbert space component of the scattering wavefunction is expanded in continuum rather than discrete basis functions in the perturbation theory.

Another general approach has been developed from the quantum field theoretical formalism of Schwinger (Csanak *et al.*, 1971b; Thomas *et al.*, 1973). This approach develops a hierarchy of coupled equations for *n*-particle Green's functions (Schwinger, 1951), which have immediate physical significance as transition amplitudes or functions describing the

response of a many-electron system to an external perturbation. Truncation of this hierarchy leads to self-consistent approximations at successive levels of complexity. In this aspect, the coupled Green's function theory is similar to the hierarchy of Bethe–Goldstone equations described above.

The formal theory suggests that an approximation referred to as the GRPA (generalized random phase approximation) should contain the essential physics of the polarization response of a target atom to an elastically scattered electron (Schneider *et al.*, 1970). In this approximation, static-exchange equations are augmented by an optical potential (response function) constructed from RPA (random phase approximation) transition amplitudes. The GRPA has been applied to e–He elastic scattering, to obtain s- and p-wave phase shifts in excellent agreement with the best polarized orbital and matrix variational calculations (Yarlagadda *et al.*, 1973). For elastic scattering, the GRPA appears to provide an internally consistent formalism at the same level of physical approximation as the polarized orbital method.

A generalized optical potential for inelastic electron–atom scattering has been derived from the coupled Green's function formalism by Csanak *et al.* (1973). The lowest order approximation for inelastic scattering is referred to as the RPA S-matrix formula (Csanak *et al.*, 1971a). This approximation has been applied to calculations of electron impact excitation cross sections for the $n = 2$ levels (^{3}S, ^{1}S, ^{3}P, ^{1}P) of He (Thomas *et al.*, 1974), in the incident energy range above the ionization threshold. This approximation is remarkably simple, requiring only matrix elements of the RPA transition potential between static-exchange continuum functions for the incident and scattered electron.

Csanak and Taylor (1972, 1973) have analyzed the coupled Green's function formalism in terms of widely used models and approximate methods, including various forms of the polarized orbital method. They show that the Green's function formalism provides a rationale for making internally consistent approximations in such methods.

VII. Applications

A. He, Elastic

As a result of recent experimental work, the e–He elastic cross section is well determined experimentally and in excellent agreement with theory for incident energies up to the first excitation threshold (2 ^{3}S at 19.818 eV). This data has been reviewed by Andrick (1973). The differential cross sections measured by Andrick and Bitsch (1975) have been
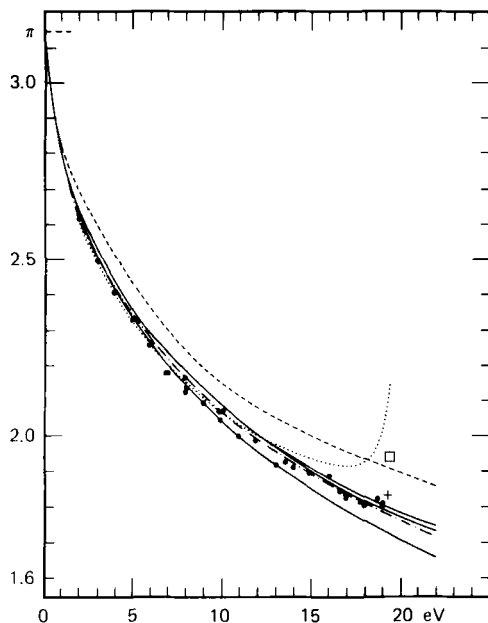
Fig. 6. e–He. $l = 0$ elastic phase shift (Andrick, 1973, Figure 10). Curves: —, Callaway *et al.* (1968), Duxler *et al.* (1971), LaBahn and Callaway (1966); – · –, Pu and Chang (1966); · · ·, Burke *et al.* (1969a); – – –, Brandsden and McDowell (1969). ●, Andrick and Bitsch (1975); +, Andrick *et al.* (1973); □, Gibson and Dolder (1969).

analyzed in terms of partial wave phase shifts, shown here in Figs. 6 and 7 (Andrick, 1973). The experimental d-wave phase shift is in good agreement with the Born approximation formula,

$$\delta_l = \frac{\pi \alpha k^2}{(2l + 3)(2l + 1)(2l - 1)} \tag{148}$$

from Eq. (141), with $s = 4$ for the polarization potential defined by the electric dipole polarizatibility of He, $\alpha = 1.39a_0^3$. This formula is used to correct differential cross sections for partial waves with $l > 2$ (Thompson, 1966; Andrick, 1973).

Absolute values of differential cross sections are obtained by combining low-order phase shifts from relative differential cross sections with the Born formula for higher l (Andrick and Bitsch, 1975). Additional data is obtained from the variation of the differential cross section at the narrow ^2S resonance near 19.3 eV (Andrick *et al.*, 1973). Figure 6 shows these results for the s-wave phase shift, compared with previous experimental and theoretical results. Figure 7 shows corresponding p-wave results.
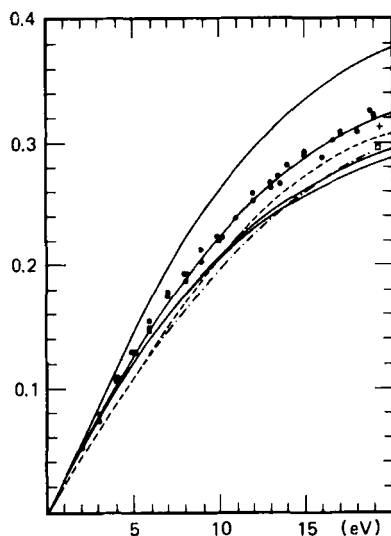
Fig. 7. e–He. $l = 1$ elastic phase shift (Andrick, 1973, Figure 11). Curves: —, LaBahn and Callaway (1964), Duxler *et al.* (1971), Callaway *et al.* (1968), LaBahn and Callaway (1966); – · – ·, Pu and Chang (1966); – – –, Brandsden and McDowell (1969). ●, Andrick and Bitsch (1975); +, Andrick *et al.* (1973); □, Gibson and Dolder (1969).

These figures indicate substantial agreement between recent experiments and theoretical calculations that include the full effect of target atom polarizability. These are all variants of the polarized orbital method, except for the optical potential calculation of Pu and Chang (1966). The p-wave results lie closest to the calculation of Duxler *et al.* (1971), a full polarized orbital calculation as originally proposed by Temkin (1957, 1959). The earlier adiabatic exchange calculation by LaBahn and Callaway (1964) apparently overestimates the p-wave phase shift. The EPOM (extended polarized orbital method) calculation of Callaway *et al.* (1968), which modifies the polarization potential by a shorter-range distortion potential, underestimates the p-wave phase shift. Other data shown in Figs. 6 and 7 include a close-coupling calculation (1 ^{1}S ground state plus 2 $^{3, 1}$S and 2 $^{3, 1}$P) of Burke *et al.* (1969); a least-squares fit of phase shifts to data from several experiments (Brandsden and McDowell, 1969); and phase shifts deduced from earlier measurements of differential cross sections near the ^{2}S resonance (Gibson and Dolder, 1969).

The matrix variational method was first applied to e–He scattering by Michels *et al.* (1969), with detailed results reported by Harris and Michels

(1971) for s, p, and d elastic phase shifts. This work was extended by Sinfailam and Nesbet (1972) by carrying the orbital basis expansion to practical completeness within the framework of the Bethe–Goldstone approximation of level [1s] for He. This approximation takes into account all polarization effects due to virtual excitation of a single target 1s orbital. Results for s, p, d, and f elastic phase shifts are shown in Figs. 8–11; solid curves, BG. For comparison, algebraic close-coupling calculations in the static exchange approximation are included in these figures; dashed curves, SE. The algebraic SE results duplicate comparable close-coupling calculations, including the R-matrix calculations of Burke and Robb (1972), while the BG results are in good agreement with polarized orbital calculations (Callaway et al., 1968; Duxler et al., 1971). The theory behind the BG approximation indicates that it includes in an internally consistent way all of the physical effects considered in the various forms of the polarized orbital method. For this reason when the
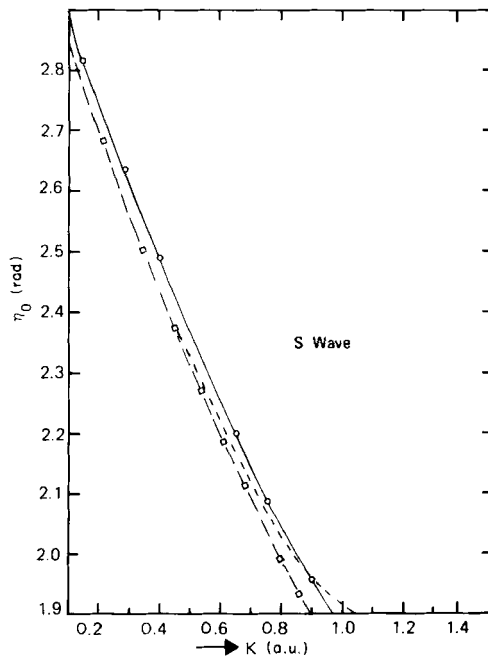
Fig. 8. e–He. $l = 0$ elastic phase shift. Curves:———, present BG; — —, present SE; ---, Burke, Cooper, and Ormonde (CC). ◯, Callaway et al. (EPOM); ☐, Burke and Robb (RM).
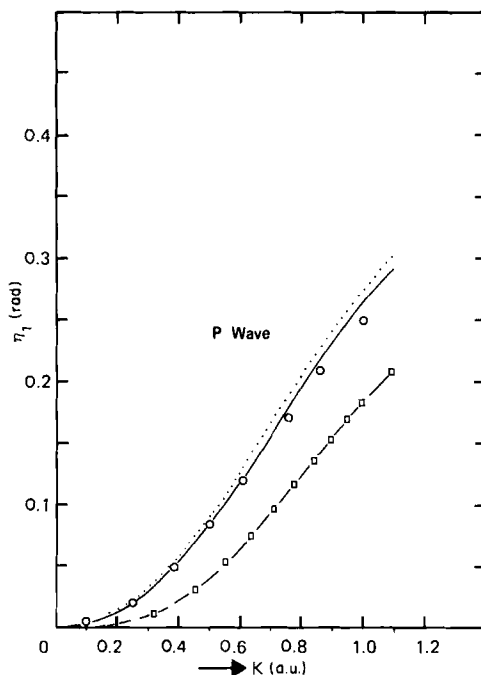
Fig. 9. e–He. $l = 1$ elastic phase shift. Curves: —, present BG; – –, present SE; ···, Duxler *et al.* (POM). ○, Callaway *et al.* (EPOM); □, Burke and Robb (RM).

orbital basis is effectively complete, the BG results should be more re-liable than the best polarized orbital results, if there is any substantial difference.

Calculations of phase shifts for e–He elastic scattering have been carried out by the GRPA coupled Green's function method (Yarlagadda *et al.*, 1973). The s- and p-wave phase shifts are in close agreement with polarized orbital and matrix variational (BG) results. There is a discrepancy in the d-wave phase shift, due to failure to include f-orbitals in the basis used to represent the GRPA optical potential. The effect of omitting such f-orbitals is illustrated for matrix variational calculations in Fig. 12 (Sinfailam and Nesbet, 1972). The figure shows that, without f-orbitals, only the d → p part of the external closed-channel orbital cor-responding to the 1s → p induced dipole of the target can be taken into account. This is equivalent to reducing the polarizability of the target atom, implying, through the partial wave Born formula, a reduction in the d-wave phase shift. When f-orbitals are available, the d → f part of the
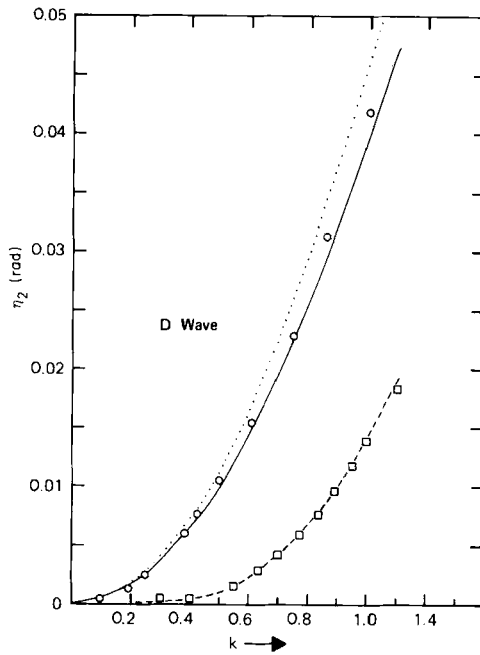
Fig. 10. e–He. $l = 2$ elastic phase shift. Curves: —, present BG; – – – present SE; ···, Duxler *et al.* (POM). ○, Callaway *et al.* (EPOM); □, Burke and Robb (RM).
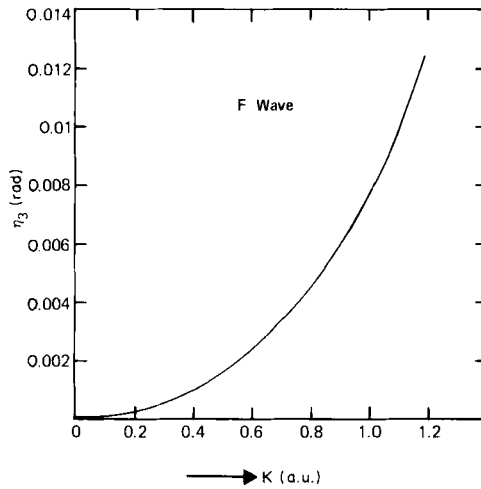
Fig. 11. e–He. $l = 3$ elastic phase shift.
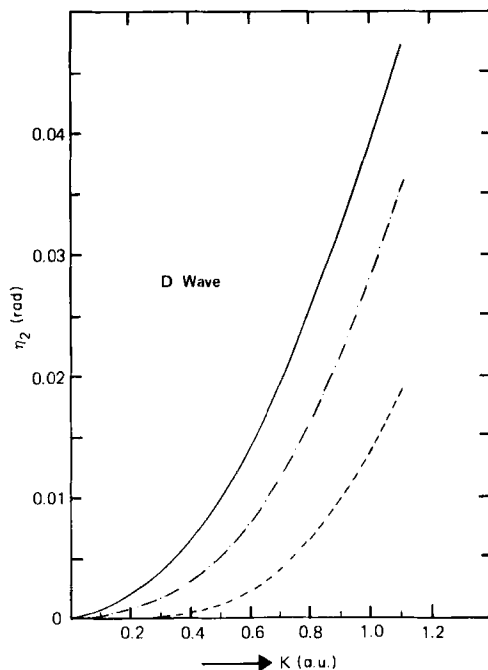
Fig. 12. e–He. $l = 2$ elastic phase shift, showing effect of basis f orbitals. Curves: —, BG (f-orbitals included); ·–·–, BG (f-orbitals excluded); – – –, SE.

external closed-channel orbital can be represented. In fact, the full BG d-wave phase shift shown in Fig. 12 is closely approximated by the Born formula, Eq. (14), in agreement with the experimental results (Andrick, 1973). In close-coupling calculations, this f-component would be obtained by numerical integration of the corresponding closed-channel equation, and in the polarized orbital method it is implicitly included in he derivation of the polarization potential.

Because the d-wave phase shift is well approximated by the Born formula, this should be true for all higher partial waves, in the elastic scattering energy range. The remarkable conclusion is that sophisticated theoretical methods are required only for s- and p-waves, higher phase shifts being adequately determined by the target atom polarizability, through Eq. (148). If this argument is applied to the f-wave phase shift shown in Fig. 9 (Sinfailam and Nesbet, 1972), obtained in the BG approximation, it is found to lie below the Born curve, implying inadequate representation of the $f \rightarrow g$ external closed-channel orbital. It should be

remarked that the partial wave Born formula is valid when the phase shift is *small*, regardless of energy. The usual application of the Born approximation is to the high energy limit, where all phase shifts are small.

The only pronounced structural feature in e–He scattering below the first inelastic threshold is the $(1s2s^2)^2S$ resonance near 19.3 eV, first observed by Schulz (1963), who has recently reviewed relevant experimental and theoretical studies (Schulz, 1973). Although evidence of other structure has appeared in some experiments, no other resonance appears in theoretical studies designed to locate all narrow resonances (Sinfailam and Nesbet, 1972; Temkin *et al.*, 1972). Observed structure near 19.5 eV has recently been concluded to be "an echo of the $1s2s^2$ resonance" (Sanche and Schulz, 1972).

From observations of Wigner cusps in e–He elastic scattering at the $2\,^3S$ and $2\,^1S$ thresholds, at 19.818 eV and 20.614 eV, respectively, Cvejanovic *et al.* (1974) calibrate the $(1s2s^2)^2S$ resonance at 19.367 ± 0.008 eV. The width measured by both Gibson and Dolder (1969) and Golden and Zecca (1971) is 0.008 eV. There is an unresolved discrepancy between this value and the results of variational calculations. The width computed by Temkin *et al.* (1972) for resonance energy 19.363 eV is 0.0144 eV, and that computed by Sinfailam and Nesbet is 0.015 eV, at a computed resonance energy of 19.42 eV. These calculations use the Hartree–Fock approximation for the target atom wavefunction, and further calculations are needed to explore the effect of target atom electronic correlation on the resonance width.

The BG calculations of Sinfailam and Nesbet (1972) locate the ^2S resonance at 19.42 eV, with background phase shifts (δ_1 and δ_2 extrapolated from the published data) $\delta_0 = 104.9°$, $\delta_1 = 18.1°$, $\delta_2 = 3.2°$. These values are very close to experimental values deduced from the resonance shape of the differential cross section (Andrick *et al.*, 1973): $\delta_0 = 105°$, $\delta_1 = 18°$, $\delta_2 = 3.2°$. At resonance, the experimental phase shifts of Andrick and Bitsch (1975), shown in Figs. 6 and 7, are $\delta_0 = 104°$, $\delta_1 = 18.5°$, $\delta_2 = 3.4°$. This agreement is somewhat closer than for other theoretical results cited by Andrick (1973).

The total elastic cross section for e–He scattering is shown in Fig. 13 (Sinfailam and Nesbet, 1972). The matrix variational (BG) and polarized orbital (EPOM) (Callaway *et al.*, 1968) results are indistinguishable. The exaggerated peak in the close-coupling cross section (Burke *et al.*, 1969a) is attributed to inclusion of only 35% of target atom polarizability in the 5-state close-coupling calculation. The experimental data of Golden and Bandel (1965) follows the theoretical curve, but lies some 5% below it.
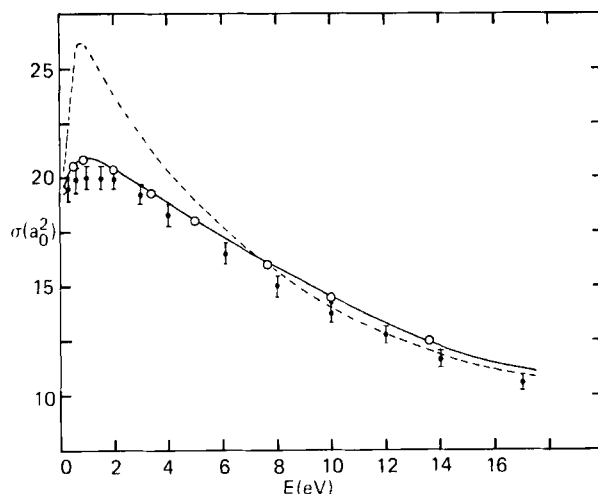
Fig. 13. e–He. Total elastic cross section. Curves: —, Sinfailam and Nesbet; – – –, Burke, Cooper, and Ormonde. ○, Callaway *et al.*; ●, experiment—Golden and Bandel.

The total cross section obtained from phase shifts fitted to recent differential cross section data (Andrick and Bitsch, 1975) is uniformly larger than that of Golden and Bandel, and is generally several percent greater than the theoretical cross section shown in Fig. 13.

The momentum transfer cross section for electron scattering is defined in terms of partial wave phase shifts by the formula

$$\sigma_M = \frac{4\pi}{k^2} \sum_{l=0}^{\infty} (l + 1)\sin^2(\delta_l - \delta_{l+1}). \tag{149}$$

This quantity has been obtained to high accuracy from measurements of the drift velocity of electrons moving through He gas in the direction of an applied uniform electric field (Crompton *et al.*, 1967, 1970). This data is compared with BG calculations (Sinfailam and Nesbet, 1972) in Fig. 14. Since this experimental data is not subject to arbitrary normalization, beyond the error bars shown, the small remaining discrepancy may be due to neglect of target atom electronic correlation in the BG calculations.

In their review of total elastic cross sections, Bederson and Kieffer (1971) use computed phase shifts to evaluate the ratio σ/σ_M, then use this ratio to convert the drift velocity data to an estimated total cross section. In the low energy range (< 5 eV), where σ_M is known, this gives a curve several percent higher than the theoretical curve (BG and EPOM) shown in Fig. 13. This result confirms the small discrepancy apparent in Fig. 14.
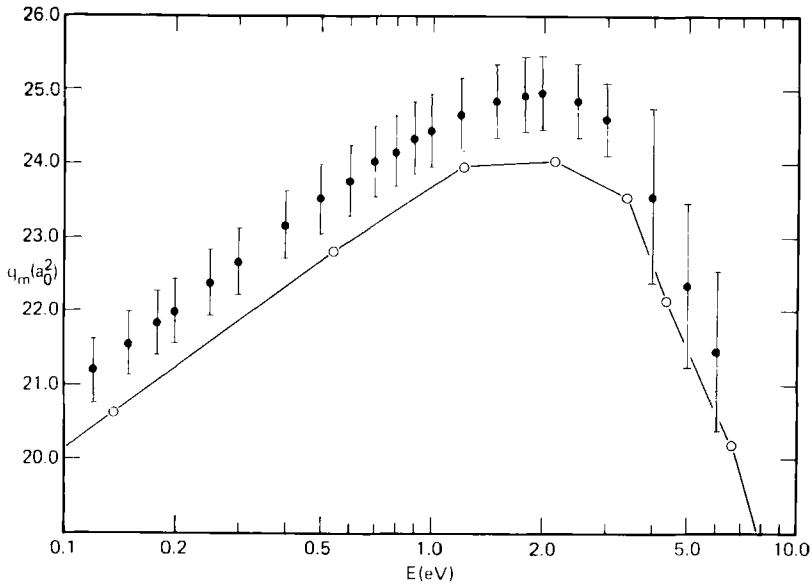
Fig. 14. e–He. Momentum transfer cross section. Solid line—Sinfailam and Nesbet; ●, experiment—Crompton *et al.*

B. He, Inelastic

The first excitation threshold in He is due to the (1s2s) 2 ^{3}S state, at 19.82 eV. The three other excited states below the $n = 3$ threshold are 2 ^{1}S at 20.61 eV, 2 ^{3}P at 20.96 eV, and 2 ^{1}P at 21.22 eV. The lowest $n = 3$ state is 3 ^{3}S at 22.72 eV. Only the 2 ^{1}P state is coupled to the ground 1 ^{1}S state by an allowed optical transition, but all of these states can be excited from the ground state by electron impact.

Experimental methods used to study inelastic e–He scattering in this energy range (19.8–22.7 eV) have been reviewed by Schulz (1973), who gives earlier references and surveys the experimental results and their theoretical interpretation. The 2 ^{3}S and 2 ^{1}S states of He are metastable, and serve as energy traps which can be de-excited by collision with other atoms (Penning ionization) or with a conducting surface. Such collisions produce secondary electrons that provide a selective detection mechanism for the metastable states. Recent experiments use a highly monochromatic incident electron beam and measure scattered intensity as a function of residual energy and scattering angle.

The main structural features found in this experimental data are in substantial agreement with cross sections computed in the 5-state (1 ^{1}S, 2 ^{3,1}S, 2 ^{3,1}P) close-coupling calculations of Burke *et al.* (1969a). This

work was simplified by approximating an exchange term, and the s-wave contribution to the cross section for metastable production had to be divided by 10 to obtain reasonable agreement with the experimental cross section. Sklarew and Callaway (1968) carried out EPOM and adiabatic exchange calculations of elastic scattering from the 2 ^{3}S state, obtaining results that were not in good agreement with experiment. It should be noted that the polarizability of He 2 ^{3}S is extremely large, $313a_0^3$ (Dalgarno and Kingston, 1958), and must be taken into account in any reasonable calculation. The full polarized orbital method has not been applied to the $n = 2$ states of He because of the inherent multichannel nature of the problem.

The matrix variational method, which includes all physical effects considered in the polarized orbital method, but is not limited to single-channel scattering, has been applied to e–He scattering between the $n = 2$ and $n = 3$ energy thresholds (Oberoi and Nesbet, 1973b). Multichannel variational equations were solved, including all significant effects of virtual excitation of reference configuration 1s2s at the level of the Bethe–Goldstone equation symbolized by [2s]. The reference configuration was augmented by ns/2s and np/2s virtual excitations, required for representation of the four $n = 2$ states and the 1 ^{1}S ground state. Scattering states with open-channel orbitals up to $l = 3$ were included in these calculations, and the orbital basis set was sufficiently large to ensure reasonable convergence. Continuum orbitals with $l > 3$ are not expected to be important below the $n = 3$ threshold.

The principal results of these calculations can be discussed in terms of Fig. 15 (Oberoi and Nesbet, 1973b). This figure shows sums of eigenphases for the principal doublet scattering states, plotted against k, the momentum relative to the 2 ^{3}S threshold. The main structural features in these computed curves correspond to observed features in the various elastic and inelastic cross sections coupling the five target states in this energy region.

Following the discussion in Section V above, a multichannel resonance corresponds to a rise through π radians of the sum of eigenphases for some symmetry component of the scattering wavefunction. From Fig. 15, the computed eigenphases show a broad ^{2}P° resonance between the 2 ^{3}S and 2 ^{1}S thresholds, a broad ^{2}D resonance near the 2 ^{3}P threshold, and several narrow resonances just below the 3 ^{3}S threshold. The computed 1 ^{1}S–2 ^{3}S excitation cross section is shown in Fig. 16, in comparison with recent experimental data (Brongersma *et al.*, 1972). Similar data, confirming these experimental results, has been obtained by Hall *et al.*
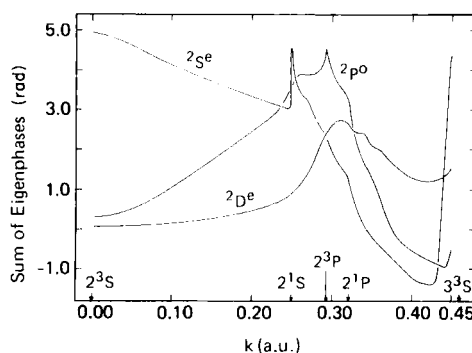
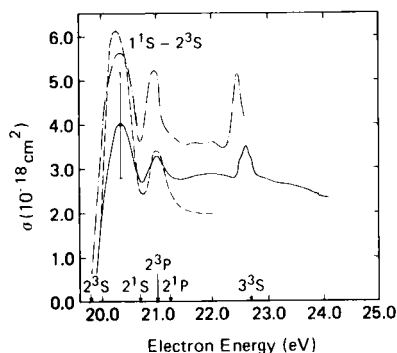**Fig. 15.** e–He. Sums of eigenphases for ^{2}S, ^{2}P°, ^{2}D partial waves.

Fig. 16. e–He. 1 ^{1}S → 2 ^{3}S excitation cross section. Curves: – · – ·, Oberoi and Nesbet; – – –, Burke *et al.*; —, experimental, Brongersma *et al.*

(1972). The error bar shown in Fig. 16 indicates the large uncertainty in the absolute normalization of the measured excitation cross section. If this data were normalized to the matrix variational calculation, the structural features of the curves would nearly coincide. The three prominent peaks, in order of increasing k, correspond to the broad ^{2}P° and ^{2}D resonances, and to the cluster of narrow resonances below the $n = 3$ threshold. The earlier close-coupling calculations (Burke *et al.*, 1969a), shown in Fig. 16, apparently overestimate the relative height of the ^{2}P° peak, and do not describe the resonances just below $n = 3$. The computed s-wave partial cross section was reduced by a factor of ten to reduce its contribution to the curve shown here. The broad ^{2}P° and ^{2}D resonances, characterized as shape resonances, are prominent features of the observed

cross section for total metastable production (Dorrestein, 1942; Schulz and Fox, 1957; Pichanick and Simpson, 1968). The $^2P^o$ resonance excitation structure was fitted to a Breit–Wigner formula by Baranger and Gerjuoy (1957). The p-wave character of the scattered electrons at this resonance was identified in differential cross section measurements (Ehrhardt and Willmann, 1967). The same experiment established the d-wave character of scattered electrons at the ^2D peak.

The narrow resonances below the $n = 3$ threshold are examples of Feshbach or core-excited (CE1) resonances. The external electron is bound to the core $n = 3$ states. Since the energy is below threshold, interaction with the continuum ($n = 1$ or 2) is weak, and the resonances are narrow. These resonances have been observed in differential inelastic scattering (Ehrhardt and Willmann, 1967; Ehrhardt et al., 1968), in metastable production (Pichanick and Simpson, 1968), and in transmission experiments (Sanche and Schulz, 1972). The variational calculations of Oberoi and Nesbet (1973b) locate two narrow ^2S resonances at 22.44 and 22.53 eV, respectively, with widths 0.15 eV and 0.03 eV. A $^2P^o$ resonance of width 0.022 eV is found at 22.45 eV. These resonances may account for the structure observed by Pichanick and Simpson (1968) at 22.44 and 22.55 eV, with widths estimated to be approximately 0.1 eV. Quartet resonances are found in the variational calculations, but they would only be observed in scattering from the target atom triplet states. A $^4P^o$ resonance of width 0.05 eV is predicted at 22.54 eV, and a ^4D resonance of width 0.01 eV is predicted at 22.56 eV (Oberoi and Nesbet, 1973b).

Figure 15 shows a priminent Wigner cusp in the $^2P^o$ eigenphase sum, at the 2 ^3P threshold. A similar structure occurs at the 2 ^1P threshold, but is not visible on the scale of the figure. As shown in Section V, such points of infinite slope can occur at a channel threshold in scattering states of symmetry such that the new open-channel orbital is an s-wave. In the present case, cusps or points of inflection can occur in $^2P^o$ scattering states at the 2 ^3P, 2 ^1P thresholds and in ^2S scattering states at the 2 ^3S, 2 ^1S thresholds.

Threshold cusps show up prominently in the computed 1 ^1S–2 ^1S excitation cross section shown in Fig. 17 (Oberoi and Nesbet, 1973b), at the $^{3,1}P$ thresholds. The rapid rise in cross section, starting at threshold, is due to the ^2D shape resonance, superimposed on a larger contribution from $^2P^o$ scattering, with threshold cusps. Resonance structure appears below the $n = 3$ threshold. The close-coupling calculation (Burke et al., 1969a) is also shown in Fig. 17, and would be in substantial agreement with a curve obtained from the variational calculations by smoothing out
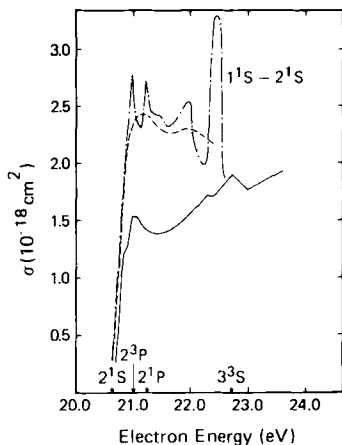
Fig. 17. e–He. $1\ ^1S \to 2\ ^1S$ excitation cross section. Curves: $-\cdot-\cdot$, Oberoi and Nesbet; $---$, Burke et al.; —, experimental, Brongersma et al.

threshold effects and omitting the $n = 3$ resonances. Comparison with experimental data (Brongersma et al., 1972) is less satisfactory for the $2\ ^1S$ excitation than for the $2\ ^3S$ excitation. Structure appears in the experimental curve, shown in Fig. 17, in the region of the $^{3,1}P$ thresholds and of the $n = 3$ resonances, but the general increase with increasing energy is not consistent with the computed excitation cross section. This discrepancy has not been resolved. It should be noted that the theoretical $2\ ^1S$ excitation curve is computed from the same multichannel K-matrices that give the $2\ ^3S$ excitation cross section shown in Fig. 16. Since this curve agrees closely with the experimental $2\ ^3S$ excitation function, it appears likely that the disagreement indicated in Fig. 17 is an artifact of the experimental data.

While expected from theory, Wigner cusps in the ^2S eigenphase sum at the $2\ ^3S$ and $2\ ^1S$ thresholds are not apparent in Fig. 15. Calculations on a finer scale near threshold would be required. Such cusps have been observed experimentally, in electron transmission measurements as structure in the total scattering cross section (Sanche and Schulz, 1972), and in the differential elastic cross section (Cvejanovic et al., 1973).

The smooth descent of the ^2S eigenphase sum from the $2\ ^3S$ threshold, shown in Fig. 15, is characteristic of threshold behavior in elastic scattering when a true bound state lies just below threshold. From Eqs. (129), (132), and (136) the phase shift δ_b would be given by

$$\tan \delta_b = -k/\kappa, \tag{150}$$

for a bound state at energy $-\kappa^2/2$ below threshold. In the present case, two channels are open, but the narrow ^{2}S resonance near 19.3 eV has the same analytic effect on the 2 ^{3}S channel opening at 19.82 eV as a similarly displaced bound state would have on a single elastic scattering channel. Ehrhardt et al. (1968) give a detailed argument based on Eq. (150) and on the assumption of weak coupling between the two ^{2}S eigenchannels near threshold, to account for s-wave structure at the 2 ^{3}S threshold observed in their experimental measurements of the differential excitation cross section. This structure appears at threshold in the 90° differential cross section computed from the eigenphases of Fig. 15. Computed differential cross sections are shown as functions of energy in Fig. 18. These calculations confirm the analysis of Ehrhardt et al. They show that the s-wave threshold structure is a consequence of the ^{2}S resonance below threshold, influencing the new eigenchannel phase shift through Eq. (150). Since the width of the 19.36 eV resonance is only 0.008 eV, the phase shift of this resonance has completed its rise through π radians at the threshold, and has no direct influence there. Thus the *width* of the 19.36 eV resonance is irrelevant to the observed structure, contrary to the qualitative argument given by Taylor (1970) who attributes this structure to an effect of the tail of the ^{2}S resonance extending beyond the 2 ^{3}S threshold.

The very sharp rise of the ^{2}S eigenphase sum at the 2 ^{1}S threshold, shown in Fig. 15, is an example of threshold behavior characteristic of a virtual state. As shown by Eq. (136), $\tan \delta_v$ rises linearly with k, but δ cannot rise more than $\pi/2$ radians. The slope at threshold is κ^{-1}, for a virtual state at energy $-\kappa^2/2$ below threshold, but displaced onto the nonphysical energy sheet. This corresponds to a potential well, without a barrier, that is not quite deep enough to produce a bound state. For s-wave scattering, Eq. (137) indicates that prominent cross section structure arises from a virtual state only if κ is quite small. Observed structure in e–He scattering has been associated with this virtual state near the 2 ^{1}S threshold by Ehrhardt et al. (1968). This virtual state was first identified by Burke et al. (1969a), whose close-coupling calculations indicated a sharp rise in the ^{2}S eigenphase commencing at the 2 ^{1}S threshold.

Computed excitation cross sections for the 2 ^{3}P and 2 ^{1}P states are shown in Fig. 19 (Oberoi and Nesbet, 1973b). The variational results are in close agreement with close-coupling calculations (Burke et al., 1969a), also shown in the figure, except for the resonance structure just below the $n = 3$ threshold. Experimental 2 ^{3}P and 2 ^{1}P excitation cross sections are in reasonable agreement with these theoretical curves (Hall et al., 1972).

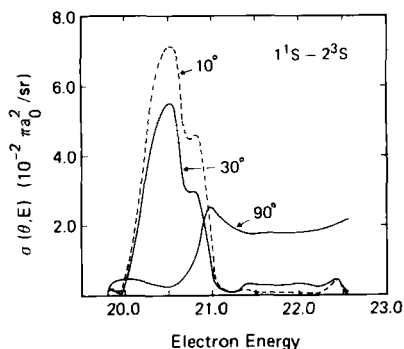The 2 ^{3}S de-excitation cross section computed by Oberoi and Nesbet

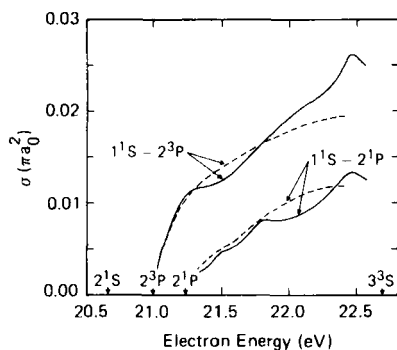**Fig. 18.** e–He. 1 ^{1}S → 2 ^{1}S differential cross section.

Fig. 19. e–He. 1 ^{1}S → 2 ^{3}P, 2 ^{1}P excitation cross sections. Curves: —, Oberoi and Nesbet; – – –, Burke *et al.*

(1973b) has been used to obtain theoretical values of the thermal deactivation rate constant for this process (Nesbet *et al.*, 1974).

C. Alkali Metal Atoms

A capsule review of theory and experimental data on low energy electron scattering by alkali metal atoms has been given recently by Bederson (1970a,b). A detailed critical review of relevant experimental techniques has been published (Bederson and Kieffer, 1971). The conclusion drawn from theoretical calculations and recent experiments is that measurements by Brode (1929) of the absolute e–K cross section were roughly twice too large at all energies, and showed spuriously exaggerated structure at the first excitation threshold. Since no comparable absolute experimental data were available until quite recently, there had

been an apparent discrepancy between theory and experiment that now is resolved in favor of theory (Bederson, 1970b).

In the elastic scattering region, electron scattering by the $(n_0 s)^2 S$ ground state of an alkali metal atom is dominated by the very large electric dipole polarizability typical of these atoms ($165 a_0^3$ for Na). The oscillator strength of the $n_0 s \rightarrow n_0 p$ optical transition is nearly unity, and the ground state polarizability is almost entirely accounted for by the transition dipole moment between these two states. In these circumstances, the two-state close-coupling expansion should give excellent results for elastic cross sections. Such calculations were carried out by Karule (1965) for elastic scattering by Li, Na, K, and Cs. Spin polarization and differential elastic cross sections have been computed from these close-coupling phase shifts, recently republished in a more accessible source (Karule, 1972). A two-state (2s, 2p) close-coupling calculation on e–Li scattering, extending into the inelastic region, was carried out by Burke and Taylor (1969). The elastic partial wave phase shifts were in agreement with those of Karule, except for a sharp peak just above threshold in the $^3 S$ phase shift computed by Burke and Taylor, similar to structure that might arise from a virtual state. This peak was shown to be a computational artifact by Norcross (1971), who repeated the $^3 S$ calculations with corrections for orthogonalization effects.

Norcross (1971) carried out two-state close-coupling calculations for both Li and Na, using an effective potential for the atomic ion core, and introducing a refined computational technique to improve the accuracy of calculations near threshold. This work was extended to the inelastic region for Na (up to 5 eV), including study of the effect of additional states (4s, 3d) in the close-coupling expansion (Moores and Norcross, 1972). Variational Bethe–Goldstone calculations by Sinfailam and Nesbet (1973) of elastic phase shifts for Li, Na, and K confirm these close-coupling results, which are in substantial internal agreement when corrected for the computational difficulties analyzed by Norcross (1971). Vo Ky Lan (1971) has shown that the polarized orbital method, including the exchange polarization potential, can reproduce the two-state close-coupling results for elastic e–Li scattering.

Figures 20–22 show computed values of the three lowest order partial wave phase shifts for Li (Sinfailam and Nesbet, 1973). Variational Bethe–Goldstone calculations are compared with two-state close-coupling calculations by Burke and Taylor (1969). The corrected $^3 S$ phase shift computed by Norcross (1971) is included in Fig. 20. With this correction, the close-coupling and variational phase shifts are in close agreement.
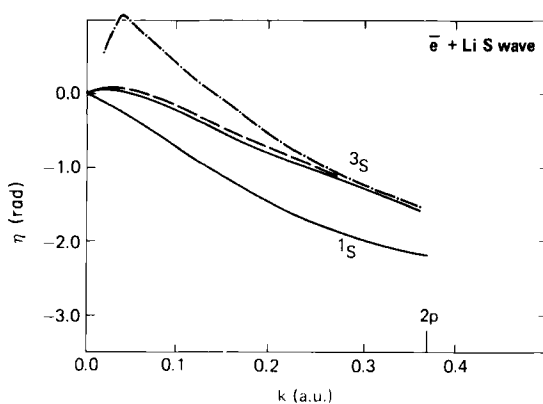
Fig. 20. e–Li. $l = 0$ elastic phase shifts. Curves: —, Sinfailam and Nesbet; – –, Norcross; – ·· –, Burke and Taylor.
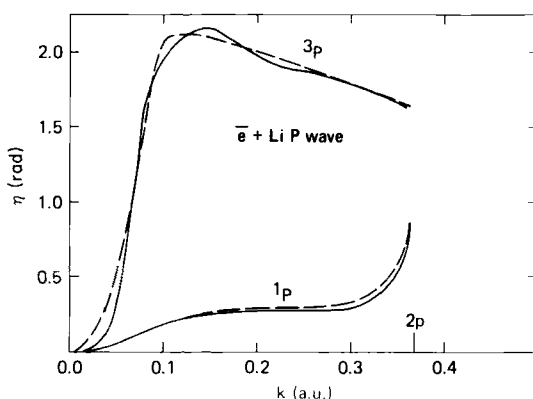

Fig. 21. e–Li. $l = 1$ elastic phase shifts. Curves: —, Sinfailam and Nesbet; – –, Burke and Taylor.

Figures 23–25 show a similar comparison for Na. Variational Bethe–Goldstone calculations (Sinfailam and Nesbet, 1973) give elastic e–Na phase shifts in substantial agreement with close-coupling results (Norcross, 1971; Moores and Norcross, 1972).

For a given partial wave, the phase shifts for Li and Na are very similar functions of k. This similarity holds for all of the alkali metal atoms. The ^1S phase shift descends linearly from its threshold value (which could be taken to be π radians) with negative initial slope, due to the ^1S ground state of the negative ion lying below the threshold. The ^3S
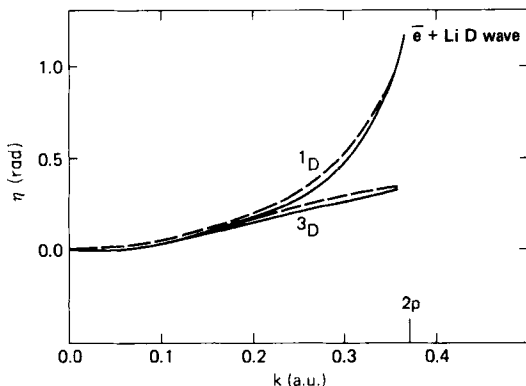
Fig. 22. e–Li. $l = 2$ elastic phase shifts. Curves: —, Sinfailam and Nesbet; – –, Burke and Taylor.
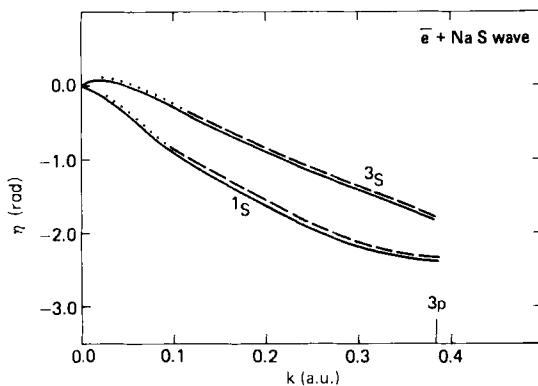
Fig. 23. e–Na. $l = 0$ elastic phase shifts. Curves: —, Sinfailam and Nesbet; – –, Moores and Norcross; ···, Norcross.

phase shift rises from threshold with positive slope, then passes through a low maximum and descends smoothly. The $^3P^o$ phase shift rises from threshold, following a somewhat truncated resonance curve. In the variational calculations (Sinfailam and Nesbet, 1973), the resonance search procedure of Nesbet and Lyons (1971) gave the following values for energy E_{res} and width Γ of the $^3P^o$ resonance:

$$Li^- \ \ E_{res} = 6.0 \times 10^{-2} \text{ eV}, \quad \Gamma = 5.7 \times 10^{-2} \text{ eV},$$

$$Na^- \ \ E_{res} = 8.3 \times 10^{-2} \text{ eV}, \quad \Gamma = 8.5 \times 10^{-2} \text{ eV},$$

$$K^- \ \ E_{res} = 2.4 \times 10^{-3} \text{ eV}, \quad \Gamma = 5.8 \times 10^{-4} \text{ eV}. \tag{151}$$
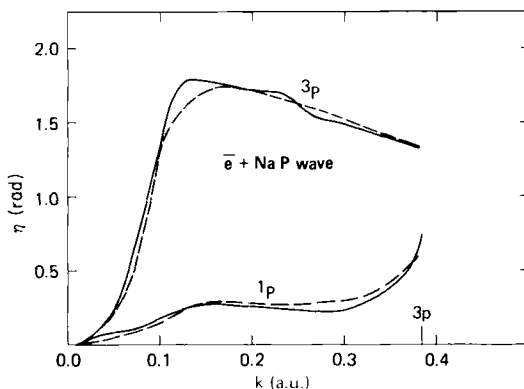
Fig. 24. e–Na. $l = 1$ elastic phase shifts. Curves: —, Sinfailam and Nesbet; – –, Moores and Norcross (3s–3p–4s–4d).
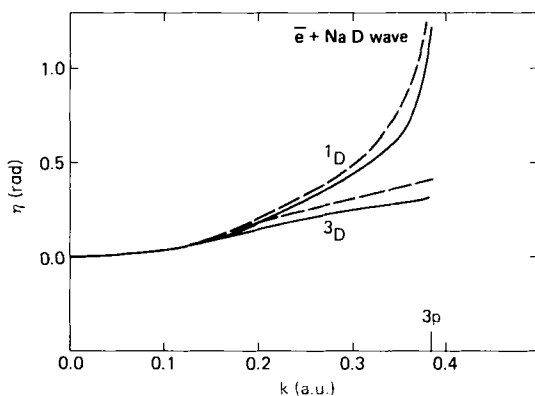

Fig. 25. e–Na. $l = 2$ elastic phase shifts. Curves: —, Sinfailam and Nesbet; – –, Moores and Norcross (3s–3p–4s–4d).

These resonances should correspond to the $(n_0 s \, n_0 p)^3 P^\circ$ first excited state of the isoelectronic alkaline earth atoms. Because of difficulties in defining low energy electron beams, there is no reliable experimental data close enough to the elastic threshold to identify these resonances.

The $^1 P^\circ$ and $^1 D$ phase shifts both rise sharply below the $n_0 p$ excitation threshold. As shown for Li in Fig. 5, this leads to a $^1 D$ resonance peak in the elastic cross section at or near threshold, and to a Wigner cusp superimposed on a $^1 P^\circ$ resonance peak (Bardsley and Nesbet, 1973), which may be associated with the $(n_0 s \, n_0 p)^1 P^\circ$ excited state of alkaline earth atoms. The effect of this threshold cusp in the $^1 P^\circ$ partial elastic
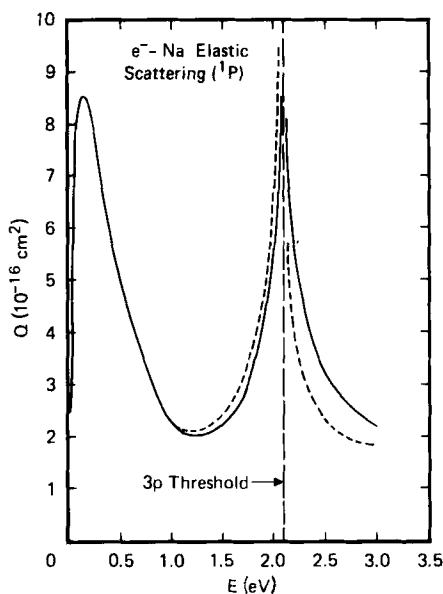
Fig. 26. e-Na. $^1P^o$ partial elastic cross section (Norcross and Moores, 1973, Figure 2; reprinted by permission). Curves: — 3s, 3p; - - -, 3s, 3p, 3d, 4s.

cross section, computed for Na, is shown in Fig. 26 (Norcross and Moores, 1973). The photodetachment cross section computed by Norcross and Moores is shown in Fig. 27. Since photodetachment proceeds by optical absorption from the ^1S negative ion ground state, the $^1P^o$ continuum state is singled out by optical selection rules. Since the np_o threshold is known to high precision with respect to the ns_o atomic ground state, observation of this cusp in photodetachment provides a precise measurement of the electron affinity of the neutral atom. Patterson *et al.* (1974) have used this technique to obtain accurate values of electron affinities of the alkali metal atoms. Narrow resonances are observed in these experiments near the excitation thresholds. This threshold structure has also been observed in the differential elastic cross section (Andrick *et al.*, 1972).

The total e-Na cross section computed by Moores and Norcross (1972) is shown in Fig. 28, compared with experimental data (Kasdan *et al.*, 1973) and with two-state close-coupling calculations (Karule, 1965; Karule and Peterkop, 1965). The theoretical cross section shows structure just above the elastic threshold due to the $^3P^o$ resonance, and a Wigner cusp at the 3p threshold. The most recent data follows the theoretical
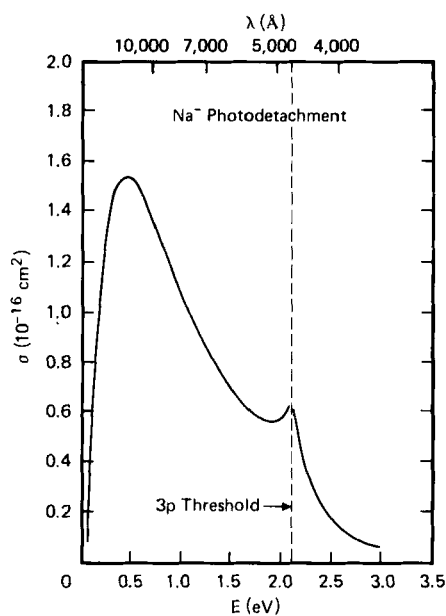
Fig. 27. e–Na. Photodetachment cross section (Norcross and Moores, 1973, Figure 4; reprinted by permission).
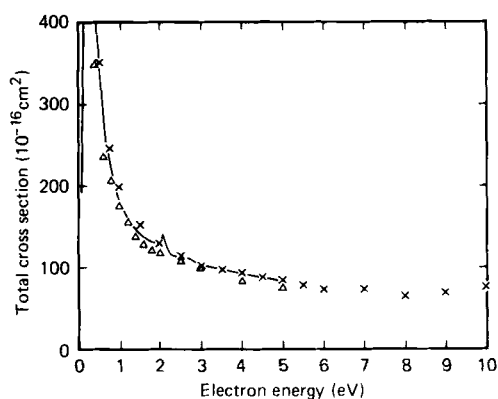

Fig. 28. e–Na. Total cross section (Kasdan *et al.*, 1973, Figure 4). ×, Present experiment; △, Karule and Peterkop; —, Moores and Norcross.

curve quite closely, but does not extend to low enough energy to trace out the $^3P^o$ resonance (Kasdan *et al.*, 1973). Good agreement with the e–Na differential cross section computed by Moores and Norcross is found in experiments by Gehenn and Reichert (1972). In computing the differential cross section, low-order phase shifts computed by two-state or four-state close-coupling were augmented by phase shifts up to $l = 150$ obtained from the partial wave Born approximation (Moores and Norcross, 1972).

Spin-dependent cross sections, relevant to experiments with state selection or alignment of incident beams, and spin analysis of recoil atoms or scattered electrons, can be computed from the theoretical phase shifts or T-matrices. Formulas for elastic scattering are given by Burke and Taylor (1969) and for inelastic scattering by Moores and Norcross (1972). These are all special cases of the general formula for the scattering amplitude, Eq. (34) here. The depolarization ratio $d(\theta)$, which measures the fractional loss of polarization by the incident electron or target atom as a result of collision, has been tabulated from two-state close-coupling calculations on Li, Na, K, and Cs by Karule (1972). Karule also tabulates the computed total spin exchange cross section

$$\sigma_{se} = \frac{\pi}{k^2} \sum_l (2l + 1)\sin^2(\delta_l^+ - \delta_l^-), \qquad (152)$$

where δ_l^+, δ_l^- are, respectively, the singlet and triplet partial wave phase shifts of angular momentum l. Direct and exchange scattering amplitudes are tabulated for Na in the energy range 0–5 eV by Moores and Norcross (1972). Collins *et al.* (1971) have measured the spin exchange cross section for e–K scattering, at four energies between 0.5 and 1.2 eV. This data is in good agreement with theoretical calculations of Karule (1972) and of Sinfailam and Nesbet (1973).

Hils *et al.* (1972) have measured the differential spin polarization of electrons scattered from polarized K atoms, at incident energy 3.3 eV. This determines the direct scattering coefficient $|f(\theta)|^2$, which is compared with two-state close-coupling calculations for energies above the first excitation threshold (Karule and Peterkop, 1965). There is general agreement between experimental and theoretical data, except for a relative shift in the angular dependence. This may be attributed to a need for more states in the close-coupling expansion, when applied above the first inelastic threshold. The differential elastic scattering cross section of Hils *et al.* is in close agreement with measurements of Gehenn and Wilmers (1971) at 3.1 eV.

D. C, N, O

Experimental measurements of electron scattering by these atoms require molecular dissociation. The few experiments that have been carried out at low energies are reviewed by Bederson and Kieffer (1971). No experiment of reasonably high precision has been performed, but e–N experiments (Neynaber *et al.*, 1963) and e–O experiments (Neynaber *et al.*, 1961; Sunshine *et al.*, 1967) give the general trend of the total ground state cross sections for low impact energies. There are no comparable experiments on e–C scattering.

Because of the open-shell structure $(2p^n)$ of the ground state configuration of these atoms, there are several distinct target states in the low energy range. In this respect, the theoretical problem is comparable to that presented by e–He scattering in the region of the $n = 2$ states. Electric dipole polarizabilities are much smaller than in the case of alkali metals, but polarization potentials are still the dominant scattering mechanism at low impact energy. The ^3P ground states of C and 0 also have a long-range static quadrupole potential, which couples partial waves l and $l \pm 2$ even for elastic scattering. For these atoms, theoretical methods must take polarization and static multipole effects into account in a formalism suitable for multichannel scattering.

The polarized orbital method was originally applied by Temkin (1957) to a calculation of the s-wave contribution to the e–O elastic scattering cross section. Temkin included only the $2p \rightarrow d$ part of the electric dipole polarizability. This work was completed by Henry (1967), who included $2p \rightarrow s$ and $2s \rightarrow p$ polarization effects, and extended the calculations to partial waves with $l \leq 2$. Higher partial wave contributions to the cross section were estimated from the Born formula, Eq. (148). The total elastic cross section computed by Henry is shown in Fig. 29, in comparison with other theoretical calculations and with experimental total cross section data (Sunshine *et al.*, 1967). The experimental points, with estimated error of 20%, do not define a smooth curve. The very low values of the cross section near threshold computed by Henry are in agreement with the value 2×10^{-16} cm^2 $(2.3\pi a_0^2)$ at 0.5 eV, deduced from shock tube measurements (Lin and Kivel, 1959).

Close-coupling calculations, including all states of the ground configuration, were first carried out for e–O scattering by Smith *et al.* (1967). An algebraic error in this work was corrected in subsequent calculations by Henry *et al.* (1969). These results agree closely with a matrix variational calculation, in the static exchange (single configuration) approximation (Thomas *et al.*, 1974). This computed total cross section is
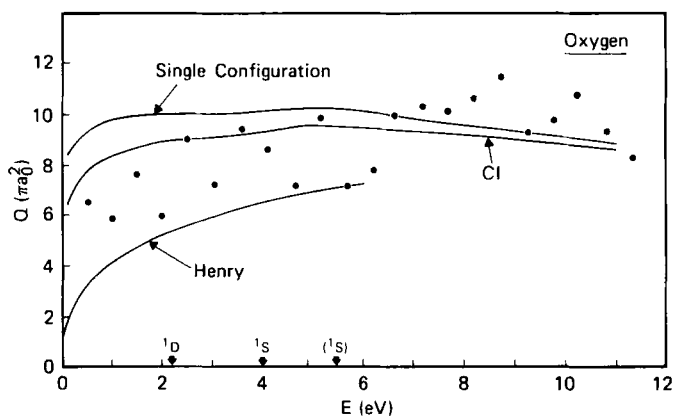
Fig. 29. e-O. Total cross section.

shown in Fig. 29. The static exchange approximation neglects the atomic polarizability. The resulting cross section is much too large at threshold, and apparently too large for energies up to 8 eV.

The current challenge to theory, for e-O scattering, is to find a computationally feasible way to include polarization effects in a multichannel formalism that can give reliable results for threshold effects and resonances. The matrix variational method can in principle include all of these effects. Results obtained allowing only for 2p-2s near degeneracy effects are shown as the curve labeled CI in Fig. 29 (Thomas *et al.*, 1974). In these calculations, configurations $2s^2 2p^4$, $2s2p^5$, and $2p^6$ were included in the target state variational basis. The second of these acts as a dipole polarizability pseudostate, and the third displaces the ^1S threshold relative to the other atomic states (^3P and ^1D). In Fig. 29, (^1S) denotes this threshold in the single configuration approximation computed with ^3P Hartree-Fock orbitals 2s and 2p. This threshold moves down to the value labeled ^1S in the CI calculations. The total cross section curve for these CI calculations is displaced downward from the static exchange curve, but only a fraction of the distance to the polarized orbital curve.

Recent calculations by a multichannel polarized orbital method (Vo Ky Lan *et al.*, 1972) obtain values of the total ground state e-O cross section that rise from approximately $6\pi a_0^2$ at 0.5 eV to approximately $8\pi a_0^2$ in a broad range extending from 4 to 12 eV. These results lie between the CI and polarized orbital (Henry, 1967) curves shown in Fig. 29, but apparently do not yet take the effect of polarization fully into account in the lowest energy range. A close-coupling calculation by Saraph (1973)

includes effects of target atom configuration interaction through configurations $2p^6$ and $2s2p^4$ 3d, and adds configurations constructed from 2s, 2p, and 3d orbitals to the Hilbert space component of the scattering wave function. The resulting cross section curve is somewhat below the CI curve shown in Fig. 29, but is still above $5\pi a_0^2$ at threshold.

Values of the e–O cross section close to the polarized orbital curve at low energies have been obtained in exploratory matrix variational calculations that include all effects of single virtual excitations of 2s and 2p orbitals (Thomas and Nesbet, 1974). A more limited expansion of close-coupling states (Rountree *et al.*, 1974) also shows a significant lowering of the cross section as a result of 2p virtual excitations. These preliminary results indicate that the polarized orbital cross section of Henry (1967) is qualitatively correct, and that the experimental value of Lin and Kivel (1959), $2.3\pi a_0^2$ at 0.5 eV, is a good estimate of the true cross section at that energy.

Calculated and experimental values (Neynaber *et al.*, 1963) of the total cross section for e–N scattering are shown in Fig. 30. The static exchange and CI results are obtained by matrix variational calculations (Thomas *et al.*, 1974). The CI calculation includes target configurations $2s^2 2p^3$, $2s2p^4$, and $2p^5$. This displaces the ^2P threshold from the value denoted by (^2P) obtained in the single configuration (static exchange) calculation. The variational single configuration cross section agrees
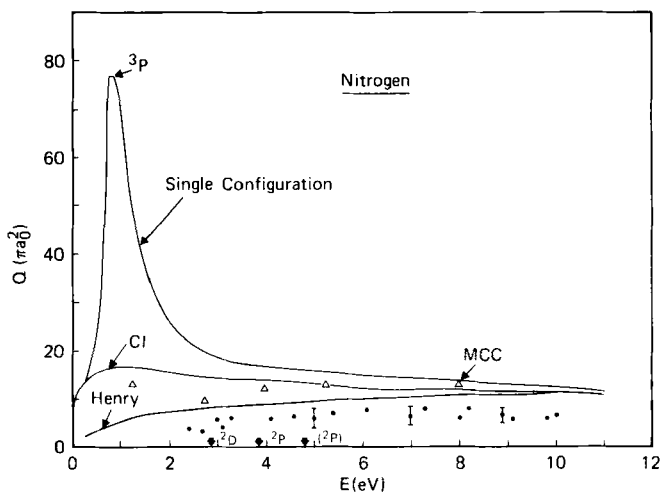

Fig. 30. e–N. Total cross section.

closely with the close-coupling results of Henry *et al.* (1969). Detailed analysis of the CI calculation shows that the prominent ^{3}P resonance has moved downward to become a weakly bound state of the negative ion. A small change of electronic correlation energy could make this a very narrow resonance just above threshold. This is in agreement with the fact that this state of N$^-$ has never been observed.

The polarized orbital e–N elastic cross section curve of Henry (1968), shown in Fig. 30, lies well below the CI curve, especially in the threshold region. As in the case of the e–O cross section, this indicates a substantial effect of target atom polarizability. Polarization effects are partially included by extension of the close-coupling expansion in the MCC (multiconfiguration close-coupling) total cross section curve (Ormonde *et al.*, 1973), shown in Fig. 30. Definitive results will require full inclusion of 2p and 2s polarization terms in the scattering wave function.

Total cross sections for e–C scattering are shown in Fig. 31. No experimental data is available. The theoretical static exchange (single configuration) and CI results are obtained by matrix variational calculations (Thomas *et al.*, 1974). This CI calculation includes target configurations 2s^{2}2p^2, 2s2p^3, and 2p^4. This introduces the ^{5}S$^\circ$ state and displaces the ^{1}S threshold significantly from its single configuration value, denoted by (^{1}S). The principal effect of the CI calculation is to displace the ^{2}D$^\circ$ resonance below threshold, and to move the ^{2}P$^\circ$ resonance
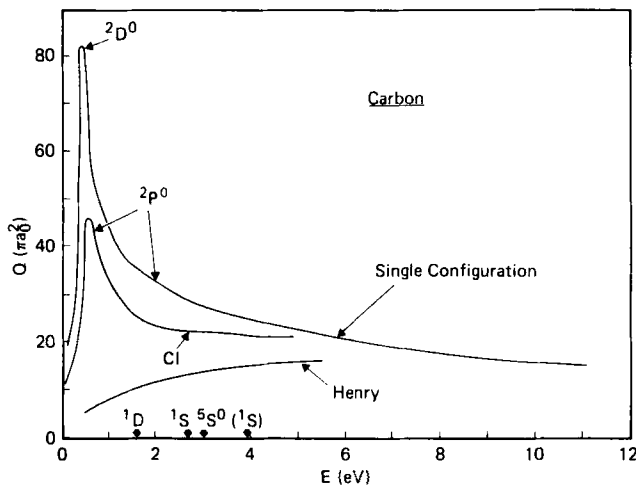

Fig. 31. e–C. Total cross section.

(appearing as a shoulder on the single configuration curve) downward in energy. This is in agreement with recent experimental data indicating that the $^2D^\circ$ state of C^- is bound by 0.035 eV (Ilin, 1973). Comparison with polarized orbital calculations (Henry, 1968) indicates that substantial polarization effects are omitted in the CI wavefunction, which contains only the $2s2p^3$ pseudostate configuration. As in the case of N and O, further 2p and 2s polarization terms must be included to obtain correct results near threshold.

REFERENCES

Andrick, D. (1973). *Advan. At. Mol. Phys.* **9**, 207.
Andrick, D., and Bitsch, A. (1975). *J. Phys. B* **8**, 393.
Andrick, D., Eyb, M., and Hofmann, H. (1972). *J. Phys. B* **5**, L15.
Andrick, D., Bitsch, A., and Eyb, M. (1973). (To be published).
Baranger, E., and Gerjuoy, E. (1957). *Phys. Rev.* **106**, 1182.
Bardsley, J. N., and Nesbet, R. K. (1973). *Phys. Rev. A* **8**, 203.
Baz, A. I. (1957). *Zh. Eksp. Teor. Fiz.* **33**, 923 [*Sov. Phys.—JETP* **6**, 709 (1958)].
Bederson, B. (1970a). *Comments At. Mol. Phys.* **1**, 135.
Bederson, B. (1970b). *Comments At. Mol. Phys.* **2**, 7.
Bederson, B., and Kieffer, L. J. (1971). *Rev. Mod. Phys.* **43**, 601.
Bethe, H. A., and Goldstone, J. (1957). *Proc. Roy. Soc., Ser. A* **238**, 551.
Bhatia, A. K. (1974). *Phys. Rev. A* **9**, 9.
Blatt, J. M., and Biedenharn, L. C. (1952). *Rev. Mod. Phys.* **24**, 258.
Brandsden, B. H. (1970). "Atomic Collision Theory." Benjamin, New York.
Brandsden, B. H., and McDowell, M. R. C. (1969). *J. Phys. B* **2**, 1187.
Brode, R. (1929). *Phys. Rev.* **34**, 673.
Brongersma, H. H., Knoop, F. W. E., and Backx, C. (1972). *Chem. Phys. Lett.* **13**, 16.
Brueckner, K. A. (1959). *In* "The Many-Body Problem" (B. deWitt, ed.), pp. 47–241. Wiley, New York.
Burke, P. G. (1965). *Advan. Phys.* **14**, 521.
Burke, P. G. (1968). *Advan. At. Mol. Phys.* **4**, 173.
Burke, P. G. (1972). *Comments At. Mol. Phys.* **3**, 31.
Burke, P. G. (1973). *Comput. Phys. Commun.* **6**, 288.
Burke, P. G., and Mitchell, J. F. B. (1973). *J. Phys. B* **6**, 320.
Burke, P. G., and Robb, W. D. (1972). *J. Phys. B* **5**, 44.
Burke, P. G., and Schey, H. M. (1962a). *Phys. Rev.* **126**, 147.
Burke, P. G., and Schey, H. M. (1962b). *Phys. Rev.* **126**, 163.
Burke, P. G., and Seaton, M. J. (1971). *Methods Comput. Phys.* **10**, 1.
Burke, P. G., and Smith, K. (1962). *Rev. Mod. Phys.* **34**, 458.
Burke, P. G., and Taylor, A. J. (1969). *J. Phys. B* **2**, 869.
Burke, P. G., and Webb, T. G. (1970). *J. Phys. B* **3**, L131.
Burke, P. G., Cooper, J. W., and Ormonde, S. (1969a). *Phys. Rev.* **183**, 245.
Burke, P. G., Gallaher, D. F., and Geltman, S. (1969b). *J. Phys. B* **2**, 1142.

Burke, P. G., Hibbert, A., and Robb, W. D. (1971). *J. Phys. B* **4**, 1153.

Buttle, P. J. A. (1967). *Phys. Rev.* **160**, 719.

Callaway, J. (1973). *Comput. Phys. Commun.* **6**, 265.

Callaway, J., LaBahn, R. W., Pu, R. T., and Duxler, W. M. (1968). *Phys. Rev.* **168**, 12.

Chen, J. C. Y., and Chung, K. T. (1970). *Phys. Rev. A* **2**, 1892.

Chen, J. C. Y., Chung, K. T., and Sinfailam, A. L. (1971). *Phys. Rev. A* **4**, 1517.

Chung, K. T., and Chen, J. C. Y. (1971). *Phys. Rev. Lett.* **27**, 1112.

Chung, K. T., and Chen, J. C. Y. (1972). *Phys. Rev. A* **6**, 686.

Collins, R. E., Bederson, B., and Goldstein, M. (1971). *Phys. Rev. A* **3**, 1976.

Crompton, R. W., Elford, M. T., and Jory, R. L. (1967). *Aust. J. Phys.* **20**, 369.

Crompton, R. W., Elford, M. T., and Robertson, A. G. (1970). *Aust. J. Phys.* **23**, 667.

Csanak, G., and Taylor, H. S. (1972). *Phys. Rev. A* **6**, 1843.

Csanak, G., and Taylor, H. S. (1973). *J. Phys. B* **6**, 2055.

Csanak, G., Taylor, H. S., and Yaris, R. (1971a). *Phys. Rev. A* **3**, 1322.

Csanak, G., Taylor, H. S., and Yaris, R. (1971b). *Advan. At. Mol. Phys.* **7**, 287.

Csanak, G., Taylor, H. S., and Tripathy, D. N. (1973). *J. Phys. B* **6**, 2040.

Cvejanovic, S., Comer, J., and Read, F. H. (1974). *J. Phys. B* **7**, 468.

Dalgarno, A., and Kingston, A. E. (1958). *Proc. Phys. Soc., London, Sect. A* **72**, 1053.

Damburg, R. J., and Geltman, S. (1968). *Phys. Rev. Lett.* **20**, 485.

Damburg, R. J., and Karule, E. (1967). *Proc. Phys. Soc., London* **90**, 637.

Dorrestein, R. (1942). *Physica (Utrecht)* **9**, 447.

Drachman, R. J. (1968). *Phys. Rev.* **173**, 190.

Drachman, R. J., and Temkin, A. (1972). *In* "Case Studies in Atomic Collision Physics" (E. W. McDaniel and M. R. C. McDowell, eds.), Vol. 2, pp. 399–481. North-Holland Publ., Amsterdam.

Duxler, W. M., Poe, R. T., and LaBahn, R. W. (1971). *Phys. Rev. A* **4**, 1395.

Ehrhardt, H., and Willmann, K. (1967). *Z. Phys.* **203**, 1.

Ehrhardt, H., Langhans, L., and Linder, F. (1968). *Z. Phys.* **214**, 179.

Fano, U. (1961). *Phys. Rev.* **124**, 1866.

Fano, U., and Cooper, J. W. (1965). *Phys. Rev. A* **137**, 1364.

Fano, U., and Lee, C. M. (1973). *Phys. Rev. Lett.* **31**, 1573.

Feautrier, N., Van Regemorter, H., and Vo Ky Lan (1971). *J. Phys. B* **4**, 670.

Fels, M. F., and Hazi, A. U. (1971). *Phys. Rev. A* **4**, 662.

Fels, M. F., and Hazi, A. U. (1972). *Phys. Rev. A* **5**, 1236.

Feshbach, H. (1958). *Ann. Phys. (New York)* **5**, 357.

Feshbach, H. (1962). *Ann. Phys. (New York)* **19**, 287.

Gailitis, M. (1964). *Zh. Eksp. Teor. Fiz.* **47**, 160 [*Sov. Phys.—JETP* **20**, 107 (1965)].

Gehenn, W., and Reichert, E. (1972). *Z. Phys.* **254**, 28.

Gehenn, W., and Wilmers, M. (1971). *Z. Phys.* **244**, 395.

Geltman, S. (1969). "Topics in Atomic Collision Theory." Academic Press, New York.

Geltman, S., and Burke, P. G. (1970). *J. Phys. B* **3**, 1062.

Gibson, J. R., and Dolder, K. T. (1969). *J. Phys. B* **2**, 741.

Golden, D. E., and Bandel, H. W. (1965). *Phys. Rev. A* **138**, 14.

Golden, D. E., and Zecca, A. (1971). *Rev. Sci. Instrum.* **42**, 210.

Gomes, L. C., Walecka, J. D., and Weisskopf, V. F. (1958). *Ann. Phys. (New York)* **3**, 241.

Hahn, Y. (1971). *Phys. Rev. A* **4**, 1881.

Hahn, Y., and Spruch, L. (1967). *Phys. Rev.* **153**, 1159.

Hahn, Y., O'Malley, T. F., and Spruch, L. (1962). *Phys. Rev.* **128**, 932.

Hahn, Y., O'Malley, T. F., and Spruch, L. (1963). *Phys. Rev.* **130**, 381.

Hahn, Y., O'Malley, T. F., and Spruch, L. (1964a). *Phys. Rev.* **134**, B397.

Hahn, Y., O'Malley, T. F., and Spruch, L. (1964b). *Phys. Rev.* **134**, B911.

Hall, R. I., Reinhardt, J., Joyez, G., and Mazeau, J. (1972). *J. Phys. B* **5**, 66.

Harris, F. E. (1967). *Phys. Rev. Lett.* **19**, 173.

Harris, F. E., and Michels, H. H. (1969a). *Phys. Rev. Lett.* **22**, 1036.

Harris, F. E., and Michels, H. H. (1969b). *J. Comput. Phys.* **4**, 579.

Harris, F. E., and Michels, H. H. (1971). *Methods Comput. Phys.* **10**, 143.

Hazi, A. U., and Fels, M. F. (1971). *Chem. Phys. Lett.* **8**, 582.

Hazi, A. U., and Taylor, H. S. (1970). *Phys. Rev. A* **1**, 1109.

Henry, R. J. W. (1967). *Phys. Rev.* **162**, 56.

Henry, R. J. W. (1968). *Phys. Rev.* **172**, 99.

Henry, R. J. W., Burke, P. G., and Sinfailam, A. L. (1969). *Phys. Rev.* **178**, 218.

Hils, D., McCusker, M. V., Kleinpoppen, H., and Smith, S. J. (1972). *Phys. Rev. Lett.* **29**, 398.

Holøien, E. (1958a). *Proc. Phys. Soc., London, Sect. A* **71**, 357.

Holøien, E. (1958b). *Proc. Phys. Soc., London, Sect. A* **72**, 141.

Holøien, E. (1961). *Phys. Norv.* **1**, 56.

Holøien, E., and Midtdal, J. (1970). *J. Phys. B* **3**, 592.

Holøien, E., and Midtdal, J. (1971). *J. Phys. B* **4**, 32.

Ilin, R. N. (1973). *In* "Atomic Physics 3" (S. J. Smith and G. K. Walters, eds.), pp. 309–326. Plenum, New York.

Jacob, M., and Wick, G. C. (1959). *Ann. Phys. (New York)* **7**, 404.

Karule, E. M. (1965). *In* "Cross Sections of Electron-Atom Collisions" (V. Veldre, ed.), pp. 33–56. Latv. Acad. Sci., Riga.

Karule, E. (1972). *J. Phys. B* **5**, 2051.

Karule, E. M., and Peterkop, R. K. (1965). *In* "Cross Sections of Electron-Atom Collisions" (V. Veldre, ed.), pp. 3–32. Latv. Acad. Sci., Riga.

Kasdan, A., Miller, T. M., and Bederson, B. (1973). *Phys. Rev. A* **8**, 1562.

Kato, T. (1951). *Progr. Theor. Phys.* **6**, 394.

Kelly, H. P. (1967). *Phys. Rev.* **160**, 44.

Kelly, H. P. (1968). *Phys. Rev.* **171**, 54.

Klar, H. (1969). *Z. Phys.* **228**, 59.

Klar, H. (1971). *Nuovo Cimento A* **4**, 529.

Knowles, M., and McDowell, M. R. C. (1973). *J. Phys. B* **6**, 300.

Kohn, W. (1948). *Phys. Rev.* **74**, 1763.

LaBahn, R. W., and Callaway, J. (1964). *Phys. Rev. A* **135**, 1539.

LaBahn, R. W., and Callaway, J. (1966). *Phys. Rev.* **147**, 28.

Lane, A. M., and Thomas, R. G. (1958). *Rev. Mod. Phys.* **30**, 257.

Levy, B. R., and Keller, J. B. (1963). *J. Math. Phys.* **4**, 54.

Lin, S. C., and Kivel, B. (1959). *Phys. Rev.* **114**, 1026.

Lyons, J. D., and Nesbet, R. K. (1969). *J. Comput. Phys.* **4**, 499.

Lyons, J. D., and Nesbet, R. K. (1973). *J. Comput. Phys.* **11**, 166.

Lyons, J. D., Nesbet, R. K., Rankin, C. C., and Yates, A. C. (1973). *J. Comput. Phys.* **13**, 229.

Macek, J. (1970). *Phys. Rev. A* **2**, 1101.

McVoy, K. (1967). *In* "Fundamentals in Nuclear Theory" (A. De-Shalit and C. Villi, eds.), pp. 419–498. IAEA, Vienna.

Massey, H. S. W., and Mohr, C. B. O. (1932). *Proc. Roy. Soc., Ser A* **136**, 289.

Michels, H. H., Harris, F. E., and Scolsky, R. N. (1969). *Phys. Lett. A* **28**, 467.

Miller, W. H. (1966). *Phys. Rev.* **152**, 70.

Miller, W. H. (1969). *J. Chem. Phys.* **50**, 407.

Miller, W. H. (1970). *Chem. Phys. Lett.* **4**, 627.

Mittleman, M. H. (1966). *Phys. Rev.* **147**, 69.

Moores, D. L., and Norcross, D. W. (1972). *J. Phys. B* **5**, 1482.

Mott, N. F., and Massey, H. S. W. (1965). "The Theory of Atomic Collisions." Oxford Univ. Press, London and New York.

Nesbet, R. K. (1967). *Phys. Rev.* **156**, 99.

Nesbet, R. K. (1968). *Phys. Rev.* **175**, 134.

Nesbet, R. K. (1969a). *Phys. Rev.* **179**, 60.

Nesbet, R. K. (1969b). *Advan. Chem. Phys.* **14**, 1.

Nesbet, R. K. (1970). *Phys. Rev. A* **2**, 661.

Nesbet, R. K. (1971). *J. Comput. Phys.* **8**, 483.

Nesbet, R. K. (1973). *Comput. Phys. Commun.* **6**, 275.

Nesbet, R. K., and Lyons, J. D. (1971). *Phys. Rev. A* **4**, 1812.

Nesbet, R. K., and Oberoi, R. S. (1972). *Phys. Rev. A* **6**, 1855.

Nesbet, R. K., Oberoi, R. S., and Bardsley, J. N. (1974). *Chem. Phys. Lett.* **25**, 587.

Newton, R. G. (1966). "Scattering Theory of Waves and Particles." McGraw-Hill, New York.

Neynaber, R. H., Marino, L. L., Rothe, E. W., and Trujillo, S. M. (1961). *Phys. Rev.* **123**, 148.

Neynaber, R. H., Marino, L. L., Rothe, E. W., and Trujillo, S. M. (1963). *Phys. Rev.* **129**, 2069.

Norcross, D. W. (1971). *J. Phys. B* **4**, 1458.

Norcross, D. W., and Moores, D. L. (1973). *In* "Atomic Physics 3" (S. J. Smith and G. K. Walters, eds.), pp. 261–267. Plenum, New York.

Oberoi, R. S., and Nesbet, R. K. (1973a). *Phys. Rev. A* **8**, 215.

Oberoi, R. S., and Nesbet, R. K. (1973b). *Phys. Rev. A* **8**, 2969.

Oberoi, R. S., and Nesbet, R. K. (1974). *Phys. Rev. A* **9**, 2804.

O'Malley, T. F., and Geltman, S. (1965). *Phys. Rev. A* **137**, 1344.

O'Malley, T. F., Spruch, L., and Rosenberg, L. (1961). *J. Math. Phys.* **2**, 491.

Ormonde, S., Smith, K., Torres, B. W., and Davies, A. R. (1973). *Phys. Rev.* **8**, 262.

Patterson, T. A., Hotop, H., Kasdan, A., Norcross, D. W., and Lineberger, W. C. (1974). *Phys. Rev. Lett.* **32**, 189.

Percival, I. C., and Seaton, M. J. (1957). *Proc. Cambridge Phil. Soc.* **53**, 654.

Pichanick, F. M. J., and Simpson, J. A. (1968). *Phys. Rev.* **168**, 64.

Pu, R. T., and Chang, E. (1966). *Phys. Rev.* **151**, 31.

Ross, M., and Shaw, G. (1961). *Ann. Phys. (New York)* **13**, 147.

Rountree, S. P., Smith, E. R., and Henry, R. J. W. (1974). *J. Phys. B* **7**, L167.

Rudge, M. R. H. (1973). *Advan. At. Mol. Phys.* **9**, 47.

Sanche, L., and Schulz, G. J. (1972). *Phys. Rev. A* **5**, 1672.

Saraph, H. E. (1973). *J. Phys. B* **6**, L243.

Saraph, H. E., Seaton, M. J., and Shemming, J. (1969). *Phil. Trans. Roy. Soc. London, Ser. A* **264**, 77.

Schneider, B., Taylor, H. S., and Yaris, R. (1970). *Phys. Rev. A* **1**, 855.

Schulz, G. J. (1963). *Phys. Rev. Lett.* **10**, 104.

Schulz, G. J. (1973). *Rev. Mod. Phys.* **45**, 378.

Schulz, G. J., and Fox, R. E. (1957). *Phys. Rev.* **106**, 1179.

Schwartz, C. (1961a). *Ann. Phys. (New York)* **16**, 36.

Schwartz, C. (1961b). *Phys. Rev.* **124**, 1468.

Schwinger, J. (1951). *Proc. Nat. Acad. Sci. U.S.* **37**, 452.

Seaton, M. J. (1953a). *Phil. Trans. Roy. Soc. London, Ser. A* **245**, 469.

Seaton, M. J. (1953b). *Proc. Roy. Soc., Ser. A* **218**, 400.

Seaton, M. J. (1955). *Proc. Roy. Soc., Ser. A* **231**, 37.

Seaton, M. J. (1961). *Proc. Phys. Soc., London* **77**, 174.

Seaton, M. J. (1966). *Proc. Phys. Soc., London* **89**, 469.

Seiler, G. J., Oberoi, R. S., and Callaway, J. (1971). *Phys. Rev. A* **3**, 2006.

Sinfailam, A. L., and Nesbet, R. K. (1972). *Phys. Rev. A* **6**, 2118.

Sinfailam, A. L., and Nesbet, R. K. (1973). *Phys. Rev. A* **7**, 1987.

Sklarew, R. C., and Callaway, J. (1968). *Phys. Rev.* **175**, 103.

Sloan, I. H. (1964). *Proc. Roy. Soc., Ser. A* **281**, 151.

Smith, K. (1971). "The Calculation of Atomic Collision Processes." Wiley (Interscience), New York.

Smith, K., Henry, R. J. W., and Burke, P. G. (1967). *Phys. Rev.* **157**, 51.

Sugar, R., and Blankenbecler, R. (1964). *Phys. Rev. B* **136**, 472.

Sunshine, G., Aubrey, B. B., and Bederson, B. (1967). *Phys. Rev.* **154**, 1.

Taylor, H. S. (1970). *Advan. Chem. Phys.* **18**, 91.

Temkin, A. (1957). *Phys. Rev.* **107**, 1004.

Temkin, A. (1959). *Phys. Rev.* **116**, 358.

Temkin, A., and Lamkin, J. C. (1961). *Phys. Rev.* **121**, 788.

Temkin, A., Bhatia, A. K., and Bardsley, J. N. (1972). *Phys. Rev. A* **5**, 1663.

Thomas, L. D., and Nesbet, R. K. (1974). Unpublished observations.

Thomas, L. D., Oberoi, R. S., and Nesbet, R. K. (1974). *Phys. Rev. A* **10**, 1605.

Thomas, L. D., Yarlagadda, B. S., Csanak, G., and Taylor, H. S. (1973). *Comput. Phys. Commun.* **6**, 316.

Thomas, L. D., Csanak, G., Taylor, H. S., and Yarlagadda, B. S. (1974). *J. Phys. B* **7**, 1719.

Thompson, D. G. (1966). *Proc. Roy. Soc., Ser. A* **294**, 160.

Truhlar, D. G., and Smith, R. L. (1972). *Phys. Rev. A* **6**, 233.

Van Regemorter, H. (1973). *Comput. Phys. Commun.* **6**, 245.

Vo Ky Lan (1971). *J. Phys. B* **4**, 658.

Vo Ky Lan, Feautrier, N., Le Dourneuf, M., and Van Regemorter, H. (1972). *J. Phys. B* **5**, 1506.

Wigner, E. P. (1948). *Phys. Rev.* **73**, 1002.

Wigner, E. P., and Eisenbud, L. (1947). *Phys. Rev.* **72**, 29.

Yarlagadda, B. S., Csanak, G., Taylor, H. S., Schneider, B., and Yaris, R. (1973). *Phys. Rev. A* **7**, 146.

SUBJECT INDEX

A

Alkali metal atoms, energy scattering
studies on, 281–288
AO basis, in excited state calculations,
70–74

C

Carbon, energy-scattering studies on,
289–293
CI techniques, for electronic spectral
calculations, 69–104
for restricted MO basis, 78–82
Coupled-channel studies, of energy
transfer, 199–214
Coupled equations, in collision
dynamics, 202–208
Cross sections, in energy transfer
studies, 208–212

E

Electron affinities, perturbation theory
for, 169–177
Electron scattering, low-energy, theory
of, 215–297
Electronic spectral calculations
CI techniques used in, 69–104
interpretation of, 94–97
for systems with twelve valence
electrons, 83–102
Electronic transitions, structural
characteristics of, 97–100
Energy transfer, rotational and
vibrational, by collision, 199–214
Ethylene, electronic spectra of, 88–91
Excited state calculations, AO basis in,
70–74
Excited states, SCF method for
description of, 74–77

F

Fock matrix elements, transferability
of, 4–41
Formaldehyde, electronic spectra of,
83–86

H

Helium, energy scattering studies on.
266–280
HNO, electronic spectra of, 91–92
Hugenholtz diagrams, 137–139

I

Ionization potentials, perturbation
theory for, 169–177

L

Low-energy electron scattering theory,
215–297
applications of, 266–293
alkali metal atoms, 281–288
C, N, O, 289–293
helium, 266–280
methods, 256–266
close-coupling, 256–257
continuum Bethe-Goldstone
equations, 259–263
matrix variational method, 258–259
polarized orbital method, 257–258
resonances and threshold effects in,
240–256
variational formalism, 232–240
wavefunction interpretation, 266–232
wavefunction structure, 218–226

M

Molecular orbital theory
   improved SCF cycling in, 58–59
   of localized orbitals, 41–58
      approximate, 46–47
      "molecules in molecules" method,
         48–55
   NEMO technique use in, 5–14
   SAMO technique use in, 14–41
   transferability in, 1–67
      of Fock matrix elements, 4–41
"Molecules in molecules" method,
   in molecular orbital theory, 48–55

N

NEMO method, 5–14
   basis of, 5–11
   modified, 11–14
Nitrogen, energy-scattering studies on,
   289–293

O

Oxygen
   energy scattering studies on, 289–293
   molecular, electronic spectra of,
      92–94

P

Perturbation theory of Fermion
   systems, 105–197
   bracketing technique for, 178–180
   diagrammatic method, 116–127
   diagrams for, 127–148
   excitation energies of closed-shell
      systems, 148–158
   Hartree-Fock diagrams of, 146–148
   for ionization potentials and electron
      affinities, 169–177
   linked cluster theorem and EPV
      diagrams in, 192–195
   normal product form of operators in,
      188–190
   particle-hole formalism, 185–187
   Rayleigh-Schrödinger theory, 103–116

second- and third-order, 158–169
sign rule in, 190–191
spin-independent formalism in,
   138–139, 152–154
time-independent second
   quantization formalism in, 180–185
Potential energy surfaces, 201–202

R

Rayleigh-Schrödinger perturbation
   theory, 109–116
Roothaan-Hartree-Fock equation, 2

S

SAMO method, 14–41
   basis of, 14–19
   bonding pathway, 31–32
   calculations using, 24–27
   conformational studies, 32–33
   cyclic systems and, 31–32
   geometry and basis sets in, 19–24
   ionic effects and, 31
   open-shell, 35–39
   pattern molecule examples, 17
   polymers, 39–41
   results and modifications of, 24
   steric effects and, 31
SCF method, for description of excited
   states, 74–77

T

Thioformaldehyde, electronic spectra of,
   86–88
Time-independent diagrammatic
   approach, to perturbation theory
   of Fermion systems, 105–197
Transferability, in molecular orbital
   theory, 1–67

W

Wick's theorem, 187–188
   diagrammatic representation of,
      121–127